Polymer Brush Carbon Nanotubes as Nanofillers in Macro and Nano Size Composites

Tony John Aitchison (BSc. Nano(Hons))

This thesis is submitted to the Faculty of Science and Engineering
of
Flinders University
for fulfillment of the requirements
for the degree of

DOCTOR OF PHILOSOPHY
in
CHEMISTRY

Dr Milena Ginic-Markovic
Dr Stephen Clarke
Prof. Janis Matisons

November 2010

Adelaide, South Australia

TABLE OF CONTENTS

Chapter 1.   CARBON NANOTUBES AND POLYMERS

Chapter 2. SYNTHESIS OF HOMOPOLYMERS AND DIBLOCK COPOLYMERS

Chapter 3. POLYMER BRUSHES: SURFACE INITIATED POLYMERIZATION (SIP)

Chapter 4. POLYMER BRUSHES AS NANOFILLERS (MACRO SIZED)

Chapter 5.   FORMATION OF BLOCK COPOLYMER MICRODOMAINS AND HYBRID MATERIALS (NANO SIZED)

Chapter 6.   GENERAL CONCLUSIONS, RECOMMENDATIONS, AND FUTURE WORK

SUMMARY

The work outlined in this thesis covers the many aspects of carbon nanotubes and polymers by combining the two into nanocomposite materials of macro and nano size. The issues of producing and combining the two are explored and results are provided.

There are four major aspects to this work;

1. *Polymer Brushed Carbon Nanotubes:* multi-walled carbon nanotubes (MWCNT) are surface functionalized with polymer brushes produced by activators regenerated by electron transfer (ARGET) atom transfer radical polymerization (ATRP). A "grafting from" approach was used as a higher grafting density would result and therefore it was necessary to functionalize the carbon nanotubes surface with hydroxyethyl-2-bromoisobutyrate (HEBI). This acted as the haloalkane (i.e. tertiary bromide) initiator sites in ARGET ATRP of styrene and methyl methacrylate. The successful growth of the polymer brushes were characterized for their chemical, kinetic and physical properties. In addition, polymer brushes of 2-hydroxyethyl methacrylate (HEMA) was grown by non-living means by attaching the HEMA monomer via the hydroxyl group to a carboxylic acid surface functionalized MWCNT and subsequently polymerized.

2. *Macro-sized Composites:* a composite of carbon nanotubes with homopolymers as the matrix, requires surface modification of the MWCNT to prevent nanotube aggregation. A homogeneous dispersion is necessary in order to produce improved properties for the composite. The 'macro' composite research involved the incorporation of polymer brush carbon nanotubes in concentrations of 0.1w/w% to 1w/w% (e.g. poly(methyl methacrylate) polymer brush carbon nanotubes in a poly(methyl methacrylate) matrix). The most

improved composites obtained used polystyrene brushes in a polystyrene matrix, which was due to π-π stacking interactions. The composite material possessed improved mechanical strength, increased glass transition temperature and increased processability. Furthermore, the dispersion was maintained after processing with shear forces.

3. *Pyrene as a Model System:* 1-pyrenecarboxylic acid has a very similar architecture to MWCNT and for this reason was used to model the chemical synthesis of aspects '1' and '2' with polystyrene. The work showed similar enhancements in terms of mechanical strength, increased glass transition temperature and increased processability. Compared to polystyrene polymer brush carbon nanotubes the improvement was not as great, however the pyrene material did not exhibit limits of dispersion like the carbon nanotubes filler.

4. *Nano-sized Composites:* This research utilized a hexagonal-packed cylindrical phase of a di-block copolymer melt, in an attempt to align the carbon nanotubes to the cylindrical phase. To ensure their affinity for the cylinder phase, polymer brushes of polystyrene were used for a 30/70 poly(styrene-b-methyl methacrylate) melt. However, the nanotubes were found to disrupt the segregation process, and the phases did not form appropriately. This ultimately did not provide strong enough forces to align the carbon nanotubes, but indicates that because of their relative massive size, greater forces are required.

Future work has been recommended with alternative polymer brush carbon nanotubes as fillers and using electric fields, as they have shown to better orientate a hexagonal-packed cylindrical phase from a parallel orientation to a perpendicular orientation. This is a suggested technique that might be able to align the carbon nanotubes.

CHAPTER SUMMARY

Chapter 1: Carbon Nanotubes and Polymers – an Introduction

What is a carbon nanotubes, what is a polymer, how are they made, and what are they used for? This first chapter is a detailed review of carbon nanotubes, polymers and combining the two.

Chapter 2: Synthesis of Homopolymers and Diblock Copolymers

Reports the findings and procedures used in this PhD research project to synthesize homopolymers of polystyrene and poly(methyl methacrylate) by activators regenerated by electron transfer (ARGET) atom transfer radical polymerization (ATRP). The chapter then extends to the synthesis of di-block copolymers of poly(styrene-b-methyl methacrylate) using polystyrene as the macro-initiator.

Chapter 3: Polymer Brushes: Surface Initiated Polymerization (SIP)

In this chapter the purification of carbon nanotubes and subsequent surface functionalization with a tertiary bromide initiator is discussed. A model system is also discussed, which uses 1-pyrenecarboxylic acid, as the chemical structure is very similar to a carbon nanotube. This model system was necessary to help verify the general functionalization procedure.

The work then extends to the use of the tertiary bromide functionalized carbon nanotubes in the synthesis of ARGET ATRP polymer brushes of polystyrene and poly(methyl methacrylate). In addition, poly(2-hydroxyethyl methacrylate) brushes were produced by a different synthetic route to the above. Further work was also performed on the pyrene model system, polymerizing one polystyrene polymer brush per pyrene molecule.

Chapter 4: Polymer Brushes as Nanofillers (Macro-Sized)

The brushes produced in Chapter 3 were used as a filler in the corresponding polymer (i.e. polystyrene brushes in polystyrene). Composite concentrations as high as 1w/w% of the polymer brush carbon nanotubes were introduced and the physical characteristics were analyzed.

Chapter 5: Formation of Block Copolymer Microdomains and Hybrid Materials (Nano-Sized)

Chapter 4 discusses the formation of macro-sized composite material, whereas this chapter takes it to the nano-sized composite material. Using block copolymer melts of a 30/70 ratio, the cylindrical phase is formed and during formation the carbon nanotube polymer brushes were added. These brushes have a stronger affinity for one of the two domains and hence it was expected to align within that phase.

Chapter 6: General Conclusions, Recommendations and Future Work

This chapter summarizes the entire work of the thesis and in particular how to optimize the composite material properties. In addition, the chapter discusses future directions the research can head towards.

OTHER SUCCESSFUL OUTCOMES

Publications & Conference Proceedings

- Trout, N.; Aitchison, T.; Clarke, S. R. *The 32nd Australasian Polymer Symposium* **2011**

- Clarke, S. R.; Aitchison, T.; Trout, N. *The 32nd Australasian Polymer Symposium* **2011**

- Aitchison, T.; Clarke, S. R. *The 32nd Australasian Polymer Symposium* **2011**

- Clarke, S. R.; Trout, N.; Aitchison T.; Habibie, S.; Brown, R. J. *Chemeca* **2010** 143, ISBN 978-085-825-9713

- Aitchison, T. J.; Ginic-Markovic, M.; Clarke, S.; Matisons, J. G. *ARNAM/ARCNN 2010 Joint Workshop* (**2010**)

- Aitchison, T. J.; Ginic-Markovic, M.; Clarke, S. *The Fourth Biennial Australian Colloid and Interface Symposium* (**2009**)

- Aitchison, T. J.; Ginic-Markovic, M.; Clarke, S.; Matisons, J. G., *ARNAM Annual Workshop* (**2008**)

- Aitchison, T. J.; Ginic-Markovic, M.; Clarke, S.; Matisons, J. G., *The 30th Australasian Polymer Symposium* (**2008**)

- Aitchison, T. J.; Ginic-Markovis, M.; Matisons, J. G., *Thinking Synergy: A Flinders Postgraduate Conference* (**2008**)

- Aitchison, T. J.; Ginic-Markovic, M.; Matisons, J. G., *Ninth International Conference on the Science and Application of Nanotubes* (**2008**)

- Aitchison, T. J.; Ginic-Markovic, M.; Matisons, J. G., *Polymer Processing Society 24th Annual Meeting Conference Proceedings* S18-925 (**2008**)

- Aitchison, T. J.; Ginic-Markovic, M.; Matisons, J. G.; Simon, G.P.; Fredericks, P. M., *J. Phys. Chem. C* **2007**, 111, 2440-2446

- Aitchison, T. J.; Ginic-Markovic, M.; Matisons, J. G., *Advanced Materials & Nanotechnology (AMN3) Conference Proceedings* (**2007**)

Grants

- Australian Research Council: Australian Research Network for Advanced Materials (ARNAM) Travel Grant (**2008**, amount $3500).

- Flinders University: Research Student Conference Travel Grant (**2008**, amount $3684)

Research Trips

- 'High Resolution Transmission Electron Microscopy,' Dr Martin Saunders, Centre for Strategic Nano-fabrication, University of Western Australia, Australia (**2009**)

- 'Polymeric characterization of nano-filled materials,' Prof. Henri Sautereau and Prof. Gerard Seytre, Institut National des Sciences Appliquees de Lyon (INSA-Lyon), France (**2008**)
- 'Optical rheology of nano-filled polymeric materials,' Dr Anson Ma, Cambridge University, England (**2008)**

Publications in Preparation

- Aitchison, T. J.; Ginic-Markovic, M.; Saunders, M.; Fredericks, P.; Valiyaveettil, S.; Matisons, J. G.; Simon, G. P. ARGET ATRP MWCNT Polymer Brushes and Their Properties, *Polymer International*
- Aitchison, T. J.; Ginic-Markovic, M.; Clarke, S.; Matisons, J. G. Kinetics of ARGET ATRP Di-Block Copolymers, *Journal of Polymer Science: Part A, Polymer Chemistry*
- Aitchison, T. J.; Ginic-Markovic, M.; Clarke, S.; Matisons, J. G. MWCNT PHEMA Polymer Brushes and Their Use *Macromolecules*
- Aitchison, T. J.; Ginic-Markovic, M.; Clarke, S.; Matisons, J. G. Polymer Brush Nanocomposites, *Chemistry of Materials*
- Aitchison, T. J.; Ginic-Markovic, M.; Clarke, S.; Matisons, J. G. Synthesis of Silicon Wafer Polymer Brushes by Using Random Tripolymers, *Chemistry of Materials*
- Aitchison, T. J.; Ginic-Markovic, M.; Clarke, S.; Matisons, J. G. Pyrene Polymer Brushes as a Nanofiller in Polymer Composites, *Chemistry of Materials*

DECLARATION

'I certify that this thesis does not incorporate without acknowledgement any material previously submitted for a degree or diploma in any university; and that to the best of my knowledge and belief it does not contain any material previously published or written by another person except where due reference is made in the text.'

Date 17/11/10

Tony Aitchison

ACKNOWLEDGEMENTS

LIST OF FIGURES

Page xvi

LIST OF SCHEMES

LIST OF TABLES

LIST OF EQUATIONS

GLOSSARY

Abbreviations

AC	Acid Cleaved – *relating to carbon nanotubes*
AFM	Atomic Force Microscopy
AGET	Activators generated by electron transfer
AIBN	2,2'-azobis(isobutyronitrile)
AR	As Received – *relating to carbon nanotubes*
ARGET	Activators regenerated by electron transfer
ATRP	Atom-transfer radical polymerization
Conv.	Conversion
CRP	Controlled radical polymerization
CVD	Chemical vapor deposition
CNT-Br	Carbon nanotubes functionalized with HEBI
CNT-PHEMA	PHEMA polymer brushes on carbon nanotubes
CNT-PMMA	PMMA polymer brushes on carbon nanotubes
CNT-PS	PS polymer brushes on carbon nanotubes
DMF	Dimethylformamide
DSC	Differential Scanning Calorimetry
DTGA	Differential Thermogravimetric Analysis
EBiB	Ethyl 2-bromoisobutyrate
EDX	Energy Dispersive X-ray Spectroscopy
FRP	Free radical polymerization
FT-IR	Fourier Transform Infrared Spectroscopy
GPC	Gel Permeation Chromatography
HEBI	Hydroxyethyl-2-bromoisobutyrate
HEMA	2-hydroxyethyl methacrylate
HRTEM	High Resolution Transmission Electron Microscopy
ICAR	Initiators for continuous activator regeneration
L-MWCNT	long multi-walled carbon nanotubes from NTP
MeOH	Methanol
Me$_6$TREN	Tris(2-dimethylamino)ethyl)amine
MMA	Methyl methacrylate

MCWNT	Multi-walled carbon nanotube
NMP	Nitroxide mediated polymerization
NMR	Nuclear Magnetic Resonance
PHEMA	Poly(2-hydroxyethyl methacrylate)
PMMA	Poly(methyl methacrylate)
ppm	parts per million
PS	Polystyrene
PS-Br	Macro-initiator of PS with an alkyl bromide functionalized end
Pyrene-HEBI	1-Pyrenecarboxylic acid functionalized with HEBI
Pyrene-PS	A PS chain covalently attached to Pyrene-HEBI
R^2	is the coefficient of determination of a linear regression. It ranges from 0 to 1 with 1 indicating the real data fits perfectly to the regression line and 0 the real data does not.
S-MWCNT	short multi-walled carbon nanotubes from NTP
SCFT	Self-consistent mean field theory
SIP	Surface initiated polymerization
$Sn(EH)_2$	Tin(II) 2-ethylhexanoate
SR & NI	Simultaneous reverse and normal initiation
SWCNT	Single-walled carbon nanotube
T_c	Crystallization temperature
T_d	Decomposition temperature
TEA	Triethylamine
TEM	Transmission Electron Microscopy
T_g	Glass transition temperature
TGA	Thermogravimetric Analysis
THF	Tetrahydrofuran
TREN	Tris(2-aminoethyl)amine
TSE	Total surface energy

- CHAPTER 1 -

CARBON NANOTUBES

AND

POLYMERS

1. INTRODUCTION: CARBON NANOTUBES & POLYMERS

Preface

This chapter reviews the current level of research that has been reported in peer reviewed journals in the fields of carbon nanotubes and polymers, more specifically carbon nanotube functionalization with long alkyl chain molecules and polymers. Furthermore, different polymerization techniques have been explored to determine the optimal technique for diblock copolymer formation and their application in thin films.

These two fields of research are to be combined to form nanocomposite materials in a macro (bulk matrix) and a nano (thin film) application.

CARBON NANOTUBES

1.1 Introduction

Carbon Nanotubes were firstly discovered in 1991 by Sumio Iijima when he was studying the material deposited on a cathode from arc-evaporation synthesis of fullerenes,[1] since then due to their remarkable properties, the research in this field has considerably grown. These carbon nanotubes have very appealing properties because they are highly anisotropic; graphene cylinders of approximately 1nm in diameter for single-walled (i.e. pictured Figure 1. 1) or could be multiple tubules packed within one another for multi-walled (diameter around 20nm), both of lengths around 1-10µm.[2] They also express exceptional mechanical properties and strength, low density, and have extremely high electrical conductivity making them the ultimate carbon fibre.[3] Nanotubes have also been described as one-dimensional molecules due to their high aspect ratio; diameter of tens of nanometres and lengths that can be as long as several microns.[4]
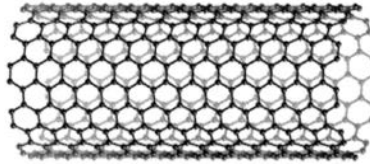
Figure 1. 1: A single-walled nanotube.[5]

1.2 Production & Synthesis

In the production of carbon nanotubes, three basic components are required; a source of heat, a source of carbon, and the presence of certain metals that act as a catalyst,[6] with the exception of Multi-Walled Carbon Nanotubes (MWCNT). MWCNT under the right conditions can be produced without the presence of a catalyst.[7] The most commonly used catalysts are iron, nickel, and cobalt.[8]

In the manufacturing of carbon nanotubes there are many techniques and the most popular ones have been discussed here. Each have there own advantages and disadvantages, but ultimately no procedure has been defined as the industry standard.

Plasma Arc Discharge

Plasma arc discharge was the first known technique to produce carbon nanotubes[1] and is the most commonly used method today. However, this process also produces graphitic impurities such as carbon soot containing amorphous carbon, onions and fullerene molecules.[9] In comparison, it can be seen as an unfavorable technique when compared to chemical vapor deposition (CVD) due to the yield of impurities formed (see section below) particularly for commercial production of carbon nanotubes. Although, the amount of graphitic impurities produced can be controlled to an extent by the conditions under which the nanotubes are formed, this ultimately affects the plasma's stability to provide optimal reaction conditions.[9]

In order to produce plasma arc discharge nanotubes, plasma is produced by using an electric discharge between two graphite electrodes, which are held within a

chamber of inert gas (He, Ar, etc…) at controlled pressure and composition. The discharge causes the carbon to vaporize from the anode and creates a plasma that surrounds the arc discharge. This plasma then deposits itself onto the facing cathode, which is usually of larger size to the anode. The deposit forms a rod shape structure and inside this rod lies the graphitic impurities and carbon nanotubes that are formed within the interelectrode plasma region; average temperature of the region is in the order of 4000K. A separation gap between the water cooled electrodes of 1mm is held while the anode is consumed and the rod grows at approximately 1mm/min. The potential applied can be either A.C. or D.C. with the electric current being dependent on the electrode's size, separation, gas pressure and anode purity; typically ~100A is used.[9,10] A setup of this process can be seen in Figure 1. 2.
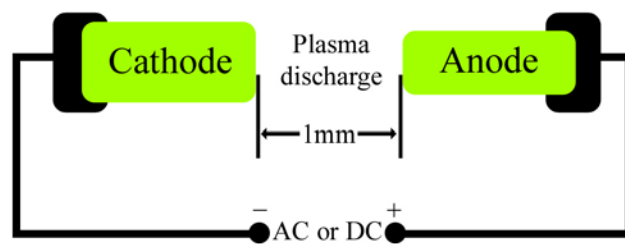
Figure 1. 2: Plasma arc discharge setup.[11]
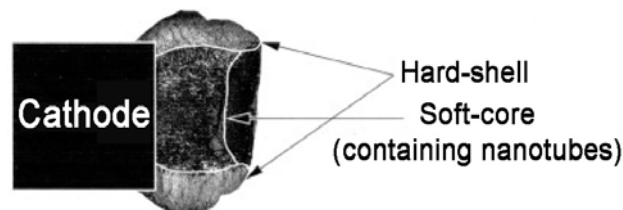
Figure 1. 3: Anode deposit, demonstrating the microstructures formed in plasma arc discharge.[12]

The cathode deposit contains two distinct microstructures (see Figure 1. 3). Firstly the outer hard-shell composed of a pyrolytic graphite mass and secondly the inside core, loosely packed columns that are aligned in the axial direction to the deposit. The nano-porous columns are composed of straight, stiff carbon nanotubes and graphitic

impurities. The best yield of carbon nanotubes for these columns is 25% of the evaporated anode material.[10]

To produce MWCNT, at its optimal conditions, a ~20V potential between the electrodes is required with a current density of 150A/cm^2, and a helium gas pressure of 500Torr.[9] In order to create Single-Walled Carbon Nanotubes (SWCNT) a metal catalyst is required and this was first achieved in 1993 by Bethune and coworkers.[13] By using a typical carbon anode, they placed a small percentage of cobalt catalyst inside the system and then found SWCNT were produced within their soot material.[13] This was the first successful method that was capable of producing substantial amounts of SWCNT by arc-discharge.[9]

Chemical Vapor Deposition (CVD)

This surface deposition technique uses a transition-metal catalyst that has been deposited on to a substrate and positioned inside a reactor to grow carbon nanotubes from a gaseous carbon source. For MWCNT growth, iron, nickel, or cobalt is often used as the catalyst because at high temperatures these metals have finite solubility for carbon.[11] Substrates such as quartz, glass,[14] alumina, silica,[15] or even silicon carbide[16] have been used, where the growth position of the nanotubes can be controlled by patterning the catalyst on to the substrate.[17] Temperatures of between 500-1000°C are used with a hydrocarbon gas (i.e. the carbon source) at a controlled concentration, in an inert atmosphere. This gas is blown through a tubular reactor for a controlled time and the carbon product is collected at room temperature.[11] A setup of this process can be seen in Figure 1. 4.

The nanotube grows by the dissociation of hydrocarbon molecules catalyzed by the transition metal, and dissociation and saturation of carbon atoms in the metal nanoparticle. The carbon precipitates from the saturated catalyst to form a tubular

carbon sp^2 structure, as this form is favored over the other forms of carbon and is of lower energy by comparison (i.e. no dangling bonds). Two growth modes can be seen in Figure 1. 5. The first being "base growth mode," which has the catalyst attached to the substrate and the nanotube grows from the base. The second being "tip growth mode," which has the catalyst attached to the end of the grown nanotube and travels with the growing end.[11]
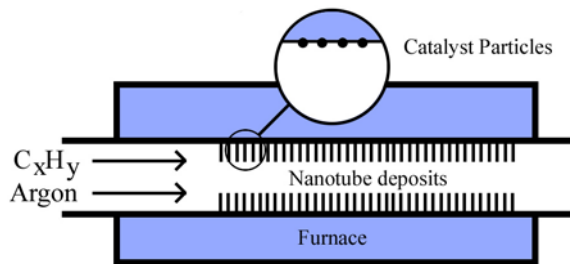
Figure 1. 4: CVD setup with inset showing the catalyst particles deposited on the reactor substrate before nanotube growth.
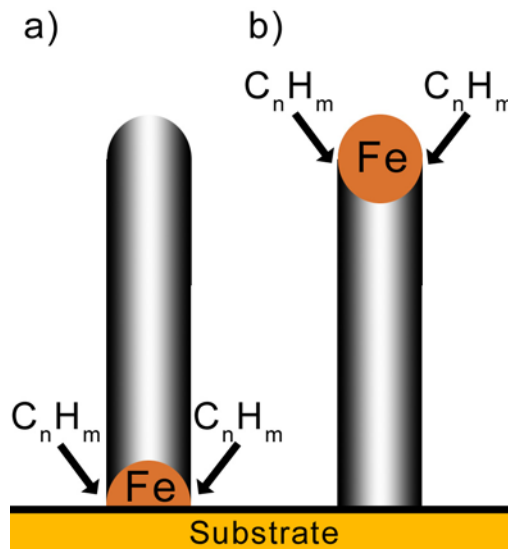
Figure 1. 5: Growth modes for CVD, a) base growth mode, and b) tip growth mode.[11]

The end product is a well-aligned, uniform mat of nanotubes on a substrate with a narrow distribution in nanotube lengths. These nanotubes are larger in diameter than that of arc discharge nanotubes because the diameter size is dependent on the catalyst particle size, growing to a maximum length, typically 50μm.[18,19] This form of

nanotube production favors the creation of MWCNT,[20] but under specific conditions SWCNT can be produced (i.e. temperature, gas, and catalyst composition).[21] It also favors the production of semi-conducting carbon nanotubes over metallic.[22] Furthermore, despite producing aligned nanotubes the major problem with this procedure is that the nanotubes produced can be highly defective.[23]
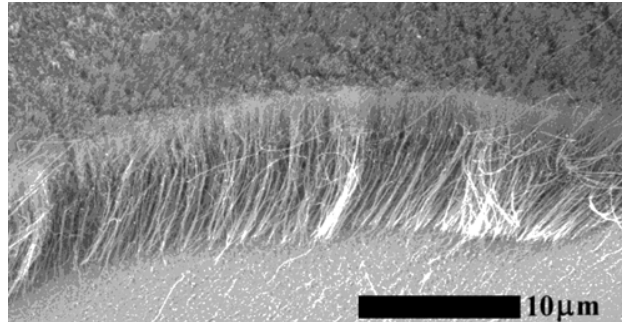
Figure 1. 6: SEM image of a CVD deposit on a 1nm Fe film, using methane/nitrogen-ammonia plasma to generate the carbon nanotubes.[24]

Laser Ablation

Laser ablation uses an intense laser pulse to vaporize a carbon target, which also contains 0.5 atomic percent of nickel and cobalt, and is placed in a tube furnace at around 1200°C. As the target is ablated, inert gas is passed through the chamber carrying the grown nanotubes to a cold finger for collection.[11] A setup of this technique can be seen in Figure 1. 7.
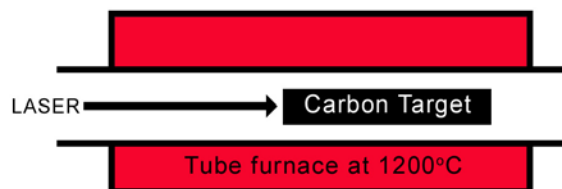
Figure 1. 7: Laser Ablation setup.[11]

The SWCNT product is in the form of ropes; nanotubes close-packed into hexagonal crystals due to van der Waals interactions (Figure 1. 8) and the by-products are the same as that produce in the arc-discharge technique.[11]
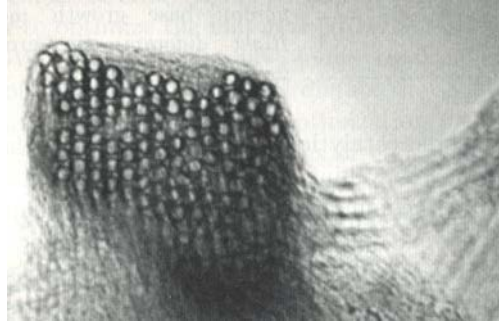
Figure 1. 8: SWCNT produced by laser ablation, demonstrating the close-packing.[11]

1.3 Chirality & Conductivity

One of the simplest ways to describe a carbon nanotube is to describe it as a rolled up sheet of graphene and depending on which direction the sheet is rolled will determine its conductivity.[25] The direction of rolling is characterized by the two chiral indices *n* and *m*, which are related to the chiral vector, $C_h = n\mathbf{a_1} + m\mathbf{a_2} \equiv (n,m)$. It can also be characterized by what is called the chiral angle θ, and the relationship between C_h and θ can be seen in Eq. (1).

$$\cos \theta = C_h \cdot \mathbf{a_1}/|C_h||\mathbf{a_1}| \qquad (1)^{[25]}$$

When rolling, depending on the combination of *n* and *m* or magnitude of θ, a specific class of nanotube is formed. There are three different classes of nanotubes; armchair and zig-zag are achiral nanotubes with a mirror image that is identical, and chiral, with the axially chiral nanotube having spiral symmetry that has a non-superimposable mirror image.[25] These are presented in Figure 1. 9.

In this model whenever $2n + m = 3q$, where *q* is an integer, the nanotube exhibits metallic conductive properties, otherwise it is semi-conducting. This calculates that all armchair nanotubes (*n,n*) are metallic and one third of all zig-zag nanotubes (*n,0*) are metallic, with the remaining two thirds being semi-conducting (refer to Table 1. 1).[25]
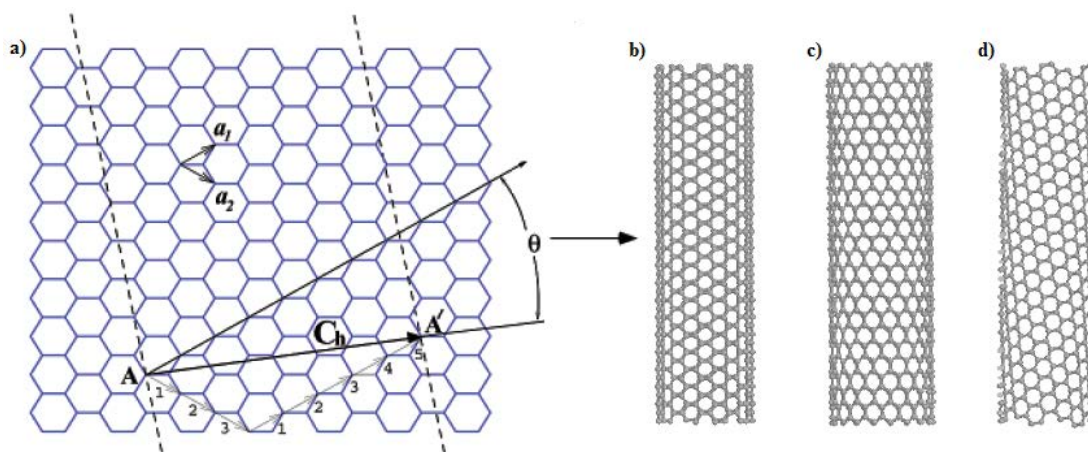
Figure 1. 9: a) Tube rolling vectors into b) armchair, c) zig-zag, or d) chiral nanotubes, with a) demonstrating a (5,3) chiral carbon nanotube.[26,27]

Type	θ	C_h	Cross Section Shape
Armchair	30°	(n,n)	Cis
Zig-Zag	0°	(n,0)	Trans
Chiral	$0^o < |\theta| < 30^o$	(n,m)	Mixture of cis and trans

Table 1. 1: n and m vector conformations where $0 \leq |m| \leq n$.[25]

1.4 MWCNT & SWCNT Modification

Structure vs. Reactivity

The carbon nanotube is composed of four different sites, all of which have a different degree of reactivity. These sites are the end caps, open ended tubule sites, defect sites, and the nanotube sidewall, pictured in Figure 1. 10.[28] This is important when chemically modifying the nanotube as any structural integrity damage that may occur on the sidewalls can result in a loss of mechanical strength and conductivity.[29,30]
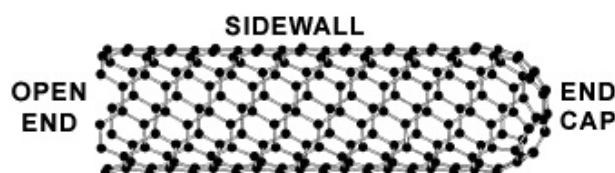
Figure 1. 10: A carbon nanotube indicating the various components of a nanotube, where a defect site is an irregularity from the above structure.[28]

The amorphous carbon impurities have the highest degree of reactivity and because of this are the easiest and the first impurity to be removed. Fullerenes and onion impurities, which are concentric fullerenes inside one another, exhibit similar properties to the nanotubes end caps, as the curved nature of the end caps is of similar structure to these impurities; the end caps have high strain on their hexagon-heptagon pairs like the onion and fullerene. When treating a crude sample of carbon nanotubes, at this level, simultaneously the impurities are removed and closed nanotubes are opened. Extended treatment shortens the nanotube as the ends are consumed, which is also known as "cutting" the nanotube. Increasing the strength of the treatment causes defects to form along the sidewalls, which can lead to larger openings and eventually nanotube destruction. Finally the sidewalls have the lowest reactivity as it is in the lowest energy form, similar to that of a graphene sheet.[31]

If, in the production of the carbon nanotube, a catalyst particle was used, acid treatment removes such particles. Often nitric acid, or a combination of nitric and sulphuric acid is used.[32,33] There have even been reports of hydrofluoric acid being used.[34]

Purifying and Cutting Techniques

The varying degrees of reactivity can allow the simultaneous consumption of graphitic impurities and the cutting of carbon nanotubes into smaller lengths.[31] As a result it can be a one step treatment, however in most treatments not all impurities result in a gaseous state (i.e. CO_2) and require filtration or centrifuging to remove the remaining impurities. As most treatments rely on oxidation, the surface oxygenated species (i.e. hydroxyl groups, carboxylic acid groups, quinone, etc...) aids in the filtration or centrifuge process.[35]

Thermal annealing is one such treatment that has the capacity to remove amorphous carbon by essentially burning off the impurities. Temperatures of between 600-1000°C are sufficient to turn the impurities into gaseous products such as carbon monoxide, carbon dioxide, hydrogen and methane. In a controlled atmosphere however, a lack of oxygen would only result in hydrogen and methane.[36,37] This technique is seen as being unfavorable for mass production, as the yield of high purity nanotubes is less than 1% and significant oxygenated moieties required for some further functionalization techniques does not occur.[9] However if the sample is rolled while heated then the expected yield can be as high as 40%.[38] The reaction mechanism for this treatment can be seen in Scheme 1. 1.

$$C \; + \; O_2 \longrightarrow CO_2$$
$$2C \; + \; O_2 \longrightarrow 2CO$$
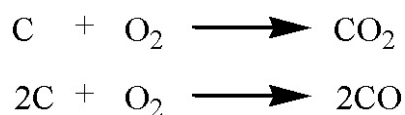
Scheme 1. 1: Thermal decomposition reaction.[36]

Nitric acid, a mild oxidant, is sufficient to oxidize/remove the impurities of graphitic carbon and metal catalyst particles with minimal damage to the nanotubes structural integrity. The nitric acid refluxing is unable to attack 6-6 ring boundaries and therefore sidewall defect generation does not occur. It can only attack the areas that express large strain, such as heptatomic rings, and $-CH_2$ and $-CH$ groups. This technique is particularly useful for opening closed nanotubes, as the end caps have large strain and cannot generate abundant functionalities (i.e. nanotube sidewalls are preserved). This process however, needs long-time refluxing as the reaction is particularly slow.[31]

Similar in nature to nitric acid refluxing, a combination of sulphuric acid and nitric acid (3:1) is one of the most well known and most popular form of carbon nanotube purification and cutting. This simple technique of sonication or refluxing

has the capacity to cut carbon nanotubes and tailor their length, since the consumption of the nanotube is dependent on reaction time.[31,39]

Ozonolysis, another technique, is used to break carbon-carbon double bonds at low temperatures, as the excess O_3 simply evolves back into gas and leaves no residual by-product such as the MnO_2 in the potassium permanganate procedure discussed below. The ozonation process produces oxygenated functional groups such as carboxylic acids, esters, and quinone moieties that can be removed by thermal annealing at temperatures of 600-800°C. This harsh oxidant readily functionalizes the end caps and defect sites to carboxylic acids, followed by the remaining rim sites.[35] This technique is largely dependent on the capability of the ozone to be dissolved into the reaction medium (i.e. solvent) and for this reason is often performed at low temperatures.[40,41] The reaction mechanism for this treatment can be seen in Scheme 1. 2.
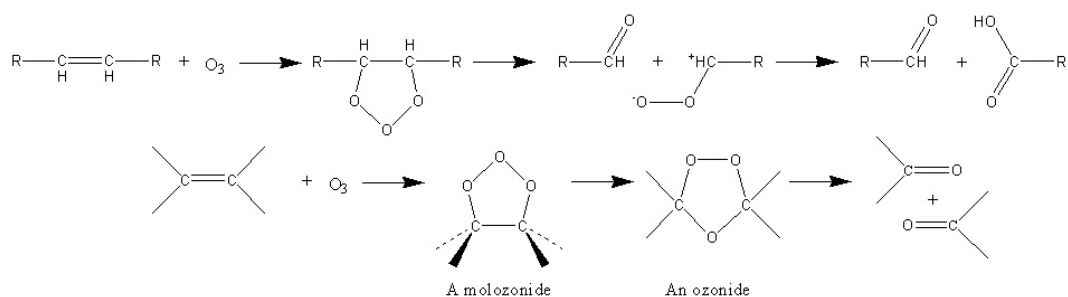
Scheme 1. 2: Chemical oxidation by ozone treatment.[42,43]

Potassium permanganate, a milder oxidant, can be used to purify carbon nanotubes in alkaline or acidic conditions. In this technique the potassium permanganate has a controllable oxidation degree, as it is dependant on the reaction time. It has the capacity to create new defect sites along the nanotube sidewalls as the quinone groups formed are an intermediate towards carboxylic acids in a later step.[31] In this process however, the by-product of manganese oxides are extremely difficult to remove, as the solid MnO_2 deposits onto the nanotube and requires hydrochloric

acid washing for removal.[44] It has however been reported that this deposit can be beneficial as it increases the dispersion stability of purified nanotubes.[45] A yield of <40% by weight is produced for SWCNT, which is extremely high for a solution phase purification.[9] This oxidant also has the ability to cut the nanotubes, but requires a long reaction time.[45] The reaction mechanism for this technique can be seen in Scheme 1. 3, where it is noted that sodium hydroxide is required to oxidize the double bond and remove the permanganate ion from the nanotube.[46]
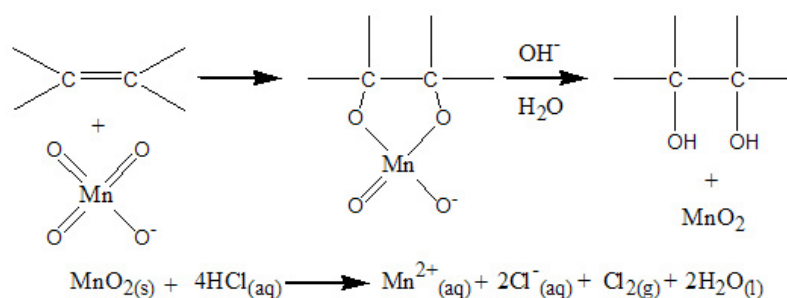
Scheme 1. 3: Reaction mechanism of potassium permanganate oxidation treatment. In this technique the hydroxyl groups formed can be oxidized further to carbonyl groups and hydrochloric acid is used to remove the MnO$_2$.[46,47]

There are many other purification techniques that have not been discussed in this chapter, such as size-exclusion chromatography,[48] but this is not the main focus of the work detailed in this thesis.

Differences in Properties

The main structural difference between a MWCNT and SWCNT is that MWCNTs are essentially many SWCNTs encased within one another. This structural difference has many benefits for future applications.[2]

It has been reported that in SWCNTs, the defect sites are often generated by chemical purification and/or functionalization, which hinders the high conductivity and mechanical strength, as the chemical procedures degrade the helical shell walls

with oxygenated functionalities.[29] This property has been observed in SWCNT self-assembled monolayers (SAM),[29] however for MWCNT this is not the case. The inner nanotubes of MWCNT are preserved in such treatments and maintain their high conductivity and mechanical strength.[30] Just to name a few other advantages, MWCNTs are excellent electron emitters like SWCNT,[49] they degrade ten times slower than SWCNTs, and the outer tubules protect the inner tubules from bombardment and radiation.[50] The most important factor being that the outer tubule can be readily modified while leaving the inner nanotubes untouched and therefore its properties effectively unaffected.

CARBON NANOTUBE FUNCTIONALIZATION

1.5 Introduction

Carbon nanotubes have a tendency to aggregate into bundles of varying size and shape limiting wider applications, however upon surface modification the nanotubes altered state can prevent these bundles from forming, increasing their dispersion stability.[51,52]

Literature papers to date have reported numerous ways in which to functionalize carbon nanotubes, often beginning with an oxidative procedure to create hydroxyl, quinone and carboxylic acid functionalities.[35] Using these groups, anything from alkyl chains[53] to nano-particles[54] have been attached through various synthetic means. A common technique is to use amide groups, either from a coupling agent[55] or acid chlorides,[56] and in the ionic method, by zwitterions (i.e. $R-NH_3^+$ ions with the negatively charged carboxylate ions).[57,58] Other functionalization techniques have been used, with a set of sub groups that include non-covalent functionalization, π-π stacking, endohedral functionalization, sidewall functionalization and defect functionalization (see Figure 1. 11).[59]
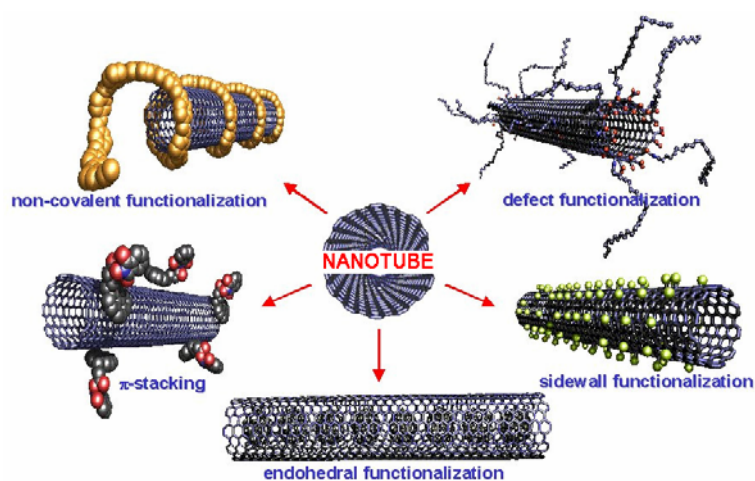
Figure 1. 11: The various types of nanotube functionalization.[59]

Often, when functionalizing carbon nanotubes, the main goal is to increase dispersion stability, because once that issue has been resolved it opens up a wider possibility for nanotube applications, such as nanotube composites.[60] However, research to date has been unsuccessful in dispersing large quantities of carbon nanotubes into solution. Quantities in the order of mg/mL is the highest recorded to date[61] and so we are yet to see any applications of such high concentrations of carbon nanotubes.

1.6 Micelle Formation

Principle

The main component of micelle formation is to use a surfactant or polymeric molecule to form a molecular aggregate that constitutes a colloidal particle.[62] The surfactant has a hydrocarbon tail with an ionic component at the other end or head, which is a sub-unit to the overall micelle structure. In the case of a polymeric molecule a similar structure to the surfactant can be used such as an amphiphilic homo-polymer or a amphiphilic copolymer, which is often a di-block copolymer with a hydrophobic tail and a hydrophilic head.[63]

In micelle formation, a loose solution (i.e. often aqueous) of surfactant and hydrophobic molecules forms the micelle from its emulsion. The hydrophobic molecule interacts with the hydrophobic hydrocarbon end of the surfactant, while the ionic component interacts with the aqueous solution. Upon dissolution, the entropic forces are lowered, and the regions align to form an aggregate with the tails directed inwards, the ionic end facing outwards, and the hydrophobic molecule contained within. Micelles can form many shapes including spheres, disks, oblate or prolate ellipsoids, long cylinders, and even bilayers.[64] Some of these formations can be seen in Figure 1. 12.

(a) linear   (b) disk-like   (c) spherical
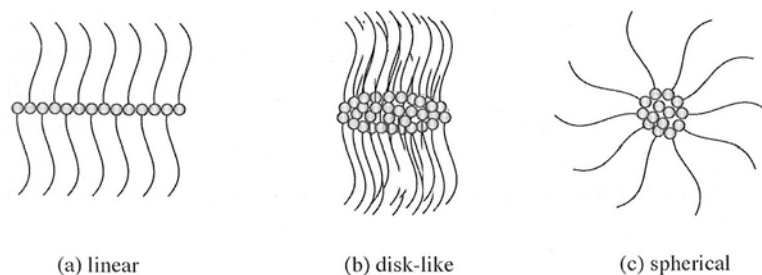
Figure 1. 12: Some of the micelle shapes that can be formed (the circles represent the hydrophilic ends and the tails represent the hydrophobic ends).[65]

Application & Synthesis

Ideally, when applying the micelle principle to carbon nanotubes, the micelle formed can wrap around the carbon nanotube forming a cylindrical shape rather than the hemispherical or disordered shape (see Figure 1. 13).[66,67] This is beneficial for nanotube dispersions, as each individual nanotube is encased in an ionic field which prevents other nanotubes from coming closer and forming aggregated bundles of nanotubes. It also disrupts the van der Waals interactions, further inhibiting bundle generation.[67,68]
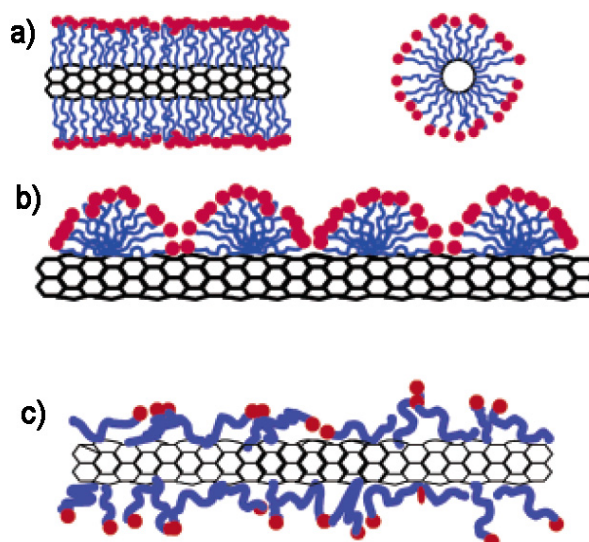
Figure 1. 13: a) Ideal micelle nanotube formation, and cross section (right), b) hemispherical micelle adsorption, and c) disordered adsorption.[66]

Kang and Taton[69] reported a process by which they formed micelles containing SWCNTs by using an amphiphilic poly(styrene)-*block*-poly(acrylic acid) (i.e. PS-*b*-PAA) copolymer (see Scheme 1. 4). The unique feature from this article comes from the fact that they then cross-linked the hydrophilic ends with one another, forming hard-shell micelle-encapsulated carbon nanotubes. This significantly improved the nanotube's dispersion capabilities in a wide variety of polar to non-polar solvents and in polymer matrices.
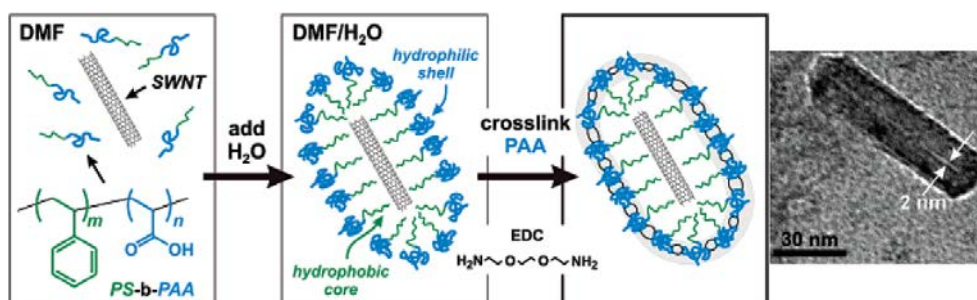
Scheme 1. 4: The Kang and Taton[69] mechanism for forming the micelle-encapsulated SWNT (TEM right). Note: EDC was the coupling agent required to catalyze the cross-linking.
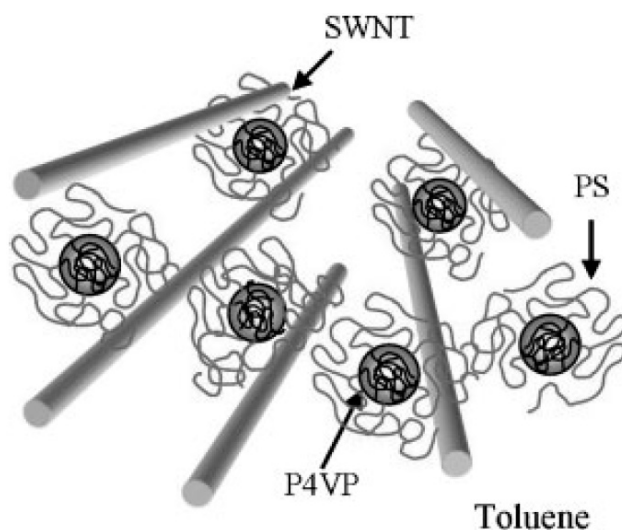
Figure 1. 14: A model representation of the end product reported by Shin et al.[70] Note: P4VP = poly(4-vinylpyridine).

Shin *et al*[70] reported a non-destructive way to disperse SWCNTs from bundles, in both polar and non-polar solvents. This was attempted in a similar way to Kang and co-workers, but in this research the amphiphilic block copolymer micelles were used as a dispersant that adhered to the nanotube surfaces rather than encapsulating them (see Figure 1. 14). The use of this amphiphilic copolymer prolonged the dispersion stability achieving greater than two months, while using a homo-polymer provided only six hours of stability. Without any polymer, the carbon nanotubes would instantly aggregate.

The use of micelles is not limited to only nanotube dispersions. It has also been used for templates that produce catalysts for nanotube growth. Bennett *et al*[71] reported the use of a poly(styrene-*block*-acrylic acid) amphiphilic block copolymer that was capable of forming micelles and self-organizing into an ordered structure on a substrate upon spin-coating. They then utilized the poly(acrylic acid) domains in an ion-exchange protocol to selectively sequester iron ions. The end result was iron-containing nanoclusters patterned on a substrate of nearly uniform size. These nanoclusters could then be used for thermal CVD as the iron-containing nanoclusters act like catalyst particles. An element of diameter control and spacing also exists in this technique, as the iron-containing nanocluster size and spacing could be controlled by altering the block copolymer molecular weight and composition. In addition, the iron-containing nanocluster formation was also altered for different metal species.

Stewart *et al*[72] composed a way of using the micelle principle to construct self-assembled block copolymer nanotubes, using the triblock copolymer, polyisprene-*block*-poly(2-cinnamoylethyl methacrylate)-*block*-poly(*tert*-butyl acrylate). They were able to produce cylindrical micelles with a diameter of 22nm, which could be

hollowed out to form nanotubes by photo-crosslinking the middle polymer, and degrading the core polymer, polyisoprene, through ozonolysis (see Figure 1. 15).
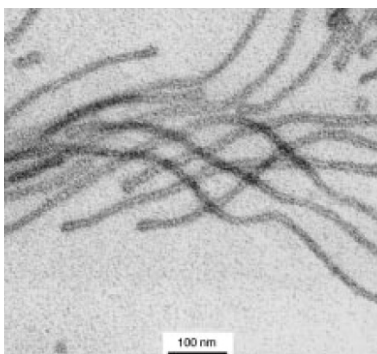
Figure 1. 15: A TEM image of the copolymer nanotubes produced by Stewart and Liu.[72]

1.7   Polymer Wrapping Nanotubes and Polymer Brush Nanotubes

Polymer wrapping is the process of attaching a polymeric chain to carbon nanotubes by covalent (i.e. polymer brushes) or non-covalent means, where the polymer wraps itself around the carbon nanotube (i.e. enveloping the surface, increasing dispersion and preventing aggregation). This "wrapping" occurs due to an electrostatic interaction, but in the absence of chemical functionalization, van der Waals forces are the main contributors. The strength of the interaction depends on the structural architecture of the polymeric chain and it has been reported that polymers with a flexible backbone comprising of aromatic rings are excellent candidates for polymer wrapping, due to π-π stacking.[73]

Many researchers have reported various polymers to wrap and the means of covalent polymer wrapping/brushes can occur by one of two synthetic techniques; the growth of the polymer from the carbon nanotube (i.e. "graft from"), or the attachment of an already grown polymeric chain (i.e. "graft to"). Polymers such as nylon 6,[74] polystyrene,[75,76] polyaniline,[77] polyurea,[78] poly(n-butyl methacrylate),[140] among others have been used, including amphiphilic copolymers.[79] Furthermore, the "graft

to" compared to the "graft from" technique has increased difficulty in purification, attachment by other forces, and a lower grafting density.[80]

1.8 Carbon Nanotube Applications

The carbon nanotube has very appealing properties that fall into three categories, which are electrical, mechanical, and chemical. These properties have been explored in many potential applications, such as conductive composites,[81] high strength composites,[82] energy storage,[83,84] field emission displays,[85] radiation sources,[86] probes,[87] and many more.

Many patents and issuances have been filed in the area of synthesis and processing of carbon nanotubes (41%), but in terms of the application of carbon nanotubes, electron emission (25%) and composite materials (9%) has had the greatest interest (Figure 1. 16).[88]
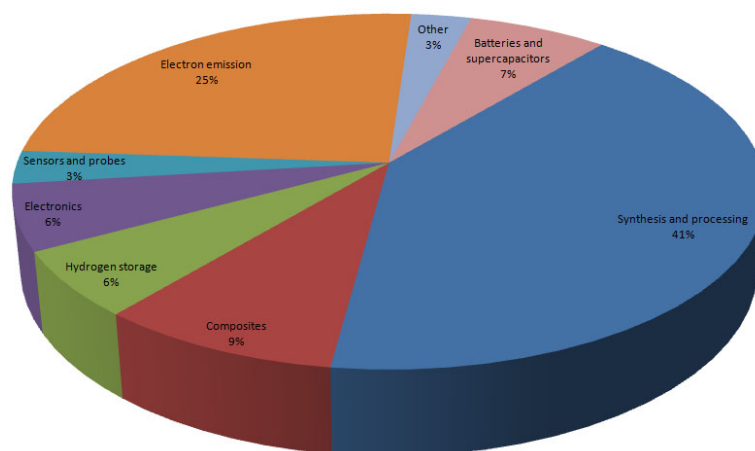
Figure 1. 16: Patent filings and issuances of carbon nanotubes in 2002.[88]

Nanotubes Used as a Nanofiller in Polymer Composites

Composites made from carbon nanotubes and polymers offer the promise of materials with high electrical, thermal, optical and mechanical properties. A significant amount of literature has been published on the mixing of pristine and acid treated carbon nanotubes into various polymer matrices.[89,90,91,92] However, a

common problem is experienced with the production of the composites as the nanotube possesses a limited solubility that results in aggregated bundles of the carbon nanotubes.

To improve the nanotubes dispersion many novel techniques have been developed that are usually post treatments of the composite.[93,94] The alternative is to chemically treat and hence functionalize the nanotube's surface, thus increasing the solubility of the nanotube.[95,96,97] Furthermore, Frankland *et al*[98] has predicted by molecular simulations that in order to strengthen the matrix mechanically ~0.3% functionalization density is required. This has been supported experimentally with a 150% increase in the storage modulus with only a 1wt % loading of the carbon nanotube. [99,100]
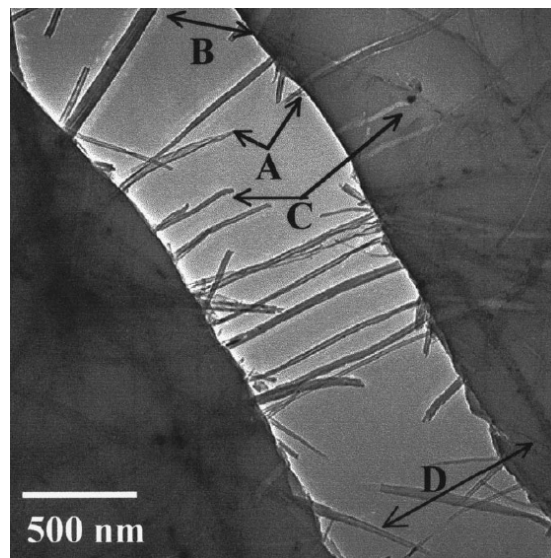
Figure 1. 17: Nanotube-polystyrene composite (non-covalent interaction), demonstrating a thermal stress fracture resulting in nanotubes pulling out of the polymer matrix (e.g. A, B, C, and D).[102]

A high strength interaction is necessary for producing good composite materials otherwise unsuccessful load transfer across nanotube-to-polymer occurs, creating mechanical fractures, with pullout of the nanotubes (see Figure 1. 17).[101,102] In this

case a non-covalent regime is preferred, as loss of mechanical strength occurs for SWCNT upon covalent functionalization as a result of lower structural integrity.[103] However, MWCNT do not have this problem as the inner tube is preserved when covalently functionalized.

One of the common reasons to increase the solubility of the carbon nanotube is to have a high concentration of evenly dispersed carbon nanotubes so that the percolation threshold is reached (i.e. becomes conductive by producing a nanotube pathway between the interfaces).[104,105] Composites of this kind also possess increased mechanical strength from the incorporation of the carbon nanotubes, but literature so far has proven this is at the cost of increasing the viscosity and hence decreasing the processability. Mitchell *et al*[106] found in their work, that upon the addition of un-functionalized carbon nanotubes to PS, the complex viscosity increased, but these composites were produced with pre-formed polymer. In comparison, work performed by Sung *et al*[107] found an increase in viscosity with acid treated carbon nanotubes in poly(methyl methacrylate) (PMMA). This was produced by a suspension of nanotubes in monomer that was initiated by 2,2'-azobis(isobutyronitrile) (AIBN). However, polymer brushes of carbon nanotubes used as a nanofiller has not been published in literature.

HOMOPOLYMERS, COPOLYMERS & THEIR BEHAVIOR

1.9 Introduction

A polymer is a large molecule composed of repeating simple units called monomers. The polymerization processes that form these polymers can be divided into two goups; condensation or step-reaction polymerization, and addition or chain-reaction polymerization.

A newer third alternative also exists, known as living polymerization, which has many different unique properties that separates it from the previously mentioned other forms.[108] This can be further sub-divided into living ionic, living covalent and living free radical mechanisms. [109]

1.10 Polymerization

Step-Reaction Polymerization

In the condensation reaction two or more polyfunctional molecules react to form a larger polyfunctional/polymer molecule, often with the expulsion of a smaller molecule (e.g. water, thus a condensation reaction). The reaction continues until nearly all of one of the reagents has been consumed. An example of a condensation polymerization can be seen in Scheme 1. 5.[108] Both linear polymers can be formed from difunctional monomers, or crosslinked polymers when overall monomer's functionality exceeds two.

$$x \, HO-R-OH \; + \; x \, HOOC-R'-COOH \longrightarrow$$

$$HO{\left[-R-\overset{\overset{\displaystyle O}{\|}}{C}-O-R'-COO-\right]}_x H \; + \; (2x-1)H_2O$$
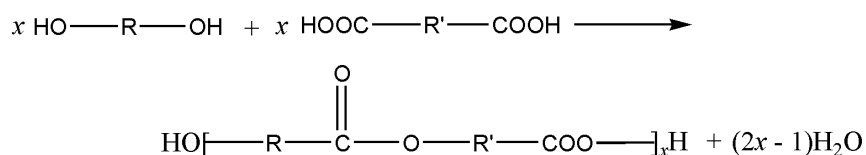
Scheme 1. 5: Step-reaction polymerization of a polyester.[108]

Chain-Reaction Polymerization

This process uses chain or addition reactions, making use of an ion or free radical (i.e. reactive unpaired electron) for its chain carrier. The free radicals are formed from thermal, UV, or other induced degradation of an initiator. A radical initiator is an unstable material that decomposes to form free radicals. These free radicals are then used to open the double bond of a vinyl monomer, which adds to the chain and still leaves the free radical at the end of that chain. This successive monomer addition occurs relatively quick until two free radicals meet in a termination reaction. An example of a chain-reaction polymerization can be seen in Scheme 1. 6.[108]
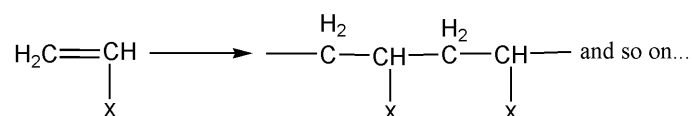
Scheme 1. 6: Chain-reaction polymerization of a polyvinyl.[108]

For comparison, the distinguishing features between step and chain polymerization have been summarized in Table 1. 2.[108]

Chain Polymerization	Step Polymerization
Adds one monomer unit at a time to limited number of growing chains.	Any two functional groups that can react will react and requires no initiator.
Steady decrease in monomer concentration.	Monomer concentration disappears quickly, with $< 1\%$ when $N^* = 10$.
Fast reaction, large molecular weight, with little change for the remainder of the reaction.	Slower reaction, steady increase in molecular weight.
Long reaction times = high yields, but minimal affect to molecular weight.	Long reaction times = high molecular weights and are necessary in order to create them.
Reaction mixture is composed of monomer, polymer, and growing chains.	Each components concentration, at any stage, can be calculated (i.e. predictable).
Chain terminating steps are involved.	No termination step, ends are still reactive.
Initiation and propagation steps are different.	Polymerization rate steadily decreases until all of the monomer has been consumed.

*Table 1. 2: Comparison of chain and step polymerization (*degree of polymerization).[108]*

1.11 Living Polymerization

Firstly defined by Szwarc,[110,111] "living polymerization" is known to be a chain growth process that has no chain breaking reactions such as transfer or termination. To inhibit the chain breaking reactions, catalysts, and sometimes chain-end stabilizers are used instead of only the initiators and monomers. In the "living" system the initiators begin the chain growth process and can be attached to a non-growing chain end (i.e. can be a polymer chain for the synthesis of block copolymers). The catalyst is used for initiation and propagation, while chain-end stabilizers slow down the polymerization rate. It is essential for molecular weight control, that the initiation step be of equal or greater rate than the propagation rate, otherwise the chains initially formed will be longer than the chains formed later on. Furthermore, due to these differences in rates the polymer chains are generally all of similar lengths.[109]

In this model initiation occurs simultaneously with all chain ends growing at the same rate and for this reason Flory noted that the molecular weight is dependent on the amount of initiator to monomer used (i.e. Eq (2).[112]

$$\text{Degree of polymerization (N)} = [\text{monomer}]/[\text{initiator}] \qquad (2)$$

where N denotes the number of monomer units per chain. Since the chain ends grow at a constant rate it also results in a very narrow molecular weight distribution with a Poisson distribution for its polydispersity (D) (i.e. Eq (3)).[109]

$$D = M_w/M_n = 1 + 1/N \geq 1 \qquad (3)$$

$$1.0 \leq D \leq 1.5 \qquad (4)$$

$$200 < M_n < 200,000 \qquad (5)$$

where M_w is the weight average molecular weight, and M_n is the number average molecular weight. This number is used to determine the distribution of molecular

weights; the closer to 1 the more uniform in chain length the polymer is and for living polymerizations this number is in the range of 1 to 1.5.[113,114]

The term living (i.e. "alive") comes from the fact that by controlling the reaction conditions, the polymerization can be stopped at anytime, giving the freedom to change the monomer for block copolymer synthesis, controlled polymer chain length, and changing its end functionalities by selective termination with the appropriate reagents.[109] Using these factors a whole range of polymer architectures can be formed, which are pictured in Figure 1. 18.
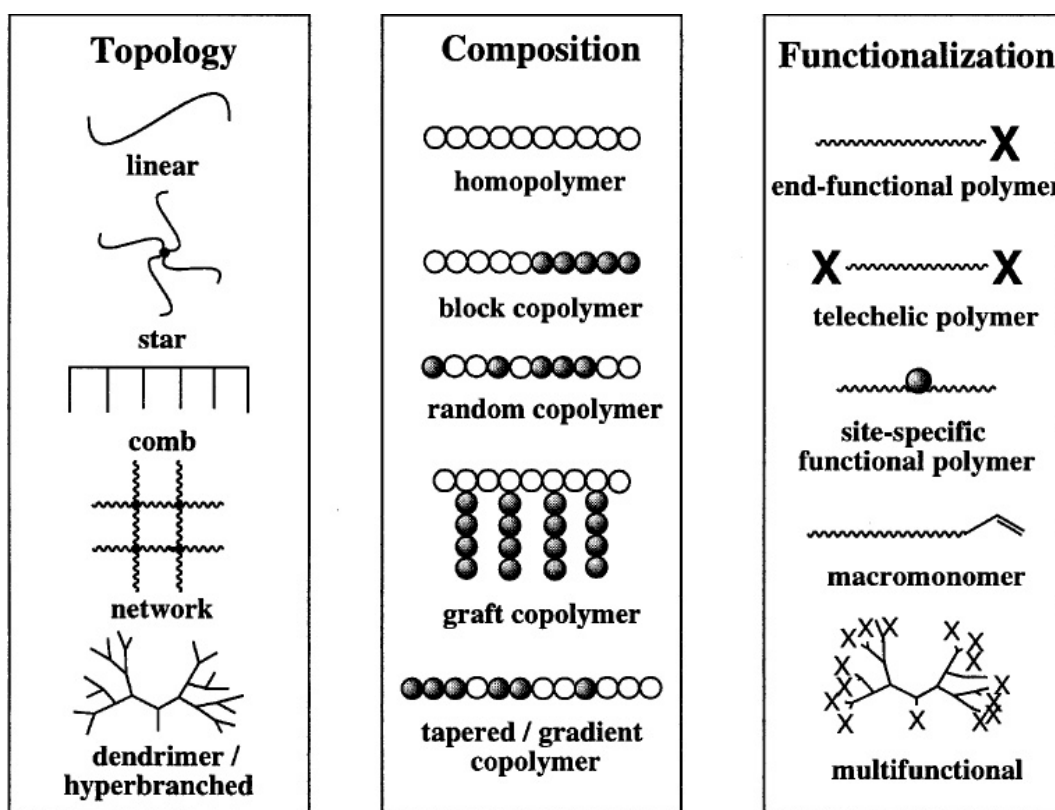
Figure 1. 18: Some of the structural architectures possible using living polymerization.[114]

By drawing a graph of the polymer's molecular weight against conversion, living polymerization can be distinguished from a free radical polymerization (chain) and a condensation polymerization (step). In Figure 1. 19 it is clear to see that in living polymerization the molecular weight is directly proportional to conversion, while for free radical polymerization, high molecular weight polymers are formed rapidly from

the onset of initiation of a polymer chain, and in condensation polymerization, the molecular weight progressively increases as conversion increases, reaching a maximum as conversion approaches 100%.[109]
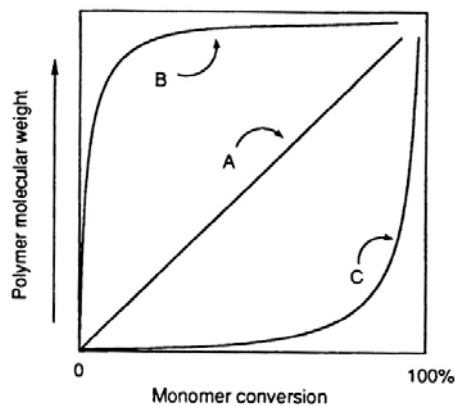
Figure 1. 19: Molecular weight conversion curves for a) living, b) free-radical, and c) condensation polymerizations.[109]

The most important factor about "living" polymerizations is once the monomer is consumed the growing end of the chain is still "alive", and remains "alive" until more monomer is added, allowing further growth of the polymeric chain, or if a terminating agent is introduced.[114]

1.12 Atom Transfer Radical Polymerization (ATRP): Living Polymerization

Atom transfer radical addition (ATRA) is a process by which an atom transfers from an organic halide to a transition-metal complex in order to create the necessary reacting radicals for addition. It is then terminated by back transfer from the transition-metal complex resulting in the final product. A schematic of the reaction mechanism can be seen in Scheme 1. 7. Metal catalysts such as copper (I) halide with 2,2'-bipyridyl,[115,116] or Ni,[117] Pd,[118] Ru,[119] Fe,[120] among others have been used for the one-electron oxidation with removal of the halogen atom from the initiator.[114]

In the ATRA process, if the reactivity of the resulting product possessed a very similar reactivity to the starting initiator-halide cleavage, then the transition-metal

catalyst could then effectively re-start the process of ATRA (i.e. activation-addition-deactivation) again and again and again. This would continue until all of the monomer is consumed, forming the chain growth polymerization process known as ATRP.[114] In this process complexes of Cu(I)[121], Ni(II)[122], Ru(II)/Al(OR)$_3$[123] and Fe[124] have been used. A schematic of this reaction can be seen in Scheme 1. 8.
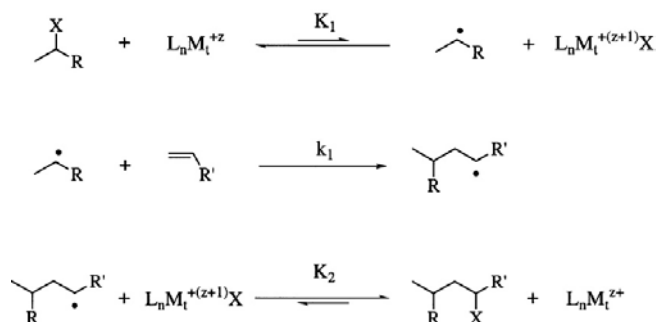
Scheme 1. 7: Reaction mechanism of ATRA.[114]
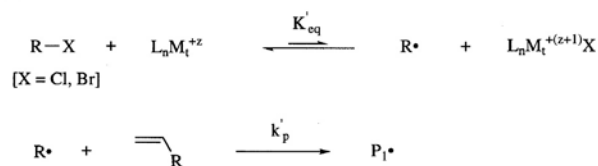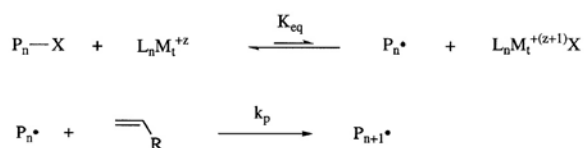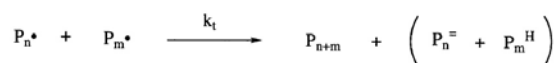
Scheme 1. 8: ATRA extended to ATRP reaction mechanism.[114]

The termination step in Scheme 1. 8 is highly un-probable, as the propagating radicals have a very low concentration. It is low because the radicals are capable of reverting back to their dormant organic-halide species.[114]

<u>Polymers formed by ATRP</u>

Styrene: Metal catalysts used for this monomer are copper,[125] iron,[124] ruthenium,[126] rhenium,[127] or molybdenum,[128] with the majority of the work focused on copper. The polymerization is conducted at $110^{\circ}C$ for bromide-mediated and $130^{\circ}C$ for chloride-mediated polymerization. When the polymerization rate is slowed, such as in dilute conditions, the termination process is observed. This is more distinct for bromide reactions than it is for chloride-mediated reactions.[129] The most common initiator for copper mediated reactions, being 1-phenylethyl halide.[130,131] However others can be used, such as benzylic halides, allylic halides, α-haloesters,[132] polyhalogenated alkanes,[133] and arenesulfonyl chlorides.[134]

Acrylate: Catalysts such as copper,[135] ruthenium,[136] iron,[137] nickel,[138] and rhenium based systems have been reported, with copper being the most efficient (i.e. low polydispersities, well-defined polyacrylates). The polymerization temperature to be used is catalyst specific, but is open to a whole range of temperatures (e.g. poly(methyl acrylate), CuBr/Me6TREN {Me6TREN = tris[2-(dimethylamino)ethyl]amine} is performed at room temperature).[139] A typical initiator for bulk polymerization is performed with an alkyl 2-bromopropionate.
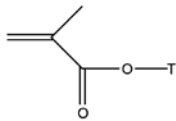
Monomer	T	Ref.
	$-CH_3$	138
	$-(CH_2)_3CH_3$	140
	$-(CH_2)_2N(CH_3)_2$	141
	$-(CH_2)_2OH$	142
	$-(CH_2)_2OSi(CH_3)_3$	143

Table 1. 3: Homopolymers produced by ATRP and their corresponding transiton-metal

catalysts.

Methacrylate: Metal-catalysts such a ruthenium,[136] copper,[144] nickel,[138] iron,[124] palladium,[145] and rhodium[146] have been reported for methyl methacrylate, with such a large list due to the highly reactive carbon-halide bonds formed from methacrylates

(i.e. high equilibrium constants). As a result, methyl methacrylate requires more dilution and lower catalyst concentrations in comparison to styrene and methacrylate to control excessive termination or side reactions from occurring. Temperatures ranging from 70°C to 90°C are typically used for methyl methacrylates.[147] Other methacrylic esters have also been successfully polymerized and have been listed in Table 1. 3.

ATRP is not restricted to styrene, methacrylates, and acrylates. It can also polymerize acrylonitrile, acrylamides, (meth)acrylamides, (meth)acrylic acids, and vinyl pyridines, among others.[147,148]

Forms of ATRP

Method	M/R-X/Cu(I)X/Cu(II)X	L	RA	AIBN
Normal	200/1/1/-	1	-	-
Reverse	200/-/-/1	1	-	0.5
SR & NI	200/1/-/0.2	0.2	-	0.1
AGET	200/1/-/0.2	0.2	0.18	-
ARGET	200/1/-/<0.01	0.1	<0.1	-
ICAR	200/1/-/<0.01	0.01	-	<0.1

Table 1. 4: Various types and conditions of ATRP.[149,150]

There are many forms of ATRP and they have been tabulated in Table 1. 4. Comparing these forms it is easy to see that simultaneous reverse and normal initiation (SR & NI) and activators generated by electron transfer (AGET) are techniques involving the generation of Cu(I) catalyst from the more stable Cu(II) species.[149] Initiators for continuous activator regeneration (ICAR) and activators regenerated by electron transfer (ARGET) are similar to the other two, but differs because the catalyst uses lower reducing agent ratios, they continuously regenerate the Cu(I) catalyst throughout the polymerization and small amounts of catalyst need to be used.[150] As for normal ATRP, the process requires the removal of all oxidants to prevent the Cu(I) catalyst from oxidizing to Cu(II).[151] Furthermore, the techniques

involving AIBN creates additional issues for the generation of block copolymers, as the AIBN can also initiate new chains resulting in a mix of homo and block copolymer when generating the second block.[152]

1.13 Other Living Polymerization Techniques

<u>Nitroxide Mediated Polymerization (NMP)</u>

NMP is a very similar process to ATRP, except in this case the organic-halide dormant species and transition-metal catalyst used is replaced with an organic-nitroxide. Development in this field was pioneered by Moad and Rizzardo[153] with their 2,2,6,6-tetra-methyl- piperidinyl-1-oxy (TEMPO) nitroxide compound, which was further refined by Georges *et al*[154] with work on polystyrene.
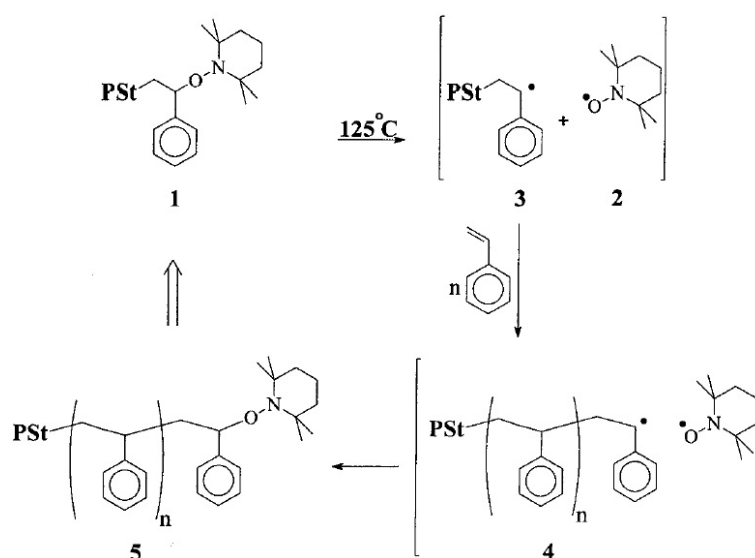
*Scheme 1. 9: PS formed by NMP, using TEMPO(**2**).[156]*
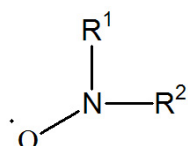
Figure 1. 20: A general nitroxide compound used in NMP.

In this technique the carbon-oxygen bond of the dormant alkoxyamine (**1**) is homolytically unstable whereby thermal fragmentation occurs, typically at $100^{o}C$ or greater, forming a stable nitroxide (**2**) and a polymeric radical (**3**). The polymeric

radical undergoes monomer addition forming a similar polymeric radical, thus increasing polymer molecular weight (**4**). This is followed by the stable nitroxide recombining with the polymeric radical, and resulting in the dormant species that this process initially started with (**5**) (see Scheme 1. 9). This cycle of homolysis-monomer addition- and recombination is repeated again and again until all of the monomer is consumed or a terminating reaction has occurred.[155,156,157] For a more general mechanism of NMP, the nitroxide (**2**) can be replaced with Figure 1. 20.

This process has its limitations and is not as versatile as ATRP and RAFT (see next section) based systems. The choice of nitroxide compound and initiator (i.e. bimolecular/1:2 radical formation, provides poorly defined initial conditions due to unknown radical formation efficiency or unimolecular/1:1 radical formation) greatly affects the possible polymers that can be grown in a "living" fashion, as well as its controllability.[156] Hawker *et al*[158] have comprised a detailed list of nitroxide structures that can be used for living free radical polymerizations and the various block copolymers that can be formed from NMP.

Reversible Addition-Fragmentation Chain-Transfer (RAFT)

This extremely versatile process is very similar in nature to both ATRP and NMP. In this case however, there is no organic-halide or organic-nitroxide, instead there is an organic-sulphur interaction. In this mechanism (see Scheme 1. 10) initiation and radical-radical termination occurs like it does in conventional radical polymerizations, however the propagation of the growing chain uses/adds a thiocarbonylthio compound (**1**). Its addition is followed by fragmentation to form the polymeric thiocarbonylthio compound (**4**) and the new radical R$^\bullet$ (i.e. the reversible chain transfer step). This new radical then undergoes monomer addition forming a new propagating radical (i.e. reinitiation). This results in a rapid equilibrium between the

dormant polymeric thiocarbonylthio compound and the active propagating radical (i.e. chain equilibration). The equilibrium formed gives equal probability for chain growth, and therefore generates a polymer with a narrow polydispersity. Once the monomer has been entirely consumed or the polymerization terminated, most of the polymeric chains retain their thiocarbonylthio end groups.[159,160]
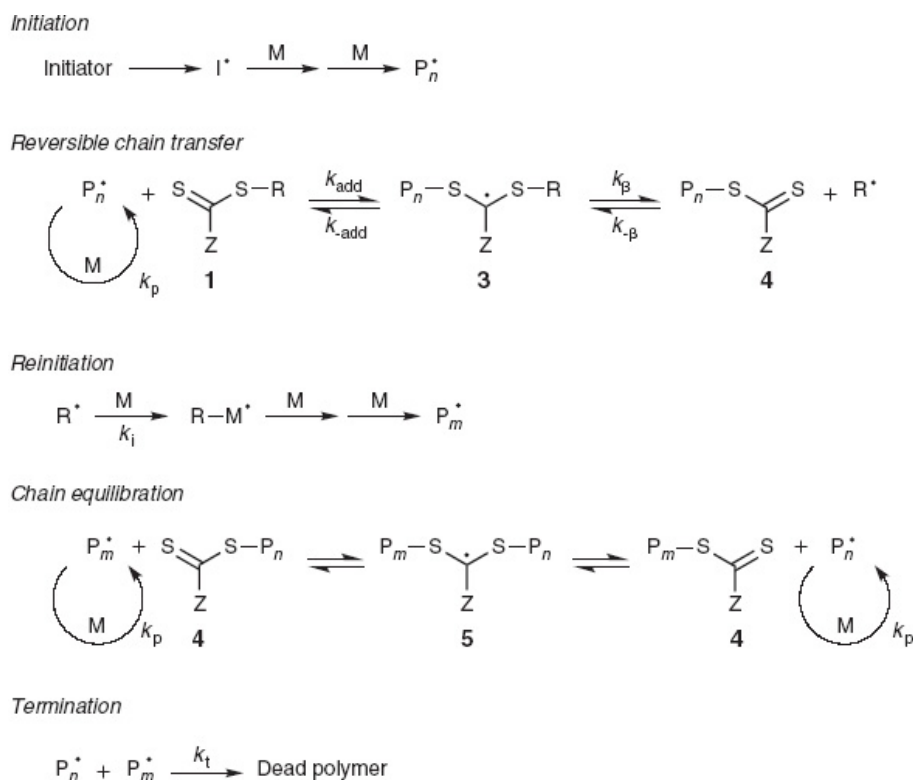
Scheme 1. 10: RAFT polymerization mechanism.
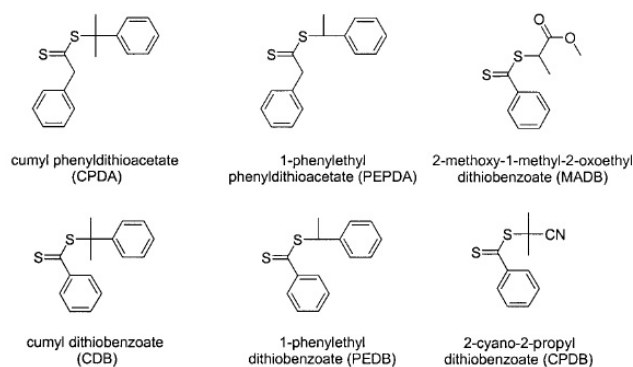
Scheme 1. 11: Some examples of RAFT agents.[160]

The choice of RAFT agent is largely dictated by what polymer is to be formed. An incorrect choice of RAFT agent only leads to difficulties of retardation, and a

decrease in molecular weight control. The defining features of the agent, which also relates to its effectiveness as a RAFT agent, is the functionality of component Z and R of its structure (see Scheme 1. 10).[161] Compounds of dithioesters, trithiocarbonates, xanthates, dithiocarbamates have all been successfully used.[159] A detailed list of polymer to suitable RAFT agent has been reported by Moad *et al.*[159] Examples of some RAFT agents can be seen in Scheme 1. 11.[160]

<u>Living Ionic Polymerization & Living Covalent Polymerization</u>

For living ionic polymerization well defined polymers of low polydispersity are possible, however in order for the generation of such polymers, very strict reaction conditions are required and the polymerization reaction is limited to only a few monomers. Such conditions of the absence of water, sometimes the absence of light, and low reaction temperatures of -80°C to 25°C to inhibit side reactions, among others are necessary, otherwise polydispersity increases, and molecular weight control is lost. Cationic polymerization is more complex than anionic, as the carbonium ion chain ends created by this process readily transfers their β-protons in the creation of a new polymeric chain. As a result the chain, the proton transferred from, dies and molecular weight control is lost with a polydispersity of higher than 1.5 and a molecular weight of less than the theoretical value.[162]

Less popular to the other forms of living polymerization, living covalent polymerization uses a nucleophile or an electrophile to initiate and propagate the chain ends with the monomer.[163] It is a more commercially attractive procedure than living ionic polymerization, due to the group transfer polymerization operating at temperatures (~80°C) that are more desirable by industry.[164,165]

The most popular techniques though are living free radical polymerizations (i.e. ATRP, NMP, RAFT), since it is more practical for industrial manufacturing; it has

less stringent processing conditions by comparison, and can polymerize a very large range of vinyl monomers. In addition ATRP is the more popular technique in comparison to NMP and RAFT for similar reasons to above (i.e. versatility and ease of execution), and is more suitable for block copolymer synthesis.

1.14 Homopolymer Mixtures

A homopolymer is a polymer that consists of only one species of monomer. Upon mixing two or more different homopolymers, a new material is formed with new properties (examples of homopolymer mixtures can be seen in Figure 1. 21). The miscibility/polymer-polymer phase behavior of a binary linear homopolymer mixture depends on four factors; choice of monomers, molecular architecture, composition, and molecular size. At equilibrium the mixture can be in either one or two phases, but upon phase separation the formation of macrophase separation, and microphase segregation occurs. This is due to interfacial tension favoring a reduction in surface area. However, the formation of defined phase separation is largely dependent on the polymers mobility (i.e. viscosity).[166] Branching for example, disrupts the polymers capability to move, resulting in increased viscosity.[167]
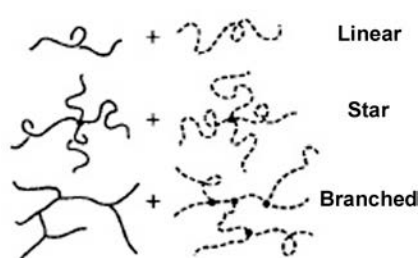
Figure 1. 21: Homopolymer mixtures (line and dotted represent two different polymers).[166]

Using mean field theory, which neglects spatial fluctuations in composition, the theoretical phase diagram can be calculated (see Figure 1. 22). The diagram represents the phase behavior of a symmetric (i.e. N of polymer A = N of polymer B)

binary linear homopolymer mixture at constant temperature and pressure.[166] It depends on three factors; degree of polymerization (N), the Flory-Huggins segment-segment interaction parameter (χ), and composition/volume fraction (Φ). The parameter χ derives from the choice of monomers, as it is used to approximate the sign and magnitude of the energy of mixing. In its simplest form χ (see Eq. (6)) is dependent on temperature, and composition; coefficients α and β determined experimentally, representing enthalpy and excess entropy.[166,168]

$$\chi = \alpha T^{-1} + \beta \qquad (6)$$
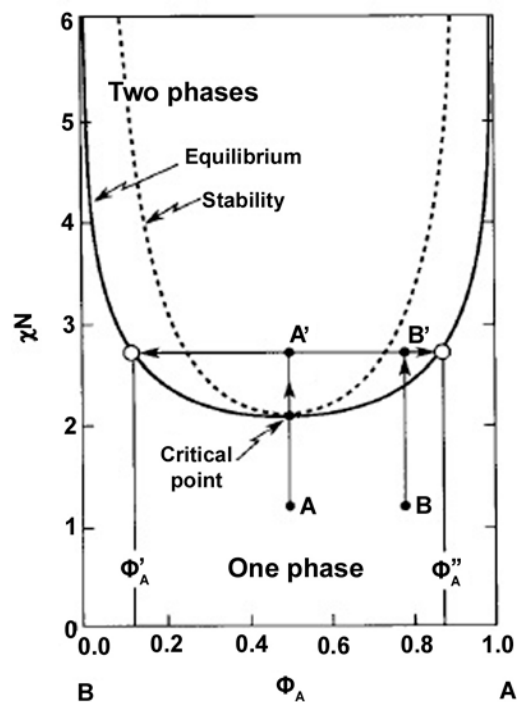
Figure 1. 22: Theoretical phase behavior of a symmetric binary mixture of polymer A and B, predicted by mean field theory, where Φ_A is the volume fraction of polymer A.[166]

In the phase diagram (see Figure 1. 22), the solid curve represents the points of equilibrium with everything outside of it forming one phase and everything inside the curve forming two phases. Between the solid curve and dashed line, thermodynamically metastable mixtures are formed, while inside the dashed curve, thermodynamically unstable mixtures are formed. The critical point (i.e. where the

two curves meet) for a symmetric mixture occurs for when $(\chi N)_c = 2$ and $\Phi_c = 0.5$. The critical point temperature (T_c) however, can be varied by altering N, and the critical composition can be varied by adjusting N_A and N_B (see Eq. (7) and Eq. (8)). As a result, the phase diagram can be adjusted to prevent any interfering factors from occurring, such as thermal decomposition temperatures.[166]

$$\Phi_c = N_A^{1/2}/(N_A^{1/2} + N_B^{1/2}) \tag{7}$$

$$\chi_c = (N_A^{1/2} + N_B^{1/2})^2/(2N_A N_B) \tag{8}$$
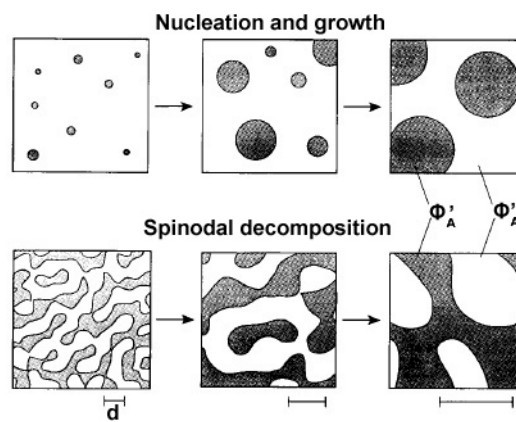
Figure 1. 23: Nucleation and growth (B → B' of Figure 1. 22) and spinodal decomposition (A→ A' of Figure 1. 22) as time progresses.[166]

Nucleation[169] occurs when small droplets, composed of the minor phase, are formed in a homogeneous mixture that has been thrusted into the metastable region (B → B'). Over time these droplets grow from the saturated mixture and when an equilibrium is established, Ostwald ripening continues the growth (i.e. consumption of smaller droplets to the larger droplets).[166] Spinodal decomposition[170] on the other hand (A → A'), although similar in formation, spontaneously forms in an uncontrolled fashion, generating a disordered bicontinous two-phase structure. As time proceeds, the interfacial tension forces the surface area to reduce by increasing "d", the size of the spinodal structure.[166] See Figure 1. 23 for a visual representation of the two phase growth methods.

1.15 Copolymers

Copolymers are composed of at least two different polymeric monomers within the one chain. Many structural architectures can result from this conformation such as diblock, triblock, and starblock (Figure 1. 18 and Figure 1. 24),[171] but the main focus of this work is diblock-copolymers.
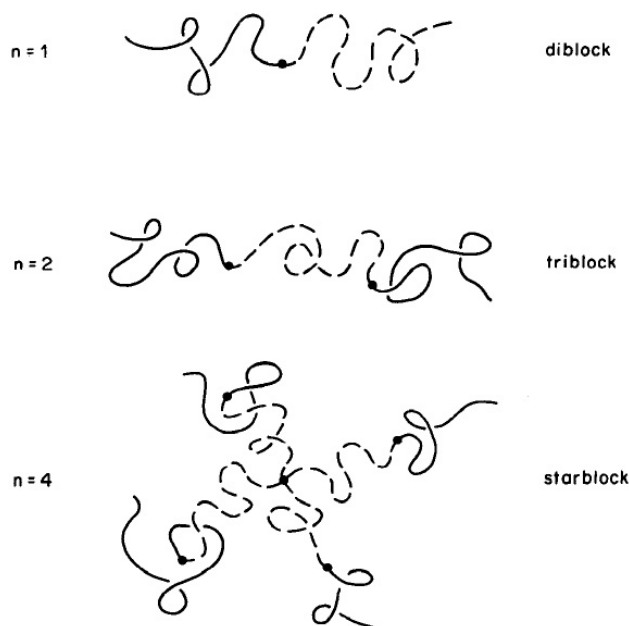
Figure 1. 24: (A-B)$_n$ block copolymer structural architectures (solid and dashed line represent two different polymers).[171]

Statistical Copolymers

Statistical copolymers are either random or alternating in nature, and in order to form such polymers both monomers are mixed together and allowed to polymerize at the same time. The nature of the polymer to be random or alternating can be determined by the copolymer equation. Using Scheme 1. 12 and a steady-state treatment the copolymer equation can be derived, Eq. (9), where [M$_1$] and [M$_2$] are the initial concentrations of the two different monomers. The reactivity ratios, Eq. (10), demonstrates the monomers tendencies to either self propagate (r > 1) or copolymerize (r < 1). For the "ideal" polymerization $r_1 r_2 = 1$, which means the

propagating chain does not have a preference to add to either monomer. This creates a random copolymer (e.g. AAABBABBBBAAAA etc…). For an alternating copolymer (e.g. ABABABABABA etc…) $r_1 = r_2 = 0$ and therefore the propagating chain prefers to react with the other monomer. However when $r_1 = r_2 \rightarrow \infty$, there is no preference to copolymerize and two homopolymers are formed instead (e.g. AAAAAA etc… and BBBBBB etc…).[113]

$$M_n^{\cdot} + M_m \xrightarrow{\ k_{nm}\ } M_m^{\cdot}$$
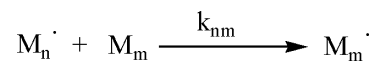
Scheme 1. 12: Monomer addition (n and m represent two different monomers), self propagation occurs when n = m, and cross-propagation occurs when n ≠ m.[113]

$$d[M_1]/d[M_2] = [M_1](r_1[M_1] + [M_2])/([M_2]([M_1] + r_2[M_2])) \qquad (9)$$

$$\text{where } r_1 = k_{11}/k_{12} \text{ and } r_2 = k_{22}/k_{21} \qquad (10)$$

Chain Extension/Block Copolymers
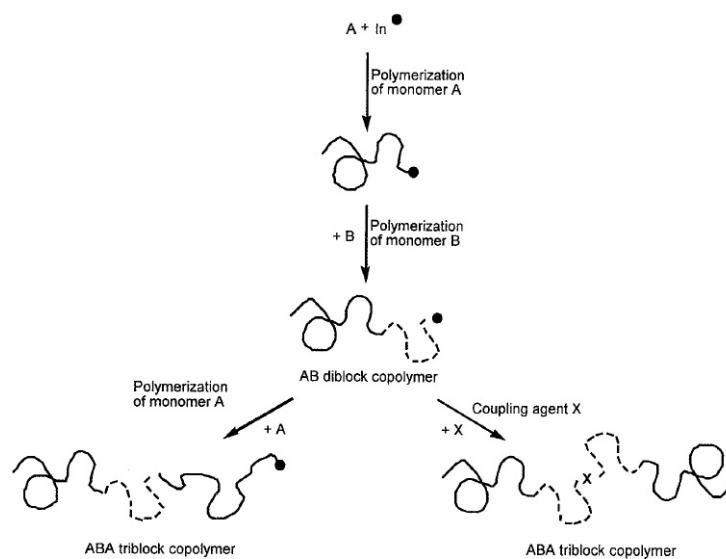
Scheme 1. 13: Block copolymer synthesis, formed from a controlled/living polymerization to maintain a low polydispersity.[172]

In this technique the polymerization of a homopolymer is carried out, however the chain's end needs to be still "alive", such as in living polymerizations. This is due to the fact that a new/different polymer chain can be grown from that end (or attached)

and thus a block copolymer is formed (see Scheme 1. 13).[172] Morphologies such as AB diblock, cyclic AB diblock, ABC triblock, mixed arm star block, ABA triblock, $(AB)_n$ star block, and $(AB)_n$ multiblock are possible.[173] As a result of this versatility and their hybrid properties, many applications are open to block copolymers.

Halogen Exchange

Block copolymer polymerization requires efficient initiation on the first and second block so that a low polydispersity polymer is formed. After the first block has been polymerized, it is used in a subsequent polymerization of a different monomer as a macroinitiator, but now the initiator has chemically changed too and in turn its efficiency. It has been found for ATRP the equilibrium constants are of the following order - acrylonitrile > methacrylates > styrene ~ acrylates > acrylamides > > vinyl chloride > vinyl acetate. This order must be obeyed to produce a well initiated polymerization and hence growth from the macroinitiator (i.e. PMMA must be extended by PS and not the reverse). In addition, this does not only apply to block copolymers, but to polymers of many blocks (i.e. ABC, BAB, ABCD, etc…).[150]

Researchers have found that to alter the above order, so that a less reactive monomer could be extended by a more reactive monomer in ATRP, halogen exchange could be used.[174,175] This method involves using an alkyl bromide macroinitiator and using a CuCl-based catalyst complex to polymerize the more reactive monomer. The system is now initiated by R-Br, propagated by the monomer and then deactivated, forming $R-P_n-Cl$ dormant polymer chains. The halogen exchange works because the K_{ATRP} of R-Cl species is smaller to that of an R-Br species (i.e. $K_{ATRP}^{initiator}k_i > K_{ATRP}^{monomer}k_p$), hence initiation is favored over propagation. This is because the R-Br species are firstly propagated to either R-P-Cl or less probable, as CuCl is in a large excess to R-Br species, R-P-Br. Afterwards the

remaining R-Br (including R-P-Br) species is more reactive than the R-P-Cl, therefore the R-Br species propagates preferentially and eventually all R-Br is consumed/initiated to propagate polymer chains of R-P$_n$-Cl (see Figure 1. 25).[176]
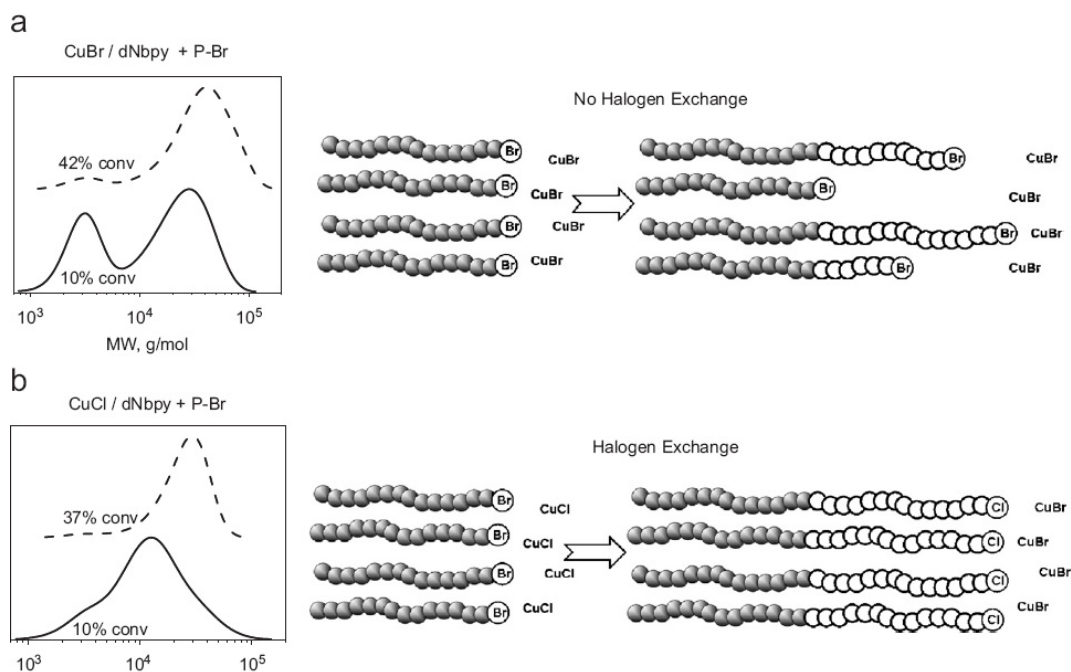
Figure 1. 25: Tsarevsky et al[177] GPC plots of PS-Br extended with MMA and their graphical representation of the polymer chains. a) no halogen exchange and b) with halogen exchange, which demonstrates efficient initiation when using the halogen exchange technique.

1.16 Phases & Transitions of Di-Block Copolymers

Similar to the homopolymers mean field theory calculation, the self consistent field theory can predict the phase diagram of a diblock copolymer. In this system however the two polymers cannot phase separate into its constituents as they are covalently joined. Instead local segregation occurs by using block-block joints at the interfaces and stretching the polymeric chains to maintain a uniform density.[171166]

Once again the product of χN determines the state of segregation, however in comparison to the homopolymers ordered phases, they are quite unique. When the product $\chi N \ll 10$ the system exists as a spatially homogeneous state, however

increasing either χ or N results in the development of local composition fluctuations that is proportional to the polymers radius-of-gyration (i.e. $R_g^2 = R_{g,A}^2 + R_{g,B}^2$).[178,179] However, if the product $\chi N \approx 10$ then at this point the curved and disordered system changes to an ordered periodic structure and is known as the order-disorder transition (ODT). Increasing the product χN further results in sharper micro-domain boundaries and when $\chi N \gg 10$ narrow interfaces with well defined/separated compositions exist (see Figure 1. 26).[173,180] This ordering occurs due to a dominancy in the systems entropic factors being overcome with energetic factors, and when $\chi N \approx 10$ these factors are balanced creating the ODT.[166]
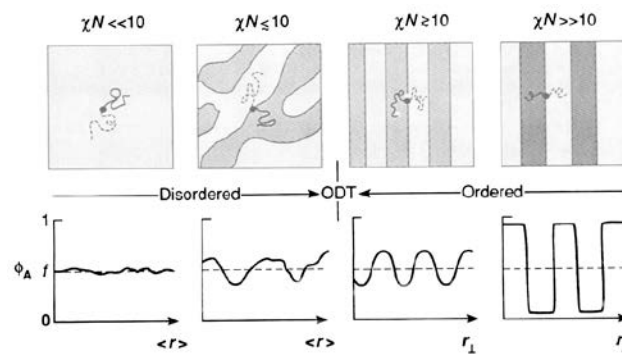
Figure 1. 26: The variation in architectural structure as the product χN increases. The graphs of Φ vs r demonstrates the strength of segregation as the product χN increases.[166]

The above discussion however, only relates to $f = 0.5$ (i.e. f is the volume fraction, and therefore 0.5 is equal portions of polymer A and B). If f is varied, different morphologies occur, as it affects the shape and packing symmetry of the ordered microstructure. Seven ordered phases exist; gyroid, hexagonal-packed cylinders, and body-centered cubic, with all of these in a positive or negative regime, with the seventh being lamellae. These phases have been predicted by the self-consistent mean field theory (SCFT) (see Figure 1. 27 and example Figure 1. 28), which can also predict domain spacing (i.e. ~ 5 to 500nm).[181,182]
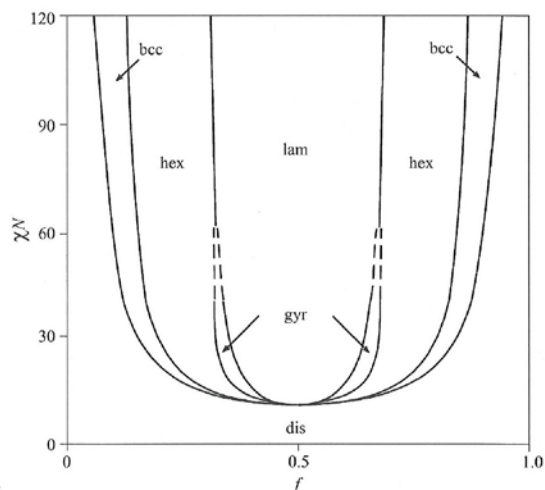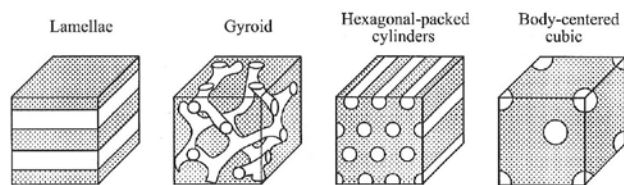
Figure 1. 27: Phase diagram of a diblock copolymer predicted by the SCFT (Note: bcc = body-centered cubic, hex = hexagonal, gyr = gyroid, lam = lamellae, dis = disordered), and the morphologies it can create.
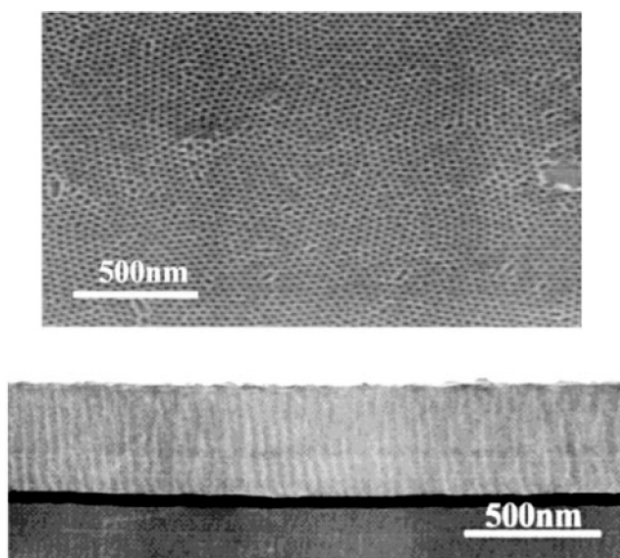
Figure 1. 28: An example of a hexagonal phase. SEM, birds-eye (top), and side-view (bottom) of a polystyrene-block-poly(methyl methacrylate) copolymer, aligned normal to a gold substrate.[183]

1.17 Polymer Melts

Polymers exist in two different geometrical arrangements, one being "configurations" and the other "conformations." Configuration polymers have an arrangement that is fixed by the chemical bonding in the polymer chain and cannot be altered unless chemical bonds are broken and reformed. These polymers exhibit properties normally associated with typical rubbers, however with increased rigidity, by crosslinking, the polymer becomes thermosetting (i.e. a hard rubber). Conformation polymers have arrangements that form from a linear arrangement of single bonds with secondary bonds, such as the interaction between polar groups. These secondary bonds are capable of breaking and re-forming as the temperature is raised or lowered, giving a limpness and flexibility to the polymer.[108]

These polymers can have a glass transition temperature (T_g) and/or a crystallization temperature (T_c) (e.g. poly(ethylene terephthalate) exhibits both).[184] A T_g can occur for a polymer, such as PS,[185] where lowering the temperature of a polymer melt (e.g. PS) causes a change in the properties to resemble ordinary inorganic glass (i.e. hardness, stiffness, brittleness, and transparency). This is due to a lack of thermal energy that is required to move segments of a polymer chain with respect to another chain. The T_c can occur for polymers, such as polyamides,[186] that have a geometrically regular structure or has some level of ordered structure within the polymer's backbone. Crystalline polymers are generally strong, tough, stiff and more resistant to solvents and chemicals than non-crystalline polymers. These polymers are also usually opaque due to the presence of crystalline regions with sizes that are in the order of the wavelength of light. Such properties can be improved by increasing the intermolecular forces and using stiff polymer chains (i.e. engineering polymers). It can also be improved by processing the polymers orientation or drawing

the polymer into a fiber. Furthermore, a diagram of these states of bulk polymer and their possible transitions can be seen in Figure 1. 29.[108]
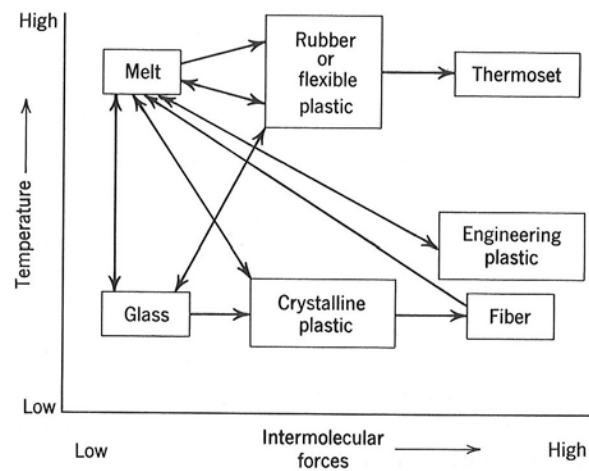
Figure 1. 29: The states of bulk polymer, where the arrows indicates the transitions from one state to another that are possible.

In this work all polymers used are conformation polymers and will exhibit a T_g. This is vital as a polymer melt is extremely viscous and is important in forming the phases discussed in the previous section. The rigidness of a polymer melt, once cooled, is required in order to maintain the phase segregation for long periods of time, as the formation of strong inter-chain forces develop during cooling.[166]

Alignment Techniques

The domains generated by phase segregation are defined by the molecular weight of the copolymer and the strength of segregation. However, in order to develop any real application, the orientation and lateral ordering must be controlled, but is largely only a concern for the lamellae and hexagonal-packed cylinder phases as the other phases are highly symmetrical.[187] To achieve the orientation, previous research has shown the use of external fields are very affective, such as electric fields,[188,189] graphoepitaxy,[190] shear,[191] crystallization,[192] temperature gradients,[193] chemically patterned substrates,[194,195] controlled interfacial interactions,[196] and droplet pinning.[197]

Solvent evaporation is also another technique that is quite simple and easy to implement. Kim *et al*[187] have reported for the hexagonal phase that by controlling the rate of solvent evaporation or annealing, the ordering of a copolymer matrix essentially grows from the surface to the entire film (see Figure 1. 30). The solvent gives an additional benefit, as it increases the mobility of the copolymer, resulting in the removal of irregularities in the phase ordering. In addition, by swelling the copolymer in a solvent vapor, the polymer T_g is effectively lowered and the material becomes flexible once again. Upon the second solvent removal, a significant improvement was noted. What is experienced overall is a disordered film that upon solvent evaporation forms a highly ordered hexagonal-packed cylindrical phase, oriented normal to the surface.
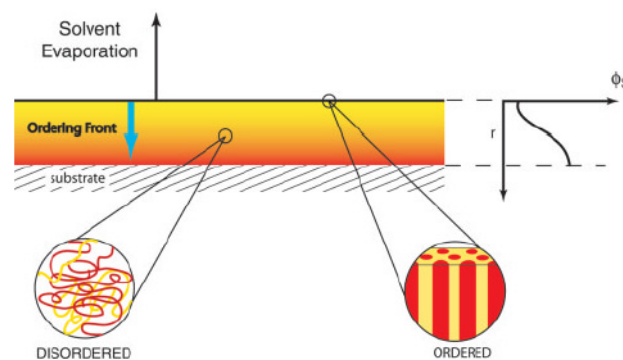
Figure 1. 30: A model of the surface induced growing order of a thin block copolymer film. (right) is the solvent gradient that helps demonstrate the concept that the concentration of solvent at the surface is low/ordered, and as the depth r increases so does the solvent concentration and so does the disorder. As the solvent evaporates from the interior, the ordered front propagates the order through the film (Note: Φ_s = solvent concentration).[187]

The ordering observed also experienced a time dependency, where the number of defects decreased with longer solvent annealing times. An exponential decay type

relationship was determined, meaning the majority of the defects were removed within the first couple of hours, with only a few defects remaining after 48 hours.

In order to achieve the normal orientation on a substrate previous research by Xu *et al*[189] found that a neutral surface was required, otherwise one of the blocks is preferential to the surface and a parallel orientation would result. Mansky *et al*[198] found that a random/statistical copolymer tethered to the surface could create a neutral surface and hence formed the normal orientation. In the case of a PS and PMMA block copolymer volume fractions of 0.58/0.42 is required for the normal alignment.[199]

1.18 Applications of Block Copolymers

Many applications for block copolymers exist, simply due to the structural and molecular weight diversity the copolymers can provide.

One such application was explored by Lu *et al*,[200,201] who developed a way to produce a regular array of Fe catalyst particles for CVD carbon nanotube growth using, either the body-centered cubic or hexagonal copolymer phases. They used a block copolymer with one of the blocks composing of a polyferrocenylsilane, which degrades upon annealing to form nano-iron clusters. These clusters were then utilized to grow SWCNT, which can be seen in Figure 1. 31.

Another use saw the removal of one of the blocks in the hexagonal phase to produce a nanoporous material or cylindrical pillars. This was achieved through chemical etching,[202,203] UV-cleavage,[204,205] and thermal cleavage.[204] Furthermore, the research has even extended to cross-linking the non-degradable block of the diblock system. Usually PS, a benzocyclobutene group can be used to crosslink the PS domain upon thermal activation to the ring-opening reaction. This cross-linking resulted in higher dimension stability and after the removal of the other block, the

stability remained for both solvent and thermal treatments.[205] Many other applications

exist and have been represented pictorially in Figure 1. 32.
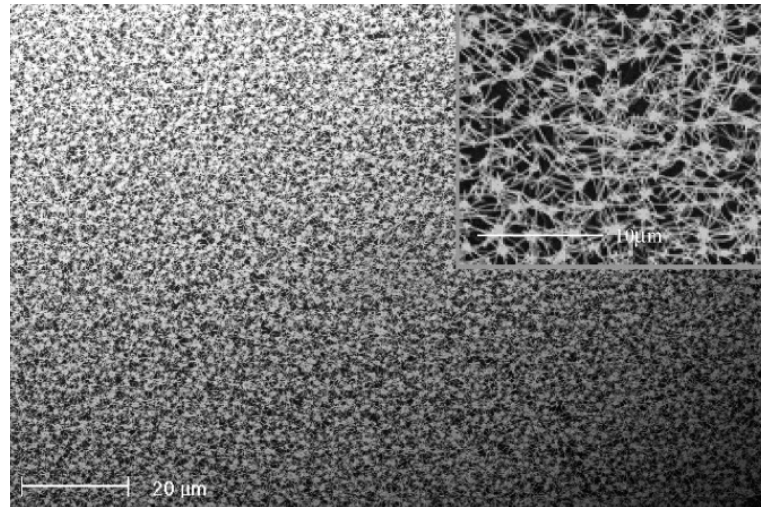
Figure 1. 31: SEM images of the carbon nanotube mat produced by the iron clusters from

a block copolymer. As can be seen in the above image the nanotubes are localized in

certain spots (i.e. where the iron clusters are and growth occurred).[200]
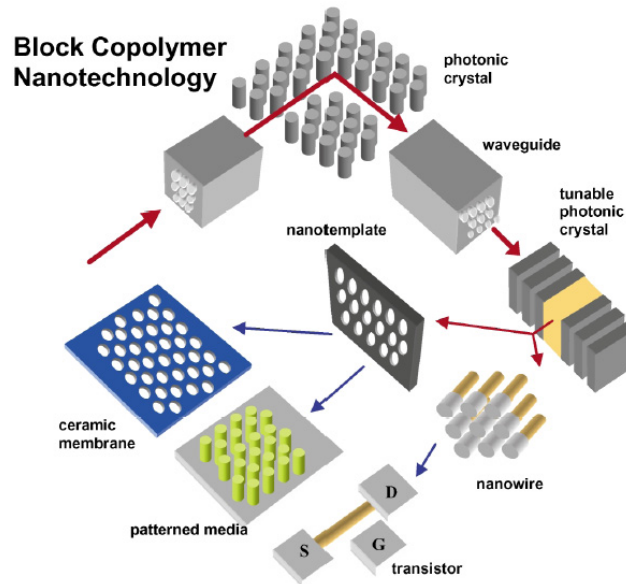
Figure 1. 32: The various applications of block copolymers in the nanotechnology

field.[206]

RESEARCH AIMS & SCOPE

The aim of the work in this thesis is to produce nanocomposite materials of macro and nano size dimensions using MWCNT and polymers. Many issues arise in producing such materials such as the nanotubes tendency to aggregate into bundles, creating a non-homogenous mixture, thus reducing the transference of properties from the incorporation of carbon nanotubes.[207]

In order to prevent the nanotube aggregation that occurs for un-functionalized carbon nanotubes, surface modification is required. The best form of modification is to alter the nanotubes surface to resemble its new surroundings and in this case that is a polymeric matrix. This infers that the nanotubes will need to be purified and functionalized with polymeric chains to produce a high degree of entanglement with its surroundings. To do this literature has shown that CVD MWCNT have less impurities than the other methods and will require less extensive treatment for purification. Furthermore, simultaneous functionalization of the carbon nanotube's walls with carboxylic acids will also occur.

Having produced oxygenated carbon nanotubes the carboxylic acids can then be used as a means to attach polymeric chains. "Grafting from" and "grafting to" are two different options, but attaching a pre-formed polymer has its own issues such as increased difficulty in purification, attachment by other forces, and low grafting density, which therefore leads to the "grafting from" technique.[80] Techniques such as ATRP,[208,209] NMP,[210,211] and RAFT[212] have been utilized in the past for their ease of production, low polydispersity, the ability to re-initiate and controllability of molecular weight. However, these techniques do possess their own complications and hence ARGET ATRP provides a novel opportunity to enact such grafting reactions due to the less stringent conditions and its ability to not initiate new polymer chains

(i.e. new polymer chains can be initiated in reverse, SR & NI, and ICAR because it uses AIBN).[213] An ARGET ATRP initiator will need to be attached to the carbon nanotube via esterification of the carboxylic acids and subsequently polymerized. Polymers of PS, PMMA, and poly(2-hydroxyethyl methacrylate) (PHEMA) are to be explored for the compatibalization of carbon nanotubes with their bulk polymer counterpart (i.e. using the polymer brush carbon nanotube as a filler).

In using the polymer brush carbon nanotube as a filler in a composite, previous research has shown that these composites can be formed by either mixing with pre-formed polymer[214] or from a polymerized solution of monomer.[215,216,217] A polymerized solution of monomer was chosen as the polymer brush carbon nanotubes will disperse more easily in a solution phase delivery (i.e. sonication and more soluble) and will create better entanglement as the polymer chains are more likely to be outstretched from the nanotube. Furthermore, increased solubility is vital to obtain enhanced properties because if the nanotubes settle out by gravity a non-homogeneous mixture will form with a varying concentration of nanotubes across the two interfaces. Li *et al*[218] found this in their work of a nanotube-ester dispersed in a polysulfone matrix, but the complications with their work came from the fact that the nanotube-ester did not provide a significant improvement of solubility in the monomer; the functionalization did not possess a high level of architectural similarity to the matrix environment. However, using the polymer brush carbon nanotubes in their counterpart bulk matrix monomer should provide a higher level of architectural similarity and hence will not settle out by gravity.

This is to be the macro size work, but heading to the nano size work will possess its own unique chemistry. The idea is to produce a polymeric thin film that incorporates the carbon nanotubes in an effort to explore the nanotubes alignment in a

di-block copolymer melt. The hexagonally-packed cylindrical phase was chosen as it was thought to be a suitably supportive network due to the structural similarities to a carbon nanotube. Having produced the polymer brushes in the macro sized work, these polymer brushes will be used in the nano size work as they will have an affinity for a particular phase (i.e. lowering the entropic factors). Similar work by Chiu *et al*[219] used poly(styrene-b-2 vinyl pyridine) as a means to demonstrate the position of polymer brush gold nanoparticles could be controlled in a di-block copolymer melt. However, nanoparticles are zero dimensional and carbon nanotubes are one dimensional. The massive size of the carbon nanotube could have issues in the positioning as greater forces could be required.

Significance

The work detailed in this thesis reports never before published research of polymer brush carbon nanotubes used as a nanofiller in polymer composites. Literature has proven that use of carbon nanotubes as a filler in polymer composites can improve the physical and electrical properties of the matrix. However, due to the carbon nanotubes limit of dispersion difficulties in creating an even dispersion can arise in their manufacture. Furthermore, a high strength interaction is necessary for producing good composite materials otherwise unsuccessful load transfer across nanotube-to-polymer occurs, creating mechanical fractures and the pullout of the nanotubes.[101,102] Using the polymer brushes as a means to aid in the nanotubes dispersion will also help in the load transfer as the polymer brushes will enhance the entanglement with the matrix.

An extensive search on the chemical synthesis of polymer brush carbon nanotubes finds polymerization techniques using "graft to", and "graft from" by living and non-living means. For the first time polymer brushes produced by ARGET ATRP will be

formed, which is a technique that is non-air sensitive, and only requires parts per million (ppm) catalyst concentrations, thus is more industry ready than the alternative techniques. Materials of this nature have been used for the production of amphiphilic copolymer brushes,[220] increasing the carbon nanotubes dispersability in common solvents,[221,222] and as a vehicle for drug delivery.[223] Producing them by using ARGET ATRP will make polymer brush carbon nanotubes more easily accessible for a commercial application. In addition, PHEMA was researched and is known as a hydrogel that was invented by Drahoslav Lim for use in soft contact lenses.[224] Using high concentrations of carbon nanotubes in a composite will make the polymer opaque and inadequate for a contact lens application. However, other uses have been found since its invention in the medical field such as artificial skin[225] or gene delivery.[226] The use of polymer brush carbon nanotubes may find similar uses in the medical field as the carbon nanotubes make the polymer conductive and has an increased glass transition temperature. Furthermore, Kumar *et al*[227] have published their findings on producing PHEMA polymer brush carbon nanotubes, which has been enhanced, in the thesis work, by developing a one-pot reaction.
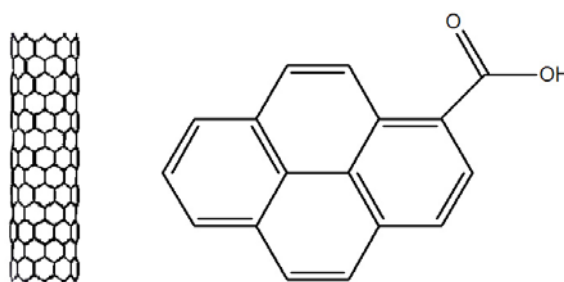
Figure 1. 33: (left) a carbon nanotube, and (right) 1-pyrenecarboxylic acid, demonstrating the architectural similarities.

To model the carbon nanotube research, 1-pyrenecarboxylic acid has been used due to the similarities in architectural structure (see Figure 1. 33). The work covered explores its use in functionalizing with a tertiary bromide for ARGET ATRP, and

further used as a nanofiller for a polymer matrix. Furthermore, the work has proven to enhance the properties of the matrix without a concern for the limit of dispersion, and has never been reported in literature as used this way.

Other significant results of this work found that ARGET ATRP is a poor technique for producing block copolymers when using a less reactive monomer as a macroinitiator. Another result was a better understanding of the necessary forces required to orient the carbon nanotube normal to the surface.

Characterization Techniques

Gel permeation chromatography (GPC), using a linear polystyrene standard and tetrahydrofuran (THF) as the moving phase, was used to determine the molecular weights and the polydispersity of the polymer samples. Samples were prepared by dissolving 5mg in 1mL of anhydrous THF (Aldrich), which was subsequently filtered using a PTFE membrane. These samples were recorded with the assistance of Dr Suresh Valiyaveettil at the National University of Singapore (NUS).

The living kinetic plots were determined by terminating the polymerization at regular intervals and performing gravimetric analysis on the resultant polymer. From the weights the $\ln([M]_o/[M])$ and conversion values could be determined and plotted.

Fourier transform infrared spectroscopy (FT-IR) was recorded using a Thermo Nicolet Nexus 870 from the Thermo electron corporation, and was used to verify and determine chemical alterations in the samples. The smart orbit attenuated total reflectance (ATR) accessory was used in absorbance mode (4000-400cm^{-1}, resolution 4cm^{-1}, and 128 scans) with the DTGS TEC detector and air as the background, but due to the carbon nanotubes having a high level of absorbance, the carbon nanotube sample spectra were recorded using a dilute concentration in a transmission disc. The discs were prepared using high purity, dried potassium bromide that was

mechanically pressed under vacuum. Data analysis was carried out using the Omnic 7.1 software to subtract the background from the sample spectra and to analyze the subsequent IR spectra.

Thermogravimetric analysis (TGA) was performed on a TGA 2950 thermogravimetric analyzer from TA instruments, using a conventional mode heating at 10^oC/min in air (i.e. flow of 50mL/min) from room temperature up to 1000^oC, using platinum pans. This technique was used to determine degradation temperatures as well as the polymer content by the weight loss concentration of the polymer degradation step. The Curie-Point method with nickel was used to perform the temperature calibration.

Differential scanning calorimetry (DSC) was carried out on a TA-DSC 2920, equipped with liquid nitrogen cooling accessory. Approximately 5mg of sample was weighed into a aluminum hermatic DSC pan and lid. First scans were heated from as low as 0^oC to as high as 200^oC at 10^oC/min in a 50mL/min air atmosphere. Second scans were recorded under the same conditions but at 20^oC/min. This technique was used to determine the T_g of the polymeric samples, and in some samples, the presence of an exotherm, which indicated a post-curing reaction. The instrument was calibrated using a sample of pure indium.

High resolution transmission electron microscopy (HRTEM) was performed with the assistance of Dr Martin Saunders at the Australian Microscopy & Microanalysis Research Facility at the Centre for Microscopy, Characterization & Analysis, at the University of Western Australia (UWA). Images were recorded on a Jeol 2100 at 120kV with a Gatan Orius camera, and an elemental mapping attachment. Samples were prepared from ethanol solution evaporations on carbon coated copper mesh discs. The microscope was used to record images of the polymer brushes that were

present on the carbon nanotubes as well as determining if localized regions of copper and tin were present in the sample.

Energy-dispersive x-ray spectra (EDX) were measured on a Philips TEM CM200 with an EDAX DX4i energy dispersive x-ray spectrometer at Adelaide Microscopy, Adelaide University, and was used to determine the atomic percentage of copper and tin in the living polymer brush samples.

Transmission electron microscopy (TEM) was performed at Flinders Microscopy & Image Analysis Facility with the aid of Kerry Gascoigne. Images were recorded using a Jeol 1200ex, with a Soft Imaging System mega View camera attached. The samples were prepared by microtome, and in the case of the block copolymer melt, stained with iodine.

Nuclear magnetic resonance (NMR) was performed on a Bruker 600MH$_z$ Ultrashield, using the Bruker TOPSPIN 2.1 software. Samples were prepared in deuterated chloroform and used for the chemical structure verification of the synthesized compounds.

The degree of tertiary bromide attachment was determined by elemental analysis, at the Campbell Micro-analytical Laboratory, University of Otago.

Raman spectroscopy was performed with the assistance of Associate Professor Peter Fredericks at the Queensland University of Technology (QUT). Spectra were collected on a Reinshaw Model 1000 using He-Ne excitation at 632.8nm. The spectra was used to verify the covalent attachment of polymer brushes to carbon nanotubes and in the case of PS, chemical verification.

The polymer brush carbon nanotubes electrical conductance was determined using the apparatus designed by Dr Gerard Seytre of the Laboratory of

Macromolecular Materials – Institut National des Sciences Appliquees de Lyon (LMM-INSA-Lyon) in France.

Contact angle measurements were carried out using a sessile drop apparatus, using both Milli Q water and diiodomethane as the liquids. The angles recorded, were averaged over ten samples and the calculations for surface energies was determined using the Windrop++ program.

Dynamic mechanical analysis (DMA) was performed on a TA DMA Q800 series instrument, with a single cantilever attachment and fastened at 10in-lb. Samples (13mm wide, 36mm long and averaging 7mm thick) were recorded at 2°C/min starting from as low as 0°C and recording as high as 150°C.

The rheology of the polymer composites was determined using TA instruments Advanced Rheometer 2000, with an environmental temperature control (ETC) attachment, using the 25mm diameter parallel plate. Nitrogen gas was used and flowed at 10L/min. Conditions of 190°C (100Pa), 280°C (100Pa), and 200°C (1000Pa) (i.e. temperature and oscillation stress) was used for PS, PMMA, and PHEMA, respectively.

Optical Rheology was performed at Cambridge University, England with the assistance of Dr Anson Ma. The apparatus models a rheometer, but has a microscope and JVC camera attached, which can view the carbon nanotube filler during measurements. A photograph of this apparatus can be seen in Figure 1. 34.

Ellipsometry was performed using a Beaglehole imaging ellipsometer, which used a 600nm light filter and Dalsa-CCD image capture technology. Measurements were performed to determine the layer thicknesses of the thin film samples.

Atomic force microscopy (AFM) was performed using a Veeco Multimode Nanoscope IV in tapping mode. NSC15/A1BS AFM probes were used and supplied

by Mikromasch. This apparatus was used to determine the surface phase images of the block copolymer thin films.

Figure 1. 34: Optical rheology apparatus that can take images of the samples while it models the affects of a rheometer.

In all of the characterization techniques, all scans and images were replicated a number of times to ensure reproducibility.

- CHAPTER 2 -

SYNTHESIS OF HOMOPOLYMERS

AND

DIBLOCK COPOLYMERS

2. SYNTHESIS OF HOMOPOLYMERS AND DIBLOCK

COPOLYMERS

Preface

This chapter discusses the polymerization technique employed for producing living free radical polymer by ARGET ATRP. Homopolymers and di-block copolymers of PS and PMMA have been investigated.

2.1 Introduction

Polymers are long chain molecules composed of many repeating units called monomers. As each unit attaches the chain becomes longer, but the rate at which the monomer attaches to one chain can be different to another, which can increase the polydispersity (i.e. the measure of chain length uniformity).[228] This was why controlled free radical polymerization was developed and over the years has grown into a variety of techniques such as ATRP,[229] NMP,[230] and RAFT,[231] to name a few. These techniques however are very sensitive and are not convenient for industrial production. Activators regenerated by electron transfer for atom transfer radical polymerization (ARGET ATRP) was invented to counteract the sensitivity, which uses a reducing agent often ascorbic acid[232] or tin(II) 2-ethylhexanoate ($Sn(EH)_2$),[233] to consume the oxygen impurities that can inhibit the polymerization. The ease of polymerization creates low polydispersity polymers that will have many uses in future applications.[234,235]

Although ARGET ATRP produces controlled polymers, the initiation efficiency has not been explored for block copolymer formation. The first part of this chapter will explore the initiation efficiency of the monomers styrene and methyl methacrylate and their homopolymer properties. A macro-initiator will then be

chosen from the best homopolymer (i.e. lowest polydispersity) and explored further in the production of diblock copolymers.

2.2 Synthetic and Preparation Procedures

Materials

Styrene and MMA were firstly dried over calcium hydride and purified by passing them through a column of basic alumina. Formic acid (88%), formaldehyde (37%), tris(2-aminoethyl)amine (TREN), sodium hydroxide, diethyl ether, sodium sulphate, Ethyl 2-bromoisobutyrate (EBiB), copper(II) bromide, copper(II) chloride, tin(II) 2-ethylhexanoate ($Sn(EH)_2$), anhydrous anisole, and methanol were used as received and obtained from Aldrich.

The macro-initiator/polystyrene, PS-Br (polydispersity 1.076, Mn 10,424g/mol) and PS-Br-2 (polydispersity 1.22, Mn 20,700g/mol) was synthesized using the procedure outlined below (ARGET ATRP of Styrene and MMA).

Synthesis of Tris(2-(dimethylamino)ethyl)amine (Me_6TREN)

A mixture of formic acid (16mL) and formaldehyde (14mL) was stirred at 0^oC. To this mixture 5mL of TREN was added drop-wise over an hour. The mixture was then allowed to come to room temperature, followed by refluxing overnight at 120^oC. The mixture was cooled to room temperature and the volatile components removed by rotary evaporator. A saturated solution of sodium hydroxide was added to the remaining mixture and an oily layer formed, which was extracted into diethyl ether and dried using sodium sulphate. Following this, the mixture was filtered using Watmann paper and the diethyl ether was removed by nitrogen flow.

ARGET ATRP of Styrene and MMA

$CuBr_2$ (2.17μmol) with 1mL of anisole, Me_6TREN (21.7μmol), styrene (43.49mmol), $Sn(EH)_2$ (21.7μmol) with 0.5mL of anisole, and a magnetic stirrer were

added to a nitrogen purged vial. The polymerization was initiated by the addition of EBiB (0.142mmol) with 1mL of anisole. The polymerization was carried out at 110°C and stopped at regular intervals by exposure to the air. In addition, the polymer was purified by precipitation in cold methanol.[236]

A similar procedure was carried out for the polymerization of MMA with some minor changes. The changes were the ratio MMA/EBiB/CuBr$_2$/Me$_6$TREN/Sn(EH)$_2$ = 200/1/0.01/0.1/0.1 and the polymerization was carried out at 90°C.[237]

The polymerization of styrene and MMA was stopped at regular intervals for the kinetic gravimetric analysis.

<u>Chain Extension of PS-Br with PMMA</u>

PS-Br (76.8μmol) with 3.5mL of anisole, CuCl$_2$ (2.34μmol) with 1mL of anisole, Me$_6$TREN (23.4μmol), Sn(EH)$_2$ (11.7μmol) with 0.5mL of anisole, and a magnetic stirrer were added to a nitrogen purged vial. The polymerization was initiated by the addition of MMA (46.74mmol), as there was nothing to polymerize until the monomer was added. The polymerization was carried out at 90°C and stopped at regular intervals by exposure to the air. In addition, the polymer was precipitated with cold methanol. The polymerization was stopped at regular intervals for the kinetic gravimetric analysis.

<u>Chain Extension of PS-Br-2 with P(MMA-co-S)</u>

PS-Br-2 (86.6μmol) with 4mL of anisole, CuCl$_2$ (2.60μmol) with 1mL of anisole, Me$_6$TREN (26.0μmol), Sn(EH)$_2$ (13.0μmol) with 0.5mL of anisole, and a magnetic stirrer were added to a nitrogen purged vial. The polymerization was initiated by the addition of MMA (46.74mmol) mixed with St (5.19mmol), as there was nothing to polymerize until the monomer was added. The polymerization was carried out at 90°C and stopped at regular intervals by exposure to the air. In addition, the polymer

was precipitated with cold methanol.[237] The polymerization was stopped at regular intervals for the kinetic gravimetric analysis.

Results and Discussion

2.3 Synthesis of Me$_6$TREN

In an ATRP system the copper catalyst works in the presence of a ligand (i.e. the formation of a complex) and therefore the choice of ligand is vital to produce a well initiated and low polydispersity polymer. Typically in ATRP, ligands such as phenanthroline and its derivatives,[238,239] substituted 2,2',6',2"-terpyridine,[240] and pyridineimines[241,242] are used, however in ARGET ATRP a more stable copper catalyst-ligand system is required.[234] Me$_6$TREN and tris[(2-pyridyl)methyl]amine (TPMA) produce a strong system and are commonly used in ARGET ATRP.[235] These compounds are not commercially available and therefore due to the ease of production, Me$_6$TREN was chosen for this work.

The synthesis of Me$_6$TREN was verified by NMR. ^{1}H NMR (CDCl$_3$) δ: 2.58 (dd,12H); 2.36(dd,12H); 2.21(s,18H)ppm (80% yield).[243]

2.4 Synthesis of PS and PMMA Homopolymers

The livingness of the polymerization technique was explored using the kinetic plot shown in Figure 2. 1 for a) polystyrene and b) PMMA. The graphs show a straight line which is typical of a living polymerization however, one thing to notice is that in Figure 2. 1a) the plot does not pass through the origin and appears to initiate approximately an hour after the reaction was started. This demonstrates the simplicity of ARGET ATRP as a plot of this nature occurs when oxygen impurities are present and then the polymerization initiates once all oxygen is consumed by the Sn(EH)$_2$. Similar findings were reported by Jakubowski *et al*[244] that polymerization had started, with good living control, once the oxygen impurities had been consumed by the

Sn(EH)$_2$ (i.e. "short induction period"). It is important to note that if the polymerization technique was "normal ATRP" the styrene would never initiate as the catalyst would be dead/oxidized to Cu(II) by the oxygen.[233] As for PMMA (i.e. Figure 2. 1b)) the plot starts at the origin indicating the absence of oxygen impurities by sufficient nitrogen purging and hence is not delayed in its initiation.
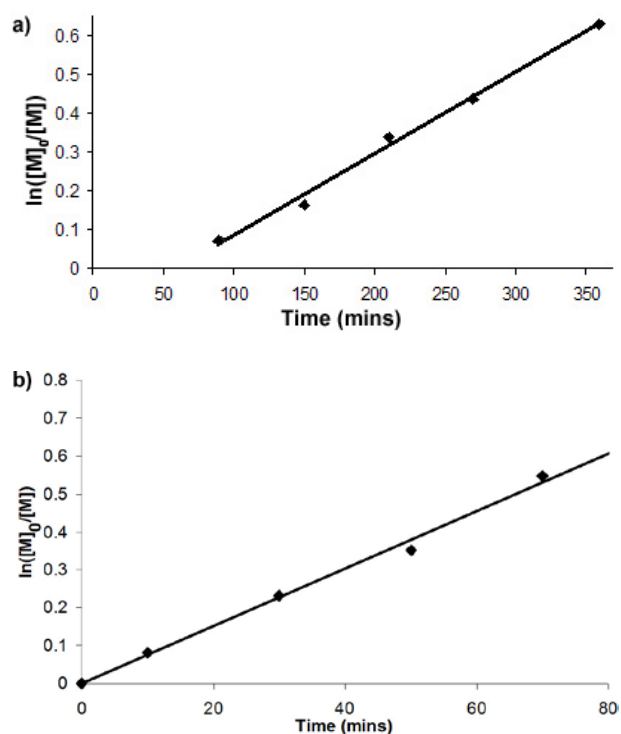
Figure 2. 1: a) Kinetic plot for ARGET ATRP of styrene (R²=0.994), b) Kinetic plot for ARGET ATRP of MMA (R²=0.994).

The livingness can further be explored by plotting the molecular weight against conversion. From Figure 2. 2a) it is noticed that the controlled polymerization of PS was unaffected by the "short induction period" as a linear plot and a polydispersity close to 1 was produced. As this plot is time independent the "short induction period" can not be determined from this graph, however the plot passes through the origin and indicates good polymer chain initiation.

In contrast the linear plot for PMMA does not pass through the origin (Figure 2. 2b)). Mueller *et al*[245] observed the same phenomenon when polymerizing homopolymers of PMMA by ARGET ATRP, due to very poor initiation; all the

polymer chains were not initiated at the same time. In addition, as the initiation was poor for PMMA, the resulting polydispersity was larger than the well initiated PS; 1.29 for 42% conversion compared to PS with 1.08 for 47% conversion (see Table 2. 1 for the summarized results). Furthermore, the polydispersity of PS tends towards 1 as the conversion increases (i.e. 1.22 decrease to 1.08), but for PMMA the opposite occurs (i.e. 1.22 increase to 1.29). PS was therefore chosen to be the macro-initiator for the di-block copolymer synthesis (i.e. section 2.5).
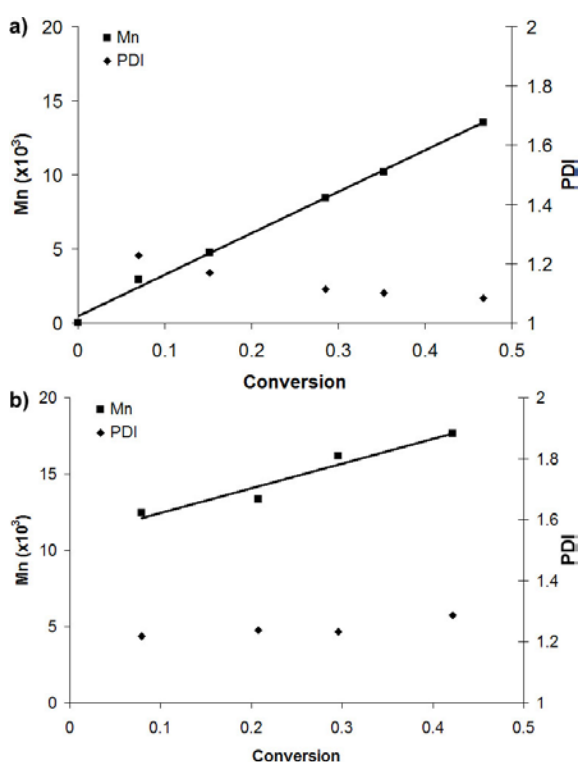
Figure 2. 2: Molecular weight and polydispersity as a function of conversion in ARGET ATRP for a) PS ($R^2 = 0.996$) and b) PMMA ($R^2 = 0.936$) using a polystyrene calibration.

An additional result comes from Table 2. 1 as it reveals that MMA has a higher reactivity than styrene; a reaction time for MMA of 70mins results in 42% conversion compared to styrene of 360mins to reach 47% conversion. This is a five times difference in reaction time and hence reactivity, which is supported by literature.[234]

Sample	Time (mins)	M_n $(\times 10^3)^b$	Conv. (%)	PDI
PS	90	2.9	7	1.22
	150	4.7	15	1.17
	210	8.5	29	1.11
	270	10.2	35	1.10
	360	13.6	47	1.08
PMMA	10	12.4	8	1.22
	30	13.3	21	1.24
	50	16.2	30	1.23
	70	17.7	42	1.29

Table 2. 1: Properties of PS and PMMA prepared by ARGET ATRP. [b] determined by GPC in THF, polystyrene standard: St/EBiB/CuBr$_2$/Me$_6$TREN/Sn(EH)$_2$ = 300/1/0.015/0.15/0.15 and MMA/EBiB/CuBr$_2$/Me$_6$TREN/Sn(EH)$_2$ = 200/1/0.01/0.1/0.1
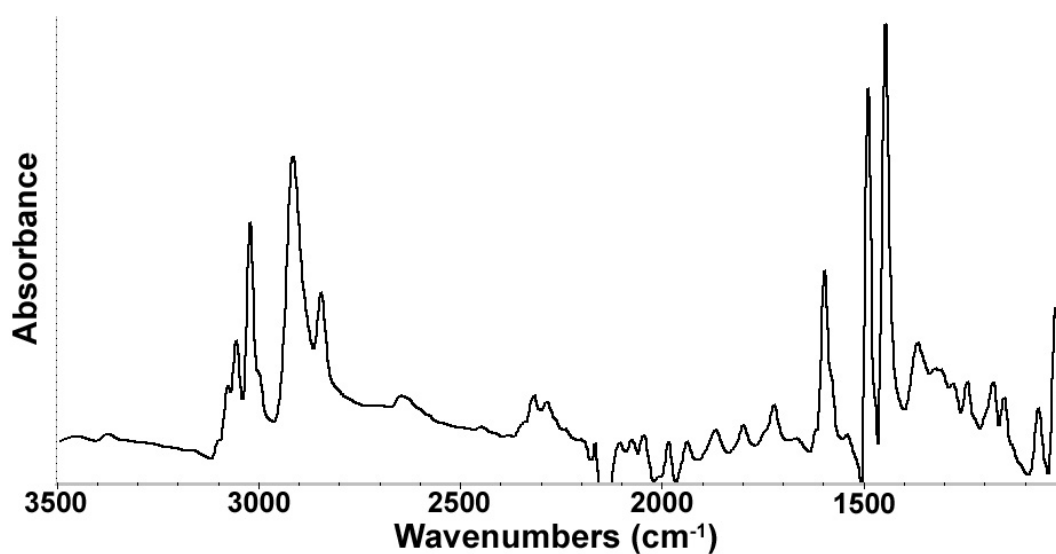
Figure 2. 3: FT-IR spectra of polystyrene produced by ARGET ATRP.
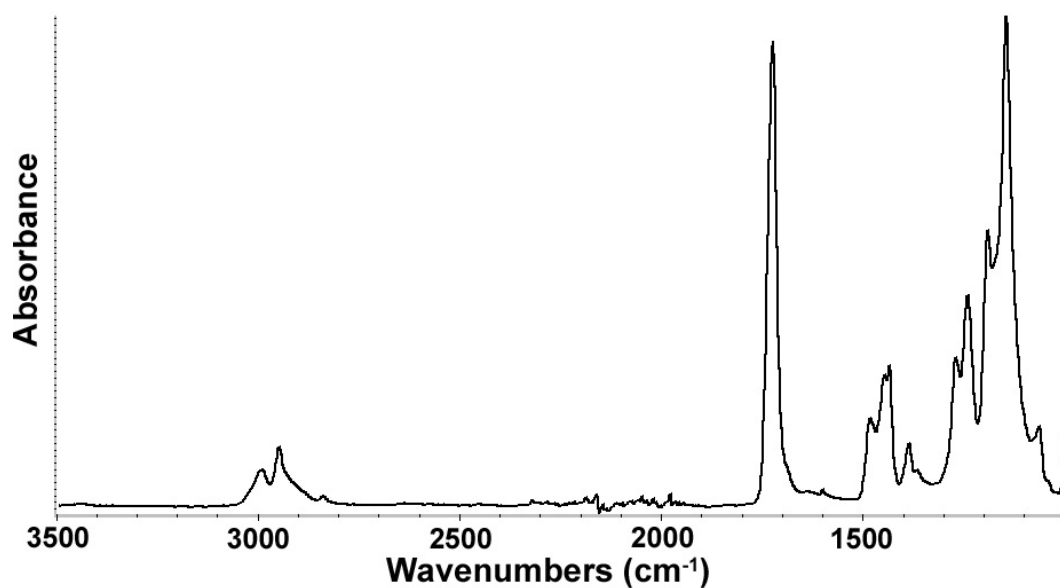
Figure 2. 4: FT-IR spectra of poly(methyl methacrylate) produced by ARGET ATRP.

The chemical structures of the living polymers were verified using Fourier Transform Infrared Spectroscopy (FT-IR). The spectra for PS and PMMA can be seen in Figure 2. 3 and Figure 2. 4, respectively. The measured PS and PMMA spectra exhibited the characteristic FT-IR peaks such as 2000-1700, 1601, 1493, 1452, 749 and 696cm^{-1} for PS[246,247] and 2952, 2866, 1730, and 1147cm^{-1} for PMMA;[248] the peak assignment is given in Table 2. 2. Some noise is present around the 2000 to 2300cm^{-1} mark and is associated to carbon dioxide. This is commonly seen in ATR-FT-IR due to the CO_2 concentration fluctuations in the air.

Sample	Wavenumber (cm^{-1})	Assignment
PS	2000-1700	Benzene ring overtones
	1601, 1493, 1452	Benzene ring carbon-carbon stretch
	749, 696	Mono substituted benzene
PMMA	2952	-CH_3
	2866	-CH_2
	1730	C=O stretch
	1147	Ester

Table 2. 2: FT-IR homopolymer peak assignment.[249]

The polymers thermal stability properties were explored using thermogravimetric analysis (TGA). It was found that in the presence of air at a ramp rate of 10°C/min that the T_d (decomposition temperature) averaged for PMMA was 289°C and for PS 354°C. Compared to literature, PMMA is in the region of 300°C[250,251] and PS is 395°C,[252] which is different from the living polymers T_d and has occurred due to the large difference in molecular weight (i.e. living M_n is in the thousands, compared to free radical/non-living in the 100,000's).

2.5 Diblock Copolymer Formation

Block copolymers consist of homopolymer fragments within a chain that is connected end to end to create a larger chain. In the case of diblock copolymers, two blocks/fragments make up the chain. For the purposes of this research a diblock copolymer of PS and PMMA was required for the final application (see Chapter 5).

The resultant polymer must have a polydispersity near 1 in order for the block copolymer phases to form and therefore good initiation of polymer chain growth is required.[253] As experienced in Section 2.4, ARGET ATRP of PMMA did not initiate well when compared to PS and the lowest polydispersity recorded was 1.22 and 1.08, respectively (see Table 2. 1). Clearly ARGET ATRP of PS produces a better homopolymer for the first block of a diblock copolymer of PS and PMMA (i.e. macro-initiator).

As we are going from styrene, a less reactive monomer, to MMA, a more reactive monomer, the halogen exchange technique must be used in order to obtain efficient initiation of the second block (i.e. PS-Br/CuCl$_2$ system instead of PS-Br/CuBr$_2$).[254] Many researchers have already shown that the halogen exchange technique works for ATRP,[255,256,257] but no reported literature has explored its use in ARGET ATRP.

2.5.1 Chain Extension of PS-Br with PMMA

The livingness of the polymerization technique was explored by using the kinetic plots shown in Figure 2. 5. From the Figure 2. 5a) a straight line is present indicating the polymerization has progressed in a living fashion, however the line does not pass through the origin as seen in section 2.4, but this is due to the use of the macro-initiator altering the initial $\ln([M_0]/[M])$ value. The plot of Mn versus Conversion (Figure 2. 5b)) does not pass through the origin and is a better indicator of how well the polymerization was initiated. However, the M_n at zero conversion is the M_n of the macro-initiator and in this case the plot should then pass through approximately 10,424g/mol (i.e. PS-Br), which it does when extrapolating the graph.

The initiation of the second block was further explored using GPC and the results are summarized in Table 2. 3. A polydispersity of the P(S-b-MMA) sample reached as high as 2.01 for a conversion of 48%. A value of this magnitude is typically

experienced with non-living free radical polymerizations and indicates a loss of control (i.e. the polymerization was not living). This strengthens the concept that MMA has poor initiation in ARGET ATRP systems as seen in the PMMA homopolymer results (i.e. section 2.4).
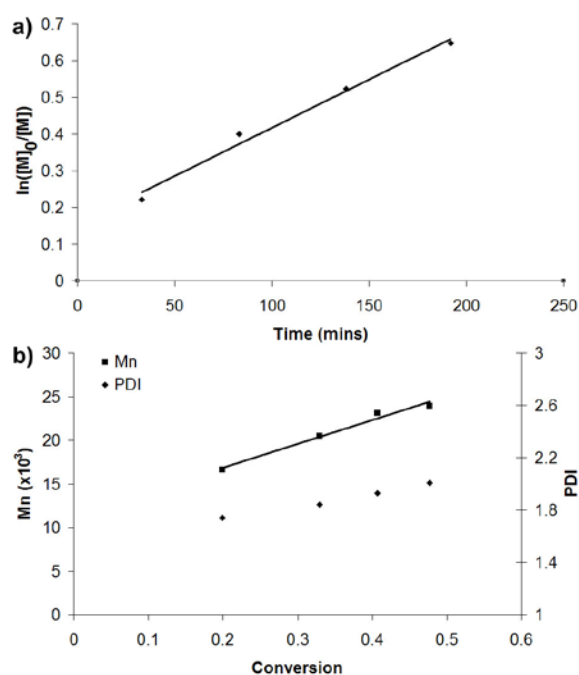
Figure 2. 5: a) Kinetic plot for ARGET ATRP of PS-b-PMMA (R^2=0.987), and b) the molecular weight and polydispersity as a function of conversion, using a polystyrene calibration ($R^2 = 0.978$).

Sample	Time (mins)	M_n (x10^3)[b]	Conv. (%)	PDI
PS-Br	360	10.4[c]	32	1.08
P(S-b-MMA)	33	16.6	20	1.74
	83	20.5	33	1.84
	138	23.1	41	1.93
	192	23.9	48	2.01

Table 2. 3: Properties of PS-Macro extended with PMMA by ARGET ATRP. [b]determined by GPC in THF, polystyrene standard: St/EBiB/CuBr$_2$/Me$_6$TREN/Sn(EH)$_2$ = 300/1/0.015/0.15/0.15 and MMA/PS-Br/CuBr$_2$/Me$_6$TREN/Sn(EH)$_2$ = 600/1/0.03/0.3/0.15. [c]the Mn is lower than the sample in Table 2. 1, which indicates oxygen was present in the PS-Br polymerization (i.e. a "short induction period").

To get a better picture of the polymerization of the second block (MMA), the GPC traces were overlaid to monitor the developing block copolymer with time (i.e.

Figure 2. 6). The initial macro-initiator (PS-Br) is shown in black and has a sharp peak at 10,400g/mol as expected (i.e. M_n of PS-Br). With the start of the polymerization, a second peak evolves and shifts to higher molecular weights as time progressed. This was not expected, as the 10,400g/mol macro-initiator peak remained and decreased with time, indicating that not all macro-initiator chains initiated at the beginning leaving some chains for later initiation, during the progress of the polymerization (i.e. poor initiation).
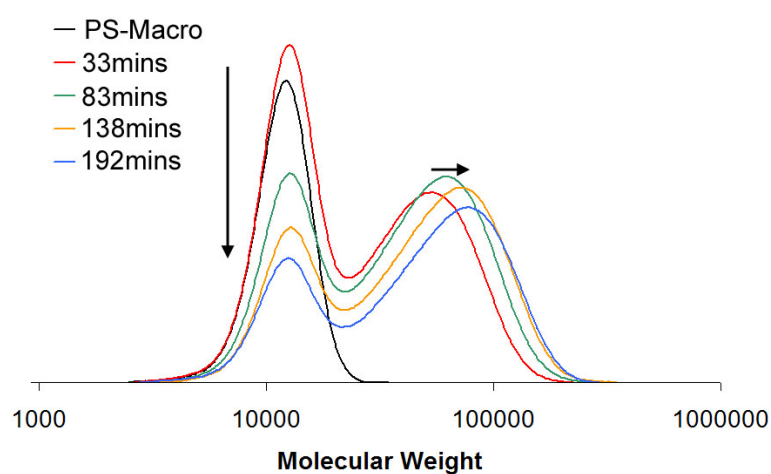
Figure 2. 6: GPC traces of PS-Macro before and after chain extension with MMA for polymerization of 33 to 192mins, using a polystyrene calibration.

In contrast to ATRP, Tsarevsky *et al*[256] showed that by using halogen exchange for the second block polymerization, efficient initiation occurred. In their results at 10% conversion a similar macro-initiator peak/shoulder was observed in the GPC trace, however the intensity of this shoulder with respect to conversion was much less intense than the results reported here for ARGET ATRP of a similar conversion. Likewise to the above results, as the conversion increased the macro-initiator peak reduced to the baseline at approximately 37% and these results can be seen in Figure 2. 7. This suggests that halogen exchange at low conversion polymerizations does not work for either polymerization process, but is effective for higher conversions of ATRP and to a much lesser extent ARGET ATRP. Furthermore, similarly to ATRP,

if the ARGET ATRP was allowed to continue, then eventually all PS-Br chains would initiate and hence the mix of PS-Br and diblock copolymer would eventually result in pure diblock copolymer. A downside to this is expected as the molecular weight of the second block was already six times the molecular weight of the first block after 192mins and not all of the PS-Br chains had initiated (see Figure 2. 6). That would mean in order to create a diblock copolymer of P(S-b-MMA) by ARGET ATRP, the PMMA second block would need to be extremely large in comparison to the first block so that all of the PS-Br chains could initiate.
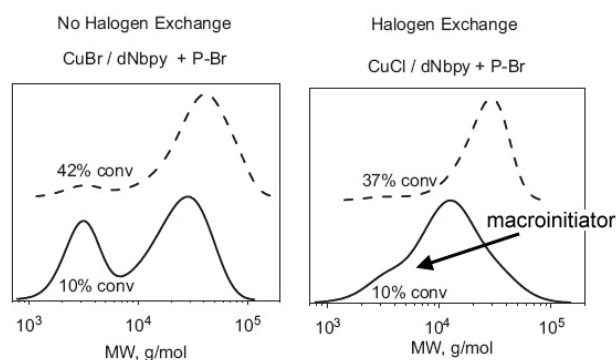
Figure 2. 7: Tsarevsky et al[256] GPC traces of no halogen exchange (left) and halogen exchange (right). The presence of the macro-initiator peak at low conversion and the disappearance at higher conversion when using halogen exchange.

2.5.2 Chain Extension of PS-Br-2 with P(MMA-co-S)

The results of section 2.5.1 suggested that a diblock copolymer of PS-b-PMMA with a polydispersity near 1 by ARGET ATRP was near impossible to produce due to the poor initiation of the second block (i.e. MMA). Charleux *et al*,[258,259] however found a way to improve the initiation efficiency of MMA, as a second block, by adding a small percentage of styrene as a comonomer in nitroxide mediated polymerization (NMP). The idea was that it would change the reactivity of the propagating chains to a comparable reactivity to the macro-initiator, thereby increasing the probability of initiation. Mueller *et al*,[245] thought this concept could be

applied to ARGET and ICAR systems with poor initiation efficiency and found that by adding 10% styrene, efficient initiation occurred. This was attempted and the research extended to get a better understanding of the process.

The typical plots to show evidence of living growth is presented in Figure 2. 8 and as expected by the report of Mueller *et al*[245] the results show efficient initiation. The kinetic plot a) is a straight line passing through the origin and plot b) is a straight line passing through the molecular weight of the macro-initiator (i.e. PS-Br-2 20,700g/mol). However, unexpected changes in polydispersity with conversion were detected; starting at 1.18 at 10% and ending with 1.52 at 56% conversion (Table 2. 4). In addition, Figure 2. 8 depicts that the polydispersity increases with respect to conversion in a linear type fashion and shows no evidence of reaching a limit.
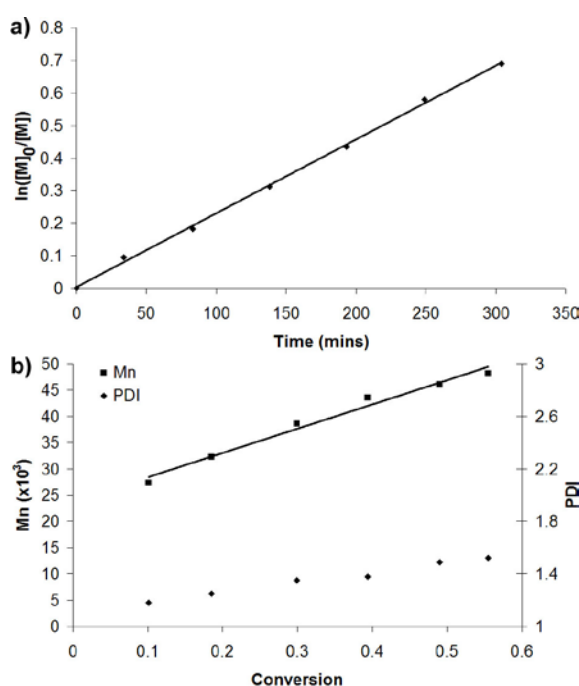
Figure 2. 8: a) Kinetic plot for ARGET ATRP of PS-b-P(S-co-MMA) (R^2=0.999), and b) the molecular weight and polydispersity as a function of conversion using a polystyrene calibration ($R^2 = 0.980$).

Although the polymerization appears to be living/controlled, the GPC traces suggested something else was occurring. Mueller *et al*[245] reported that their GPC

traces (Figure 2. 9) showed good initiation, however they only show the results of one chain extension length, which is increased from 19,500g/mol to 38,200g/mol (i.e. doubled in size). This study reflects an extension of their work for longer chain extensions of five times the macro-initiator M_n, where the additional affects are more pronounced.

Sample	Time (mins)	M_n (x10^3)^b	Conv. (%)	PDI
PS-Br-2	360	20.7^c	58	1.22
P(S-b-(S-co-MMA))	34	27.3	10	1.18
	83	32.3	19	1.25
	138	38.6	30	1.35
	192	43.6	39	1.38
	249	46.1	49	1.49
	300	48.1	56	1.52

Table 2. 4: Properties of PS-Br-2 extended with PMMA and 10% PS by ARGET ATRP. ^{b}
determined by GPC in THF, polystyrene standard: St/EBiB/CuBr2/Me6TREN/Sn(EH)2 =
300/1/0.015/0.15/0.15 and MMA/St/PS-Br/CuBr2/Me6TREN/Sn(EH)2 =
540/60/1/0.03/0.3/0.15. ^{c} *the Mn is higher than PS(360mins) and PS-Macro, which*
indicates sufficient de-oxygenation occurred and that no "short induction period"
occurred.
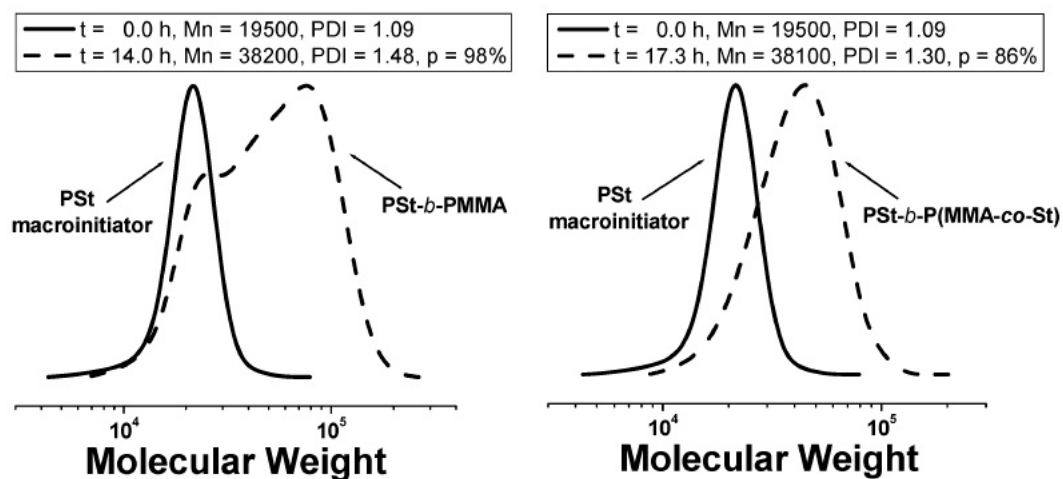
Figure 2. 9: (left) showing poor initiation and (right) demonstrating efficient initiation,
from Mueller et al paper.[245]
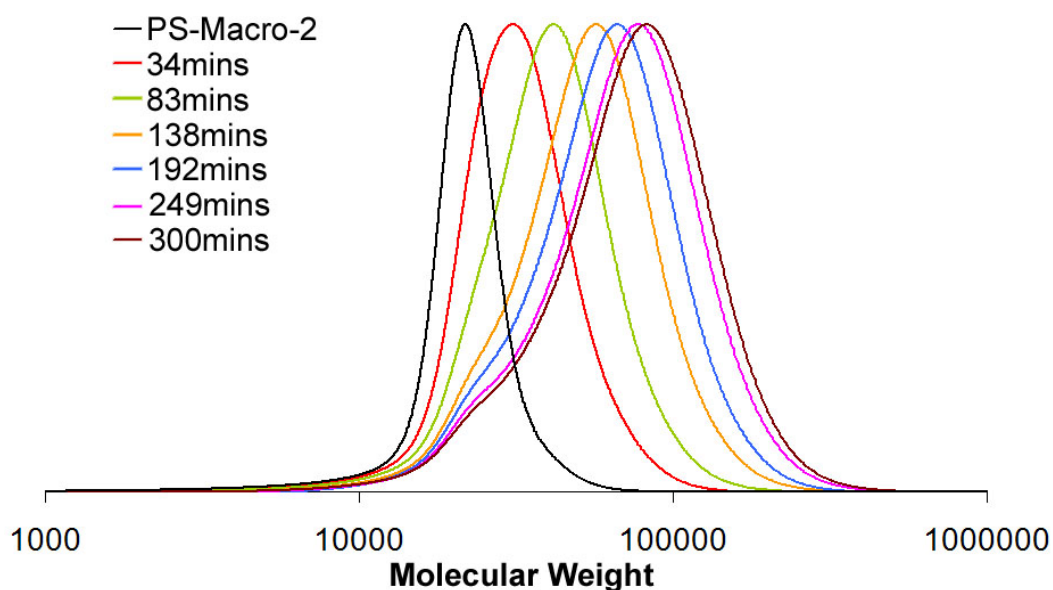
Figure 2. 10: GPC traces of PS-Br-2 before and after chain extension with MMA and 10% styrene for polymerization of 34 to 300mins, using a polystyrene calibration. Note the development of a shoulder.

In this work, the GPC traces of Figure 2. 10 show the macro-initiator has a good polydispersity by its sharp peak. Upon chain extension this peak does move to a higher molecular weight appearing with no shoulder like Figure 2. 9, but the propagating peak begins to broaden also like Figure 2. 9. The subsequent results continued moving the peak to larger molecular weights, but at approximately 30% conversion a shoulder appeared and became more prominent as the polymerization continued. This suggested that some of the PS-Br-2 chains were initiated and extended with the MMA, however the remaining PS-Br-2 chains continued their growth with the added 10% styrene. As the polymerization continued the block copolymer continued to grow and more of the lengthened, with styrene, PS-Br-2 chains were extended with MMA. Eventually all of the styrene was consumed in lengthening PS-Br-2, but not all of the lengthened PS-Br-2 had a chance to switch monomer (i.e. extend with MMA), leaving un-initiated macro-initiator chains; a graphical representation of this explanation can be seen in Figure 2. 11. Furthermore, this was evident by the increasing polydispersity with conversion (Table 2. 4) and

only when all of the styrene was consumed by the PS-Br-2 growth, the residual lengthened PS-Br-2 chains appeared as a shoulder. This was a similar result to the GPC traces seen in section 2.5.1, except the PS-Br/macro-initiator does not increase in molecular weight by any presence of styrene monomer. In addition this would mean that the samples produced are actually a mixture of lengthened PS-Br-2 and P(S-b-MMA) of unknown PS/first block chain length and not the expected P(S-b-(S-co-MMA)) (see Figure 2. 11).
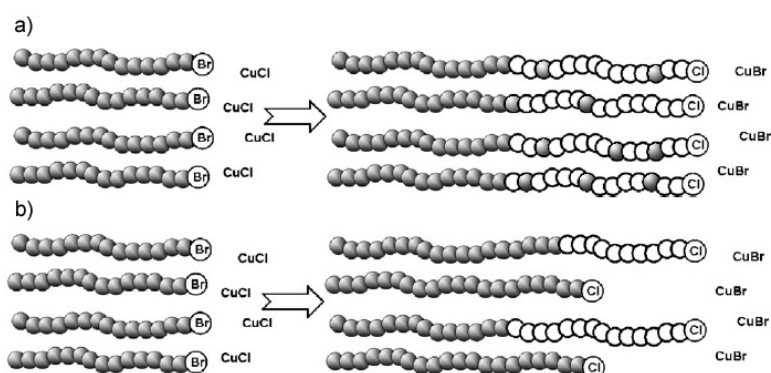
Figure 2. 11: A representation of the polymeric material produced using halogen exchange and adding 10% styrene to the subsequent chain extension polymerization. a) the expected polymer of P(S-b-(S-co-MMA)) and b) the produced polymeric mixture of PS-Br-2 and P(S-b-MMA).

The physical properties, such as the T_g and T_d of the polymeric samples were determined using Differential Scanning Calorimetry (DSC) and TGA. In the DSC results, presented in Table 2. 5, the lower molecular weight polymeric samples (i.e. P(S-b-(S-co-MMA)) for 34 and 83mins) express one T_g that starts at 97.5°C and increases to 107.6°C. This is an increase of 19.6°C from the PS-Br-2 sample, and is attributed to the increase in molecular weight. This finding demonstrates and supports that PS-Br-2 of lower molecular weight produces a lower T_g compared to Commercially Available PS (CA-PS, purchased from Aldrich) having a larger molecular weight producing a higher T_g (i.e. 88°C increased to 102.2°C). This is

supported by the work of Fox *et al*,[260] as they too found that with increasing molecular weight the T_g also increased.

At 138mins of polymerization, the DSC results show the already present T_g at approximately 107°C, which remains and persists for the rest of the samples, but as the polymerization progressed a second T_g emerges at 119.1^{o}C (see Figure 2. 12). The 107°C T_g is associated to the PS block and is supported with the CA-PS sample, however the second T_g at 119.1^{o}C is associated with the second block/PMMA, which is supported with the PMMA (70mins) sample. In addition, after 138min when the conversion reached 30%, the material expressed the two T_g's, which was also the point of where the shoulder appeared in the GPC traces and was an indication that a mixture of homopolymer and copolymer was present. In comparison to the work by Holoubek *et al*[261] they found for a similarly sized molecular weight that their block copolymer of PS-b-PMMA expressed only one T_g. However, when the sample was mixed with a shorter molecular weight block copolymer, two T_gs were observed. This further supports the concept that the block copolymer produced by ARGET ATRP is a mixture of two different molecular weight polymers.

Sample	T_g (^{o}C)	T_g' (^{o}C)	T_d (^{o}C)
CA-PS	102.2	-	400
PS-Macro-2	88	-	346
PMMA (70mins)	120	-	295
P(S-b-(S-co-MMA))			
34	97.5	-	343
83	107.6	-	339
138	107.2	119.1	331
192	108.3	121.3	310
249	107.9	121.3	298
300	107.6	122.1	304

Table 2. 5: physical properties of P(S-b-MMA) and their homopolymers. The T_g was measured at 20°C/min second heating, and T_d was measured at 10°C/min in air.
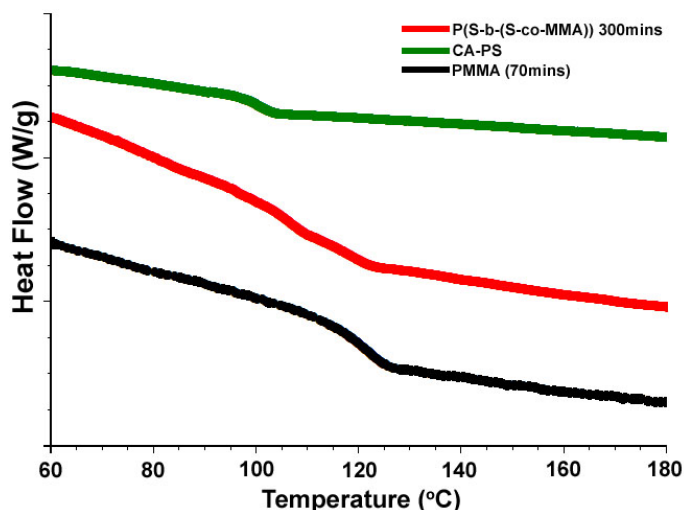
Figure 2. 12: A typical DSC curve of P(S-b-(S-co-MMA)) with CA-PS and PMMA (70mins) for comparison
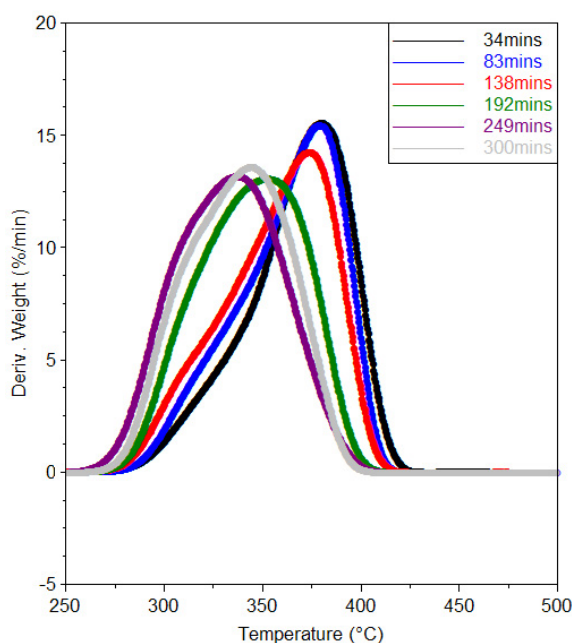
Figure 2. 13: TGA thermograms of P(S-b-MMA) mixture with PS homopolymer, measured at 10^oC/min in air, demonstrating a shift in T_d towards lower temperatures as the polymerization time increased and a shoulder.

The TGA results demonstrated an initial T_d of 346^oC, however as the block copolymer polymerization progressed the T_d decreased to 304^oC (see Table 2. 5). This suggests that the thermal stability of the samples decreased, but as the extension was with MMA then the T_d, originally 346^oC for PS-Br-2, was expected to decrease towards the PMMA's T_d of 300^oC[250,251] and therefore the results are in good

agreement with literature. In addition, the thermograms of the block copolymers in Figure 2. 13 show that the lower polymerization times produce a shoulder in the peak, which becomes more dominant at higher polymerization times. This shoulder proves the existence of a heterogeneous material, as a pure material would have a sharper peak with no shoulders.

2.6 Conclusion

The results showed that ARGET ATRP of styrene produces an efficiently initiated homopolymer, however produces a poorly initiated PMMA homopolymer. When this research was extended to block copolymers, the well initiated PS was used as a macro-initiator, but upon chain extension with MMA many chains did not propagate. As the conversion increased these un-initiated chains started to propagate, but in order for all the macro-initiator chains to eventually initiate the second block, the polymerization time needs to be large and hence an extremely large second block results.

To increase the efficiency of chain extension, halogen exchange was used, but had proven to be ineffective for ARGET ATRP. A new technique was employed to add 10% styrene into the subsequent block polymerization to aid in the initiation. However, upon higher conversions this technique showed new qualities, which were not seen in the referred paper as only lower conversions were presented.[245] From this it was determined that the technique produced a mixture of PS and P(S-b-MMA).

In summary, halogen exchange at low conversion polymerizations does not work for ATRP or ARGET ATRP, but is effective for higher conversions of ATRP and to a much lesser extent ARGET ATRP. Upon adding 10% styrene for the second block ARGET ATRP polymerization the appearance of a well initiated polymer was

observed, however at greater conversions the results clearly demonstrated the production of a homo/copolymeric mixture

- CHAPTER 3 -

POLYMER BRUSHES:

SURFACE INITIATED POLYMERIZATION

(SIP)

3. POLYMER BRUSHES: SURFACE INITIATED

POLYMERIZATION (SIP)

Preface

This chapter discusses the purification technique employed to remove carbonaceous impurities from the carbon nanotube wall. In addition, the formation of hydroxyethyl-2-bromoisobutyrate (HEBI) is discussed and how this chemical is used to functionalize the multi-walled carbon nanotube (MWCNT) further with tertiary bromides in preparation for use as an initiator for ARGET ATRP. Furthermore, the research explored in this chapter, has shown that the extent of functionalization is in the low percentile and so 1-pyrenecarboxylic acid has been used to model the MWCNT work due to its chemical similarities (Scheme 3. 1).
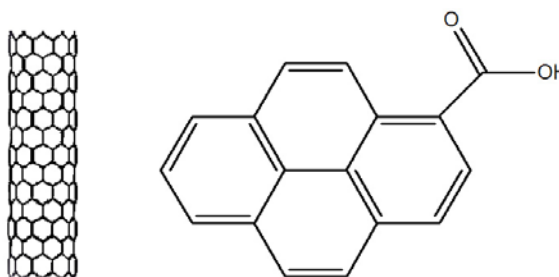
Scheme 3. 1: (Left) A MWCNT, which is composed of many aromatic groups and the defects are functionalized with oxygenated species, primarily in the form of a carboxylic acid. (Right) 1-pyrenecarboxylic acid, which is chemically similar to a MWCNT.

This chapter then discusses the synthesis of polymer brushes on carbon nanotubes; polystyrene (PS) and poly(methyl methacrylate) (PMMA) have been synthesized by ARGET ATRP using an adapted method from chapter 2, and poly(2-hydroxyethyl methacrylate (PHEMA) has been produced by free radical polymerization (FRP). Each method produced a polymer layer that surrounded the

outside of the carbon nanotube and was observed using high resolution transmission electron microscopy (HRTEM). In addition, Pyrene-HEBI was used in the production of one PS polymer brush per pyrene molecule.

The chemical and physical properties of the polymer brushed carbon nanotubes and the polymer brush pyrene were also explored.

3.1 Introduction

Carbon nanotubes have been considered as the ultimate carbon fiber due to their high aspect ratio, high tensile strength, excellent mechanical and electrical properties. They appear in two primary morphologies: single and multi-walled carbon nanotubes.[262] Their extraordinary properties have stimulated extensive interest in their use as reinforcing nanoadditives for polymers.[263] However, the poor dispersion and poor interfacial bonding of the carbon nanotubes limit their full utilization for reinforcing polymeric media.
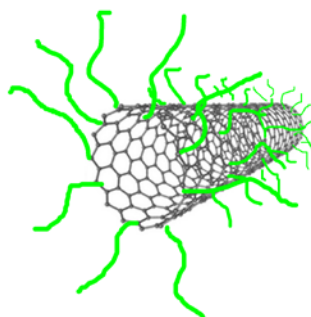
Figure 3. 1: A model drawing of polymer brushes attached to a carbon nanotube.

There are generally four methods used in modifying carbon nanotubes for dispersion in polymer matrices: (i) solution mixing carbon nanotube suspensions into dissolved polymers;[264] (ii) mechanical mixing of carbon nanotubes into polymer melts;[265,266] (iii) in situ polymerization of monomer-carbon nanotube mixtures[267] and (iv) emulsion polymerization to generate polymer-wrapped carbon nanotubes.[268] Functionalized carbon nanotubes, and in particular polymer brushed carbon

nanotubes (see Figure 3. 1), allow a synthetic "bottom-up" approach to the creation of nanomaterials; their organic functional groups being manipulated to be compatible with polymer matrices, thus ensuring the good dispersion and strong interfacial interactions needed in nanocomposite applications. Materials of this nature have been used for the production of amphiphilic copolymer brushes on carbon nanotubes,[269] to increase the dispersity in common solvents,[270,271] as a vehicle for drug delivery,[272] as well as conductive fillers in nanocomposite films.[273]

Controlled/living radical polymerization, in which the polymerization process occurs by the propagation of radicals, has previously been used for the production of nanotube polymer brushes. A variety of synthetic techniques such as atom-transfer radical polymerization (ATRP),[220,274,275,276,277] nitroxide mediated polymerization (NMP),[278] reversible addition-fragmentation chain transfer (RAFT),[279,280] and non-covalent attachment[281] have all previously been reported for the creation of such polymer brushes. Although, ATRP is well suited for surface modification, it has to be carried out in the complete absence of oxygen and generally uses a relatively high Cu(I) catalyst concentration of 10,000ppm, making the subsequent removal of the catalyst a non-trivial process.[282]

In this chapter ARGET ATRP was used for the first time on carbon nanotubes in the formation of dense polymer brushes, based on a "grafting-from" approach. An important aspect of this process (compared to normal ATRP) is that a substantially lower amount of copper catalyst was used (i.e. 10-50ppm, compared to 10,000ppm), and this is particularly important in that previous research has shown the removal of transition metal ions from nanotubes to be very difficult.[283] Additionally, the polymerization can be carried out in the presence of limited amounts of air.

In a controlled radical polymerization the polymer chains start at the initiator/alkyl bromide and continue to propagate uniformly (i.e. polydispersity of 1, and greater than 2 for uncontrolled polymers).[284] The reaction can be terminated by air exposure, but can reinitiate when a sufficient amount of reducing agent is added, thereby allowing polymer extension or the production of block copolymers.[285] The alkyl bromide end functionality can also be displaced using electrophilic, nucleophilic, and radical transformations, changing the polymer end group.[286]

Previous research reported the importance of a "sacrificial initiator" in surface-initiated polymerizations in order to evaluate the molecular weight of the covalently bonded polymer[285] and to assist in controlling the initiation from the surface for styrene, MMA and HEMA graft ATRP.[285,287,288,289] In contrast, Matyjaszewski *et al*[290] reported that the addition of the "sacrificial initiator" creates unnecessary complexity and also the presence of unwanted, unattached polymers on a silicon wafer surface. The necessity of a sacrificial initiator is explored and whether it leads to any additional benefits.

In this chapter, high purity chemical vapor deposition (CVD) nanotubes (i.e. the purity is greater than 95%) are functionalized in a series of simple steps to produce an alkyl bromide terminal group, which then was used as the macro-initiator in ARGET ATRP. This work focuses on the polymerization of styrene and methyl methacrylate to carbon nanotubes and systematically investigates the structural and chemical properties that such polymer modified MWCNTs afford. Furthermore, HEMA was polymerized using a non-living polymerization technique in the formation of PHEMA polymer brush carbon nanotubes and pyrene was explored as a model system in forming living brushes.

3.2 Synthetic and Preparation Procedures

Materials

CVD-MWCNT used in this work were purchased from NTP Shenzhen Nanotech Port Co., LTD; the purity is $\geq$ 95% with a diameter of 40-60nm. Two types were purchased for this work L-MWCNT with a length of 5-15μm and S-MWCNT with a length of 1-2μm. The L-MWCNT were used for all the work reported in this chapter and chapter 4. S-LMWCNT were used in chapter 5 for the block copolymer hybrid materials. The concentrated sulfuric acid, concentrated nitric acid, anhydrous ethylene glycol, 2-bromoisobutyryl bromide, chloroform, magnesium sulphate, thionyl chloride, dimethylformamide (DMF), triethylamine (TEA), diethyl ether, 1-pyrenecarboxylic acid, toluene, copper(II) bromide, copper(II) chloride, tin(II) 2-ethylhexanoate ($Sn(EH)_2$), anhydrous anisole (99%), and methanol were obtained from Aldrich and used as received. The PTFE membranes were obtained from the Pall corporation. Styrene (Aldrich, 99%) and methyl methacrylate (MMA) (Aldrich, 99%) were dried over calcium hydride and passed through a column filled with basic alumina. Tris(2-(dimethylamino)ethyl)amine (Me_6TREN) was synthesized following a previously reported procedure, but dried over sodium sulfate instead (for full details see chapter 2).[291] 2-hydroxy ethyl methacrylate (HEMA) (Aldrich) was purified by a previously recorded procedure[292] to remove impurities such as dimethacrylates and methacrylic acid.

Nanotube Purification

In the production of carbon nanotubes many carbonaceous impurities are formed. Arc discharge produced nanotubes creates the greatest amount of impurities whereas CVD produced nanotubes have impurities as low as 5%.[293,294] CVD nanotubes were chosen because of this.

Although CVD has the highest purity, further purification is required which typically involves an acid mixture of sulphuric and nitric (3:1).[295,296] This results in an increase in carboxylic acid functionality and creates opportunities for further functionalization, as the carboxylic acids can be manipulated to form ester linkages.[283] In addition, using a strong acid technique creates additional problems as the reaction temperature and time play a key role in the purification technique. Too high of a temperature would result in exfoliating the MWCNT and the destruction of SWCNT, rather than just removal of the carbonaceous material. It can also result in the opening of the nanotube ends and cutting/shortening the carbon nanotubes.[295] In this case we have used an ice bath to avoid these issues and have experienced minimal damage.

In this process 2g of L-MWCNT were mixed with a 100mL 3:1 acid mixture of sulfuric acid to nitric acid. This mixture was sonicated for 7hrs in an ice bath. The reaction was stopped by the addition of a liter of distilled water and filtered with a PTFE membrane until a neutral pH was reached. Dried at 20°C at 100mbar. In addition, care was taken in filtering the acid solution as a low pH could destroy the membrane.

Synthesis of Hydroxyethyl-2-bromoisobutyrate (HEBI)

45mL of anhydrous ethylene glycol was added to a flame dried round bottom flask filled with nitrogen. This was cooled to 0°C and while vigorously stirring, 4mL of 2-bromoisobutyryl bromide was added slowly. The mixture was stirred for a further 3hrs and then quenched with 40mL of distilled water. The product was extracted using chloroform and the organic phase was dried over magnesium sulphate, followed by filtration with Watmann paper. The solvent was removed by

nitrogen flow and purified by distillation (85°C, 30mTorr) yielding approximately 90%.[297]

Carbon Nanotube Functionalization with HEBI

250mg of acid treated L-MWCNT were sonicated for 20mins in 25mL of thionyl chloride, followed by 20 drops of DMF to help catalyze the reaction (a white gas evolved during its addition). This mixture was then refluxed at 70°C for 24hrs in a nitrogen atmosphere. After this period the thionyl chloride was removed by vacuum and a catalytic amount of TEA (0.1g) and 20mL of HEBI was injected. Once again the mixture was refluxed at 70°C for six days under nitrogen. Excess HEBI was removed by filtration and washed thoroughly with diethyl ether. The reaction scheme can be seen in Scheme 3. 2.
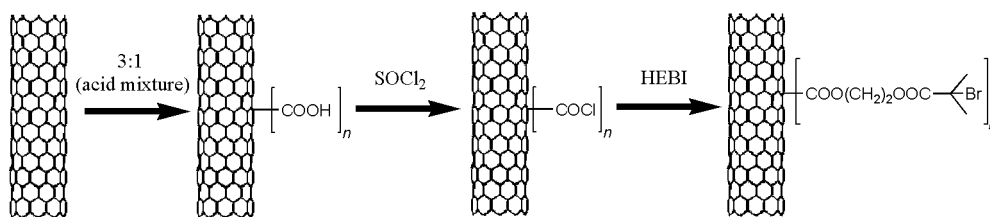
Scheme 3. 2:Mechanism to CNT-Br formation.

Model system: 1-Pyrenecarboxylic acid Functionalization with HEBI

250mg of 1-pyrenecarboxylic acid was sonicated for 20mins in 25mL of thionyl chloride. 20 drops of DMF was also added to help catalyze the reaction (a white gas evolved during its addition). This mixture was then refluxed at 70°C for 24hrs in a nitrogen atmosphere. After this period the thionyl chloride was removed by vacuum and a catalytic amount of TEA (0.05g) and 10mL of HEBI was injected. Once again the mixture was refluxed at 70°C for six days under nitrogen. Excess HEBI was removed by vacuum and the product was washed with toluene/water. The toluene was removed by nitrogen flow and dried at 40°C, 100mbar for 24hrs.

CNT-Br as the Initiator: Polystyrene Brushes

15mg of CNT-Br with 1mL of anisole, and a magnetic stirrer were added to a nitrogen purged vial. Following this, $CuBr_2$ (2.17μmol) with 1mL of anisole, Me_6TREN (21.7μmol), and styrene (43.49mmol) were added to the vial. The polymerization was initiated by the addition of $Sn(EH)_2$ (21.7μmol) with 0.5mL of anisole. The polymerization was carried out at 100^oC and stopped at regular intervals by exposure to the air. In addition, the nanotube-polymer was filtered using the PTFE membranes and washed with room temperature methanol (CNT-PS).

Polystyrene Polymer Brush Hydrolysis

10mL of a 1M KOH/ethanol solution was added to 20mg of CNT-PS in 40mL of THF. The mixture was refluxed at 80^oC for 72hrs, followed by filtration and then re-dissolved into THF. The resultant polymer was precipitated by the addition of acidified methanol.

CNT-Br as the Initiator: Poly(methyl methacrylate) Brushes

15mg of CNT-Br with 1mL of anisole, and a magnetic stirrer were added to a nitrogen purged vial. Following this, $CuCl_2$ (2.34μmol) with 1mL of anisole, Me_6TREN (23.4μmol), and MMA (46.74mmol) were added to the vial. The polymerization was initiated by the addition of $Sn(EH)_2$ (23.4μmol) with 0.5mL of anisole. The polymerization was carried out at 90^oC and stopped at regular intervals by exposure to the air. In addition, the nanotube-polymer was filtered using the PTFE membranes and washed with room temperature methanol (CNT-PMMA).

Acid Treated MWCNT: Poly(2-hydroxyethyl methacrylate) Brushes

250mg of acid treated MWCNT were sonicated for 20mins in 25mL of thionyl chloride. 20 drops of DMF was also added to help catalyze the reaction (a white gas evolved during its addition). This mixture was then refluxed at 70^oC for 24hrs in a

nitrogen atmosphere. After this period the thionyl chloride was removed by vacuum and the resultant acid chloride nanotubes were chilled in an ice bath with the addition of 10mL of purified HEMA and 50mL of diethyl ether. The mixture was refluxed at 50^oC for 24hrs, followed by filtration using a PTFE membrane and washed with diethyl ether.

Model System, Pyrene-HEBI: Polystyrene Brushes

15mg of Pyrene-HEBI with 1mL of anisole, and a magnetic stirrer were added to a nitrogen purged vial. Following this, $CuBr_2$ (2.17μmol) with 1mL of anisole, Me_6TREN (21.7μmol), and styrene (43.49mmol) were added to the vial. The polymerization was initiated by the addition of $Sn(EH)_2$ (43.4μmol) with 1mL of anisole. The polymerization was carried out at 100^oC and stopped at regular intervals by exposure to the air. In addition, the nanotube-polymer was precipitated with cold methanol and captured by filtration using the PTFE membranes (Pyrene-PS).

Results and Discussion

3.3 Nanotube Purification

High resolution electron microscopy (HRTEM) was used to observe the removal of the carbonaceous impurities along the carbon nanotube wall. As can be seen in Figure 3. 2 the successful removal of the carbonaceous material from the carbon nanotube wall has occurred after acid treatment without damaging the exterior walls.

Fourier Transform Infrared (FT-IR) spectroscopy was performed on the L-MWCNT to observe the chemical changes when acid treated and from what can be seen in Figure 3. 3 only minor changes have occurred from the original material. In the spectra, three distinct peaks can be seen; $1380cm^{-1}$, $1460cm^{-1}$, and $1630cm^{-1}$, corresponding to the C-H bend, $-CH_2$ vibrations, and the stretching mode of the quinone groups, respectively.[298]
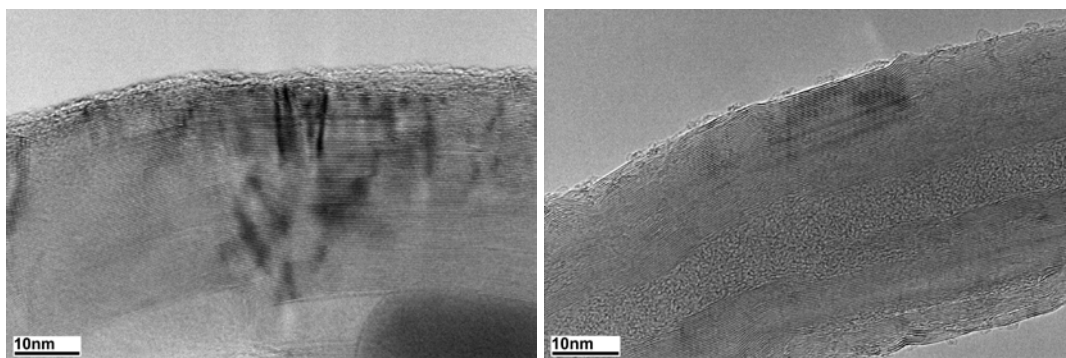
Figure 3. 2: HRTEM images, Left: L-MWCNT starting material, Right: after acid treatment, showing the removal of the carbonaceous impurities from the nanotube wall.

The peak at 1380cm^{-1}, corresponding to a C-H bend, has a lower intensity in CVD nanotubes when compared to pristine arc-discharge nanotubes.[283] This is expected due to the lower concentration of carbonaceous impurities found in CVD nanotubes and furthermore decreases upon acid treatment purification, as shown in Figure 3. 3. In addition, the absorbance band at 1460cm^{-1} follows similar intensity changes, as it is similar in nature to that of the 1380cm^{-1} peak.

The 1630cm^{-1} peak has a small decrease in intensity, which is a result of the 0°C acid treatment. The low temperature used in the purification process is not strong enough to generate a significant increase in new defect sites on the sidewalls, such as the quinone species.[295] This means the acid treatment attacks the already present quinone species and changes their chemical structure to carboxylic acids. This has resulted in a small decrease in the peaks intensity.

A shoulder also appears at 1580cm^{-1}, which corresponds to the stretching mode of carbon-carbon double bonds near oxygenated carbon atoms.[299] Only a small peak can be seen for the L-MWCNT, however this peak increases when acid treated and is a clear indication that an increase of oxygenated species has occurred.

The peak at 1730cm^{-1} supports the results found for the 1580cm^{-1} peak and 1630cm^{-1} peak, as it is assigned to the ν(C=O) of carboxylic acid groups and

symbolizes an increase in oxygenated species,[298] which will be subsequently used for further functionalization. The greater this peak, the greater the possibility to functionalize by forming ester or amide bonds with the carboxylic acid groups.
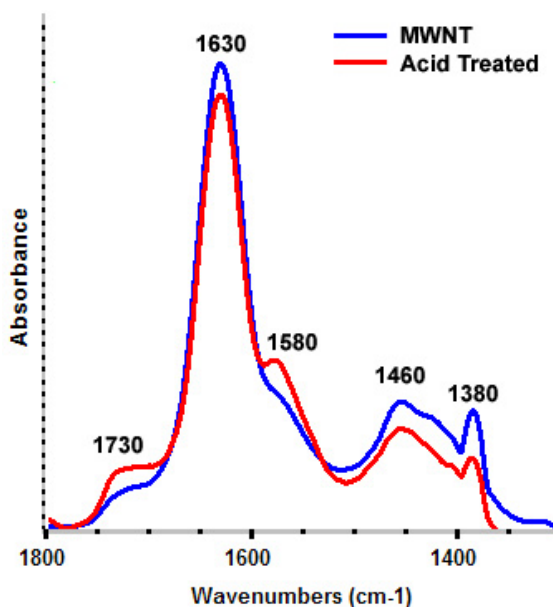
Figure 3. 3: FT-IR spectra of L-MWCNT and acid treated L-MWCNT, demonstrating an increase in carboxylic acid functionality.

3.4 Synthesis of Hydroxyethyl-2-bromoisobutyrate (HEBI)

The hydroxyl terminated HEBI (Scheme 3. 3) was used in the later synthetic steps for esterification of carbon nanotubes, turning them into a macroinitiator with tertiary bromide functionality. The tertiary bromide acts as an initiator for any ATRP process and as it is tertiary, it is a more stable species than primary or secondary bromides.[300]
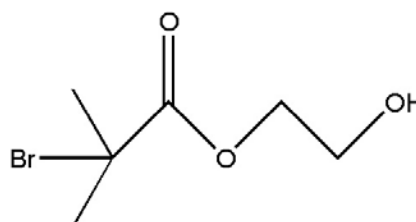
Scheme 3. 3: Chemical structure of HEBI.

The chemical structure was verified using ^{1}H NMR (200MHz, CDCl$_3$) and the same signals as Jakubowski *et al*[301] were observed (i.e. Scheme 3. 4). In addition, the

residue after distillation was also characterized by ^{1}H NMR (200MHz, CDCl$_3$) and it is clear from the signals that the hydroxyl group of HEBI also underwent esterification with 2-bromoisobutyryl bromide resulting in the chemical structure of Scheme 3. 5.

1 - 1.95ppm (s, 6H)

2 - 3.21ppm (s, 1H)

3 - 3.87ppm (t, 2H)

4 - 4.41ppm (t, 2H)
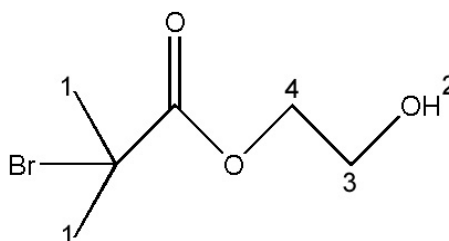
Scheme 3. 4: NMR signals of HEBI.

1 - 1.95ppm (s, 12H)

2 - 4.41ppm (s, 4H)
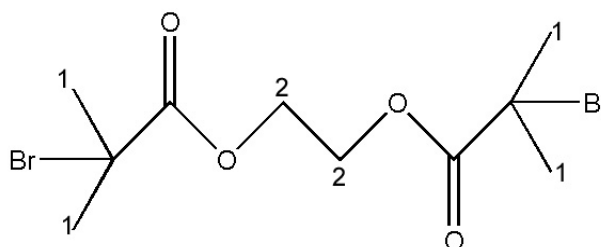
Scheme 3. 5: NMR signals of residual product.

3.5 Carbon Nanotube Functionalization with HEBI

The detection of functionalization was extremely difficult as the extent of functionalization was quite low. No signals relating to the HEBI was detected in FT-IR, or Thermogravimetric analysis (TGA) therefore samples were analyzed by microanalysis. Each carboxylic acid that was functionalized with the HEBI has one bromine atom and therefore the atomic bromine concentration was measured as a way to see the extent of functionalization.

Firstly the oxygen content for the L-MWCNT and the acid treated nanotubes were measured and an increase from 2.37% to 6.70% was observed. When functionalized with the tertiary bromide, readings as high as 5.19% of atomic bromine were observed. This translates to a 77% yield of the HEBI to oxygenated species.

3.6 Model system: 1-Pyrenecarboxylic acid Functionalization with HEBI

The synthetic route to functionalizing 1-pyrenecarboxylic acid with HEBI (Pyrene-HEBI) is similar to the functionalization route of the acid treated L-MWCNT with HEBI (CNT-Br). The major difference between the systems is the ratio of carboxylic acids to aromatic groups is higher in the Pyrene-HEBI than that of the CNT-Br. As a result the signals of characterization have been a lot stronger for the Pyrene-HEBI.
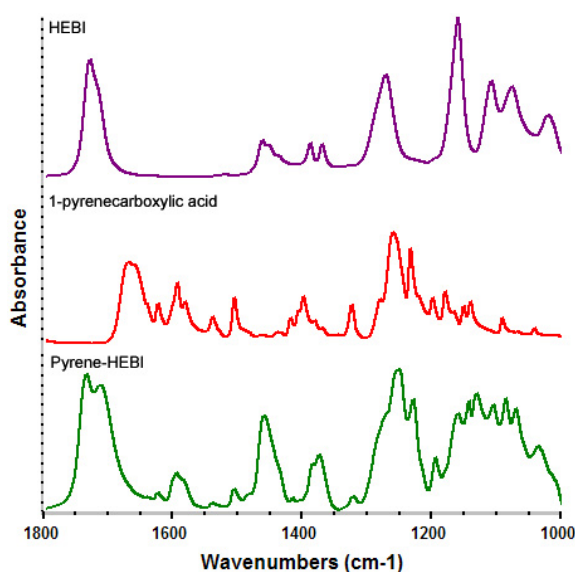
Figure 3. 4: FT-IR spectra of HEBI, 1-pyrenecarboxylic acid, Pyrene-HEBI.

The chemical modification of 1-pyrenecarboxylic acid to Pyrene-HEBI was verified using FT-IR and the spectra can be seen in Figure 3. 4. Firstly the spectra of HEBI and 1-pyrenecarboxylic acid was recorded to find their distinctive peaks and typically these peaks appeared between 1800-1000cm^{-1}. In the HEBI spectra three distinct peaks can be seen; 1730cm^{-1}, 1270cm^{-1}, and 1160cm^{-1}, which can be assigned to the v(C=O) of an ester group, -COO- stretch, and an ester group respectively. Two additional peaks, not shown in Figure 3. 4, 3400cm^{-1} and 2950cm^{-1}, are also present and are responsible for bonded hydroxyl groups and –CH$_2$, -CH$_3$ stretch, respectively.[298] In addition, the 1-pyrenecarboxylic acid spectra had many peaks, all

relating to the main aromatic structure (i.e. 1625cm^{-1} and 1510cm^{-1}) and the carboxylic acid group (i.e. 1660cm^{-1}, 1600cm^{-1}, and 1390cm^{-1}).[298,302]

When the Pyrene-HEBI spectrum was recorded two specific changes to the FT-IR spectra of the reacting components were expected. One of these changes was the loss of the bonded hydroxyl peak at 3400cm^{-1} as the functionalization with HEBI occurs by esterification (i.e. forms by using the hydroxyl groups). The second change was the appearance of a new ester vibration around 1730cm^{-1}, which would indicate the esterification functionalization reaction proceeded. These two changes were observed in the Pyrene-HEBI spectrum; the loss of the 3400cm^{-1} peak and the generation of a new ester vibration at 1713cm^{-1} (i.e. in addition to the already present ester peak of HEBI at 1740cm^{-1}). In addition, the peak at 2950cm^{-1}, responsible for the –CH$_2$, -CH$_3$ stretch was enhanced in strength and three peaks were resolved (i.e. 2950cm^{-1}, 2922cm^{-1}, and 2853cm^{-1}). This has occurred because of the increased concentration of aliphatic carbons from the HEBI.
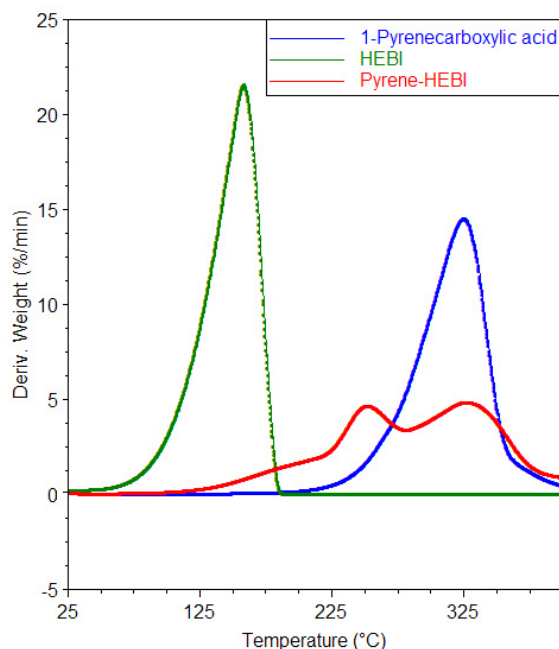
Figure 3. 5: Thermograms of the model system: 1-pyrenecarboxylic acid functionalization.

The thermal decomposition of HEBI, pyrene and Pyrene-HEBI were studied in air, using TGA. The overlay of the related Differential Thermogravimetric Analysis (DTGA) curves are presented in Figure 3. 5. From the DTGA curves the temperature of decomposition of HEBI occurs at 166°C while the decomposition temperature of 1-pyrenecarboxylic acid was found to be 329°C. In the HEBI functionalized pyrene thermogram two broad peaks at 250°C and 329°C were observed, which are related to the decomposition of the ester bonded HEBI groups and pyrene, respectively.

The extent of functionalization was determined using the Pyrene-HEBI thermogram. Using the weight percentage step losses, the calculation found that 0.1629mol of HEBI at 250°C and 0.1978mol of pyrene at 329°C had degraded. This corresponds to a 82% attachment, and indicates that 18% of un-functionalized 1-pyrenecarboxylic acid is present in the material. However, 1-pyrenecarboxylic acid will not act as an initiator in an ARGET ATRP living polymerization as the molecule does not possess the alkyl bromide functionality and therefore will not affect the reaction. Furthermore, after the Pyrene-HEBI has been used in a polymerization, the remaining 1-pyrenecarboxylic acid will be removed by subsequent polymer purification steps.

3.7 CNT-Br as the Initiator

3.7.1 Polystyrene

HRTEM was used to visualize the extent and thickness of the polymer coverage on the MWCNT (see Figure 3. 6). Here it is clear that the amorphous graphitic layer was removed by acid treatment and successful polymerization has subsequently occurred on the exposed nanotube wall. A 10nm thick layer was observed on polymerization for 2640mins. As the polymerization was living, the thickness of the

layer can be altered by the reaction time, or by a subsequent polymerization for chain extension and/or addition of a new monomer to produce copolymer brushes.
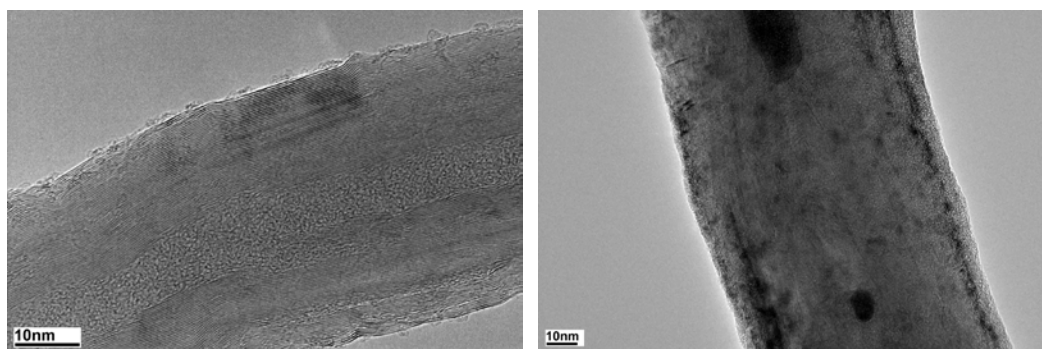
Figure 3. 6: HRTEM images, Left: acid treated nanotubes, Right: CNT-PS, showing the approximately 10nm PS layer.

The extent of polymer attachment was subsequently studied using TGA in an air environment. Polymers have lower decomposition points than MWCNTs so the amount of polymer attached to MWCNTs can be readily determined by the controlled increase in temperature while carefully monitoring the weight loss in the TGA. A typical thermogram of L-MWCNT, CNT-Br, and CNT-PS5 can be seen in Figure 3. 7.

CNT-PS5 decomposes in two steps with the first step (step 1) involving the decomposition of PS, and the second (step 2) the carbon nanotubes themselves. The amount of polymer at approximately $360^{o}C$ (step 1) increased with polymerization reaction time, achieving results as low as 9.5% for 420mins and as high as 84.7% for 3000mins. The complete set of data is summarized in Table 3. 1 and clearly shows an increase in polymer content with reaction time, further supporting the concept that the polymerization is indeed living.[286] An additional step, representing the decomposition of the ester linkage group between the polymer and the nanotube, was not able to be detected. The thermogram of CNT-Br also does not exhibit a separate step for the ester linkage group because the weight percentage contribution of this material is very

small compared to the other components. As the TGA resolution is less than 1%, the signal to noise ratio also made detection impossible.
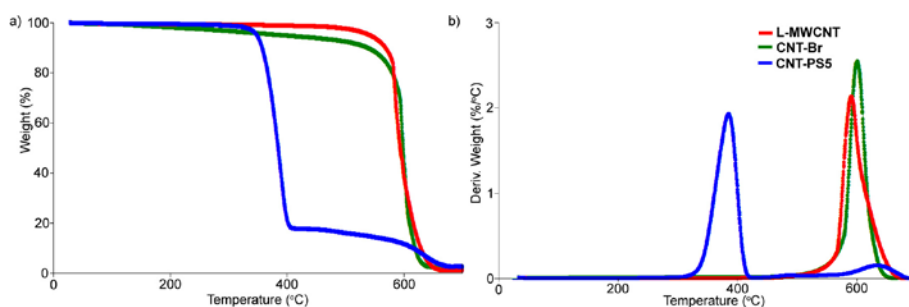
Figure 3. 7: a) Thermogram of L-MWCNT, CNT-Br and CNT-PS5 and b) DTGA of the thermograms, measured in air at $10^{o}C$/min.

Sample	Time (mins)	M_n $(x10^3)^b$	Conv.	Polydispersity[b]	Polymer T_d (^{o}C)	% Polymer
Homo-PS1	90	2.9	0.07	1.22	338	100
Homo-PS2	150	4.7	0.15	1.17	350	100
Homo-PS3	210	8.5	0.29	1.11	353	100
Homo-PS4	270	10.2	0.35	1.10	362	100
Homo-PS5	360	13.6	0.47	1.08	365	100
CA-PS[c]	-	140	-	1.64	400	100
CNT-PS1	420	-	0.0045	-	306	9.5
CNT-PS2	600	-	0.0043	-	334	11.4
CNT-PS3	1140	-	0.0102	-	340	60.4
CNT-PS4	2640	-	0.0157	-	343	72.3
CNT-PS5	3000	94.8	0.0250	1.78	361	84.7

Table 3. 1: Polymerization for ARGET ATRP of styrene [b] determined by GPC in THF, polystyrene standard. Homo-PS(1 to 5) St/EBiB/CuBr₂/Me₆TREN/Sn(EH)₂ (300/1/0.015/0.15/0.15) and CNT-PS(1 to 5) St/CuBr₂/Me₆TREN/Sn(EH)₂ (300/0.015/0.15/0.15) with 15mg of CNT-Br. [c] Commercially available polystyrene was purchased from Aldrich.

In order to study the amount of homopolymer non-covalently attached to the carbon nanotubes surfaces, a control experiment was conducted, where all the components of the polymerization were again mixed, with the exception that acid treated L-MWCNT was added instead of the CNT-Br. This created a mixture that was not initiated by living polymerization. After heating for 12hrs and

purification/filtration, the TGA thermogram showed 12% polymer content (see Figure 3. 8 Left). This 12% did not change with the reaction time, and therefore clearly demonstrates that under these experimental conditions some spontaneous polymer growth can still occur. It also shows that the 12% free polymer produced is independent of reaction time. Now in the polymer brushed material, the amount of non-covalently bound polymer is expected to be less than 12%. When a CNT-PS material is formed, the attached polymer would preferentially π-π stack to the nanotube walls due to the restricted freedom and proximity, than to free polymer chains. In addition, any free polymer chains are likely to be washed away during the filtration process leaving only the covalently-bound chains attached to the isolated MWCNTs. In addition, acid treated L-MWCNT was also mixed with CA-PS in heated anisole for an extended period of time, and this too resulted in a 12% polymer content (see Figure 3. 8 Right), further supporting the finding that a maximum of 12% of PS can associate with carbon nanotubes through the physical mixing of the components.
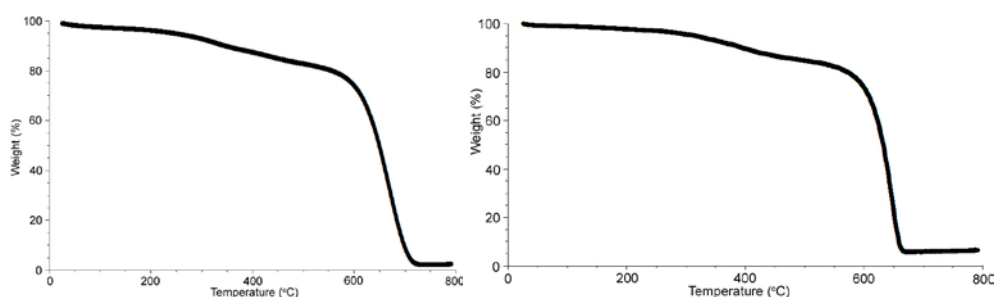
Figure 3. 8: thermograms of the controlled experiments, Left: a mixture of styrene and acid treated nanotubes and Right: a mixture of CA-PS and acid treated nanotubes. Each thermogram shows 12% polymer content.

The decomposition temperatures (T_d) are shown in Table 3. 1. The T_d increases with increasing molecular weight; the homo-PS1 showing a T_d of 338°C, which increases to 365°C for the higher molecular weight homo-PS5, and increases further

for commercially-available PS (CA-PS) (i.e. 400°C), having the highest molecular weight. Due to the living nature of the polymer-brush nanotubes, they too have an increasing molecular weight with increasing polymerization time that then leads to the higher polymer content (see Table 3. 1). It was therefore expected that the T_d of the CNT-PS series (1,2,3…5) would also show an increasing trend for T_d with increasing molecular weight. The thermograms of the polymer brush nanotubes exhibited two T_ds, one relating to the decomposition of carbon nanotubes at approximately 600°C, which remains unaffected by the polymer content, and the lower T_d corresponding to the polymer. The polymer T_d occurs at approximately 306°C for CNT-PS1 and increases to 361°C for CNT-PS5. This supports the trend found for the homopolymer, and also suggests that by growing the chains longer, the T_d becomes closer to the T_d of the CA-PS.

The polydispersity and molecular weight was studied using gel permeation chromatography (GPC) and can also be seen in Table 3. 1. From Table 3. 1, the polydispersity for the homopolymers falls in the range 1.08-1.22; however the polydispersity of the polymer brushes reaches 1.78 (i.e. after cleavage from the MWCNT by basic hydrolysis). Generally polydispersities of 1.78 are considered large for living free radical processes. However, in previous research by Kong *et al*[303] where polymer brush carbon nanotubes were produced using conventional ATRP, a polydispersity of 1.77 was found, and similarly other reports, where surface initiation of ATRP is used, have recorded values as high as 3.08.[269,304] Typically EBiB is used as the initiator in ARGET ATRP due to the stability of the tertiary bromide creating well initiated and controlled living polymers as evident by the GPC results in Table 3. 1.[305] It was thus expected that the polymer brush polydispersity would also be in the range of 1.1, as the chemical structure of HEBI was similar to that of EBiB. The key

difference that accounts for the increase is the HEBI is being anchored to the nanotube, and is no longer mobile like EBiB in solution. This would suggest that the polymerization acts more like surface initiated (SI) ARGET ATRP, rather than non-SI ARGET ATRP. Previous research by Matyjaszewski *et al*[285] has shown that SI ARGET ATRP on planar surfaces (i.e. Si wafer) leads to polymers with a higher than normal polydispersity due to the restricted movement of the tertiary bromides and the high reactant ratios. The nanotubes large amount of cylindrical surface area then produces a similar affect in this case, but with a lesser degree of this restricted movement as the CNT-Br has some dispersion through the solution. Although polydispersity has increased, the benefit comes from the ease of polymerization and with the resulting polymer having no catalyst contamination, makes this approach of considerable commercial benefit. The living nature of the polymerization was then further explored using the kinetic plot shown in Figure 3. 9, where the linear trend in the graph shows that the polymerization was indeed living.
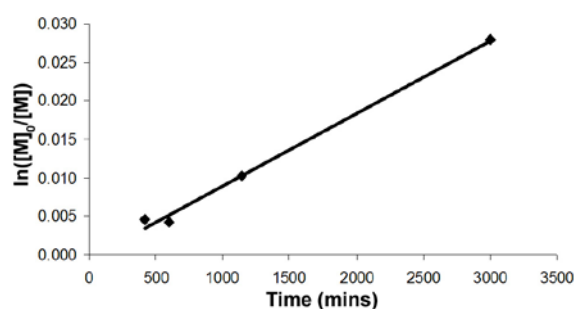
Figure 3. 9: Kinetic plot for ARGET ATRP of styrene using a CNT-Br initiator (R^2 = 0.9946).

The benefits of the ARGET ATRP procedure are (i) a reduced amount of copper catalyst is required (i.e. the resultant polymer lacks the green tinge commonly seen in normal ATRP-produced polymers) and (ii) with the use of $Sn(EH)_2$ as a reducing agent, less sensitivity to air is encountered. As the molar ratio of Sn used is quite low, its removal should be relatively easy like that for the trace amounts of copper.

TEM/Energy Dispersive X-ray (EDX) spectroscopy was used to see if any residual tin was still present in the polymer brush samples. An extremely weak tin signal was barely visible above the background noise. Elemental mapping of this signal indicated that no localized regions of elemental tin, or for that matter copper, existed. These results demonstrate that although the elemental catalysts are there, they are not in significant quantities to allow ready detection.
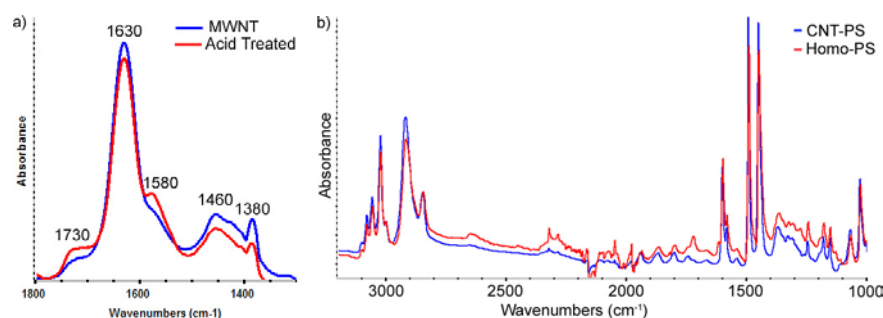
Figure 3. 10: FT-IR spectra of a) as received MWCNT and acid treated MWCNT. An increase in the 1730cm^{-1} peak can be seen indicating an increase in carboxylic acid functionality. b) CNT-PS and Homo-PS. The spectra of CNT-PS does not exhibit any peaks of the nanotube.

Using FT-IR, the carbon nanotubes and polymer brush chemical composition were examined. The typical peaks associated with carbon nanotubes were observed at 1380cm^{-1}, 1460cm^{-1}, and 1630cm^{-1} corresponding to the C-H bend, -CH$_2$ vibrations, and the stretching mode of quinine groups respectively.[306] Upon acid treatment, an increase of the peak at 1730cm^{-1} was observed (Figure 3. 10a)) and is related to carboxylic acid functionality that results from the oxidation of the carbon nanotubes during acid treatment.[283] Once polymer growth occurred from the CNT-Br surface, these characteristic carbon nanotube peaks were no longer seen as the signal was too weak to detect in comparison to the strong PS spectra seen in Figure 3. 10b). This

strong PS spectra arises from the PS polymer brushes that are clearly seen in the HRTEM images (Figure 3. 6 Right).

Carbon nanotubes alone show no melting (T_m), crystallization (T_c), or glass transition temperature (T_g). However upon addition of polymer chains to the carbon nanotubes, a T_g is observed using differential scanning calorimetry (DSC) (see Figure 3. 11). The T_g recorded for the CA-PS was measured to be 102.2°C, whilst for CNT-PS3, the T_g increases to 116.2°C and another 1-2°C as the molecular weight/content of the brushes increased for CNT-PS4 and CNT-PS5. Both CNT-PS1 and CNT-PS2 samples showed no detectable T_g as the polymer brush content was too small (i.e. 9.5% and 11.4%, respectively). Overall this represents a 14.0°C increase in T_g and defines the nanotube as a reinforcing agent in long polymer brush carbon nanotubes. The carbon nanotubes here not only reduce polymer chain mobility on attachment,[307] but also promote new π-π stacking between the nanotube and the aromatic polymer.[263]
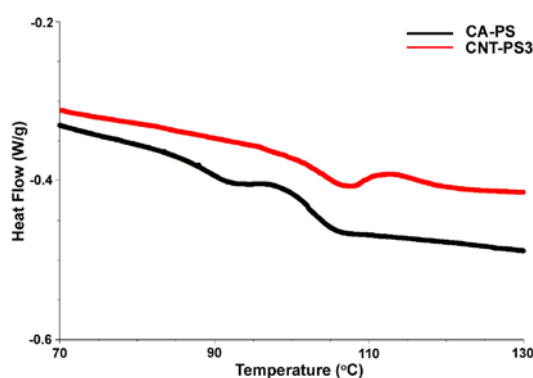
Figure 3. 11: The first detectable T_g in the CNT-PS samples, which did not change significantly when increasing the polymer chain length.

The presence of the PS produces additional, weak peaks in the Raman spectra (see Figure 3. 12 and Table 3. 2) of these functionalized nanotubes at 1000cm^{-1}, 1029cm^{-1}, and 3056cm^{-1} corresponding to ring out-of-plane deformation, ring in-plane CCH bend, and CH ring stretching respectively.[308] The main focus however, of the Raman

measurements remains on the typical D and G modes of carbon nanotubes; (i) the D mode (disorder mode) at 1330cm^{-1} is caused by sp^3-hybridized carbon atoms (e.g. COOH) in the nanotube sidewalls or defects that break the translational symmetry, and (ii) the G mode (tangential mode) at 1580cm^{-1} corresponds to the movement in opposite directions of two neighboring carbon atoms in a graphitic sheet.[309,310,311] Barros *et al*[312] found that in SWCNT, an upshift to the Raman peaks occurs due to the charge transfer from the nanotube to its carboxylic acid functional group, and was similarly observed as an increase of approximately 2cm^{-1} for the G band upon acid treatment occurred (i.e. an increase due to carboxylic acid functionalization). However, once the CNT-Br were polymerized, the long polymer chains effectively neutralized this charge transfer affect causing a downshift (see Table 3. 2). In addition, like Wu *et al*,[313] it was found that the I_D/I_G intensity ratios increased when functionalized with oxygen moieties (i.e. upon acid treatment) yet alter again when functionalized with PS. In the Raman spectra of Figure 3. 12, the I_D/I_G ratio increased from 0.65 to 1.28 upon acid treatment, and had changed again once the PS chains had grown, providing further evidence for covalently bound PS.

In comparison to the control reaction, a charge transfer affect occurred as well, but was then neutralized by the π-π stacked, non-covalently bound, polymer chains physically associated with the nanotube (see Table 3. 3). The charge transfer affect can be neutralized by covalently bound alkyl chains as short as six carbons long.[283] This would indicate that the charge transfer affect can be neutralized by covalently bound species as well as other additional forces.
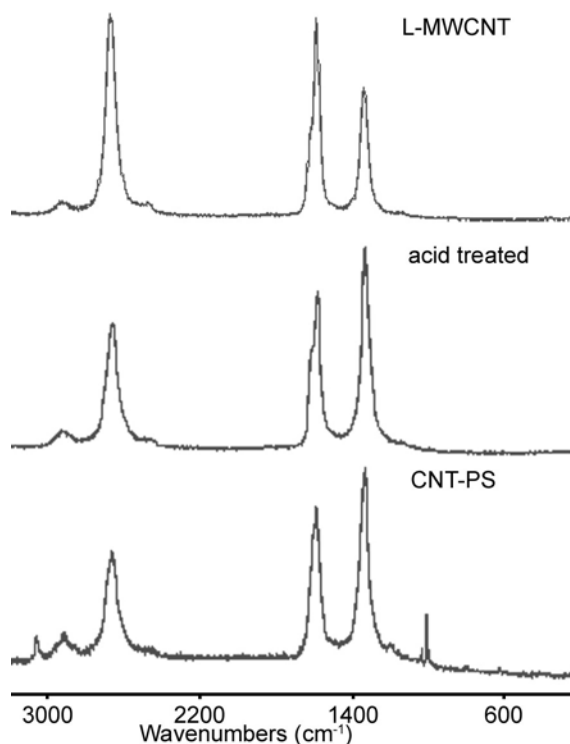
Figure 3. 12: Raman spectra of L-MWCNT, acid treated L-MWCNT, and CNT-PS. The

CNT-PS spectra has additional peaks typical of a polystyrene spectra.

Sample	G' band	G band	D band
L-MWCNT	2663	1582	1332
Acid treated	2662	1584	1332
CNT-Br	2663	1585	1334
CNT-PS	2660	1583	1332

Table 3. 2: Raman Peak Positions (cm^{-1}).

Sample	G'band	G band	D band
L-MWCNT	2663	1582	1332
Acid Treated	2662	1584	1332
CNT-Br	2663	1585	1334
Controlled[a]	2660	1582	1333

Table 3. 3: Raman Spectra results of controlled styrene experiment. [a]Produced by

heating a mixture of CA-PS with acid treated nanotubes in anisole.

The polymer brush-MWCNT electrical conductance was measured by obtaining

IV curves of mechanically pressed samples. These curves can be seen in Figure 3. 13

where the polymer brush nanotubes had a shiny film appearance that could be

stretched by hand. The L-MWCNT and acid treated L-MWCNT samples measured

0.020S and 0.016S, respectively, which decreased further to 1μS for CNT-PS5. This

was in line with the previous work by Curran *et al*,[314] who found that pristine MWCNT are better conductors than acid treated L-MWCNT; the acid treatment generates defect sites, which disrupt the electron ballistic transport of carbon nanotubes, and therefore decreases their conductance. Furthermore, the concentration of nanotubes within a polymer matrix affects conductance, as CNT-PS5 has 84.7% polymer in the sample compared to no polymer in the L-MWCNT and the acid treated L-MWCNT, the conductance is lower in the CNT-PS5. While the polymer interrupts the flow of electrons, it can be readily pressed into films and so possible applications still exist in making electrically or thermally conductive films/coatings, depending on the nanotube concentration that can be attained.

Contact angle measurements of the representative sample CNT-PS5 are summarized in Table 3. 4. Due to the very low mismatch of surface energies between Homo-PS5 and CNT-PS5 it is expected that the CNT-PS samples will be well dispersed in a PS matrix. Despite the fact that the total surface energies of Homo-PS5 and CNT-PS5 are very similar, the polar components and non-polar components of the polymer brushes decreased by 1.5 and 3.6mN/m, respectively. From Table 3. 4 it is clear that the non-polar components of the total surface energy are dominant in the samples, indicating that the CNT-PS has now developed an affinity for the non-polar PS matrix.
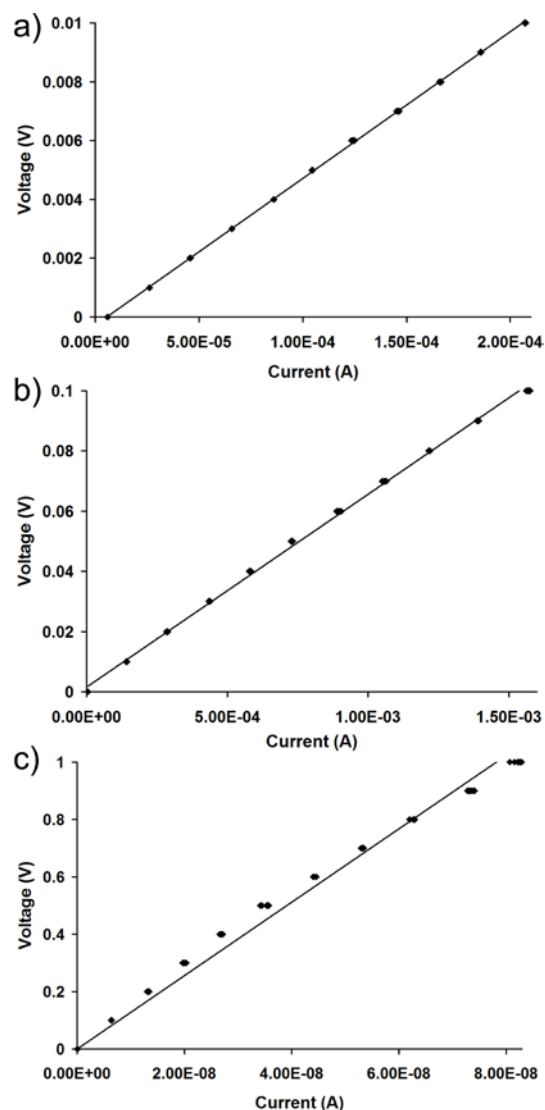
Figure 3. 13: IV curves for a) L-MWCNT, b) acid treated L-MWCNT, and c) CNT-PS5.

Sample	Water Angle	CH_2I_2 Angle	Polar Component (mN/m)	Non-Polar Component (mN/m)	Total Surface Energy[α] (mN/m)
Homo-PS5	$83.70^o \pm 4.32^o$	$24.63^o \pm 2.60^o$	1.5	46.3	47.8
CNT-PS5	$98.91^o \pm 1.27^o$	$31.66^o \pm 1.78^o$	0	42.7	42.7

Table 3. 4: Sessile drop contact angle measurements. [α] calculated using Windrop++.

It is clear from these results that the properties of the PS polymer brush carbon nanotubes are greatly benefited by the π-π stacking capabilities and hydrophobic nature. However, not all polymers possess this ability and therefore PMMA has been explored as a polymer brush in the next section.

3.7.2 Poly(methyl methacrylate)

In contrast to PS as a hydrophobic polymer, MMA was used to create PMMA polymer brushes. The chemical differences in this particular monomer were that it has no aromatic groups and is a more polar monomer than styrene. This should produce a material that can not π-π stack with the carbon nanotubes graphene aromatic walls and would have a tendency to repel from the much less polar nanotube walls.

The evidence of polymeric growth was observed by HRTEM, which was also used to determine the thickness of the polymer coverage. It is clear in Figure 3. 14 that after the successful removal of the amorphous graphitic layer and tertiary bromide functionalization, MMA can be successfully polymerized, using ARGET ATRP, from the nanotube wall just like styrene in section 3.7.1. A layer as thick as 15nm has been observed after 480mins.

It is important to note that a much thicker layer is produced in the CNT-PMMA samples in only a fifth of the CNT-PS reaction time. The increase in the polymeric layer is due to the higher reactivity of MMA in ATRP systems.[300] Furthermore, PMMA on its own is naturally a more dense polymer than PS, indicating longer PMMA polymer chains for the same thickness (i.e. PMMA 1.17g/cm^3, PS 1.05g/cm^3).[315]
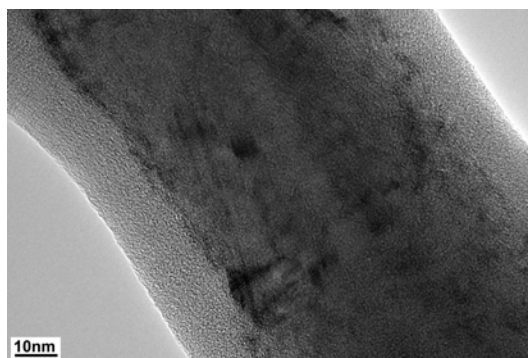
Figure 3. 14: HRTEM image, CNT-PMMA1, showing the approximately 15nm PMMA layer.

The livingness of the polymerization was explored using the kinetic plot shown in Figure 3. 15. The kinetic plot is linear and provides evidence of a living polymerization occurring. However, the results of Chapter 2 indicated that using ARGET ATRP to polymerize MMA with EBiB, provided poor initiation and due to the similar chemical structure of the HEBI, used for the polymerization to CNT-PMMA, a similar result is expected. This would also result in a higher polydispersity than the result found for the CNT-PS and is recommended as a future study.
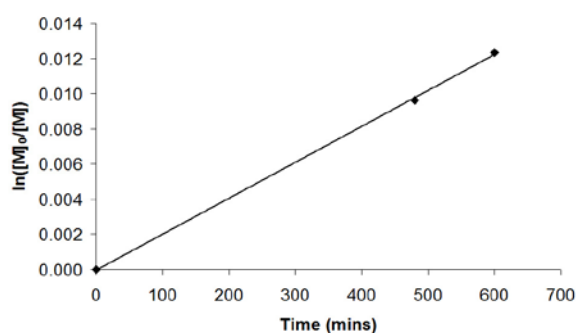
Figure 3. 15: Kinetic plot for ARGET ATRP of MMA using a CNT-Br initiator (R^2 = 0.9995).

The glass transition temperatures presented in Table 3. 5 were determined using DSC, and no noticeable pattern with respect to molecular weight was observed. The average T_g found for the Homo-PMMA(1,2,3,4) was approximately 122°C, for the CA-PMMA it was 117°C and for CNT-PMMA(1,2) it was 134°C. These results show that the samples produced by ARGET ATRP (i.e. living polymerization) exhibited a polymer with a higher T_g than the commercially, free radical polymerization, produced polymer (CA-PMMA). This represents a 12°C increase for the homopolymers and a 17°C increase for the polymer brush material. The large increase in the CNT-PMMA T_g was also experienced for the CNT-PS (i.e. 14.0^{o}C increase) and infers that the increase is independent of the type of attached polymer; whether it is polar or non-polar, or if it has π-π stacking capabilities. Furthermore, the results indicate that for PMMA the increase is due to the living polymerization technique,

which increases further when covalently attached to carbon nanotubes (i.e. the nanotubes ability to act as a reinforcer).[307]

Sample	Time (mins)	M_n $(x10^3)^b$	Conv.	Polydispersity[b]	Polymer T_d (^{o}C)	% Polymer	T_g (^{o}C)
Homo-PMMA1	10	12.4	0.08	1.22	282	100	117
Homo-PMMA2	30	13.3	0.21	1.24	286	100	124
Homo-PMMA3	50	16.2	0.30	1.23	293	100	126
Homo-PMMA4	70	17.7	0.42	1.29	295	100	120
CA-PMMA[c]	-	120	-	-	303	100	117
CNT-PMMA1	480	-	0.013	-	338	75	134
CNT-PMMA2	600	-	0.016	-	339	78	134

Table 3. 5: Polymerization for ARGET ATRP of MMA [b] determined by GPC in THF, polystyrene standard. Homo-PMMA(1 to 4) MMA/EBiB/CuCl$_2$/Me$_6$TREN/Sn(EH)$_2$ (200/1/0.01/0.1/0.1) and CNT-PMMA(1 to 2) MMA/CuCl$_2$/Me$_6$TREN/Sn(EH)$_2$ (200/0.01/0.1/0.1) with 15mg of CNT-Br. [c] Commercially available poly(methyl methacrylate) was purchased from Aldrich.

The decomposition temperatures reported in Table 3. 5 were determined using TGA. The average T_d for the homo-PMMA(1,2,3,4) was 289°C (note: the T_d increases with increasing molecular weight), and for the CNT-PMMA(1,2) the T_d was approximately 338°C. The CA-PMMA was 303°C, which shows a good agreement with the homo-PMMA(1,2,3,4) samples. However, these results are at a minimum 35°C lower than the CNT-PMMA(1,2) samples and demonstrates that the carbon nanotube thermally stabilizes the PMMA. This is a similar result found by Chowdhury *et al*[316] where they experienced a 37°C increase in thermal stability upon adding 0.5wt% of SWCNT to PMMA.

In addition, the polymer content was determined from the thermograms and in the CNT-PMMA1 sample the polymer content was 75% for 480mins, which increased to 78% for the CNT-PMMA2 at 600mins. This increase with reaction time was expected

as the polymerization was living, which supports the results found in the kinetic plot of Figure 3. 15, and was a similar affect found in the CNT-PS samples. However, the CNT-PS samples produced a smaller polymer content in comparison to the CNT-PMMA samples of similar reaction time; for a reaction time of 600mins CNT-PS creates 11.4% polymer content compared to CNT-PMMA creating 78%. This supports the concept that MMA is a more reactive monomer than styrene in an ARGET ATRP polymerization.[300]
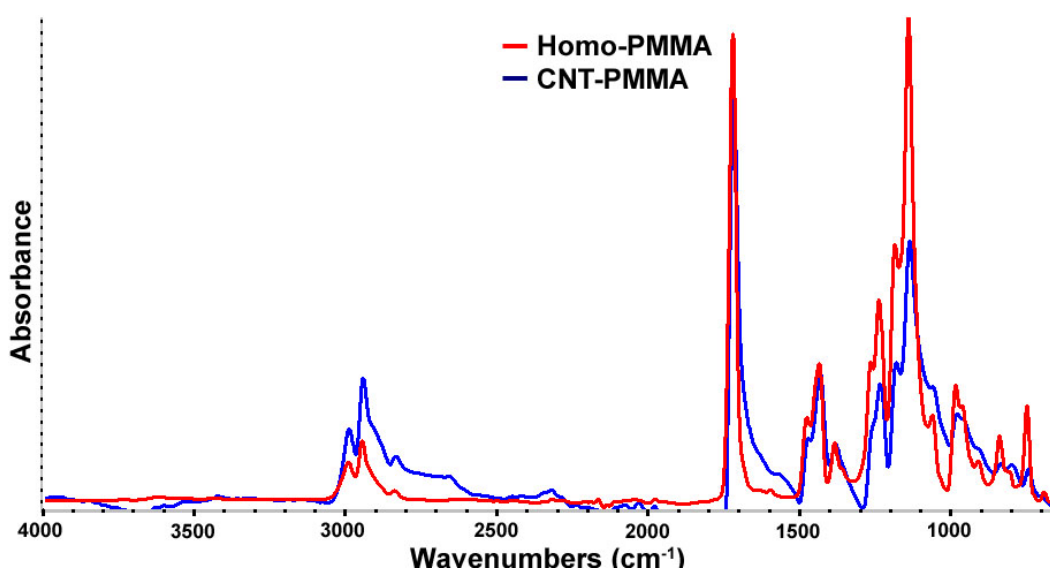
Figure 3. 16: FT-IR spectra of CNT-PMMA and Homo-PMMA. The spectra of CNT-PMMA does not exhibit any peaks of the nanotube, only the PMMA signals.

The chemical composition of the CNT-PMMA samples were studied using FT-IR, and as can be seen in Figure 3. 16 the characteristic peaks of carbon nanotubes were not observed, only the signals of PMMA. This has been discussed before in section 3.7.1, which deduced that the concentration of carbon nanotube functional groups is significantly small to detect by FT-IR, and therefore only the polymer signals can be detected.

It is clear that the properties of a living polymer brush can be affected by its hydrophobicity and by its ability to π-π stack. To extend on this work PHEMA has

been studied in the next section as a non-living polymer brush that can not π-π stack. In addition, it is comparable to PMMA as they are both of the same polymer family (i.e. methacrylates).

3.8 Acid Treated MWCNT: Poly(2-hydroxyethyl methacrylate) brushes

In addition to the materials produced in section 3.7, a FRP polymer brush nanotube was produced. In this technique the nanotube was not synthetically modified into a "macroinitiator" by functionalizing it with tertiary bromides, instead the nanotube was functionalized with vinyl groups turning the nanotube as a whole into a poly-monomeric unit. This was accomplished by firstly creating acid chloride nanotubes, followed by the addition of HEMA. The hydroxyl group of the HEMA creates an ester bond to the nanotube resulting in a vinyl group functionalized nanotube, which can then be polymerized. The synthetic route of vinyl functionalized nanotubes can be seen in Scheme 3. 6.
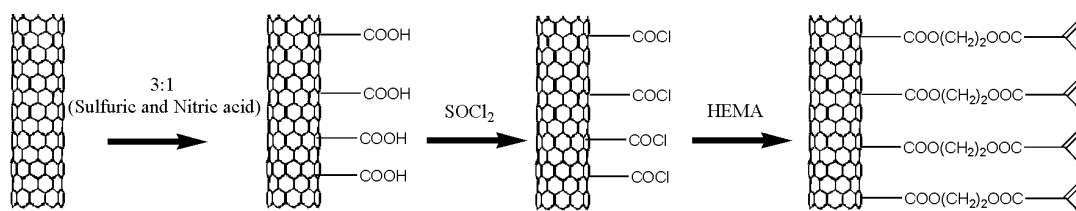
Scheme 3. 6: The synthetic route to vinyl functionalized nanotubes.

The use of a nanotube monomer to create polymer brushes has some chemical and structural differences in comparison to using the nanotube "macroinitiator" in living polymerizations. As the technique for using the nanotube monomer is an uncontrolled free radical polymerization, this would create a material with a high polydispersity (i.e. greater than 2) and an uncontrolled polymer chain length independent of reaction time.[317] Furthermore, when compared to the living technique the end of the polymer chain is "alive", can be reinitiated, but in the PHEMA brushes the material is "dead",

can not be reinitiated, which also creates a non-distinctive chain end for further functionalization or block copolymer formation.[318]

Chemically the HEMA nanotube acts differently in the polymerization as the nanotube has many vinyl groups. Each vinyl group is a possible site for polymerization, which can propagate to produce a material of highly cross-linked nanotubes having more than one nanotube within a polymer chain or contain no nanotubes within a chain (refer to the model diagram in Figure 3. 17). In an attempt to avoid nanotube cross-linking the polymerization was carried out at low temperatures to favor terminating reactions, as well as using low concentrations of nanotubes to decrease the probability of the nanotubes aggregating.[319] However, in the attempt to avoid nanotube cross-linking, the probability of homopolymer creation increases, which can be difficult to separate from the brushes due to the strong hydrogen bonding from the hydroxyl groups. Matyjaszewski *et al*[290] also reported this problem in his work of removing free homopolymer from a polymer brush silicon wafer surface and therefore is seen as an unavoidable outcome in the PHEMA polymer brush nanotubes.
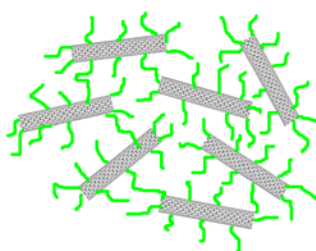
Figure 3. 17: A model drawing of how PHEMA could react in this system. Some polymeric chains have more than one nanotube.

The carbon nanotube sample increased in weight due to the growth of PHEMA brushes on the carbon nanotube wall and the production of free PHEMA polymeric chains. These brushes were observed using HRTEM and can be seen in Figure 3. 18.

The image shows an approximately 5nm thick coating of PHEMA polymer around the nanotube. This thickness was not dependent on reaction time like in the previous section (i.e. section 3.7: living brushes) nor could it be increased by a subsequent polymerization.
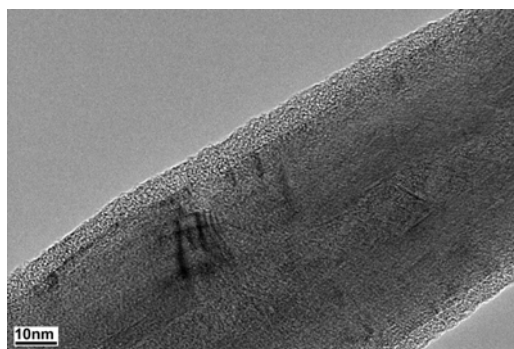
Figure 3. 18: HRTEM image of CNT-PHEMA, showing the approximately 5nm PHEMA layer.

The polymer content was study using TGA and a typical thermogram can be seen in Figure 3. 19. In the thermogram it is clear that the first step is due to the PHEMA polymer and the second was produced by the degradation of the carbon nanotube. However, the FRP procedure for producing CNT-PHEMA is uncontrolled and therefore the polymer content would also change between samples (i.e. the height of the first step). The results seen in Table 3. 6 are therefore a representation of what was observed for many samples and typically the polymer content ranged from 50 to 80%. This polymer content further supports the HRTEM results that polymer brushes were formed on the carbon nanotube.

The decomposition temperatures were determined and the results are displayed in Table 3. 6. What is observed is a reduction by 4°C of the T_d and this particular affect was also seen previously in the CNT-PS samples (section 3.7.1). When these results are compared, it is clear that the PHEMA is also a polar polymer like PMMA and could experience similar repulsion properties to the non-polar nanotube walls.

PHEMA also has an inability to π-π stack as it is not an aromatic polymer. Overall the CNT-PS decreases by approximately 40°C when compared to CA-PS, CNT-PMMA increases by 35°C when compared to CA-PMMA, and CNT-PHEMA decreased by 4°C. However, structurally PHEMA has many similarities to the nanotube in terms of oxygenated moieties,[320] which therefore has the greatest attraction and was unlikely to hinder the T_d compared to the chemically dis-similar PS or PMMA. Furthermore, the large decrease in the CNT-PS sample was due to the large difference in molecular weight. The difference in the T_d is expected to decrease with an increase in molecular weight (i.e. following the trend exhibited in the results, until comparable to the CA-PS molecular weight).
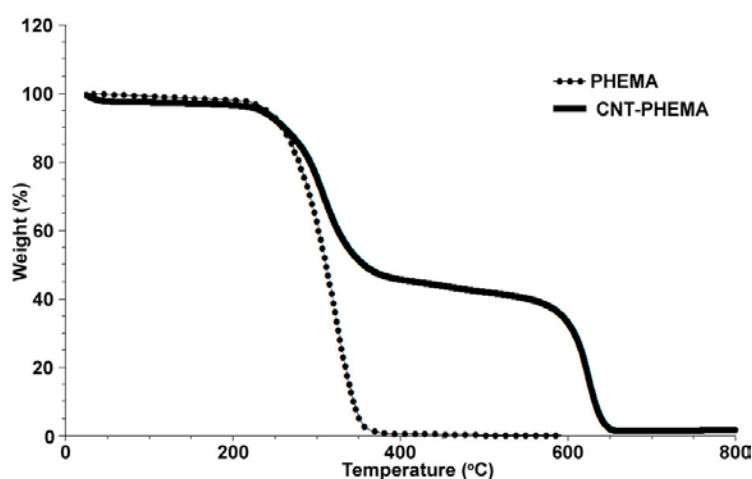
Figure 3. 19: Thermograms of PHEMA and CNT-PHEMA produced by FRP.

Sample	Polymer T_d ($^{\circ}$C)	T_g ($^{\circ}$C)	% Polymer
PHEMA[a]	276	96	100
CNT-PHEMA	272	113	50-80

Table 3. 6: Thermal properties of PHEMA and CNT-PHEMA. [a] The PHEMA was

produced using purified HEMA, benzoyl peroxide (1000:1) and light in a bulk

polymerization.

The CNT-PHEMA samples also exhibited a T_g as other polymer brush nanotube samples have done in the previous sections when there was sufficient polymer content. These results are tabulated in Table 3. 6, which exhibit a T_g of 96°C for the

bulk polymerized PHEMA and a T_g of 113°C for the CNT-PHEMA. Overall this represents a 17°C increase in the T_g. Similarly the PMMA T_g increased by 17°C, which has a comparable chemical structure to PHEMA and hence the similar increase. In addition, PS increased to a lesser extent by 14°C. These increases were attributed to the stronger hydrogen bonding forces in the PHEMA and PMMA polymers, compared to the π-π stacking capabilities of the PS,[321,322] creating a more rigid structure in the hydrogen bonded polymers.

Using FT-IR, the chemical structure was determined and as previously seen, no signals of the carbon nanotubes were detected due to the low concentration/ratio of carbon nanotube functional groups to polymer functional groups. An overlay of CNT-PHEMA and PHEMA spectra are shown in Figure 3. 20 with significant similarities in the peaks, however two particular peaks have greatly changed in intensity. These peaks are 1710cm^{-1} and 3430cm^{-1} corresponding to ester vibrations, and hydroxyl groups respectively.[323] A cross-linking reaction can occur between the hydroxyl groups and in this case these two peaks are related to one another; the more cross-linking that occurs the lower the hydroxyl peak and hence the greater the ester peak.[324] It is noticed that in the PHEMA material, produced by bulk polymerization, a greater extent of cross-linking has occurred compared to the CNT-PHEMA brushes produced in a solution based polymerization. This happened because the solution based polymerization has low concentrations of nanotubes, which lowered the probability of cross linking,[319] whereas in bulk polymerization no solvent is used, hence the cross-linking occurred. In addition, the strong presence of hydroxyl groups allow for future functionalization, previously thought impossible when compared to the distinct living tertiary bromide end of ARGET ATRP polymer brush nanotubes.[318]
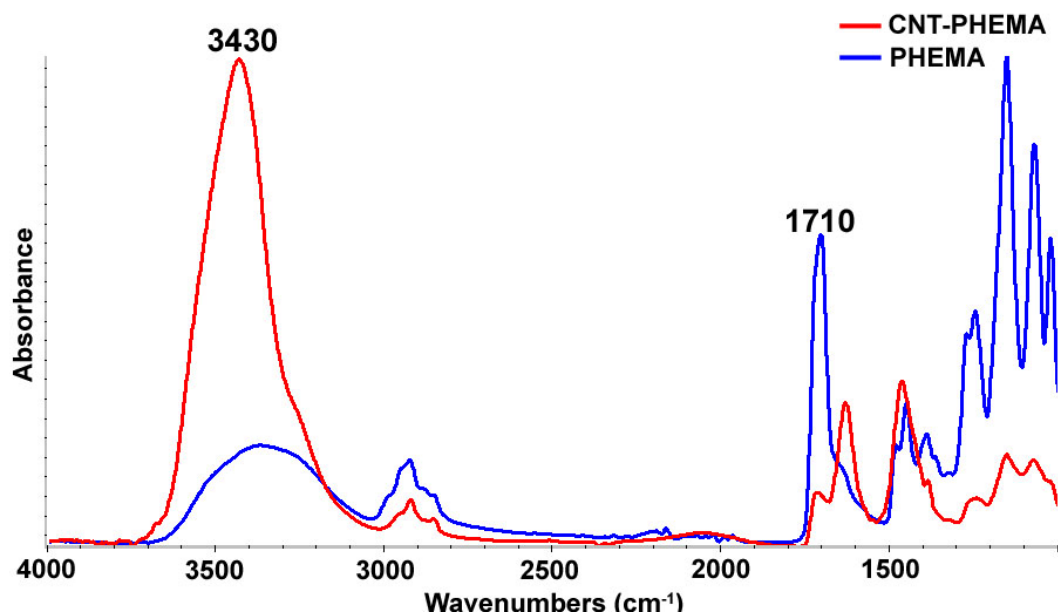
Figure 3. 20: FT-IR spectra of CNT-PHEMA and PHEMA. The spectra of CNT-PHEMA does not exhibit any peaks of the nanotube.

The polymer brush electrical conductance was measured by obtaining an IV curve of the mechanically pressed sample (see Figure 3. 21). From this curve it was found that the CNT-PHEMA sample had a conductance of 3μS and in comparison to section 3.7.1 the conductance result of CNT-PS5 was 1μS. This is a three times increase in conductance and was expected due to the difference in polymer content. In the CNT-PS5 sample the polymer content was 84.7%, however in the CNT-PHEMA sample the polymer content ranged from 50-80% between samples; the content is lower and therefore less polymer to impede the flow of electrons thus the increase in conductance. Furthermore, the conductance is lower than the L-MWCNT, and the acid treated L-MWCNT as those samples contain no polymer to impede the flow of electrons. Similar to the CNT-PS5 sample, this material can also be pressed into films and therefore possible applications exist in the area of conductive films/coatings provided a high enough concentration of nanotubes is achieved.
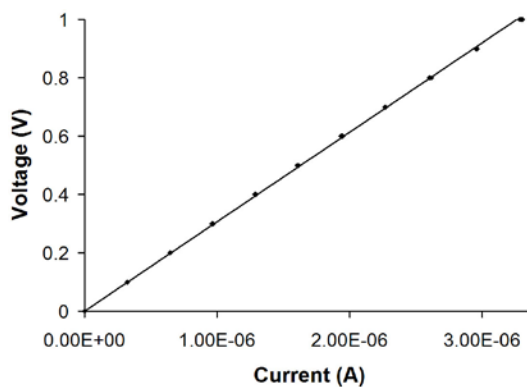
Figure 3. 21: IV curve of CNT-PHEMA.

3.9 Model System, Pyrene-HEBI: Polystyrene Brushes

In section 3.6, 1-pyrenecarboxylic acid was used as a model system, as it is comparable to MWCNT, in the functionalization with HEBI. Successful attachment was achieved and the product, Pyrene-HEBI, was formed. This product was used further to create Pyrene-PS brushes, using ARGET ATRP to model the similarities with creating CNT-PS brushes.

Although the end product has many similarities in terms of chemical structure, during ARGET ATRP some differences do exist that could affect the efficiency of the polymerization. One of these differences is the solubility of the Pyrene-HEBI, which is much greater than that of the HEBI functionalized carbon nanotubes (i.e. CNT-Br). To combat this difference the same weight of CNT-Br used in section 3.7.1 was used in the living polymerization of Pyrene-HEBI. This is different to the molar ratio that would typically be used in EBiB initiated homopolymer type reactions (see Chapter 2). Another difference is the ratio of initiation points in Pyrene-HEBI is one initiation point to each molecule, whereas the HEBI functionalized carbon nanotubes have many initiation points to each nanotube. In this situation the polymer chain of the Pyrene-HEBI propagates in one direction, whereas the polymer chains attached to the nanotube propagate in all directions (i.e. many propagating polymer chains from the

one carbon nanotube). Such a difference could not be adjusted without changing the original starting material, however in the solution polymerization, the pyrene structure will exhibit similar π-π stacking capabilities as the carbon nanotube, due to the molecular structure similarity.
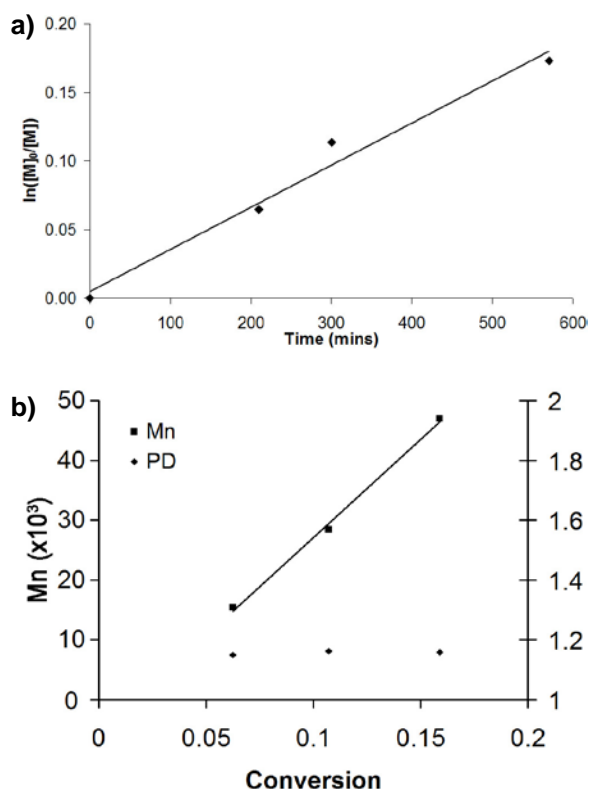
Figure 3. 22: a) Kinetic plot for ARGET ATRP of styrene using Pyrene-HEBI as the initiator (R^2 = 0.9775), and b) the molecular weight and polydispersity as a function of conversion, using a polystyrene calibration (R^2 = 0.9966).

The efficiency of polymerization was determined using the kinetic plot presented in Figure 3. 22a). From the graph a straight line is revealed indicating living polymerization has occurred. The graph also begins at the origin, which demonstrates that successful purging of oxygen with nitrogen had occurred, unlike the PMMA results of Chapter 2 requiring a "short induction period" (i.e. consumption of oxygen with Sn(EH)$_2$).[325]

GPC results confirm that the polymerization was living as a polydispersity of 1.16 was achieved (Table 3. 7 and the kinetic plot of Figure 3. 22b)). Erdogan *et al*[326] found a similar result using a similar pyrene initiator, however in ATRP, to achieve a polydispersity of 1.15-1.18. In comparison to the Pyrene-PS work, Erdogan and coworkers did achieve higher conversions of 30-67% compared to the 6-16% by ARGET ATRP. However, Erdogan and co-workers used a monomer to initiator ratio of approximately 100/1 unlike the ratio used here of approximately 1300/1. Furthermore, as the ratio was higher, higher molecular weights resulted (i.e. 46,900g/mol compared to 8,760g/mol by Erdogan and co-workers).

Sample	Time (mins)	M_n (x10^3)^b	Conv.	Polydispersity^b	Polymer T_d (^{o}C)	T_g (^{o}C)
CA-PS^c	-	140	-	1.64	400	102.2
Pyrene-PS1	210	15.3	0.06	1.15	352	101.5
Pyrene-PS2	300	28.4	0.11	1.16	357	106.1
Pyrene-PS3	570	46.9	0.16	1.16	361	108.1

Table 3. 7: Polymerization for ARGET ATRP of styrene ^{b} determined by GPC in THF, polystyrene standard. Pyrene-PS(1 to 3) St/CuBr$_2$/Me$_6$TREN/Sn(EH)$_2$ (300/0.015/0.15/0.3) using 15mg of Pyrene-HEBI. ^{c} Commercially available polystyrene was purchased from Aldrich.

When comparing the GPC results to the results of the CNT-PS samples it is clear that some element of control is lost. The carbon nanotube brushes have a higher polydispersity of 1.78 compared to the Pyrene-PS samples of approximately 1.16. This loss in polymerization control has occurred due to the carbon nanotubes limited dispersion and limited mobility capabilities in the solution polymerization. The Pyrene-HEBI does not possess a limit of dispersion, nor does it have limited mobility and therefore has shown good initiation and growth in the kinetic plots of Figure 3. 22 with a near 1 polydispersity. Furthermore, for a similar conversion, higher molecular weights are formed for the CNT-PS samples than the Pyrene-PS samples, which

indicates that the ratio of monomer to initiator is higher in the CNT-PS reaction; the tertiary bromide initiator sites are more dense in the Pyrene-HEBI compared to the CNT-Br.

The decomposition temperature of Pyrene-PS(1,2,3) was determined using TGA. The thermograms showed a similar trend seen in section 3.7.1. In section 3.7.1 the CNT-PS and Homo-PS material demonstrated a trend of increasing T_d with increasing molecular weight and this was also observed for the Pyrene-PS samples (Table 3. 7). The T_d of Pyrene-PS1 occurs at 352°C for 210mins with a molecular weight of 15,300g/mol, which increased to 361°C for 570mins with a molecular weight of 46,900g/mol for Pyrene-PS3. Furthermore, the T_d is tending towards the T_d of the CA-PS, which is a similar result to the Homo-PS samples.

In previous measurements of T_g, determined using DSC, an increase in the carbon nanotube polymer brushes T_g compared to the homopolymers T_g was observed due to the rigidity of the carbon nanotubes reinforcing the material and the π-π stacking capabilities. However, as the pyrene structure is significantly smaller than a nanotube the strength of this effect was not seen (Table 3. 7). The trend observed in this case was still an increase in the T_g, but only by a maximum of 5.9^{o}C for Pyrene-PS3 when compared to CA-PS. In comparison to the results of section 3.7.1, an increase of 14°C was detected for the CNT-PS samples, which is more than double the increase of the Pyrene-PS samples. This result was due to the effectiveness in the π-π stacking capabilities of the pyrene structure compared to the carbon nanotube. In the carbon nanotube the chains are anchored to the nanotube and coat that particular nanotube making a very rigid structure, whereas in the Pyrene-PS material the π-π stacking pyrene structure is significantly smaller and planar in shape. It would therefore exhibit similar properties to graphite, which is layered planar graphene sheets that can

slide over one another,[327] and hence the Pyrene-PS samples have less rigidity than carbon nanotubes, making them less effective reinforcing agents.

The chemical structure was re-affirmed using FT-IR, and is presented in Figure 3. 23. The spectra of Pyrene-PS has the same characteristic absorption peaks to that of Homo-PS and does not exhibit any signals of the pyrene structure. The small concentrations of pyrene is overwhelmed by the high concentration of PS functional groups, resulting in only the detection of the PS signals by FT-IR, which is a similar result obtained with CNT-PS brushes as well as the other polymer brush materials of this chapter.
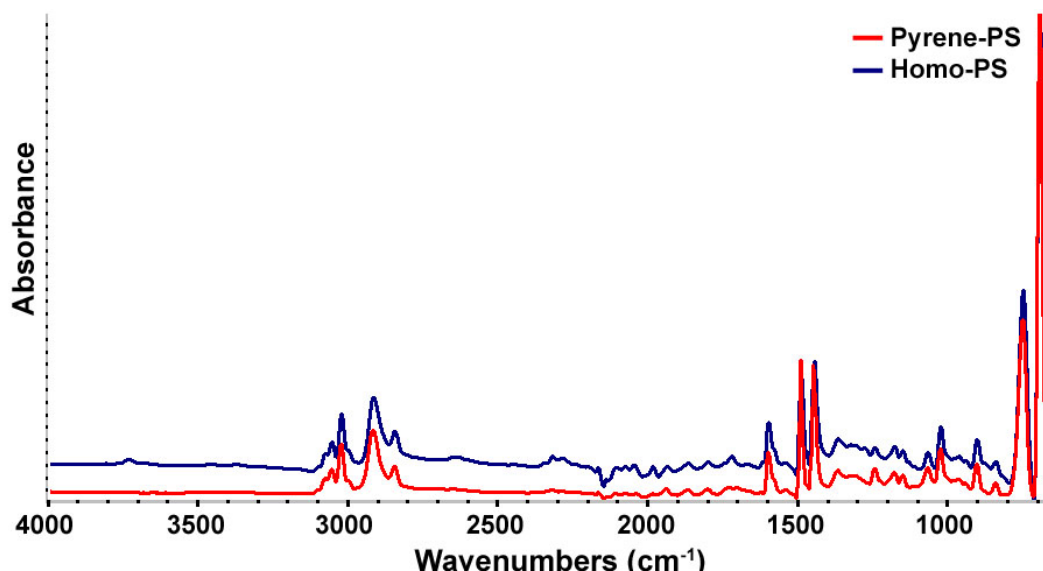
Figure 3. 23: FT-IR spectra of Pyrene-PS and Homo-PS, showing no noticeable differences in the absorbance peaks.

3.10 Conclusion

In conclusion, it was shown that the polymerization technique of ARGET ATRP can be used to produce polymer brushes of polystyrene on multi-walled carbon nanotubes with polymer coverage as high as 84.7%. This technique proved to have many benefits over existing techniques such as normal ATRP and other more sensitive living polymerization techniques. Benefits such as low catalyst

concentration, ease of polymerization technique, and the living capacity to reinitiate polymer growth. In addition, a polydispersity of 1.78 was determined and found to be of similar magnitude to previous research using normal ATRP.

This research was explored further by the production of PMMA polymer brushes on carbon nanotubes by ARGET ATRP (living polymerization) and PHEMA polymer brushes on carbon nanotubes (free radical polymerization). Physical differences occurred due to the technique used to produce them, and PHEMA's capability to crosslink. A comparison was then made between controlled living polymer brushes to uncontrolled polymer brushes on carbon nanotubes and many differences and similarities occurred. One of these differences came from the reactivity of the monomer and hence the polymer layer thickness or content was affected. In the living polymerizations this thickness depended on the reaction time and it was found that the PS was much less reactive compared to the PMMA; the same approximately 80% polymer content of PMMA in the CNT-PMMA was achieved in a fifth of the time to produce the CNT-PS. When compared to un-controlled polymer brushes, CNT-PHEMA, the polymer content was anywhere between 50 and 80%, which could not be controlled by reaction time. Generally the polymer layer of the three different types of brushes was in the range of 10nm. However, this did not reflect the molecular weight as PS, PMMA, and PHEMA all have different densities and therefore for the same thickness of PMMA as to PS, the molecular weight of PMMA is much greater than PS (i.e. similarly to PHEMA).

In addition, for the living polymerizations, living plots were created to re-affirm that the ARGET ATRP of CNT-Br did in fact polymerize in a living fashion. Linear plots were obtained, however more study is needed in the areas of molecular weight and polydispersity to establish the efficiency of initiation. As a guide, what was

observed in Chapter 2 was a well initiated polymer of PS and poorly initiated polymer of PMMA, meaning a similar trend in the CNT-PS and CNT-PMMA materials could have been expected.

An increase in T_d with respect to the molecular weight was noticed only in the CNT-PS material and was not observed in the other polymer brush materials. Although this trend was not observed in the other materials, changes did occur to the T_d for the three types of brushes synthesized in this chapter; CNT-PS decreased approximately 40^oC and CNT-PMMA increased by 35^oC when compared to the commercially available products, and CNT-PHEMA decreased by 4^oC. However, structurally PHEMA has many similarities to the nanotube in terms of oxygenated moieties, therefore has the greatest attraction and was unlikely to significantly alter the T_d compared to the chemically dis-similar PS or PMMA.

The T_g of the material acted to increase the temperature, by 14^oC for CNT-PS, by 17^oC for CNT-PMMA and also 17^oC for CNT-PHEMA. This increase was attributed to the rigidity of the carbon nanotube and hence it acted as a reinforcing agent.

The chemical structure of the brushes was determined using spectroscopy techniques. FT-IR was used, however the nanotubes could not be detected due to the extremely low concentration of specific nanotube groups that were covered by the thin layer polymer coating. Raman spectra of the CNT-PS material was used to determine if a charge transfer affect could be detected and then not detected, to prove the covalent attachment of the polymer brushes. This was observed, and therefore the brushes were covalently attached instead of solely due to additional forces, such as π-π stacking.

Electrical conductance measurements found that the polymer brush carbon nanotubes were less conductive than pristine or acid cleaved nanotubes and that the

strength of conductance was dependent on the polymer content (i.e. more polymer, less conductive). In addition, the preparation technique found that the polymer brush carbon nanotubes can be formed into films and hence applications exist in conductive coatings or films.

The model system of Pyrene was also used to produce polymer brushes using ARGET ATRP with Pyrene-HEBI as the initiator. What was observed was a well initiated polymer, a $5.9^{o}C$ increase in the T_g, and the T_d increased as the molecular weight increased. These properties resembled the properties of the CNT-PS and demonstrated that the pyrene is a good model system for carbon nanotubes.

- CHAPTER 4 -

POLYMER BRUSHES

AS

NANOFILLERS (MACRO SIZED)

4. POLYMER BRUSHES AS NANOFILLERS (MACRO SIZED)

Preface

This chapter discusses the application of polymer brushes as re-inforcers in polymer matrices. The concentration of polymer brushes was varied from 0 to 1w/w% and the composite materials were characterized for their physical properties.

4.1 Introduction

Nanocomposites made from carbon nanotubes and polymers offer the promise of composites with substantially improved material properties, such as high electrical, thermal, optical and mechanical properties. A large amount of literature has been reported on the mixing of un-functionalized or acid treated carbon nanotubes into polymer matrices.[328,329,330,331] However, in these reports they all experience problems with the nanotube's limited solubility in the liquid polymer matrix, therefore resulting in aggregated bundles of nanotubes inside the composite instead of an even dispersion. To combat this they have reported various procedures for mixing/processing in an attempt to get an even dispersion.[332,333] The alternative is to chemically treat the nanotubes surface increasing solubility of MWCNT,[334,335,336] hence the research undertaken to develop polymer brushes, reported in Chapter 3.

The reason for increasing the solubility of the carbon nanotubes in the molten polymer matrix is to create a material with a high dispersion of nanotubes so that the percolation threshold is able to be reached at relatively low carbon nanotube concentrations, thus making the composite conductive.[337,338] It is seen as advantageous to not only mix the nanotubes into the material to strengthen it, but to also utilize the nanotube's property of conductivity. Extending these two properties of

the nanotube into the material can only increase the possible applications when it comes to commercialization of the composite.

An additional application of one composite can also be created that has these two properties (i.e. strength and conductivity), which depends on the nanotube concentration. When the concentration of nanotubes are higher than the percolation threshold then the composite becomes conductive, and when it is lower the composite is non-conductive. This therefore creates two materials; one that is conductive, which can be used to conduct a current in a circuit and the other can act as a barrier to impede electron flow. Essentially a circuit can be produced using and supported by the one composite material.

In this work polymer brushes on carbon nanotubes have been used to create composite materials. This was done to increase the limit of solubility of carbon nanotubes in polystyrene (PS), poly(methyl methacrylate) (PMMA), and poly(2-hydroxyethyl methacrylate) (PHEMA), by employing like polymer brushes, on carbon nanotubes, of PS, PMMA, and PHEMA, respectively. Concentrations of between 0 to 1w/w% were produced then characterized to identify the physical properties of the composites. Furthermore, the model system of pyrene has also been investigated as a potential nanofiller using the Pyrene-PS developed in Chapter 3 in a PS matrix.

4.2 Synthetic and Preparation Procedures

Materials

Styrene (Aldrich, 99%) and methyl methacrylate (MMA) (Aldrich, 99%) were dried over calcium hydride and passed through a column filled with basic alumina. 2-hydroxyethyl methacrylate (HEMA), and dibenzoyl peroxide were obtained from Aldrich and used as received. The polymer brushes on the carbon nanotubes were

synthesized using the procedures outlined in Chapter 3; CNT-PS5, CNT-PMMA2, and Pyrene-PS3 of Chapter 3 were chosen due to their high polymer content, which would have a greater solubility than the lower polymer content polymer brush carbon nanotubes.

General Composite Formation Procedure

Purified styrene or methyl methacrylate was mixed with dibenzoyl peroxide in a 1000:1 ratio, followed by the addition of the corresponding polymer brush carbon nanotube (i.e. CNT-PS5 in styrene to make CNT-PS5 in PS) in 0.00, 0.10, 0.25, 0.50, and 1.00w/w% concentrations. The mixture was then mixed for 30mins, followed by 10mins sonication. Once the brushes were evenly dispersed into the solution, the mixture was transferred to Teflon moulds and polymerized in an oven at 80°C for 24hrs.

The procedure for polymerizing HEMA is similar to the above procedure and was repeated, but with some minor changes. The polymerization temperature was reduced from 80°C to 60°C, and during the 24hr reaction time the mixture in the moulds was exposed to a constant incandescent light source.

For comparison, four additional composites were produced using the above general procedure for the PS and PMMA composites. 0.25w/w% of as received (AR), also known as pristine carbon nanotubes and 0.25w/w% acid cleaved (AC) nanotubes were used as a filler in a PS and PMMA matrix, as well as un-filled PS and PMMA. This was performed as a control in the following experiments to observe the differences occurring between polymer brushed nanotubes, non-polymer brushed carbon nanotube, and un-filled polymer composite materials.

THE TEFLON MOULDS: Teflon moulds, as pictured in Figure 4. 1, were constructed to the dimensions required for the dynamic mechanical analysis (DMA) –

single cantilever attachment (13mm wide, 36mm long and averaging 7mm thick) and in the dimensions for the 25mm diameter parallel plate attachment for the Rheometer. As the composite was polymerized into the shape required for characterization, no post-cutting was required.
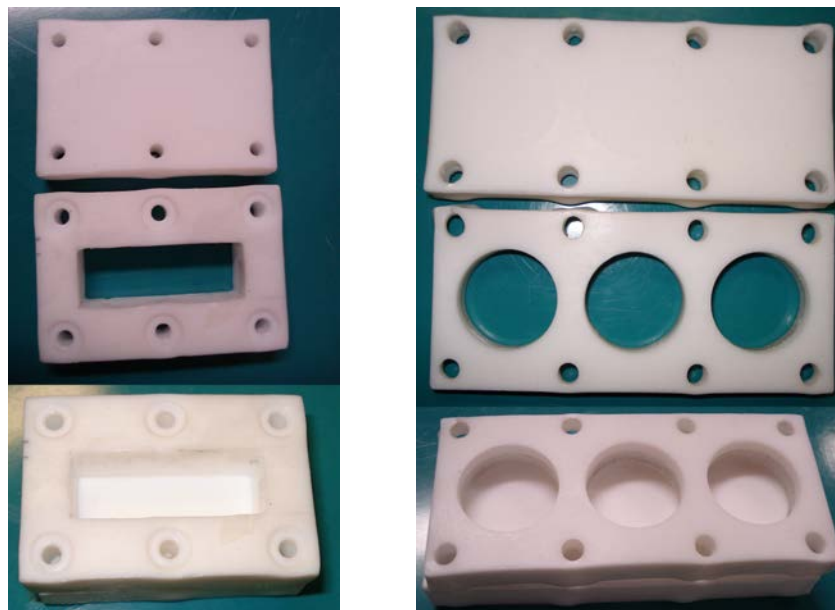
Figure 4. 1: digital photos of the Teflon moulds used; separated and stacked, held together with nuts and screws, (left) is the DMA – single cantilever mould, and (right) is the 25mm discs required for the parallel plate rheometer.

NOTE

Some values in the following results may appear different to those found in common literature. The composites have had no post-curing and therefore contains a small percentage of unreacted monomer due to the bulk polymerization procedure. This was deliberate as literature does not explore the efficiency of the polymerization in similar materials and was determined using DSC (i.e. exotherms), and NMR. In addition, as the composites were polymerized into their desired shapes, the possibility as a ready-made material that requires no post-moulding was explored. However

some characterization procedures, such as rheology, were pre-heat treated, which ultimately removed the unreacted monomer.

Another item to note is that the polymers are amorphous polymers which are typically transparent, however the photograph images of the un-filled composites are not, due to the polymer forming/moulding to the rough surface of the Teflon.

Results and Discussion

4.3 AR and AC Nanotubes as Fillers in PS and PMMA

The initial observation in the storage modulus, measured using DMA, found that upon adding AR nanotubes the storage modulus of the material decreased and decreased further when using AC nanotubes. As can be seen from Figure 4. 2 at 0°C the storage modulus of PS drops by 200MPa from 1800MPa unfilled to 1600MPa when 0.25w/w% AR nanotubes is added to the polymer. Similarly for PMMA the storage modulus reduces by about 400MPa from 3200MPa unfilled to 2800MPa when 0.25w/w% AR nanotubes is incorporated into the polymer. The situation was worse when AC nanotubes were incorporated into these polymers. In PS the storage modulus reduced by 500MPa from 1800MPa to 1300MPa when 0.25w/w% AC nanotubes was added to the polymer. Similarly for PMMA a reduction of 450MPa was seen, with the storage modulus reducing from 3200MPa for the unfilled polymer, down to 2750MPa when 0.25w/w% AC nanotubes was included.

These changes in storage modulus were attributed to the nanotubes limited dispersability within a polymer matrix, which decreased further when AC nanotubes were used, because they are more polar, due to oxygen moieties (i.e. the most chemically dissimilar from the matrix when compared to AR). In the case of inclusion in PS, the nanotubes have an additional aromatic π-π stacking attraction that is not possible in the PMMA composite material and therefore the initial decrease of adding

AR nanotubes is less for the PS. The PS polymeric chains have a capability to π-π stack with the nanotubes graphene type walls increasing the dispersability, whereas PMMA does not possess such a capability and is in fact a more polar polymer which lowers the dispersability limit of the nanotubes. Furthermore, Andrews et al[339] and Velasco-Santos et al,[340] found a similar trend in their work with the PMMA storage modulus changing more greatly than with a PS matrix.
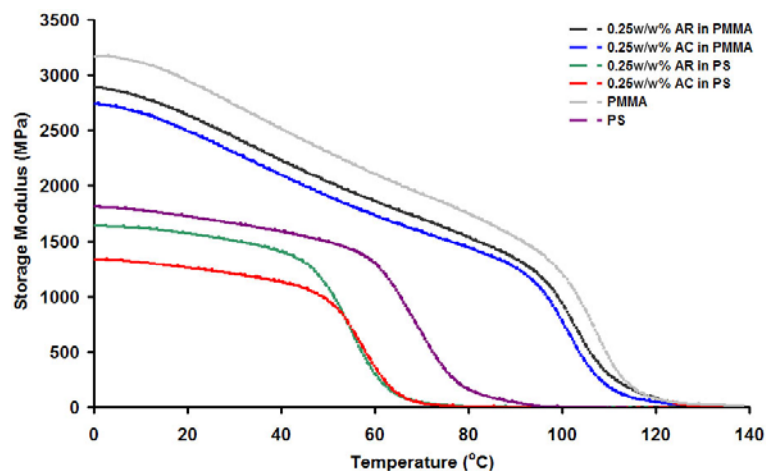
Figure 4. 2: DMA results of AR and AC nanotubes as nanofillers in PS and PMMA.

The polymerization was a bulk technique and when compared to literature, solution polymerizations[215,216,341] and preformed polymer,[342] tend to create composite materials of increased storage modulus. However, these techniques have post processing steps to remove excess monomer, which can act as an impurity weakening the polymer. Upon removal by heating, the polymer chains can reorganize into the most thermodynamically stable state, producing a harder, stronger material, and hence the increased storage modulus.[343,344] Compared to the technique seen here, which has no post processing or post curing (i.e. trapped monomer), the reorganization has had no chance to form and trapped monomer is still present, hence the decrease in storage modulus. Furthermore, modeling work performed by Odegard et al[345] found that these increases in storage modulus only occur when the nanotubes

are evenly dispersed. With the support of Odegard and coworkers work it implies that to have an increase in storage modulus the trapped monomer must be removed and the nanotubes must be evenly dispersed.

Differential scanning calorimetry (DSC) was performed on the composite materials to determine the change in the glass transition temperature (T_g) with the incorporation of AR and AC carbon nanotubes. The results are shown in Table 4. 1. From the table it is obvious that in the first heating cycle T_g decreases following the trend, PS then AR in PS, followed by AC in PS. Overall the most significant decrease in T_g occurred for the AC composite with a decrease of 2.48^{o}C. In addition, within this first heating run an exotherm at 110-180°C was observed for all samples (i.e. the heat of the post curing reaction). This exotherm was attributed to trapped unreacted monomer, which subsequently polymerized when sufficient heat was supplied. The unfilled PS, displayed an exotherm of 30.4J/g, which was significantly lower for the AR composite with 0.62J/g and was higher for the AC composite with 35.33J/g.

Sample	T_g (1st run)(^{o}C)	T_g (2nd run)(^{o}C)	Exotherm (110-180°C) (1st run)(J/g)	Mn (x10^3)[*]	Polydispersity[*]
AR in PS	54.26	76.54	0.62	57.40	2.86
AC in PS	52.52	Not detected	35.33	71.20	2.94
PS	55.00	72.00	30.40	24.40	2.86
AR in PMMA	108.40	103.80	2.94	82.06	5.62
AC in PMMA	108.40	99.23	2.38	102.79	5.77
PMMA	105.77	104.04	8.26	90.60	3.60

Table 4. 1: DSC and GPC results of AR and AC nanotubes (0.25%) in PMMA and PS matrix. [*]Mn and polydispersity is of the PS or PMMA matrix with no post treatments from specified experimental of section 4.2, PS calibration.

The formation of these exotherms is a common phenomenon in bulk polymerizations due to the production of trapped radicals and trapped monomer.[346,347,348,349] To remove the trapped monomer the sample needs to be heated

above the T_g, increasing the mobility of the free monomer, whereby it is removed from the sample. The removal occurs by a combination of evaporation of unreacted monomer and polymerization on heating in a post curing reaction. This observation was confirmed when for the second DSC heating of the samples, virtually no exotherm was observed. This removal of the monomer increased the T_g to 72°C and 76.54^{o}C for PS and AR in PS, respectively (AC in PS did not show a T_g). The increase in T_g of 20°C in the second run suggests that unreacted monomer acts like a plasticizer. It is important to note that the smallest exotherm and increase in T_g, is found for the AR in PS, which is due to its π-π stacking capabilities pulling the chains closer together and decreasing the free volume.[350] Furthermore, trapped monomer and its concentration was verified with ^{1}H-NMR by comparing the vinyl group protons of the styrene monomer with the methylene protons of polystyrene.[351] A monomer concentration of 3.5% was calculated for the unfilled PS (Figure 4. 3). It is assumed that the exotherm/post curing reaction is a reflection of concentration, which therefore implies the AC in PS has a higher concentration of trapped monomer.
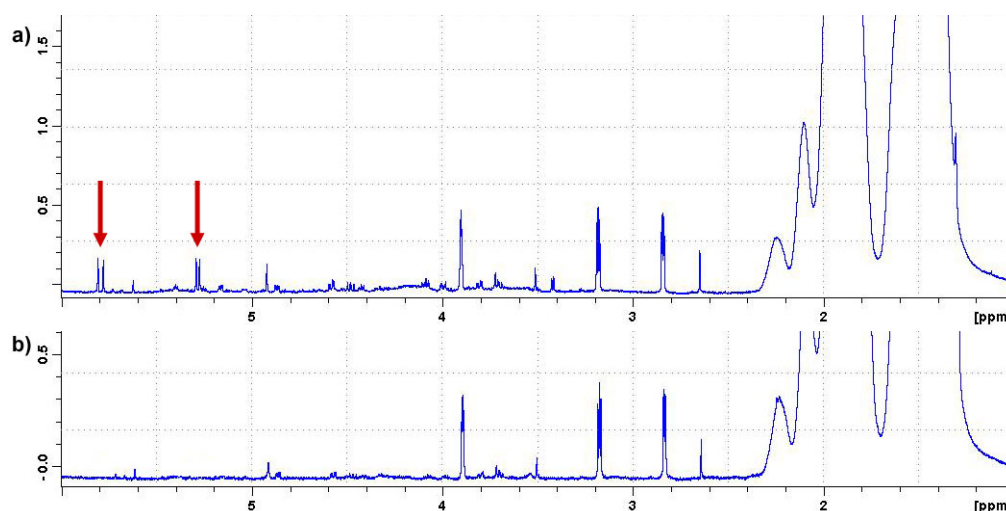
Figure 4. 3: NMR spectra of a) bulk PS with free monomer and b) bulk PS, after the first DSC heat treatment, with no free monomer. The arrows indicate the styrene monomer NMR shifts.

The PMMA material exhibited different characteristics to the PS material as the carbon nanotubes surface chemistry is more dissimilar to that of the PS. The T_g of the PMMA material was found to be 105.77^{o}C and when compared to the AR and AC in PMMA an increase of 2.63^{o}C occurs for each sample, however upon second heating the T_g decreases by 4.6^{o}C and 9.17^{o}C for the AR and AC, respectively when compared to the first heating. Furthermore, the presence of a post curing reaction was observed again, like the PS composites, however the addition of either AR or AC nanotubes substantially decreased the exotherm from 8.26J/g for the PMMA (i.e. 0.81% by ^{1}H-NMR, Figure 4. 4), to approximately 25%.[352] The fact that the exotherm has decreased upon addition of carbon nanotubes for both the PS and PMMA samples, with the exception of AC in PS, indicates that the nanotube acts to aid in the polymerization reaction, preventing the termination reactions occurring so that higher conversions are reached.
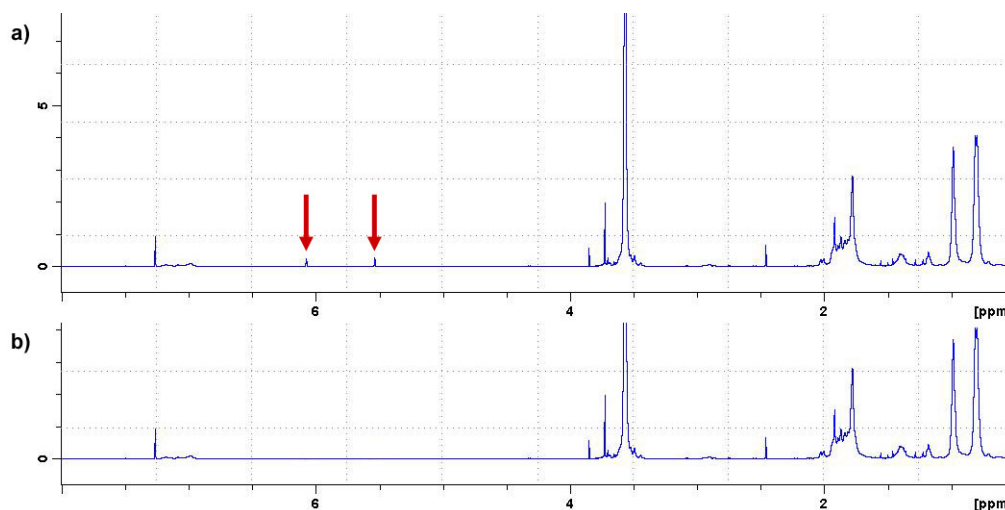
Figure 4. 4: NMR spectra of a) bulk PMMA with free monomer and b) bulk PMMA, after the first DSC heat treatment, with no free monomer. The arrows indicate the MMA monomer NMR shifts.

When the PS and PMMA samples are compared, it is clear to see that two competing factors are affecting the T_g. The first factor is the presence of trapped

monomer, as the results indicate that for PS the trapped monomer acts like a plasticizer, lowering the T_g, but in the PMMA samples the trapped monomer increases the T_g (i.e. the difference between first and second heating). The second factor is the carbon nanotube as a filler. In the PS composites the nanotubes act to increase the T_g, whereas in PMMA the carbon nanotubes act like a plasticizer lowering the T_g (i.e. the difference between filled and unfilled of second heating, which has no trapped monomer). These variations in the T_g are due to the composite's changes in free volume where an increase in the T_g indicates a decrease in the free volume and vice versa.[350] Furthermore, this indicates that the trapped monomer increases the free volume in the PS and lowers the free volume in the PMMA. Similarly carbon nanotubes lower the free volume in the PS and increase the free volume in the PMMA.

It is interesting to note that the normal T_g literature value for PS is 95°C and for attactic PMMA is 105°C.[353] The fact that the observed T_gs for unfilled PS is still approximately 20°C lower than the literature value upon removal of the trapped monomer, suggests that additional polymer properties are affecting the T_g. However, literature has also shown that the T_g is affected by low molecular weights due to more free volume at the chain ends. A relationship was determined by Fox and Flory that relates an infinitely large molecular weight polymer to a smaller molecular weight polymer Eq. (11).[354]

$$T_g = T_g^{\infty} - KM^{-1} \tag{11}$$

where T_g^{∞} is the T_g of an infinitely large molecular weight polymer and T_g is the glass transition temperature at molecular weight M and constant K.[354] Using this equation, it predicts the unfilled PS polymer of 24,400g/mol to have a T_g of approximately 88°C, but the calculation overestimates the T_g.[355] However, the results of

Couchman[355] compared the calculated to the observed T_g and found that for a calculated result of $88^{o}C$ the observed was approximately $73^{o}C$, which is in good agreement with the unfilled PS gel permeation chromatography (GPC) result of $72^{o}C$.

The GPC results of the PS samples are shown in Table 4. 1, which demonstrates an approximate two times and three times increase in Mn upon addition of AR and AC, respectively for the PS material (the polydispersity was unaffected). These results indicate that the nanotubes aid in the polymerization of styrene to increase the Mn. In comparison to the PMMA results, shown in Table 4. 1, a much higher Mn to the PS results has occurred due to MMA having a higher reactivity than styrene (see Chapter 2 and 3). The AC nanotubes ability to aid in the polymerization (i.e. increase in Mn) was also present in the PMMA like the PS, however the addition of AR nanotubes to MMA does not act to increase the Mn, instead the Mn decreases. In the AR composites, the PS creates π-π stacking with the nanotubes, whereas PMMA does not possess this ability and when the two are mixed, the non-polar AR nanotubes do not disperse well in the MMA creating a resistance to blending, therefore in this mixture it has inhibited longer chain growth. In contrast, the AC nanotubes have polar oxygenated species, and therefore is better at blending with the polar MMA. In addition, the presence of the carbon nanotubes in the polymerization of MMA decreases the level of control in the polymerization as the polydispersity increased from 3.6 to as high as 5.77.

Sung *et al*[356 and Park *et al*357] found a similar trend in their work of an increased Mn upon the addition of acid treated carbon nanotubes to the polymerization of MMA. However, they attributed the increase in Mn as a result of the vinyl groups, present on the carbon nanotube, consuming the radical intiator 2,2'-azobis(isobutyronitrile) (AIBN) and therefore increasing the ratio of monomer to initiator (i.e. forming a

higher Mn). Although in the results of Table 4. 1 this is possible with benzoyl peroxide as the initiator, the increased Mn trend should occur for all samples and monomers as the AR and AC nanotubes possess the vinyl groups. Contrary, Mn of AR in PMMA has decreased, indicating that additional properties such as the blending capabilities with the monomer must also affect the Mn.
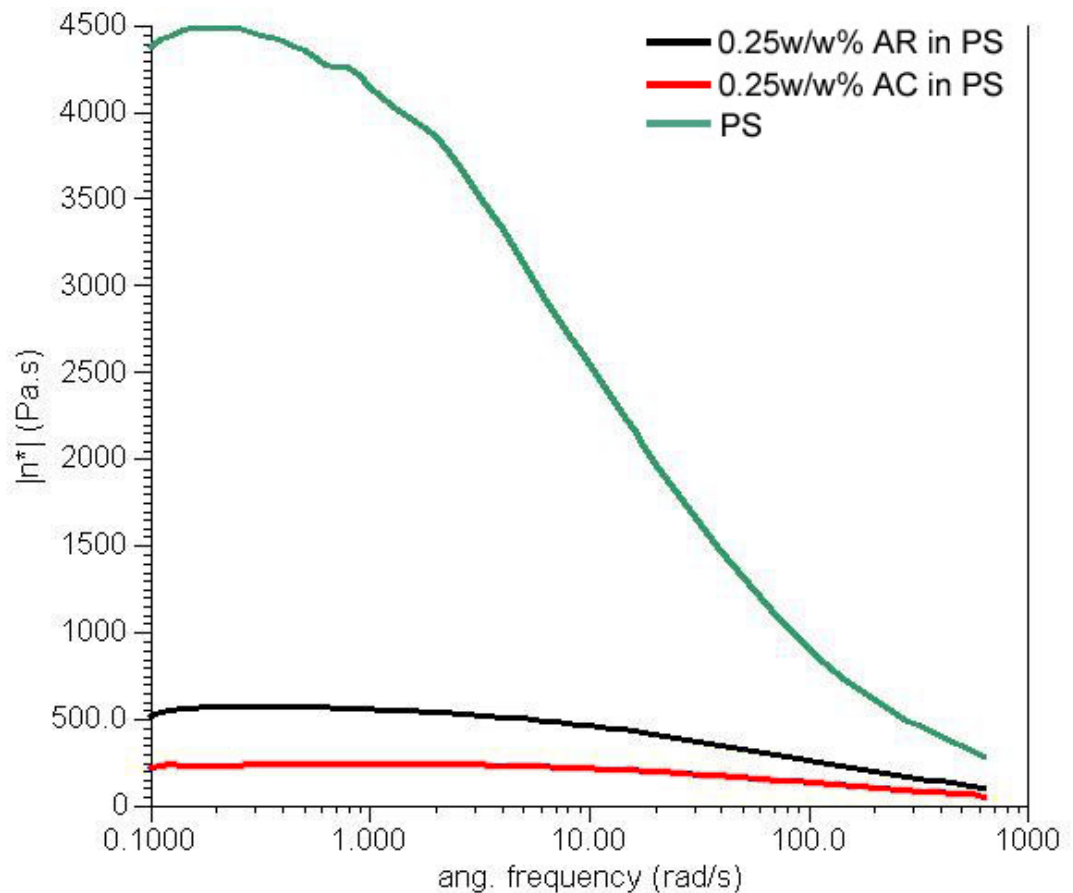
Figure 4. 5: Rheological results of AR and AC nanotubes in PS and PS.

The composite materials have shown that the nanotubes aid in the polymerization, increasing the Mn and in some composites reaching higher conversions. The nanotubes have also affected the physical properties, such as T_g and the storage modulus. It was therefore expected that additional affects in the processability of the material would occur. This was explored using a 25mm parallel plate ETC rheometer setup and the results of the PS samples can be seen in Figure 4. 5. It is clear from the

complex viscosity plot that the addition of 0.25w/w% of either AR or AC nanotubes has a significant affect in lowering the viscosity at low shear rates and the difference decreases with increasing shear rate. At the initial measurements of $0.1s^{-1}$ the decrease is approximately to 11% for the AR composite and to 4.5% for the AC composite when compared to un-filled PS. At the higher shear rates this difference decreases approximately to 30% for both the AR and AC materials of the un-filled PS result. The rheology also demonstrates that the unfilled PS has a shear thinning effect in contrast to filled composites behaving almost like a Newtonian fluid. Mitchell *et al*[358] found in their work that upon addition of the carbon nanotubes to the PS, the complex viscosity increased, which is the opposite affect of the results found above. However, some differences exist between Mitchell and co-workers samples to the samples reported here. One such difference is that Mitchell's polymer was pre-formed before mixing, and therefore contained no trapped monomer. However, in the AR and AC rheology tests, the operating temperature was higher than the post curing reaction temperature (i.e. the exotherm) experienced in the DSC results, indicating that the samples tested did not contain trapped monomer (i.e. see Figure 4. 3). This therefore leaves the conclusion that the pre-formed polymer creates a different material to when the composite is formed from the monomer. These two techniques would have a difference in dispersion as the nanotubes solubility limit is higher for the styrene monomer, than the PS polymer. Furthermore, the AR and AC in PS samples were sonicated compared to no-sonication in the work of Mitchell and co-workers.
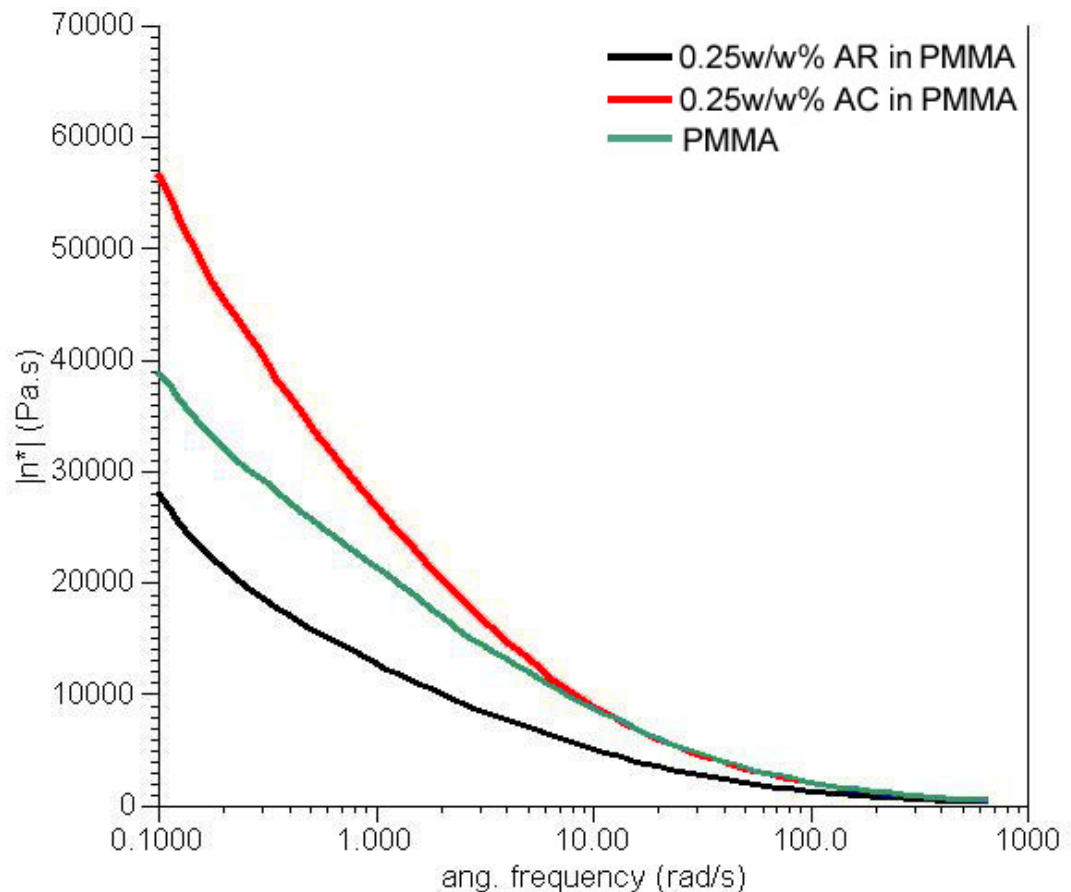
Figure 4. 6: Rheological results of AR and AC nanotubes in PMMA and PMMA.

In the PMMA material, the complex viscosity difference was significantly less than the PS material, which was expected due to the resistance to blending of the two mediums. The complex viscosity plot of Figure 4. 6 shows an approximate decrease to 72% for the AR composite and increase to 144% for the AC composite when compared to un-filled PMMA. This difference decreases with increasing shear rate to a point where viscosity is the same for all materials. The AR nanotubes are highly non-polar and upon mixing with the polar PMMA, the material acts to lower the viscosity, which was a similar affect seen for the AR in PS composite. The extent of the AR composite changes is a result of the differences in polarity. The non-polar nanotube is more easily incorporated into the non-polar PS compared to the polar PMMA, hence the change in viscosity is higher for the PS than the PMMA. For the

AC composite, Sung *et al*[356] found in their work an increase in viscosity with increasing acid treated carbon nanotube concentration. This is similar to the results found above as the AC in PMMA also increased in viscosity, but Sung and co-workers used 2,2'-azobis(isobutyronitrile) (AIBN) as the initiator. This created a matrix of a higher Mn, which is a more viscous substance; at 1% nanotube filler, Sung obtained 110500g/mol, whereas AC in PMMA was lower at 102790g/mol.

In contrast to the AR in PMMA composite, the AC in PMMA composite demonstrates an increase in viscosity, therefore the AC nanotubes act as a thickener in PMMA. Previous research has shown that to thicken water, which is a very polar liquid, the use of high viscosity polar substances such as hydrophilic polymers of polyethyleneoxide[359,360] are needed. These are used in industry and are very effective in small concentrations. In referring to the AC composite the PMMA is acting like the water and the highly viscous thickening agent is the AC nanotubes. Chemically the affect has occurred due to increased hydrogen bonding effects from the carboxyl groups on the AC nanotubes causing an increase in the viscosity of the composite. This also explains why the affect is not seen in the AR in PMMA composite as the AR nanotubes do not possess the hydrogen bonding due to having very little carboxyl group functionality.

Typically in literature the complex viscosity increases when incorporating carbon nanotubes into a polymer matrix,[361,362] but this was not the case for the above results (except for AC in PMMA). Additional affects must be interacting in the system to lower the complex viscosity that otherwise is not seen in literature. Some of these affecting factors could be explained by the work of Fangming *et al*.[363] In their work they found that a rheological percolation threshold could be reached, which was the point where the nanotubes start to impede the flow of the polymer chains. Fangming

and co-workers also found that the alignment and dispersion of the carbon nanotubes also had an affect on the rheological properties. These results indicate that the above composites had not reached the rheological percolation threshold (except AC in PMMA), the dispersion was poor, and that some form of alignment had occurred. A poor dispersion was expected, as previously mentioned, because un-functionalized carbon nanotubes are well known for their limits of dispersion in various common solvents and matrices.

A strong decrease in complex viscosity, upon the addition of carbon nanotubes to a PS matrix, could also explain why higher Mn values were achieved in the GPC results. This was due to lower viscosities increasing the propagating chain end mobility, and lowering the probability of terminating reactions. Similarly, solvent is used in living polymerizations to lower the viscosity and in turn higher Mn values are achieved by reaching higher conversions.[364]

These composites must be explored further for their unique viscosity properties, but is recommended as a future study. In this chapter they have been used as a comparative composite for the polymer brush carbon nanotube composites explored in the following sections.

4.4.1 Polystyrene Brushes in a Polystyrene Matrix

In section 4.3 it was found that PS composites produced by the method stated in this chapter created a material with improved properties. These properties are increased Mn, increased processability and higher T_g, however the material had a lower storage modulus attributed to the nanotubes limited dispersion. To increase dispersability and hence improve the storage modulus, polymer brush carbon nanotubes were utilized. In these materials, the nanotube wall would no longer be a graphene wall, but instead have been functionalized to have the same polymer chains

as the polymer matrix, thus increasing the dispersability in the composite. For a PS composite, π-π stacking occurs between the carbon nanotube and the PS polymer, but with the addition of the polymer brushes the increase in architectural similarity leads to their better interaction with the matrix and hence a uniform dispersion results. The photograph in Figure 4. 7 is of CNT-PS (refer to Chapter 3) in PS and to the naked eye demonstrates no aggregated particles. In addition, conductivity measurements were performed and the results found that the percolation threshold had not been reached for the concentrations tested (i.e. insulating material).
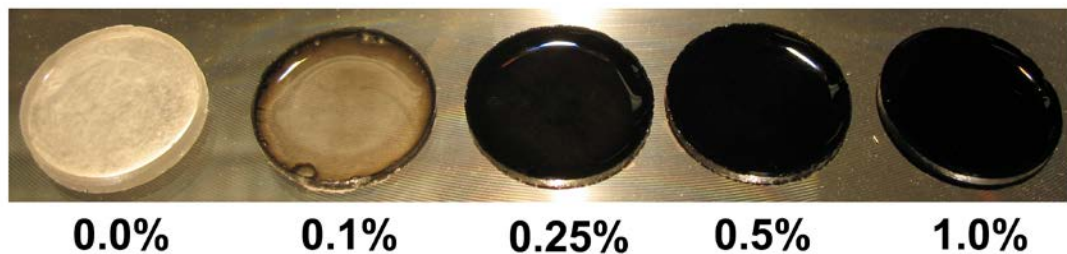
Figure 4. 7: CNT-PS in PS of various w/w concentrations. The composite becomes

opaque at 0.25w/w%.

Although by appearance the limits of dispersion had not been reached, the polymer brushes were expected to change the physical properties. Therefore the storage modulus of the composite was measured by DMA. The results are shown in Figure 4. 8 and shows an improvement to the previous composites of AR and AC in PS discussed in section 4.3. In this series of experiments the composite has not suffered a decreased storage modulus like before, but rather has shown an increased storage modulus of at least 200MPa. The plot in Figure 4. 9 shows the relationship between concentration and the storage modulus, and it is clear from the graph that the most significant result comes from the 0.25w/w%. This critical concentration reflects a peak in the storage modulus, which subsequently decreases and begins to plateau

around 1w/w%, providing a storage modulus of 2000MPa. This trend occurred because as the concentration of nanotubes increased, the attraction to the neighboring nanotubes become a stronger force than the polymer brushes ability to prevent nanotube aggregation. Hence the nanofiller condensed, creating the observed peak in the storage modulus. The plateau that follows heads towards the storage modulus of the original PS material because of the condensed affect, but still maintains an improvement in the storage modulus. This indicates that at higher concentrations, greater than 1w/w%, the storage modulus is higher than the PS material. Essentially it is 'like' a limit of dispersion, but still maintains an improvement to the composites properties.

Figure 4. 8: DMA results of CNT-PS in PS of various w/w concentrations.
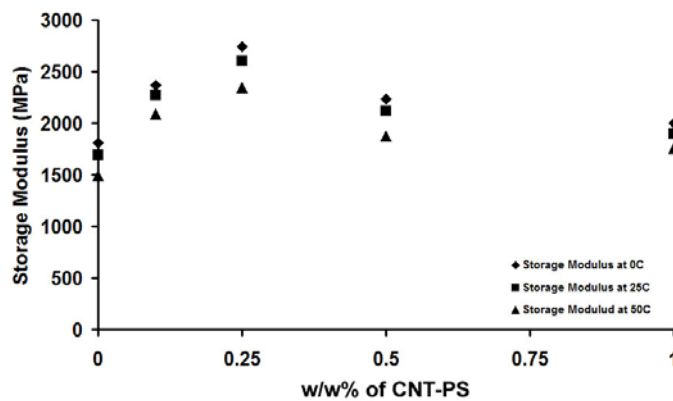
Figure 4. 9: The storage modulus at specific temperatures and concentrations of CNT-PS

in PS. What is noticed is an increase in strength with 0.25w/w% filler concentration

obtaining the maximum.

In contrast to literature, Frankland *et al*[365] predicted from molecular simulations that the strength of the matrix could be increased with only ~0.3% grafting density, which has been supported experimentally by others with an approximate increase of 150% in the modulus with 1wt % loadings.[366,367] Compared to the CNT-PS in PS it too possessed an increased modulus, however to obtain the 150% increase in this research only a 0.1w/w% of functionalized nanotubes was required. In addition, at 0.25w/w% the storage modulus increased by 180%, which is higher than the results of Frankland and coworkers.

Sample	T_g (1st run)(^{o}C)	T_g (2nd run)(^{o}C)	Exotherm (110-180°C)(J/g) (1st run)	Mn (x10^3)*	Polydispersity*
0.00%	55	72	30.4	24.4	2.86
0.10%	65	77	10.6	25.0	2.76
0.25%	70	83	11.9	82.6	2.97
0.50%	65	85	25.5	28.9	3.03
1.00%	56	74	1.2	26.0	3.05

*Table 4. 2: DSC and GPC results of CNT-PS in PS. *Mn and polydispersity is the PS matrix, PS calibration.*

From the DMA curves seen in Figure 4. 8, the Tanδ peak depicts the T_g, which shows a T_g around 70-75°C for all materials. To verify this DSC was performed and the results can be seen in Table 4. 2. In the first heating the T_g of PS is 55°C, which is increased upon the addition of the CNT-PS; the greatest increase was to 70°C for the 0.25w/w% and the smallest increase was to 56°C for 1w/w%. Upon second heating and hence the removal of the unreacted monomer (i.e. the post curing reaction), the same trend is observed, but occurs at higher temperatures with the PS increasing to 72°C and even higher for the CNT-PS composites. This supports the concept that the unreacted monomer acts as a plasticizer, previously seen in the AR and AC in PS composites. It is important to note that the values of the DMA T_gs are comparable with the DSC T_gs during the second heating ramp. In the DMA results, the heating

rate is significantly lower than the DSC rate, giving time for the monomer to evaporate or react and hence depicts a T_g of an un-plasticized PS composite. In the second heating of DSC the monomer has been removed (i.e. the exotherm or the heat of post curing polymerization) and hence this too depicts a T_g of an un-plasticized PS composite, hence the similarities to the DMA. Furthermore, the presence of trapped monomer in a sample after a DMA run was not detected by NMR, which supports the findings that the T_g is of an un-plasticized polymer.

Increases in T_g can also reflect an increase in Mn, which was observed in the GPC results (Table 4. 2). The PS material has an Mn of 24,400g/mol and increases by a few thousand upon the addition of the CNT-PS, which indicates that the polymer brush carbon nanotubes aid in the polymerization, also seen in the AR and AC composites. One particular result is very unique with an Mn of 82,600g/mol for 0.25w/w% and indicates an optimum concentration. This was also the material that exhibited the highest storage modulus and is thought to be the critical point where the CNT-PS gives the greatest affect. In addition, like the previous materials of AR in PS and AC in PS, no loss of polymerization control was experienced; the polydispersity remained relatively constant. Furthermore, these results support the concept that the Mn does not increase solely due to the carbon nanotube consuming the vinyl groups, thus altering the ratio of initiator to monomer (i.e. previously thought by Sung *et al*[356] and Park *et al*[357]). This is an improbably affect in the composite as the nanotubes surface is coated in PS, protecting any vinyl groups on the nanotubes surface from reacting.
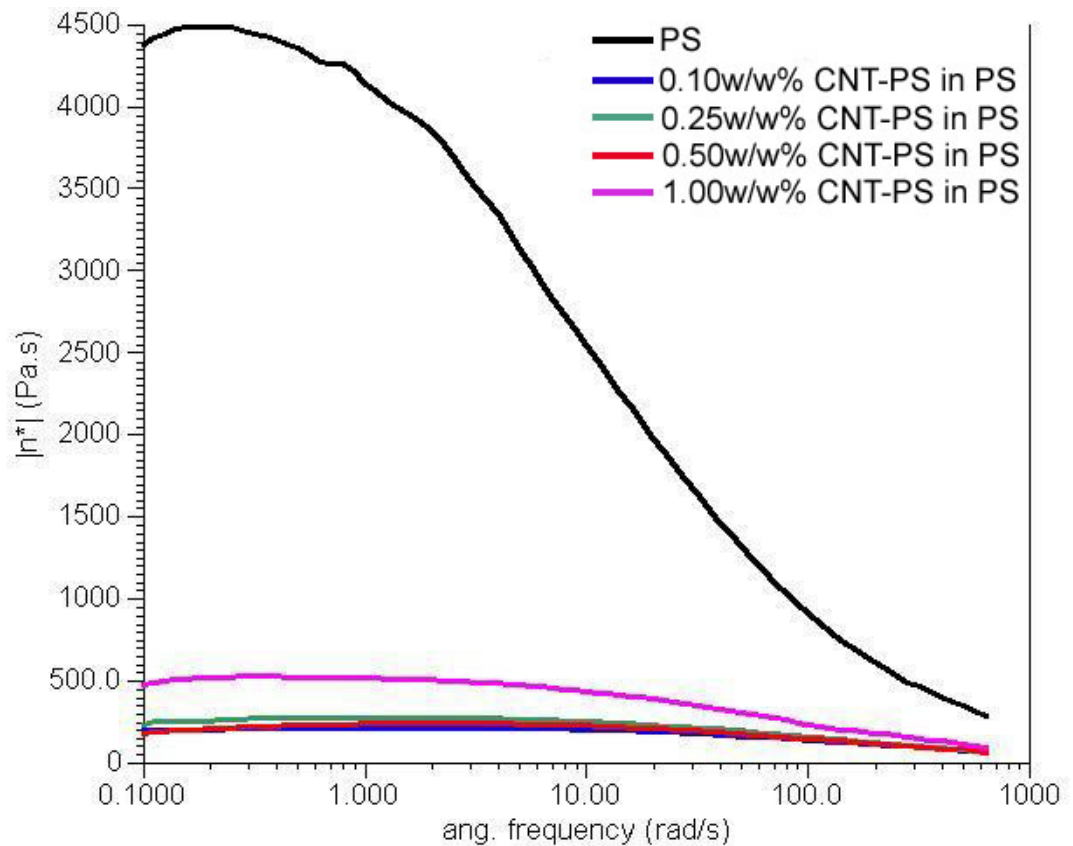
Figure 4. 10: Complex viscosity plot of CNT-PS in a PS matrix. The graph shows a decrease in viscosity upon adding as little as 0.10w/w% of CNT-PS.

In section 4.3 a decrease in the complex viscosity was observed upon the addition of carbon nanotubes to the PS matrix. This decrease was also observed for the CNT-PS composites and the rheological plots can be seen in Figure 4. 10. At the low angular frequencies the data plots demonstrate a decrease to 4.5% in the complex viscosity for all concentrations except 1w/w% with a decrease to 11% when compared to un-filled PS (i.e. difference due to limited solubility). This difference becomes less significant as the angular frequency increases due to a shear thinning effect of the PS and the filled composites almost acting like a Newtonian Fluid. When comparing this plot with Figure 4. 5, which is the complex viscosity versus angular frequency plot of AR and AC in PS, there is a strong similarity between them. The curve of AC in PS has the same complex viscosity trend as the CNT-PS in PS, except

the 1w/w% composite matching the AR in PS composite. This affect has occurred because although the surface of the carbon nanotube is now functionalized, the PS brushes are composed of aromatic rings, which are architecturally similar to the PS matrix thus increasing the limit of dispersion.[368] It was therefore expected that the processability would not change significantly compared to the AC or AR in PS composites, which appears to decline only when the concentration exceeds 1w/w% (i.e. approaching the limit, but still produced an increase in processability). Furthermore, the limit of dispersion has increased beyond 1w/w% as an increase in storage modulus was observed in the DMA results. The PS brushes on carbon nanotubes also do not disrupt the processability, which further supports the concept that they are a better filler than AR or AC nanotubes.

The composite so far has shown remarkable properties, providing an increased storage modulus, and an increase in processibility, but when the composite is moulded into a specific form using shear forces, the carbon nanotubes collide and could start to aggregate. For this reason an optical rheometer was used to model the affect of shear forces. This work utilized an optical microscope to observe the dispersed nanotubes. A series of images from the machine can be seen in Figure 4. 11, which clearly shows the filler is evenly dispersed within the matrix and remains evenly dispersed after shear forces have been applied. A previous study by Ma *et al*[369] showed that upon applying shear forces to a composite of MWCNT in an epoxy matrix the formation of ribbons occur, which are also described as helical bands. These helical bands formed because of increased inter-particle collision, which is otherwise known as orthokinetic aggregation.[370] Studies with colloidal suspensions have also shown this property and is seen as an unfavorable trait as the end product does not have an even dispersion.[371,372] It occurs because as the nanotubes collide

they become interlocked with one another and gradually grow in size as they collect more nanotubes. The key property of the CNT-PS filler that prevents this from happening is the polymer brushes ability to repel the other nanotubes, lowering the aggregation forces and hence once they collide, no interlocking occurs. The fact that the dispersion is maintained demonstrates an improvement in the field of intricate molding, where otherwise the build up of aggregated nanotubes would occur during processing, forming weak points in the structure.
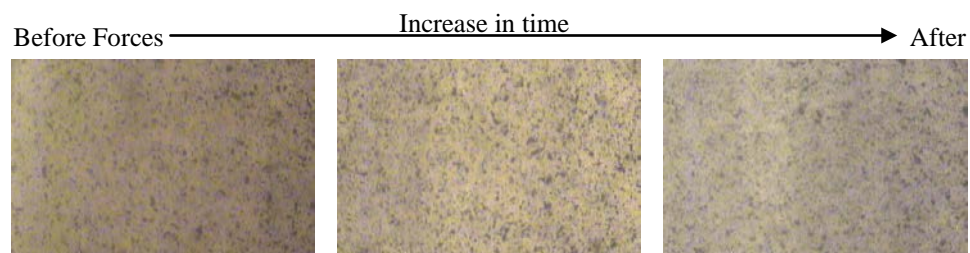
Figure 4. 11: Optical rheology of 0.25w/w% CNT-PS in PS with $100s^{-1}$ shear rate, downward forces. The images show that the dispersion is maintained after shear forces have been applied.

4.4.2 PMMA Brushes in a PMMA Matrix

In section 4.4.1, CNT-PS were used as a filler in a PS matrix. This material had improved properties, which were mainly attributed to the architectural similarities between the polymer brush carbon nanotube and the polymer matrix. In this section the effect of PMMA polymer brush carbon nanotubes on the properties of a PMMA composite material was studied.

To observe the production of any optically sized bundled nanotubes, the composites were photographed on a light table (Figure 4. 12). Clearly seen is a decrease in optical transparency as the concentration of CNT-PMMA increases, which becomes completely opaque at 0.5w/w%. At 0.1w/w% the composite already shows visible signs of aggregation, which was previously not seen in the CNT-PS in PS composite material (Figure 4. 7). In addition, the presence of aggregation is an

indication that the properties of the composite may not improve upon the addition of the CNT-PMMA filler into a PMMA matrix.

Figure 4. 12: CNT-PMMA in PMMA (left to right – 0.00, 0.10, 0.25, 0.50, 1.00w/w%).

To verify the above statement DMA was performed on the composite materials to determine the CNT-PMMA affect on the storage modulus. As can be seen in Figure 4. 13 the composite does not show an improvement in the storage modulus. The initial un-filled PMMA matrix shows a storage modulus of 3100MPa, which subsequently begins to decrease upon the addition of the filler with the greatest decrease for 1w/w% to 2500MPa (i.e. at 0°C). This decrease can clearly be seen in the plot of storage modulus versus specific temperature and concentration (Figure 4. 14). In this graph, as the concentration increases the storage modulus decreases, however a localized peak develops at 0.5w/w%, which has occurred due to similar interactions seen between the CNT-PS in PS material. In the PS material architectural similarity increased the storage modulus and peaked at 0.25w/w%. This peak was the attraction to the neighboring nanotubes becoming stronger than the polymer brushes ability to repel them, and hence the nanofiller was condensed creating adverse affects. Comparing this phenomenon to the PMMA material, the architectural similarity is strong between the brushes and the matrix, however the similarity between carbon nanotubes and the brushes is low, causing the decrease in storage modulus when compared to un-filled PMMA. However, compared to the AC in PMMA (i.e. Figure 4. 2, and 0.1w/w% and 0.5w/w% of AR in PMMA), the CNT-PMMA in PMMA

composites are stronger for concentrations less than 0.5w/w%, which was due to the polymer brushes. In addition, the 0.5w/w% was the critical concentration where the carbon nanotube forces of attraction and repulsion were balanced (i.e. the localized peak). These results indicate that the PMMA polymer brushes of the CNT-PMMA sample show an increase in the carbon nanotubes limit of dispersion in a PMMA matrix, but more research is required to increase the limit of dispersion further so that the composite is stronger than un-filled PMMA.
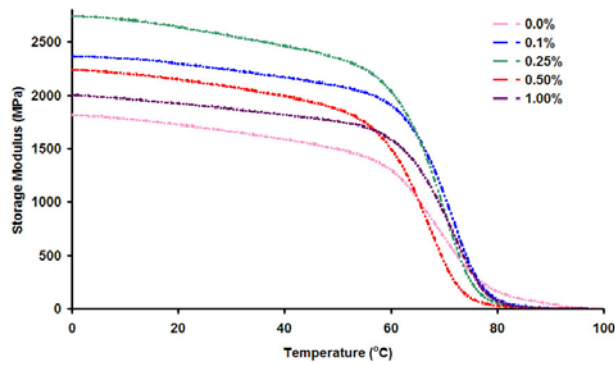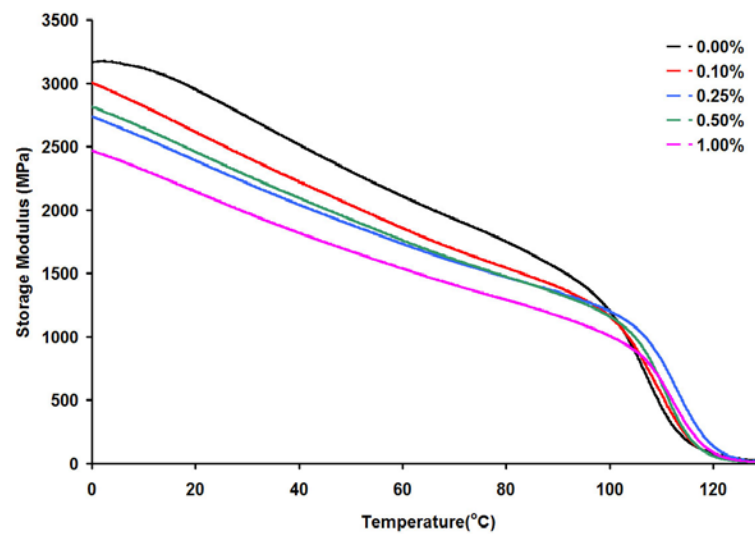

Figure 4. 13: DMA results of CNT-PMMA in PMMA of various w/w concentrations.
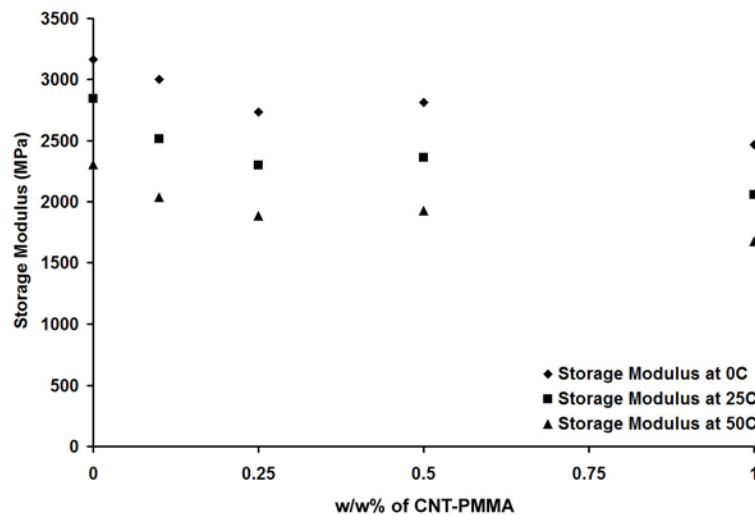
Figure 4. 14: The storage modulus at specific temperatures and concentrations of CNT-PMMA in PMMA. The graph exhibits an overall decrease in strength.

Previous research found that to obtain a 150% increase in the modulus a 1wt% loading was required.[373,374] However, the CNT-PS in PS increased by 150% at only 0.1w/w% achieving the greatest result at 0.25w/w% (i.e. ~180%). In the CNT-PMMA in PMMA, the 150% increase in the modulus was not achieved, but literature has shown with post processing a nanotube PMMA composite can increase with as little as 1wt% loading (i.e. 167% increase)[216] and as high as 10wt% loading (i.e. 137%).[375] This indicates that with post processing the storage modulus would increase, and due to the polymer brushes presence achieve stronger results at lower concentrations. Furthermore, longer polymer brushes would aid in increasing the architectural similarity, and entanglement with the matrix, which would help to increase the carbon nanotubes limit of dispersion.

From the DMA curves in Figure 4. 13 the Tanδ peaks determined the T_g to be 105°C for PMMA and increased to a maximum of 115°C for 0.25w/w%. DSC was used to verify these results and to determine the heat of post curing that formed due to the release of trapped monomer in the composite. The Table 4. 3 shows the results of the thermograms for the first and second heating. The T_gs determined by DSC are very similar to the T_g results obtained by DMA with 105°C for the PMMA, which increased to 119.38^{o}C for 0.25w/w% and 1.00w/w%.

In the first heating run, an exotherm forms in the DSC thermogram, which is the heat of the post curing reaction. Upon addition of the CNT-PMMA the exotherm decreases from 8.26J/g (i.e. un-filled PMMA) to 5.34J/g for 0.10w/w% and further to 0J/g for higher concentrations. The reduction of the exotherm was previously seen in Table 4. 1 of AR and AC in PMMA, which was attributed to the nanotubes ability to aid in the polymerization. This exotherm is not detected for 0.25w/w% and higher concentrations, which means no trapped monomer was found. In these cases the

CNT-PMMA must act as an efficient means to aid the polymerization so that no trapped monomer is formed. In addition, the T_g of the CNT-PMMA in PMMA is higher than the addition of AR, AC or no nanotubes. CNT-PMMA therefore is acting as a re-enforcing agent in the PMMA matrix, which is a similar affect to that observed in the CNT-PS in PS composite. Furthermore, this affect was observed in Chapter 3 as the polymer brush nanotubes also exhibited a higher T_g (i.e. when not in a polymer matrix). This was attributed to the nanotubes ability to reduce chain mobility[376] as well as the π-π stacking capabilities between the nanotube and the aromatic polymers.[377]

Upon second heating the T_g of all the PMMA composites (i.e. with and without CNT-PMMA) decreased, which correlated to the removal of trapped monomer, as previously seen in section 4.3. However the 0.25w/w% and higher concentrations do not possess an exotherm and hence no trapped monomer. For these materials a decrease in the T_g was observed due to a re-organization of the polymer chains when heated above the T_g. This therefore means the removal of excess monomer and/or heating above the T_g, causes the T_g to decrease.

Sample	T_g (1st run)(^{o}C)	T_g (2nd run)(^{o}C)	Exotherm (110-180°C)(J/g) (1st run)
0.00%	105.77	104.04	8.258
0.10%	109.83	103.75	5.343
0.25%	119.38	111.56	0
0.50%	118.80	104.04	0
1.00%	119.38	104.62	0

Table 4. 3: DSC results of CNT-PMMA in PMMA.

The T_g was not the only property to decrease, as the rheometer measurements showed a decrease in complex viscosity. In section 4.3 the addition of AR nanotubes decreased the complex viscosity, however when the AC nanotubes were used as a filler it acted to thicken the composite mix due to polar interactions.[359,360] The results

of the CNT-PMMA in PMMA, presented in Figure 4. 15, show no evidence of thickening, instead at low angular frequencies the complex viscosity decreased to approximately 59% and to as low as 40% for 0.25w/w% when compared to unfilled PMMA. This change from acting as a thickening agent has occurred due to the loss of carboxylic acid groups on the nanotube. The once polar nanotube, aiding in restricting flow, has had its carboxylic acid groups replaced with long PMMA chains that mimic the free polymer chains surrounding it. This results in the CNT-PMMA acting very similar to the AR filler in processability, but can possess a stronger storage modulus and a higher T_g than AR in PMMA.
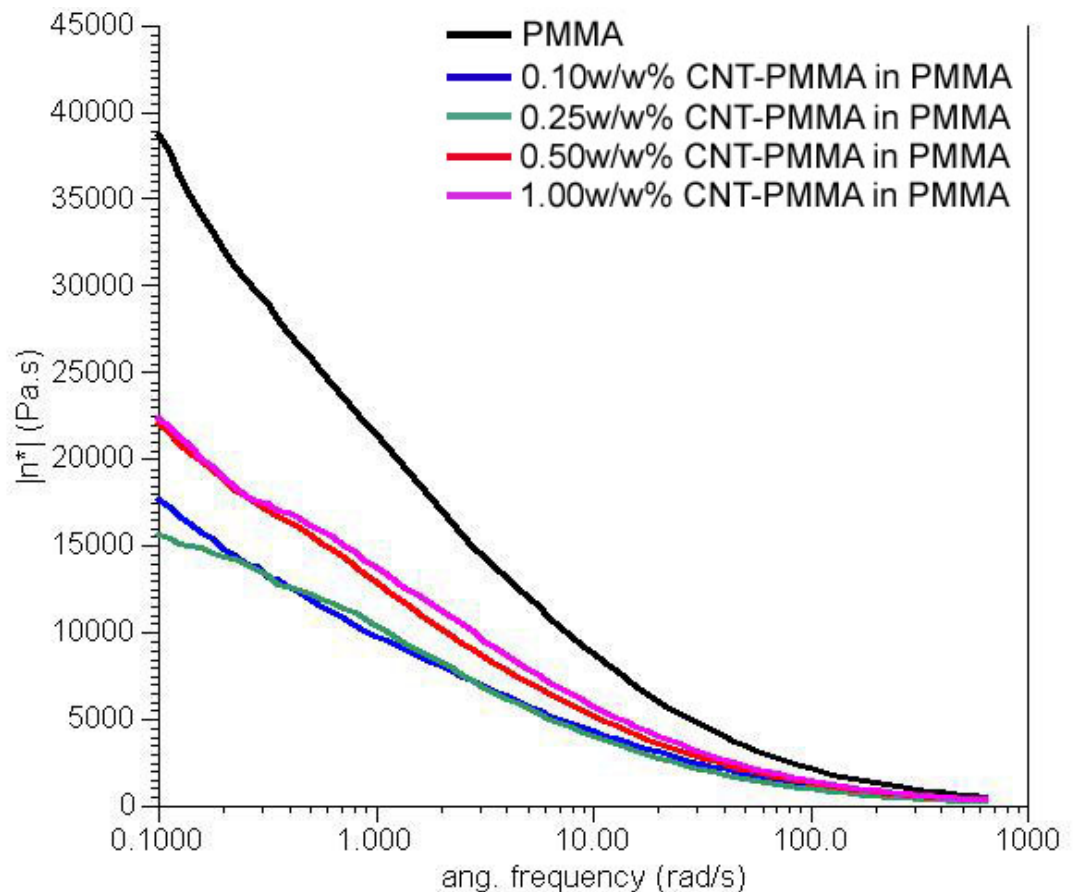
Figure 4. 15: Complex viscosity plot of CNT-PMMA in a PMMA matrix. The viscosity decrease approximately by half upon adding as little as 0.10% of CNT-PMMA.

The large change in rheological properties indicates that the percolation threshold is higher for the polymer brushed carbon nanotubes compared to the AC nanotubes due to a decrease in the interfacial tension (i.e. the loss of carboxylic acid surface functionality). Similarly to literature, Gelves *et al*[378] found using copper nanowires functionalized with 1-octanethiol that the rheological threshold could be increased by decreasing the interfacial tension between the nanowire and the polymer matrix.

4.5 PHEMA Brushes in a PHEMA and a PMMA Matrix

In the previous section the filler used had un-cross-linked polymer chains produced by ARGET ATRP. In this section, the filler has been replaced with CNT-PHEMA that can contain some cross-linkages, and is dispersed into a PHEMA matrix that can also cross-link.[379] A PMMA matrix was also investigated due to the large similarity in chemical structure.

The research on the CNT-PHEMA was performed so a comparison could be made between a free radical polymerization (FRP) and a controlled radical polymerization (CRP) filler. The results of the CRP filler (CNT-PS and CNT-PMMA) has shown increased processability, and with a high architectural similarity, the storage modulus also increased. The FRP was investigated to determine if these properties are a result of the polymerization technique employed or if it is due to the addition of a CRP polymer brushed nanotube; a CRP polymer brush nanotube contains linear chains unlike the cross-linked FRP polymer brush nanotube.
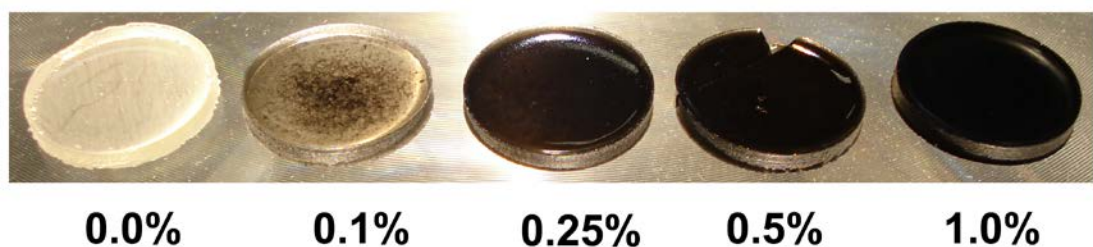
Figure 4. 16: CNT-PHEMA in PHEMA of various w/w concentrations.
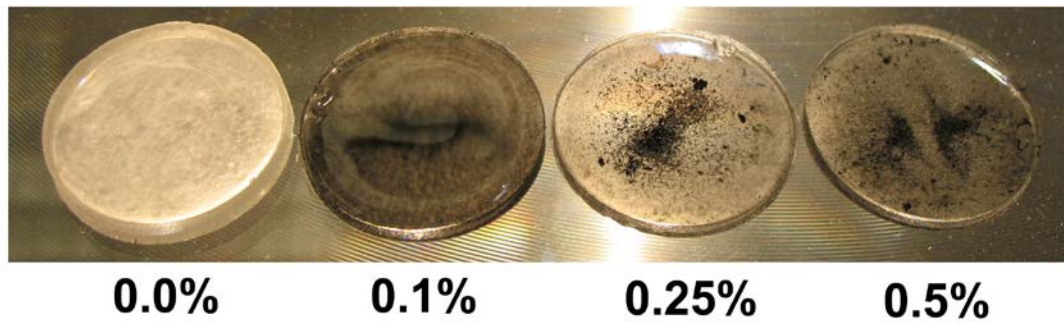
Figure 4. 17: CNT-PHEMA in PMMA of various w/w concentrations.

In the photographs of Figure 4. 16 and Figure 4. 17, it is clear that the CNT-PHEMA disperses better in the PHEMA matrix rather than the PMMA. This was due to the CNT-PHEMA filler having a higher polarity than PMMA, which comes from the hydroxide groups along the polymer chain. Further investigation using microtome slices of the matrix in transmission electron microscopy (TEM) found that the CNT-PHEMA were more abundant in the lower portion of the matrix (Figure 4. 18). This demonstrated that the CNT-PHEMA did not disperse well in the monomer/MMA and hence settled by gravity before the polymer matrix was formed. The end result is a material with a concentration gradient of filler that creates different physical properties to the lower and upper portions of the matrix (i.e. heterogeneous composite). This was a similar result to that found by Li *et al.*[380] In their results they found that some of their nanotube-ester products did not disperse well in a polysulfone matrix and hence settled out by gravity. This created varying degrees of electrical properties through the composite as well as across the two surfaces (i.e. bottom and top). Relating to the CNT-PHEMA in PMMA, this therefore indicates that varying properties across and through the composite might be expected.
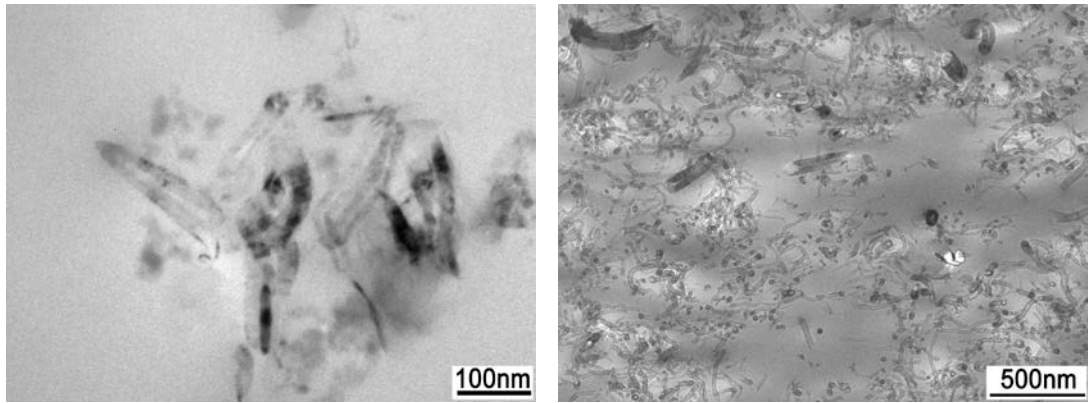
Figure 4. 18: Microtome TEM images at the top (left) and at the bottom (right) of CNT-PHEMA in PMMA. Due to the limited solubility in PMMA the filler aggregates and settles out by gravity.

The CNT-PHEMA in PHEMA showed a lesser degree of limited dispersion than when it was in PMMA. The 0.1w/w% filler loading of Figure 4. 16 does show some visibly sized aggregated particles, but as the concentration increases the uniformity of the filler appears to increase. This was associated to higher concentrations creating a greater supportive network for the cross-linked nanotubes and the PHEMA's capability to change its polarity by chain rearrangement;[381] evenly spaced filler due to equal forces of attraction and repulsion to the other nanotube-polymer chains. Too low a concentration favors aggregation and the nanotubes within the single polymer chain come together, while higher concentrations favors relaxation of the filler with PHEMA chain rearrangement, and hence the nanotubes in the chains stretch outwards to neighboring nanotubes/filler creating a better dispersion. It is important to note that this phenomenon only occurred in the CNT-PHEMA and not the CNT-PS or CNT-PMMA as their chemical structure is different containing only one nanotube per chain, compared to many nanotubes per chain in the CNT-PHEMA. Furthermore, microtome slices of the CNT-PHEMA in PHEMA of the top and bottom showed no identifiable difference in nanotube concentration (i.e. has not settled by gravity). This

indicates that the CNT-PHEMA in PHEMA will exhibit different properties to the heterogeneously dispersed CNT-PHEMA in PMMA.
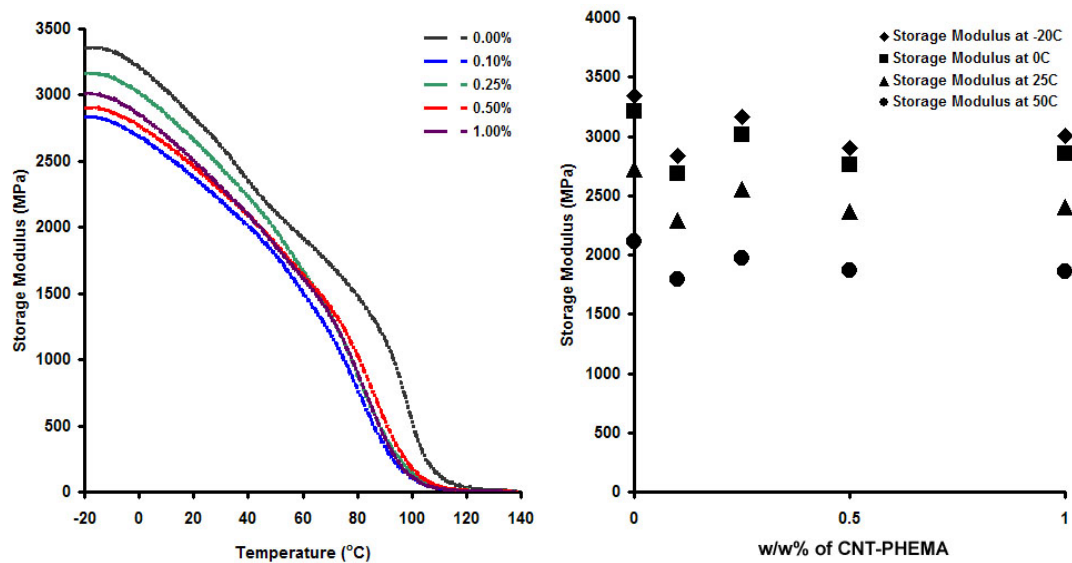
Figure 4. 19: DMA results of CNT-PHEMA in PHEMA, which demonstrates an overall decrease in the strength, however a localized peak occurs for 0.25w/w%.

As the composite of CNT-PHEMA in PHEMA aggregates at low concentrations and disperses in high concentrations the storage modulus should increase at the critical point. DMA was performed on the composites of CNT-PHEMA in PHEMA and CNT-PHEMA in PMMA to observe this change. Figure 4. 19 shows the CNT-PHEMA in PHEMA curves and it was clear to see that upon addition of the filler the storage modulus decreased, but then increased. This was to be expected as poorly dispersed fillers degrade the storage modulus and well dispersed fillers can increase the storage modulus. Referring to Figure 4. 16, the 0.1w/w% composite is poorly dispersed and the 0.25w/w% composite is well dispersed corresponding to decreased storage modulus and increased storage modulus, respectively. As the concentration increased further, the strength of the modulus lowered, indicating the effective concentration had been reached with the production of the condensed affects (i.e. aggregation forces were stronger than repulsion forces). This same trend was

observed for the CNT-PS in PS (Figure 4. 9), except the introduction of the CNT-PS filler in PS is favored creating an overall positive affect when compared to the unfilled PS. In addition, both localized peaks occur at 0.25w/w%, which could reflect a nanotube polymer brush optimal concentration that relates to the volume it occupies. Further studies on different monomers are required to determine the validity of this concept.

DMA curves of Figure 4. 20 show a similar trend to that observed in Figure 4. 14, which is of CNT-PHEMA in PMMA and CNT-PMMA in PMMA, respectively. This decreasing trend on the storage modulus was expected due to the presence of visibly sized aggregates, as observed in Figure 4. 17, which was a result of the architectural dis-similarity between PHEMA and PMMA. Although the main difference between PMMA and PHEMA is a hydroxyl group, Holly *et al*[381] found in their work that PHEMA possesses an ability to increase or decrease its polarity by the reorientation of the polymer side chains, depending on the nature of the adjacent phase. However, in this material the phenomenon experienced by Holly and coworkers must be retarded by the large nanotubes in the polymer brush chains, as the PHEMA would otherwise adjust the polarity to disperse the nanotubes uniformly in the PMMA. However, the results of section 4.4.2 suggested that post processing the PMMA composites would increase the storage modulus and is suggested as future work. Furthermore, the localized peak of the CNT-PHEMA in PHEMA, presented in Figure 4. 19, corresponds to the increase in dispersion upon the 0.25w/w% loading, observed in the photograph of Figure 4. 16. These changes in the DMA and the observable dispersion further supports the concept that the CNT-PHEMA in PHEMA can disperse more easily at concentrations between 0.25w/w% to 1w/w%. This was

associated to the affect seen by Holly and coworkers, and the architectural similarity between brush and matrix.
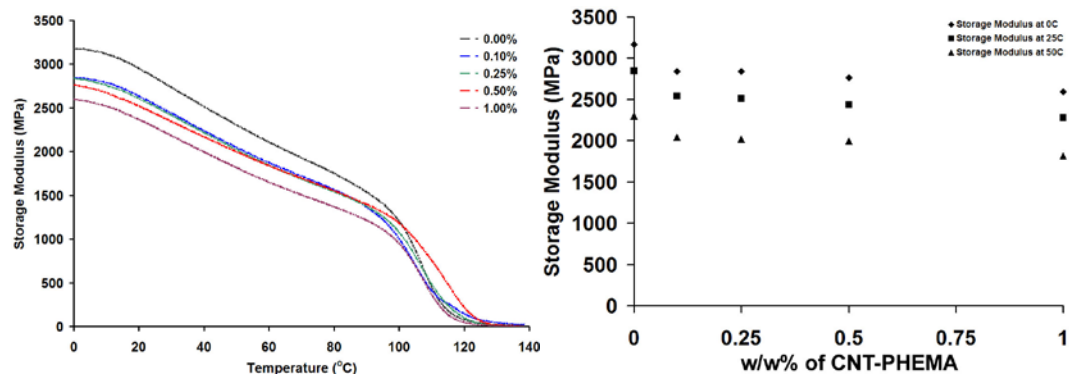
Figure 4. 20: DMA results of CNT-PHEMA in PMMA. These results show an overall decrease the in strength of the material with the greatest decrease for 1.00w/w%.

The T_g of the composites were determined from the DMA Tanδ peaks, which showed that when the CNT-PHEMA was in PHEMA the T_g decreased and in PMMA it was unchanged (exception of 0.5w/w%). DSC analysis complimented this and the results can be seen in Table 4. 4 and Table 4. 5. The CNT-PHEMA in PHEMA decreased by approximately 40^oC upon the addition of the filler, but after the second heating run the T_g fluctuated about the un-filled PHEMA T_g. This is similar to the other composites presented in this chapter and was associated to a loss of trapped monomer in the first heating. However, in the un-filled PHEMA when the trapped monomer was removed the T_g remained constant. An affect such as this would indicate that the un-filled PHEMA matrix is already a very rigid structure, which strengthens the concept that the un-filled PHEMA is highly cross-linked as determined in chapter 3.[382] In addition, the filled PHEMA composites do not exhibit an exotherm, which verifies that the trapped monomer is not the only property to affect the T_g. The increase occurred due to relaxation/reorientation of the matrix polymer chains when heated to high temperatures; the free volume lowered in the

polymer chain re-organization, increasing the T_g. This indicates that the filled PHEMA matrix was cross-linked to a lesser extent when compared to un-filled PHEMA, as the matrix polymer chains had some freedom for reorientation to occur.

Sample	T_g (1st run)(^{o}C)	T_g (2nd run)(^{o}C)	Exotherm (110-180°C)(J/g) (1st run)
0.00%	105.6	105.6	4.2
0.10%	65.0	109.0	0
0.25%	62.4	101.9	0
0.50%	60.9	104.9	0
1.00%	58.7	108.6	0

Table 4. 4: DSC results of CNT-PHEMA in PHEMA.

Sample	T_g (1st run)(^{o}C)	T_g (2nd run)(^{o}C)	Exotherm (110-180°C)(J/g) (1st run)
0.00%	105.77	104.04	8.258
0.10%	111.27	103.17	0
0.25%	114.70	102.89	0
0.50%	111.56	104.04	3.895
1.00%	108.96	102.01	3.109

Table 4. 5: DSC results of CNT-PHEMA in PMMA.

The results of CNT-PHEMA in PMMA showed for the first heating the same trend as seen in Table 4. 3 (CNT-PMMA in PMMA), but in the second heating run the T_g of all the concentrations decreased to approximately 103°C. This was attributed to the removal of trapped monomer, but as 0.10w/w% and 0.25w/w% do not possess an exotherm it suggests relaxation/reorientation of the composites occurred as well. This could indicate that in all of the composites, a change in the T_g could be a combination of the removal of trapped monomer and relaxation/reorientation of the polymer chains.

Literature concerning PHEMA composites found that the T_g increases when paired with an equally polar substance. Caykara *et al*[383] found in their work that upon the addition of silica particles to a PHEMA matrix the T_g increased by 26°C

regardless of the concentration. This was attributed to a decrease in mobility of the chains near the filler particles. Mohomed *et al*[384] found that when they dispersed [(DMSO)(methanol)Cu$_2$(benzene-1,3-dicarboxylate-5-OH)$_2$]$_{12}$ nanoballs into PHEMA, the T$_g$ increased due to similar reasons that Caykara and coworkers found. In this work, the CNT-PHEMA composites did not experience an increase in the T$_g$ as carbon nanotubes are not an equally polar substance to the PHEMA matrix. However, as the PHEMA can adjust its polarity by chain reorientation,[381] the PHEMA brushes should have counteracted the nanotubes presence. This indicated that the structure of the polymer brushes were cross-linked, which hindered this affect.

In the previous sections, the composites containing nanotubes or polymer brush nanotubes decreased the viscosity upon the addition of the filler, but in AC in PMMA an increase occurred due to hydrogen bonding, which retarded the polymer flow. A similar affect was observed for the CNT-PHEMA in PHEMA, as evident from the rheology curves of Figure 4. 21. These plots show an increase in viscosity to approximately 119% when compared to the un-filled PHEMA, but for 0.25w/w% the complex viscosity is the same as the un-filled PHEMA. Comparing these results to the photograph of Figure 4. 16 the 0.25w/w% concentration is also the point when the filler becomes evenly dispersed, which occurred due to a structural expansion of the filler and also coincides with the localized peak of the DMA results. As in this concentration the filler is more out stretched the affect of the filler does not act as a thickening agent. Instead the CNT-PHEMA has been more easily incorporated into the mix and as a result the matrix is unchanged. However, increasing the concentration changed the volume which the filler could occupy, creating the condensed affects and increasing complex viscosity. Similarly El-Tahlawy *et al*[385]

found in their work that upon the addition of chitosan-PHEMA, the viscosity increased.
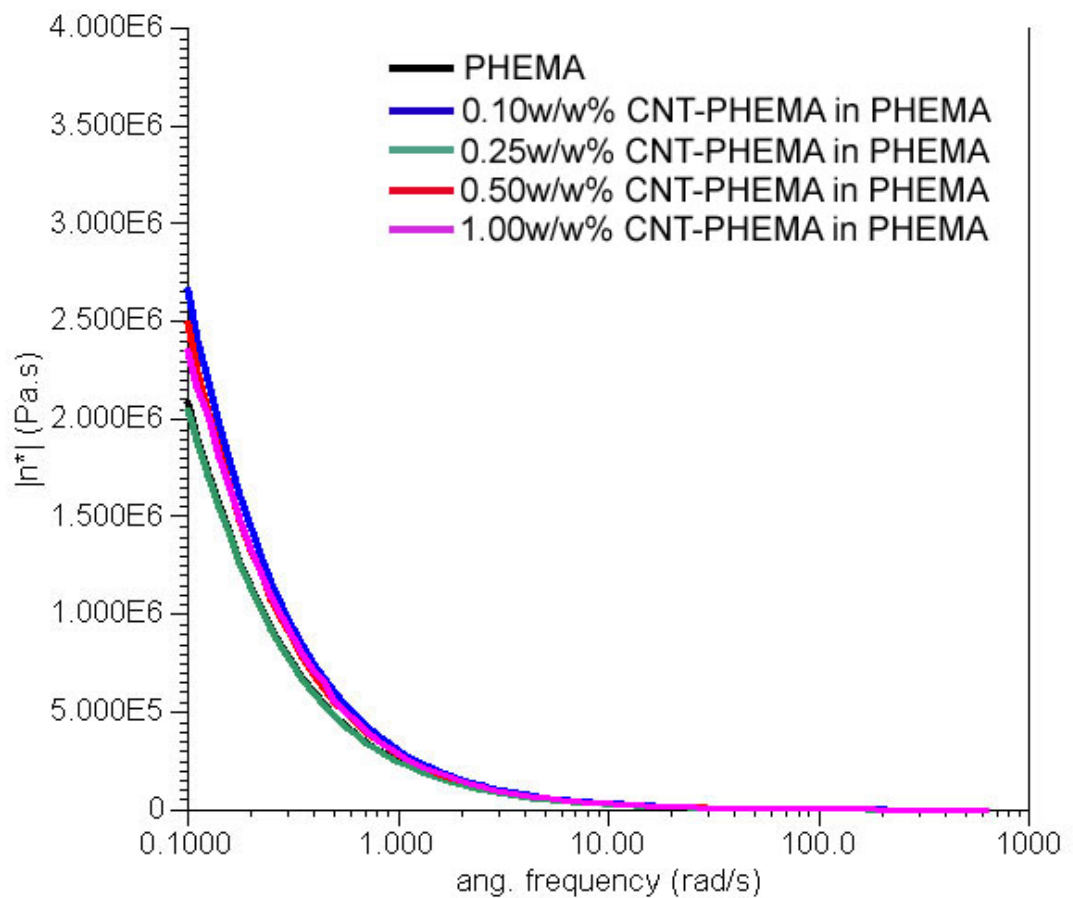
Figure 4. 21: Complex viscosity plot of CNT-PHEMA in a PHEMA matrix.

The rheological plots of CNT-PHEMA in PMMA (Figure 4. 22) showed different results to the CNT-PHEMA in PHEMA. This is because the filler is not evenly dispersed, and the matrix is weaker in its hydrogen bonding capabilities. Previously hydrogen bonding was found to increase the complex viscosity (i.e. AC in PMMA) and hence the filler acted like a thickening agent. In this case the strength of hydrogen bonding between the two mediums is not as strong and the filler acts to decrease the complex viscosity. All concentrations showed some increase in processability, with 0.25w/w% complex viscosity decreasing approximately to 50% at the low angular frequencies (note: 0.50w/w% complex viscosity is higher at low angular frequencies and lower at high angular frequencies when compared to the un-filled PMMA). These

changes showed no observable trend, but overall a decrease in the complex viscosity occurred.
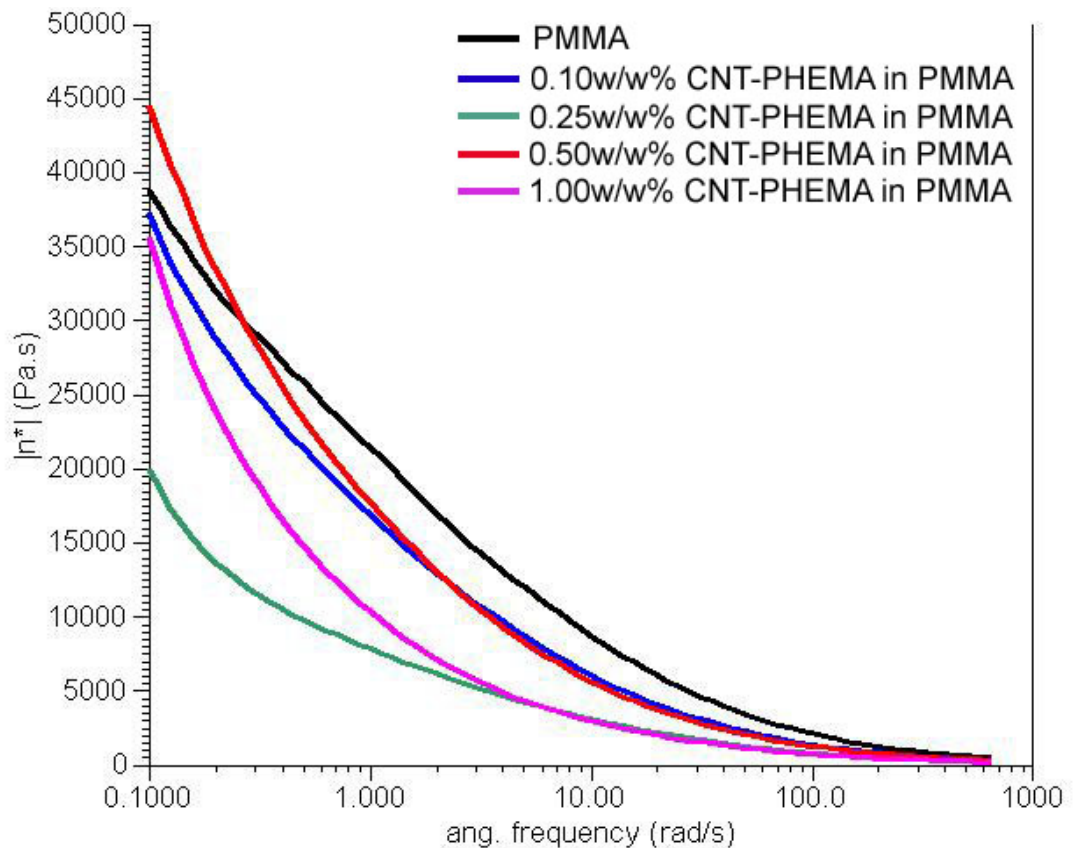
Figure 4. 22: Complex viscosity plot of CNT-PHEMA in a PMMA matrix.

4.6 Pyrene-Polystyrene brushes in a Polystyrene Matrix

Pyrene-PS was used previously to model the effects of growing polymer brushes on carbon nanotubes. This work was extended further to a Pyrene-PS in PS composite to determine the affect it would have on the PS. As the CNT-PS is similar in chemical structure, similar changes in the properties were expected, but does possess one structural difference. The Pyrene-PS possesses one polymer chain to every one pyrene group, whereas the CNT-PS has many polymer chains to every one nanotube. This ultimately changes the effective volume the filler occupies and greatly increases the limit of dispersion.

Figure 4. 23 is a photograph depicting the increasing concentration of the Pyrene-PS in PS. What is observed is no change in its transparency when previously the addition of polymer brush carbon nanotubes resulted in visibly sized aggregates or semi to complete opaque composites. Although the filler appears uniformly dispersed there is no visual change to verify the finding. However, work in this chapter has indicated that measurements using DMA, when the filler was poorly dispersed, would result in a decrease in the storage modulus, due to it acting like an impurity. What was found from this research is that the DMA curves of Figure 4. 24 do not show a decrease, but instead show an increase in the storage modulus. This indicates that an even dispersion was formed in the composite.

Figure 4. 23: Pyrene-PS in PS.

The plot of Figure 4. 25 examines the DMA curves more closely in relation to the filler concentration. What can be seen is an increase in concentration, creates an increase in storage modulus. Within the first 1w/w% of filler addition to the composite there appears to be a steady increase until a maximum is reached. As there appears to be no limit of dispersion this maximum could be the storage modulus of pure Pyrene-PS and would become more evident with significantly higher concentrations of the filler. Overall the storage modulus increased to a maximal 130% with the addition of 1w/w% Pyrene-PS, which showed no sign of it acting as an impurity.
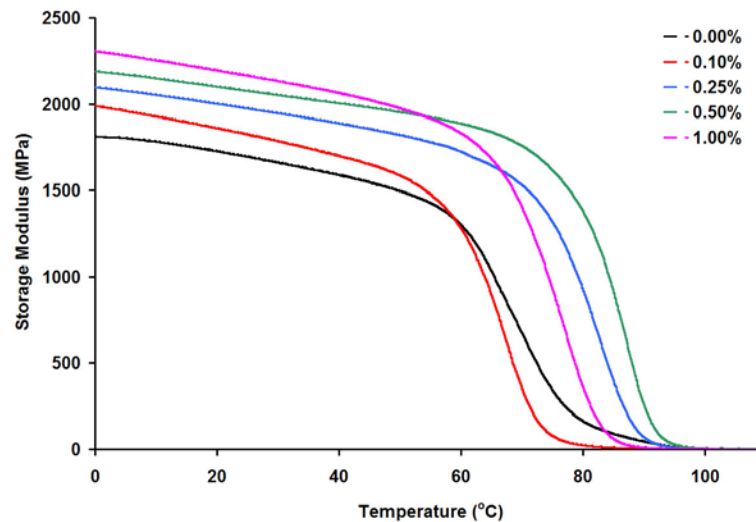
Figure 4. 24: DMA results of Pyrene-PS in PS of various w/w concentrations.
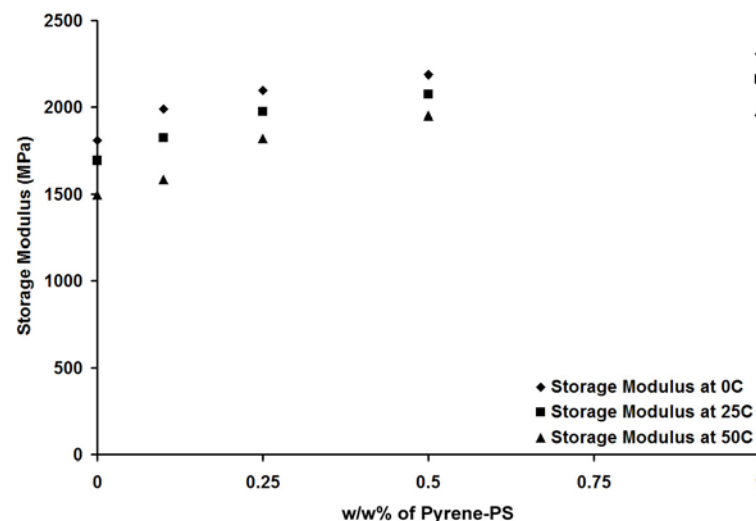
Figure 4. 25: The storage modulus at specific temperatures and concentrations of

Pyrene-PS in PS. What is noticed is an increase in strength with increasing filler

concentration.

Comparing these results to the CNT-PS in PS a localized maximum occurred at 0.25w/w%, which was associated to the limit of dispersion and was not observed in the Pyrene-PS in PS. This difference occurred due to the presence of the carbon nanotubes and ultimately the chemical structure. In the case of the CNT-PS it occupied more volume and had stronger π-π stacking capabilities, but the most significant property was the transference of mechanical strength. The carbon

nanotube on its own possesses a very high mechanical strength,[386] but the pyrene does not possess an equal strength and as a result the greatest storage modulus increase observed was 180% at 0.25w/w% and 130% at 1w/w% for CNT-PS in PS and Pyrene-PS in PS, respectively (i.e. a 500MPa difference). This demonstrates that the CNT-PS is a better filler due to the lower concentrations required for a greater storage modulus improvement. This also indicates in conjunction with the results of Figure 4. 2 (i.e. AC in PS composite) that the polymer brushes are covalently attached. If they were not attached they would disperse during the matrix polymerization and the nanotubes would decrease the storage modulus due to their limited dispersibility.

Sample	T_g (1st run)(^{o}C)	T_g (2nd run)(^{o}C)	Exotherm (110-180°C)(J/g) (1st run)
0.00%	55	72	30.4
0.10%	87.83	94.49	5.066
0.25%	84.36	90.72	2.184
0.50%	85.22	95.64	1.926
1.00%	86.67	93.91	0

Table 4. 6: DSC results of Pyrene-PS in PS.

The results of the DSC, presented in Table 4. 6, demonstrated a similar trend to that observed for the CNT-PS in PS (see Table 4. 2). In the previous results, upon addition of the CNT-PS fillers the T_g generally increased by 10°C, however in the Pyrene-PS filled material a larger increase in the T_g was observed. In the first run the Pyrene-PS in PS composites increased by approximately 30°C, which is three times greater than the CNT-PS in PS. The reason for this increase is obviously due to the absence of the carbon nanotube, as the Pyrene-PS, being smaller than the MWCNT, significantly decreases the free volume in the PS matrix and hence increases the observed T_g.[350]

Further study of the DSC results in Table 4. 6, found that the heat of the post curing reaction was lower for the Pyrene-PS. This is obviously associated to the release of trapped styrene monomer, but indicates that Pyrene-PS is a better filler than CNT-PS in a bulk polymerization (see section 4.4.1). In addition to this finding, comparing only the results of the second heating, it is clear that the T_g does increase upon the addition of either filler. For the CNT-PS filler this increase does not significantly change the T_g, but the Pyrene-PS increases the T_g by a minimum of 18.72^{o}C. This difference is not associated to trapped monomer as it was vaporized in the first heating and so these results are solely due to the filler acting only on the PS matrix.
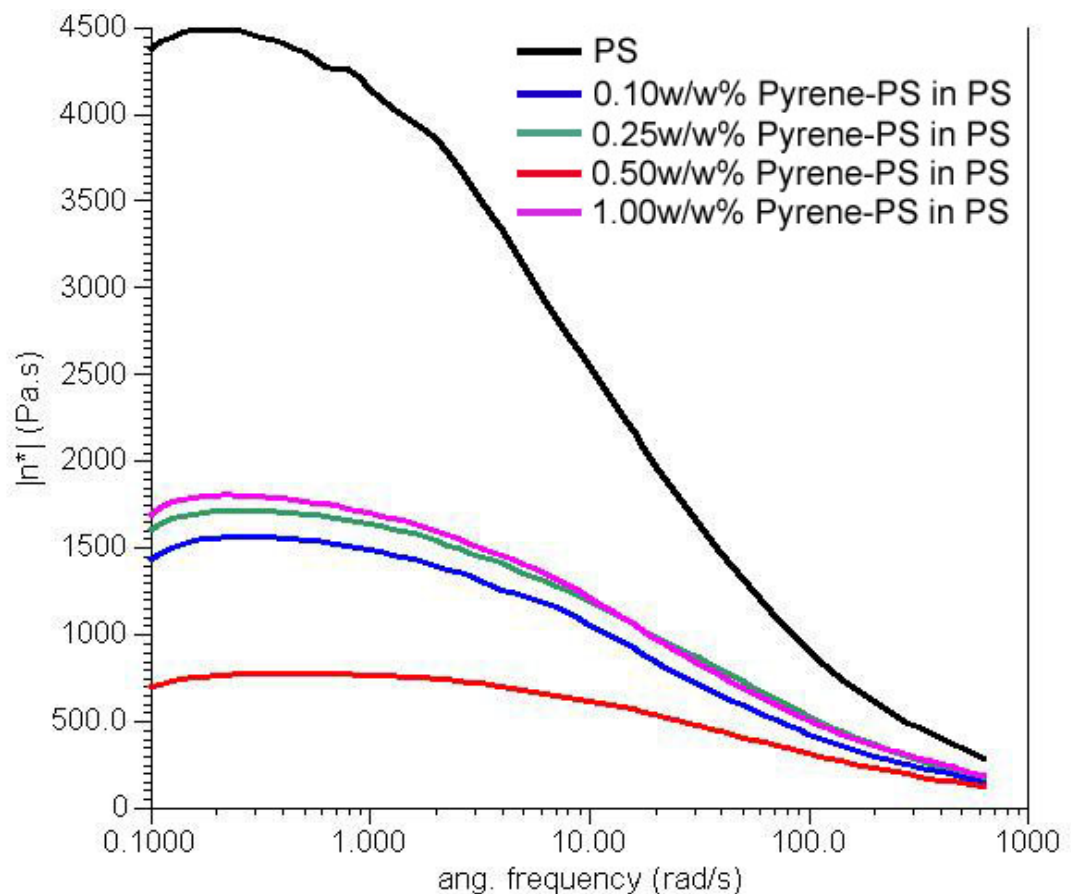
Figure 4. 26: Complex viscosity plot of Pyrene-PS in a PS matrix. The graph shows an increase in processability upon adding as little as 0.10w/w% of Pyrene-PS.

As previously found in section 4.4.1 the presence of the CNT-PS significantly increased the processability with an average decrease in complex viscosity to 4.5% when compared to the un-filled PS. In comparison to the Pyrene-PS the average decrease in complex viscosity was to 36%, except 0.50w/w% decreasing to 16%, when compared to un-filled PS. However, results from section 4.3 found AR in PS to have the same decrease in complex viscosity as the CNT-PS (i.e. 4.5%). From these results it is clear that the nanotube is a vital component in significantly reducing the complex viscosity, and the presence of the polymer brushes aid in increasing the limit of dispersion.

4.7 Conclusion

The results of this chapter indicate that the carbon nanotube is an excellent filler for a composite material, however due to the chemical structure and hence the limit of dispersion, it often leads to an increase in properties of one characteristic and a corresponding decrease in another. Typically this was an increase in processability, which resulted in a decrease in the storage modulus. To combat this, polymer brushes were covalently attached to the carbon nanotube to increase the nanotubes architectural similarity with the polymer matrix.

Polymers such as PS, PMMA, and PHEMA were produced and generally the properties of the PS material gave better results due to the presence of the aromatic groups (i.e. π-π stacking capabilities). The methacrylate polymers did not possess π-π stacking capabilities, but experienced greater affects due to a difference in polarity between the nanotube and the polymer. This led to a decrease in the storage modulus of the PMMA and PHEMA composites, but did not affect the T_g of the materials and still produced an increase in processability in the PMMA composites. Furthermore, localized peaks in the DMA results often occurred at the low concentrations and

indicated, in the PS composites, an optimal concentration for the CNT-PS to be most affective.

In comparison to PS, the model system of Pyrene-PS did not exhibit a limit of dispersion for concentrations less than 1w/w%. The results showed that the storage modulus continued to increase with increasing concentration to a final increase of 130% for 1w/w%. In addition, the T_g increased by approximately $20^{o}C$ and the complex viscosity decreased to 36%. These property changes were very similar to the CNT-PS composites, but a limit of dispersion was reached at 0.25w/w%. This did not create an issue as at 0.25w/w% the increase in the storage modulus was 180%, which was 500MPa greater than that experienced with Pyrene-PS. In addition, the processability also increased more than the Pyrene-PS. Overall the nanotube played an important part in increasing the storage modulus and increasing the processability that was not matched by the Pyrene.

Ultimately the carbon nanotube was found to be an affective filler. However, polymer brushes are required and to observe the greatest enhancements, aromatic groups within the chains are essential. This helps in fostering its strengths into the matrix due to the π-π stacking capabilities.

- CHAPTER 5 -

FORMATION

OF

BLOCK COPOLYMER MICRODOMAINS

AND

HYBRID MATERIALS (NANO SIZED)

5. FORMATION OF BLOCK COPOLYMER

MICRODOMAINS AND HYBRID MATERIALS

(NANO SIZED)

Preface

This chapter details the procedures employed to obtain successful di-block copolymer lamellae and hexagonal cylindrical phase segregation. The technique was altered to include the polymer brush carbon nanotubes and the final orientation of the nanotubes were determined.

5.1 Introduction

Block copolymers, with contiguous sequences, sufficiently incompatible, spontaneously self-assemble in order to minimize interactions between incompatible components. Depending on the structure considered, the block copolymers and the incompatible segments could have a different contrast such as compositional contrast (i.e. hydrophilic/hydrophobic, polar/non-polar, etc…). The chemical link between different blocks prevents phase separation in macroscopic length scale and the phase separation leads to regular structures with periodicity in the nanometre range, whereas dilution with solvent produces highly associated, but disordered phases. Depending on the composition of the block copolymers and the interaction between constituent segments, different packaging (i.e. spherical, cylindrical, gyroid, lamellae) and morphologies of typical domain size in the nanometre range emerge.[387]

The clever manipulation of this architectural contrast and self-organization has lead researchers to create different nanomaterials with various applications in nanotechnology. The cylindrical packing phase has received considerable interest in the generation of nanoporous templates or in the generation of cylindrical pillars. This

was achieved by chemical etching,[388,389] UV-cleavage,[390,391] and thermal cleavage[390] of the second block with subsequent washing for its removal.

In this work hexagonal-packed cylindrical and the lamellae phase of PS-b-PMMA was used as a template for exploring the alignment of carbon nanotubes on a silicon wafer surface.

In order to achieve perpendicular orientation of block copolymer phases on a silicon wafer surface, previous research by Xu *et al*[392] found that a neutral surface was required, otherwise one of the blocks align preferentially to the surface and a parallel orientation would result. Mansky *et al*[393] found that a random/statistical copolymer tethered to the surface could create a neutral surface and hence formed the perpendicular orientation.

However, due to the high viscosity of block copolymers the formation of the phases do not occur unless the temperature is raised above the order-disorder transition (ODT) temperature for long periods of time. This is typically above the glass transition temperature (T_g) as the polymer segments can move more freely and segregate themselves to lower the entropic forces; the copolymer block junctions align at the phase boundaries in the lowest energy form (see Figure 5. 1).[166]
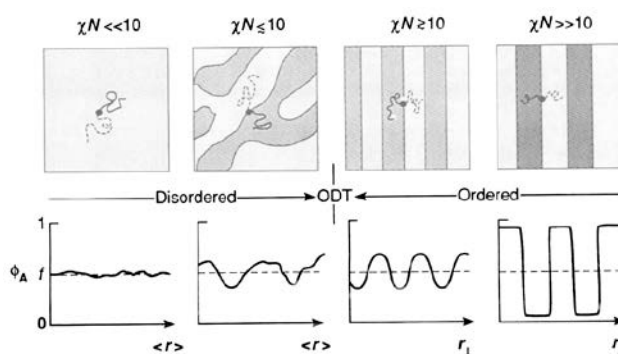
Figure 5. 1: The block copolymer junctions aligning at the phase boundaries and the orientation of the domains as the block copolymer is brought into the ordered phase. [166]

Literature to date has not combined the two fields of carbon nanotubes with block copolymers, except in patterning a surface with catalytic particles for the generation of chemical vapor deposition (CVD) nanotubes.[394,395] This chapter therefore explores for the first time the merging of the two fields in an effort to explore the nanotube's orientation in a cylindrical phase melt.

Some difficulties arise in merging the two materials as their surface energies do not match and the nanotubes tend to aggregate.[396] To combat this in a "30/70" hexagonal cylindrical phase melt, a polymer brush of the "30" polymer was used to create the composite. The "30" polymer was targeted specifically as the cylindrical morphology it creates is similar to that of a carbon nanotube and hence will not interfere with the long range ordering of the polymer cylinders. Furthermore, in the polymer melts effort to lower the entropic forces the polymer brush carbon nanotube will have an affinity to orient within the "30" phase, which is orientated perpendicularly to the surface, making the "70" polymer the supportive matrix.

Using the results of the previous chapters, it is clear that a polymer brush of PS will be more suited for this application. As seen in Chapter 4 the CNT-PS disperses better than the CNT-PMMA, due to the PS π-π stacking capabilities to the carbon nanotube enhancing the dispersion properties. This makes the CNT-PS ideal for this application, as a CNT-PMMA would be attracted to the PMMA phase, but as the carbon nanotube is still present in the core of the structure, it could express some π-π stacking capabilities and still have an affinity to enter the PS domain. This would ultimately interfere with the melt and it is probable that no segregation would occur.

Previous research has shown that when surface functionalized nanoparticles are mixed into a block copolymer phase melt, the nanoparticle position could be

controlled.[397] Compared with carbon nanotubes, the nanoparticle is very small and hence could require stronger forces than what the polymer segregation can provide.

Foreseeable applications of this composite are, but not limited to, conductive materials, solar cells, and membranes. A perpendicular alignment is particularly favored as the carbon nanotube could traverse both the top and bottom interface of the thin film. This would create a channel for electrons to pass through the composite (i.e. ballistic transport through the nanotube and hence conductive)[398] or a small molecule such as water[399] in desalination membranes.

5.2 Synthetic and Preparation Procedures

<u>Materials</u>

Styrene and MMA was dried over calcium hydride then purified by passing through a column of basic alumina. 2-hydroxy ethyl methacrylate (HEMA) was purified by a previously recorded procedure.[400] Me$_6$TREN was synthesized as previously discussed in Chapter 2. (100)-oriented single-crystal silicon (Si100) was obtained from Mick Bjelopavlic at Monsanto, St Lewis. Anionic polymerized di-block copolymer was purchased from Polymer Source Inc. P(S-b-MMA) lamellae Mn: 105,500g/mol and PS cylinder Mn: 187,800g/mol. CNT-PS(Short) was prepared using the procedures outlined in Chapter 3 to produce CNT-PS with reaction time 1440mins, but S-MWCNT were used (1-2μm in length), which are comparable in length to the thickness of the thin films produced. Ethyl 2-bromoisobutyrate (EBiB), copper(II) bromide, tin(II) 2- ethylhexanoate (Sn(EH)$_2$), anhydrous anisole, methanol, sulphuric acid, hydrogen peroxide, and anhydrous toluene were obtained from Aldrich.

Preparation of Neutral Surface

   - Copolymerization of Styrene and HEMA

$CuBr_2$ (6.54µmol) with 1mL of anisole, Me_6TREN (65.4µmol), styrene (25.28mmol), HEMA (18.30mmol), $Sn(EH)_2$ (32.7µmol) with 0.5mL of anisole, and a magnetic stirrer were added to a nitrogen purged vial. The polymerization was initiated by the addition of EBiB (0.218mmol) with 1mL of anisole. The polymerization was carried out at 90^oC and stopped at regular intervals by exposure to the air. In addition, the polymer was purified by precipitation in cold hexane (PS-co-PHEMA).

   - Tripolymerization of Styrene, HEMA, and MMA

$CuBr_2$ (2.06µmol) with 0.5mL of anisole, Me_6TREN (20.6µmol), styrene (23.09mmol), HEMA (1.65mmol), MMA (16.49mmol), $Sn(EH)_2$ (30.9µmol) with 0.5mL of anisole, and a magnetic stirrer were added to a nitrogen purged vial. The polymerization was initiated by the addition of EBiB (0.206mmol) with 0.5mL of anisole. The polymerization was carried out at 90^oC and stopped at regular intervals by exposure to the air. In addition, the polymer was purified by precipitation cold in methanol (PS-co-PHEMA-co-PMMA).

   - Silicon Wafer Surface Functionalization with Polymer

Si100 was cut into squares measuring 4cm x 4cm. The organic residues on the surface of the silicon substrate were removed by submersing the wafer in "Piranha" solution (i.e. 70vol% sulphuric acid, 30vol% hydrogen peroxide) for 15mins at room temperature.[401] After being rinsed with copious amounts of distilled water and blown dry by nitrogen flow, the newly produced hydrolyzed surface (Si-OH) had a 0.1w/v% (0.8vol% THF, 0.2vol% methanol) solution of the PS-co-PHEMA spin coated onto

the surface at 1000rpm. The wafer was then heated in a vacuum oven at 170°C for 48hrs followed by rinsing with THF and blown dry by nitrogen flow.

The above procedure was repeated for the PS-co-PHEMA-co-PMMA polymer, but used a 0.1w/v% toluene solution and was rinsed with toluene.

Lamallae and Cylindrical Phase Di-Block Copolymer Melt

A 10w/v% solution of the commercial PS-b-PMMA (lamellae and cylindrical) in toluene was spin coated onto the PS-co-PHEMA-co-PMMA polymer brush wafer at 1000rpm and subsequently heated at 200°C for 48hrs.[403]

Cylindrical Phase Di-Block Copolymer Melt with CNT-PS(Short)

A 10%w/v solution of the commercial PS-b-PMMA mixed with 3%w/v of CNT-PS(Short) in toluene was spin coated onto the PS-co-PHEMA-co-PMMA polymer brush wafer at 1000rpm and subsequently heated at 200°C for 48hrs.[403]

Results and Discussion

5.3 Random Polymer Synthesis for Silicon Wafer Polymer Brushes

To form a lamellae or cylindrical block copolymer melt with perpendicular alignment the first step was to change the surface tension of the silicon wafer so that there was no preference for either the PMMA or PS block during a polymer melt. Previous research has shown that this neutral surface can be formed by a random copolymer brush that is composed of PS with a fraction of between 0.42 to 0.58 with PMMA as the other monomer.[402] Typically these polymer brushes are made by controlled polymerizations as the end functional group used in the polymerization is later changed into a hydroxyl group (e.g. NMP, ATRP, etc…). These polymer chains terminated by a hydroxyl group then undergo a reaction with the hydroxyl groups on the silicon wafer, tethering them to the surface, creating a neutral polymer brush surface (Figure 5. 2).[403,404]
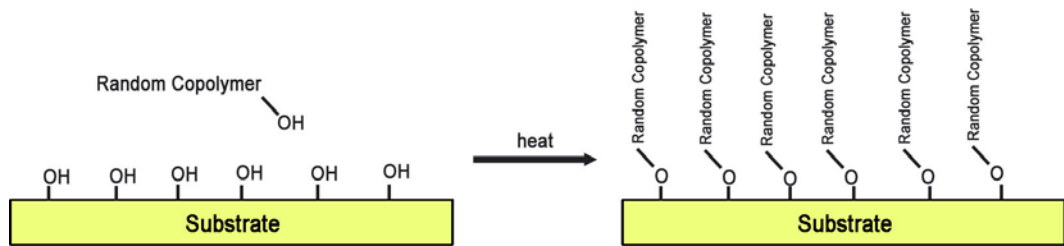
Figure 5. 2: The formation of the neutral silicon wafer polymer brush surface.

In this chapter a different style of brush to that described above was attempted. The brush was not composed of PMMA and PS, but instead is composed of PHEMA and PS. The use of HEMA was considered an excellent substitute to MMA due to the architectural similarities, but also due to the hydroxyl group that is present in the monomer creating a one pot process for forming ready to attach polymer brushes. In addition, the higher polarity of the HEMA hydroxyl groups is thought to decrease during the random copolymer attachment, as cross-linking can also occur (i.e. stronger adhesion to the wafer surface).[405] This therefore increases the similarities to a PS-co-PMMA polymer brush silicon wafer surface.

As the reactivity of styrene and HEMA is not equal, one will react faster than the other, which could create a copolymer that favors the more reactive monomer. In these types of situations the copolymer equation (Eq. 12)[406] is used to determine the composition of the final polymer, however this only predicts the average composition of the polymer formed. The integrated copolymer equation (Eq. 13)[407,408] is more accurate in this case as it takes into consideration the overall polymer composition with respect to the conversion.

$$F_1 = \frac{r_1 f_1^2 + f_1 f_2}{r_1 f_1^2 + 2 f_1 f_2 + r_2 f_2^2}$$

(12)

$$\log\left(\frac{M}{M_0}\right) = \frac{r_2}{1 - r_2}\log\left(\frac{f_1}{(f_1)_0}\right) + \frac{r_1}{1 - r_1}\log\left(\frac{f_2}{(f_2)_0}\right) + \frac{1 - r_1 r_2}{(1 - r_1)(1 - r_2)}\log\left(\frac{(f_1)_0 - \varepsilon}{f_1 - \varepsilon}\right)$$

$$\text{where } \varepsilon = (1 - r_2)/(2 - r_1 + r_2)$$

(13)

The variables r, f, and M represent the monomer reactivity ratios, mole fractions in the monomer feed, and moles of monomer respectively.

Eq. 13 was therefore used to calculate the PS volume fraction and hence its capability to create a neutral surface.

Random Copolymer (PS-co-PHEMA)
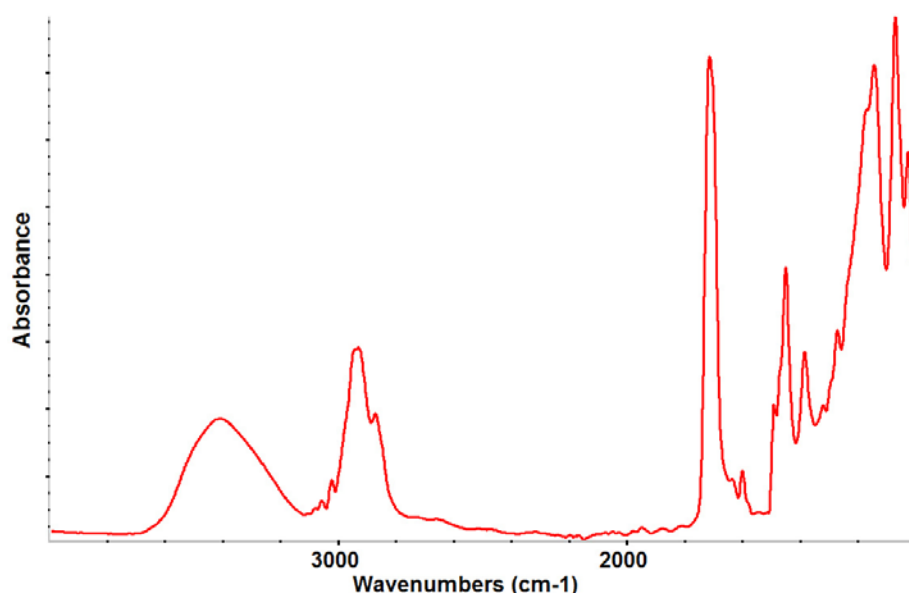
Figure 5. 3: FI-IR spectrum of PS-co-PHEMA.

The chemical structure of the random copolymer was tested using fourier transform infrared (FT-IR) spectroscopy. As the polymer is composed of styrene and HEMA monomeric units the FT-IR spectrum should show absorption peaks of both polymers. As can be seen in Figure 5. 3 there are many strong peaks that are characteristic to PS such as 1601, 1493, 1452, 749, and 696cm^{-1},[409,410] similarly HEMA peaks are also exhibited in the spectrum (i.e. 1710cm^{-1} and 3430cm^{-1}).[411] However, the most vital peak to observe is an absorption peak at approximately 3400cm^{-1}, which is ascribed to hydroxyl groups and it is a very strong peak in the

spectrum. Essentially a random copolymer of styrene and HEMA has been successfully made while maintaining the hydroxyl groups, which are to be used as the anchoring group to a silicon wafer.

It has been proven that the necessary functional groups are present to functionalize the surface of a silicon substrate, however as previously mentioned above, literature has shown that in order for it to create a neutral surface, the PS fraction has to be between 0.42 to 0.58.[402] To determine this fraction the integrated copolymer equation (Eq. 2) was used, which relates the polymer composition to conversion and these results can be seen in Table 5. 1. These results show that for a reaction time of 83mins and 193mins, the PS fraction is within the necessary requirements to create the neutral surface. It also shows that a reaction time between 83mins and 193mins will also create a compatible PS fraction. In addition, the gel permeation chromatography (GPC) results show a low Mn, which is required to produce the dense brushes needed for the neutral surface and the polydispersity of the samples are typical for a living polymerization.[412]

Reaction Time (mins)	$\ln([M_o]/[M])$	Fraction (HEMA/Styrene)[*]	Mn	Polydispersity
83	0.09406	0.48/0.52	1878	1.383
193	0.17237	0.54/0.46	2741	1.363

Table 5. 1: PS-co-PHEMA monomeric fractions and GPC measurements.[*]Calculated using the reactivity ratios from the Polymer Handbook.[413]

For the polymer to act successfully as a neutral surface for a phase separation polymer melt, a specific PS fraction is required, but as the random copolymer consists of styrene and HEMA, it may not act well as a neutral surface for PS-b-PMMA. To verify the suitability, contact angle measurements using milli Q water and diiodomethane were taken. The samples were prepared by using a mechanical press of 10,000 pounds of pressure and the results are tabulated in Table 5. 2. It is clear

from the results that the PS-co-PHEMA has shown strong repulsion to polar and non-polar liquids whereas the PS-b-PMMA has shown a greater affinity for the polar and non-polar components. This ultimately has resulted in a total surface energy (TSE) that is not similar (i.e. a difference of 27.3mJ/m^2) and therefore due to this dis-similarity the polymer is unlikely to produce a neutral surface. In addition, due to the chemical similarities between the two polymers, the difference in TSE can be attributed to the abundant hydroxyl groups and hence decreasing the amount of hydroxyl groups, decreases the difference in the TSE.

Sample	Water	diiodomethane	TSE
PS-co-PHEMA[*]	100.7^o	70.37^o	23.8mJ/m^2
PS-b-PMMA$^\alpha$	67.45^o	32.02^o	51.1mJ/m^2

Table 5. 2: Contact Angle and surface energy measurements determined using the Owens Wendt theory.[414] [*]the 193min sample was measured. $^\alpha$Averaged from the samples produced in Chapter 2.

<u>Random Tripolymer (PS-co-PHEMA-co-PMMA)</u>

The random copolymer did not show a compatible result to create a neutral surface for a perpendicular alignment, which was attributed to the abundant hydroxyl groups of the PHEMA. To improve the TSE the polymerization was carried out with styrene and HEMA, but also with MMA. The concept was to use a small ratio of HEMA to the styrene and MMA, which would create a copolymer of PS and PMMA, with some monomeric units being HEMA. These HEMA units are not abundant, therefore the polarity of the material would reduce to that of a PS-co-PMMA polymer and similar to the TSE of PS-b-PMMA, while maintaining the ability to covalently bond to a silicon wafer.

In the previous results the copolymer has shown that a combination of monomeric units within a polymer chain produces an FT-IR spectrum that exhibits vibrations from both polymers. Vibration peaks characteristic to PS as well as characteristic

peaks of PHEMA were present in the FT-IR spectra (Figure 5. 3). In this case, there are three different monomeric units, styrene, HEMA, and MMA, therefore the spectrum should exhibit characteristic peaks of all three. The FT-IR spectrum of Figure 5. 4 clearly demonstrates this concept, showing the characteristic peaks of PMMA (i.e. 2952, 2866, 1730, and 1147cm^{-1}),[415] in addition to the previously described PS and PHEMA peaks. The crucial hydroxyl functional group that has an absorption at approximately 3400cm^{-1}, is still present, but weaker than that observed in Figure 5. 3. This was expected as the peaks of an FT-IR spectrum can reflect concentration, therefore the spectrum has also shown the intended successful reduction in the concentration of hydroxyl groups (i.e. functional group used to anchor the polymer to a silicon wafer).
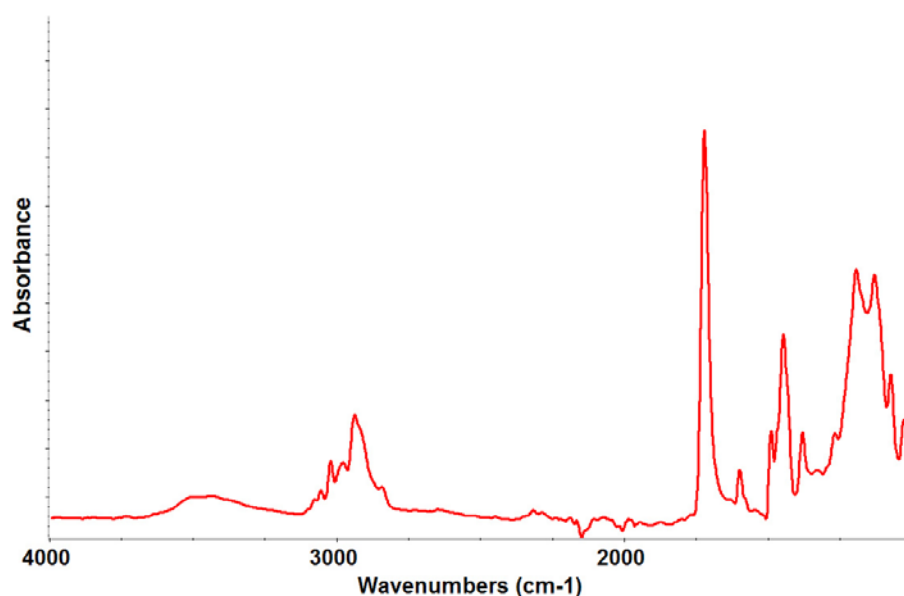
Figure 5. 4: FT-IR spectrum of PS-co-PHEMA-co-PMMA.

Although the polymer has reduced polarity by decreasing the amount of hydroxyl groups, the polymer still needs to create a neutral surface. The primary aspect which should be satisfied was the PS polymer fraction needs to be between 0.42 and 0.58, and was calculated using the integrated copolymer equation (Eq. 2). In this situation,

using the equation creates an issue because there are more than two different monomers. There are three monomers in the reaction, but due to the large structural similarity between the MMA and HEMA, and the low concentration of HEMA, the HEMA was considered negligible in the calculation. The results have been tabulated in Table 5. 3 and clearly shows that a polymerization time of 360mins creates a polymer with the desired PS fraction. In addition, the GPC results indicate that the polymerization occurred in a living fashion as the polydispersity is near 1, and the Mn is small, which is typically desired in the production of such brushes (i.e. thin monolayers are formed when attached to a wafer).[412]

Reaction Time (mins)	ln([M_o]/[M])	Fraction (MMA/Styrene)*	Mn	Polydispersity
240	0.15080	0.26/0.74	4867	1.39
360	0.21406	0.42/0.58	5748	1.11

*Table 5. 3: PS-co-PHEMA-co-PMMA monomeric fractions and GPC measurement.*Calculated by using the integrated copolymer equation and the reactivity ratios from the Polymer Handbook[413] with PHEMA considered a negligible component in the calculation due to the comparatively low amount used.*

Sample	Water	diiodomethane	TSE
PS-co-PHEMA-co-PMMA*	80.83^o	21.75^o	49.3mJ/m^2
PS-b-PMMA$^\alpha$	67.45^o	32.02^o	51.1mJ/m^2

*Table 5. 4: Contact Angle and surface energy measurements determined using the Owens Wendt theory.[414] *the 360min sample was measured, $^\alpha$averaged from the samples produced in Chapter 2.*

The other factor the polymer needs to satisfy in order to create that neutral surface, is it requires a similar TSE. This was determined by contact angle measurements with milli Q water and diiodomethane. The samples were prepared in a mechanical press with 10,000 pounds of pressure and the results have been tabulated in Table 5. 4. The results demonstrate that the PS-co-PHEMA-co-PMMA produces a polymer that differs by approximately 10° in the contact angle, and a very small

difference of 1.8mJ/m^2 in the TSE. This is an improvement to the previous results, which had a difference of 30-40° and a TSE difference of 27.3mJ/m^2 (i.e. PS-co-PHEMA). This decrease in the difference was attributed to the reduction in the hydroxyl group concentration, seen in the FT-IR results. Due to these improved factors, the PS-co-PHEMA-co-PMMA would create a more suitable neutral surface for a PS-b-PMMA di-block copolymer melt.

5.4 Attachment of Random Polymers to Silicon Wafers

As previously discussed a neutral surface is required for a lamellae or cylindrical polymer melt that has perpendicular alignment on a silicon wafer. The results of section 5.3 clearly show that the tripolymer formed of PS, PMMA, and PHEMA is a better material for this application. This was due to a similar TSE, which creates the neutral surface required for the polymer melt.

Sample	Layer Thickness (nm)	Surface Roughness (nm)$^\alpha$
Si-OH	~500*	4.46
PS-co-PHEMA	~1000	6.95
PS-co-PHEMA-co-PMMA	~100	6.86

Table 5. 5: Ellipsometry and AFM results of the copolymer and tripolymer that is anchored to a silicon substrate. * Is the thickness of the native silicon layer. $^\alpha$ determined by AFM.

The wafers were characterized by ellipsometry and AFM for the layer thickness and surface roughness, respectively. These results have been summarized in Table 5. 5 and it clearly demonstrates that the PS-co-PHEMA-co-PMMA creates the most suitable substrate for the di-block copolymer melt. The thinner layer produced by the PS-co-PHEMA-co-PMMA creates a surface that is unlikely to show porous properties as it is approximately 100nm thick and is limited in the number of groups that can cross-link. In the PS-co-PHEMA, due to the highly abundant hydroxyl

groups and hence strong cross-linking ability, the polymer has cross-linked many times creating a thicker layer, which could exhibit porous properties. This would interfere with the copolymer melt as the di-block would flow into the PS-co-PHEMA layer and result in an uneven coverage affecting phase formation. Furthermore, there is no significant change in surface roughness compared to the PS-co-PHEMA.

5.5 Spin Coating Di-Block Copolymer Melt (With and Without Nanotubes)

From section 5.3 and 5.4 it has been determined that a PS-co-PHEMA-co-PMMA polymer brush silicon wafer will create a neutral surface for perpendicular orientation of a PS-b-PMMA polymer melt. This section explores its potential in producing thin films of PS-b-PMMA that has a lamellae or hexagonal cylindrical packed polymer melt, orientated perpendicular to the surface.
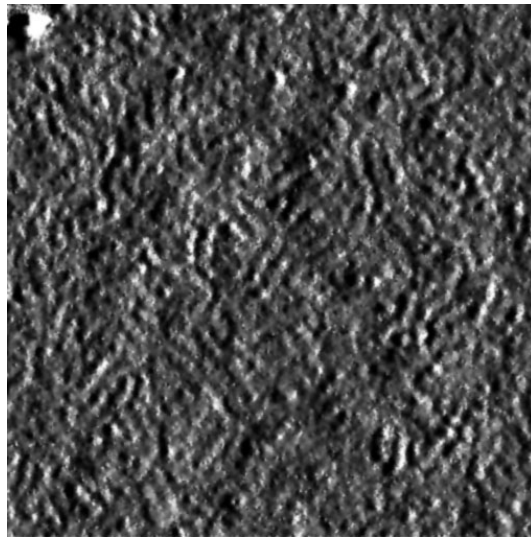
Figure 5. 5: AFM phase image (1.25x1.25μm) of lamellae PS-b-PMMA polymer melt on a PS-co-PHEMA-co-PMMA polymer brush silicon wafer.

The use of PS-co-PHEMA-co-PMMA as a neutral surface for a block copolymer melt was verified using a P(S-b-MMA) of 50/50 volume fractions. It is expected that this block copolymer will create a lamellae phase segregation that is orientated perpendicularly to the surface. Otherwise a preference to the surface will occur with parallel alignment. As can be seen in the AFM phase images of Figure 5. 5 strong

Page 184

vertical alignment has occurred, indicating the successful production of a neutral surface for P(S-b-MMA). The melt expresses an average domain size of 30nm. Furthermore, ellipsometry found that the polymer layer thickness was approximately 1μm.
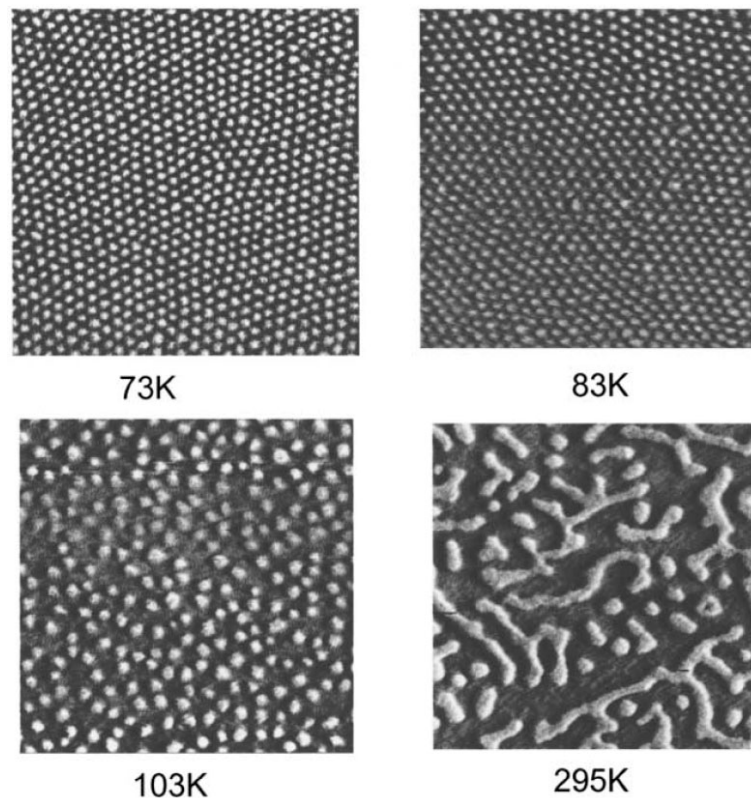
Figure 5. 6: Xu et al[416] AFM Phase images (1μm x 1μm) of P(S-b-MMA). Note: the numerical values refer molecular weight (K=1000).

Successful vertical alignment has occurred using a novel approach to producing neutral polymer brush wafer surfaces, however to align the carbon nanotubes to the phases, comparable domain sizes are required. The S-MWCNT used in the synthesis of CNT-PS(Short) have a thickness of 40-60nm, therefore the "30" domain of a 30/70 cylindrical melt must be at least 60nm in size to fit the nanotubes. Xu *et al*[416] found in their work that in order to achieve these large domain sizes high molecular weights are required. Using their results a Mn between 103,000g/mol and 295,000g/mol would create the large domains required, however within this region the regular array

of hexagonal-packed cylinders starts to deform (see Figure 5. 6). Furthermore, at 103,000g/mol it is clear that the cylinders are still present, but has no hexagonal-packed distribution.

In this work a high molecular weight of 187,800g/mol was used and the melt can be seen in the AFM phase image of Figure 5. 7. The cylinder domains are still present, but are not hexagonally-packed, which is in agreement with Xu and coworkers research.[416] The domain size was found to be averaged at 80nm, which is suitable to contain the CNT-PS(Short) filler.
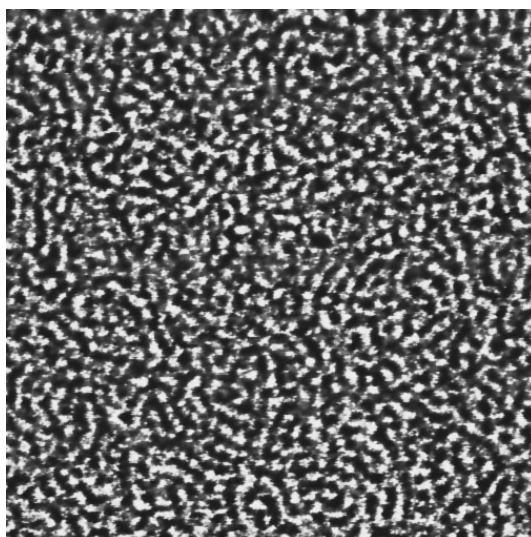
Figure 5. 7: AFM phase image (2μm x 2μm) of 30/70 polymer melt.

When the above melt was incorporated with CNT-PS(Short) the resultant morphology was disrupted and CNT-PS(Short) aggregation occurred (note: aggregation was observable under an optical microscope as well as to the naked eye). The material formed this distribution of nanotubes because the matrix is not purely PS and hence did not disperse uniformly creating weak entanglement towards the PS phases. This ultimately created the aggregated bundles of CNT-PS(Short) due to the greater affinity for one another over the PS and PMMA chains within the matrix. Furthermore, the relative massive size of the nanotubes also presented a problem as MWCNT can settle out by gravity within a matrix.[417]
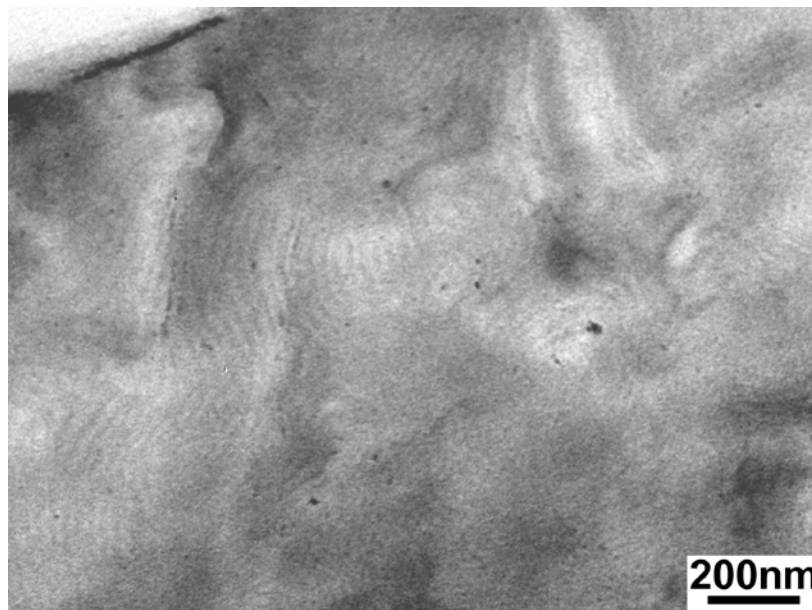
Figure 5. 8: 30/70 ARGET ATRP P(S-b-(S-co-MMA)) bulk polymer melt. Stained with

Iodine.

The disruption was further explored using a bulk polymer melt of the same

procedure, but a 30/70 ARGET ATRP P(S-b-(S-co-MMA)) of 249mins from Chapter

3 that has a lower molecular weight and hence has stronger packing (see Figure 5. 8).

As can be seen in the microtome TEM image of Figure 5. 9, the formation of the

phases has still occurred, however in the localized region of the nanotubes the phases

are disrupted (i.e. smaller concentration of CNT-PS(Short) was used to lower

probability of aggregation). In the TEM image of Figure 5. 10 the arrows help to

clearly indicate that the alignment of the phases is essentially cut off at right angles,

by the nanotube. This is a result of the block copolymers high viscosity, present

during the polymer melt, which lowered the mobility of the nanotube. It is clear that

the segregation forces of a polymer melt is not strong enough to change the

orientation of the carbon nanotubes and therefore greater forces are required to aid in

the alignment with the cylindrical phases. Furthermore, the results indicate that the

reverse affect has occurred. Instead of the block copolymer phase formation

orientating the carbon nanotube, the results demonstrate that the nanotube orientated the block copolymer's localized domain. Essentially the nanotube is encased by the PS block of the block copolymer in an effort to lower the systems entropic forces.
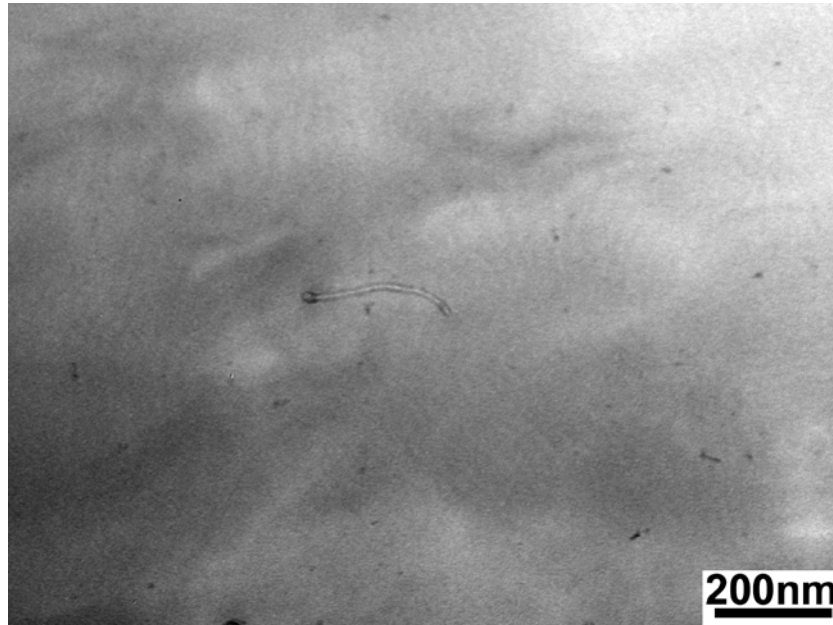
Figure 5. 9: 30/70 ARGET ATRP P(S-b-(S-co-MMA)) bulk polymer melt with CNT-PS(Short). Stained with Iodine.
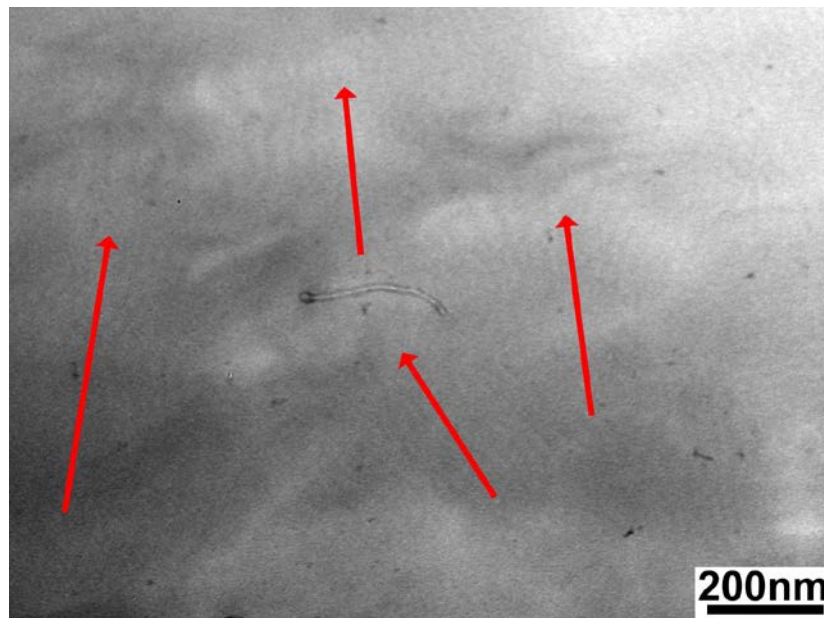
Figure 5. 10: 30/70 ARGET ATRP P(S-b-(S-co-MMA)) bulk polymer melt with CNT-PS(Short), demonstrating the alignment of the phases around the nanotube. Stained with Iodine.

Compared to literature the positioning of particles by a block copolymer segregation melt has been achieved with nanoparticles. Chiu et al[397] was able to control the position of gold nanoparticles in a poly(styrene-b-2 vinyl pyridine) melt. This was achieved when the particles were coated with either PS or poly(2 vinyl pyridine) and the system, in an attempt to lower the entropy, positioned the particles in the corresponding phase. Further work found that by coating the nanoparticles with both PS and poly(2 vinyl pyridine), the nanoparticles positioned themselves along the interfaces. Similar results were achieved by Bockstaller et al,[418] using gold nanoparticles and silica nanoparticles in a poly(styrene-b-ethylene propylene) system (pictured in Figure 5. 11).
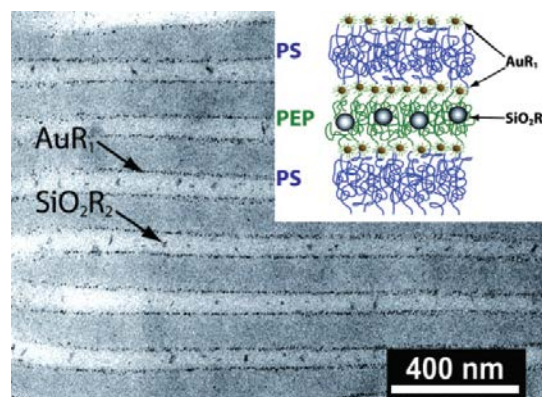
Figure 5. 11: Bright field electron micrograph showing the controlled position capabilities of nanoparticles in a block copolymer melt.[418]

On the other hand, in the reverse fashion, Lacier et al[419] found in their work that the orientation of a bulk block copolymer melt could be controlled by coating a gold nanorod with dodecanethiol (i.e. orientation controlled by the particle). The nanorod was found to be in the centre of the cylindrical domain, but long range order was not achieved. It is suggested in the article that they are looking into using externally applied fields to combat this. In contrast to carbon nanotubes, nanorods are less rigid and have weaker inter-particle forces, hence the nanotube disrupting the block

copolymer phase formation. However, a similar result was found in Figure 5. 10, as the nanotube disrupted and altered the localized orientation of the block copolymer. Furthermore, due to structural differences between nanorods and carbon nanotubes, an externally applied field for long range nanorod orientation may not be sufficient for carbon nanotube orientation.

5.6 Conclusion

The results of this chapter has clearly demonstrated a new technique in the production of neutral surfaces for a P(S-b-MMA) polymer melt. Thin films of lamellae and hexagonal-packed cylindrical phases were orientated perpendicularly to a silicon wafer surface by using a tripolymer neutral surface.

The hexagonal-packed cylindrical phase was then manipulated to incorporate polystyrene polymer brushes on carbon nanotubes, in an attempt to explore the resultant nanotube orientation. The resultant material found that the segregation forces of the di-block copolymer melt were not strong enough to move and hence orientate the nanotubes within the cylindrical phase. This concept was further verified using a bulk di-block copolymer melt. Furthermore, the TEM images demonstrated that the phase formation was disrupted by the presence of the nanotubes and hence greater forces were required.

- CHAPTER 6 -

GENERAL CONCLUSIONS,

RECOMMENDATIONS,

AND

FUTURE WORK

6. GENERAL CONCLUSIONS, RECOMMENDATIONS AND FUTURE WORK

Preface

This chapter summarizes the work of the entire thesis, discussing the key outcomes and possible future directions to enhance the research.

6.1 General Conclusions and Recommendations

Polymer Brush Carbon Nanotubes

Polymer brushed carbon nanotubes were successfully synthesized using a "graft from" approach in a new polymerization technique called ARGET ATRP.[420,421] This technique proved to have many benefits over existing methods such as normal ATRP,[422] and other more sensitive living polymerization techniques.[423,424] Benefits were obtained such as low catalyst concentration, ease of polymerization, and the living capacity to reinitiate polymer growth. Brushes of PS and PMMA were grown using this technique reaching a polymer coverage as high as 84.7% and 78%, respectively. In addition, a polydispersity of 1.78 for the PS brushes was determined and found to be of similar magnitude to previous research using normal ATRP.[425]

Living plots were created to re-affirm that the ARGET ATRP of CNT-Br did in fact polymerize in a living fashion. Linear plots were obtained, however more study is needed in the areas of molecular weight and polydispersity (i.e. GPC measurements) to establish the efficiency of initiation. As a guide, in Chapter 2, well initiated polymer of PS and poorly initiated polymer of PMMA was observed when using EBiB, thus indicating a similar trend in the CNT-PS and CNT-PMMA materials and verified using the pyrene model system.

This research was explored further by the production of PHEMA polymer brushes on carbon nanotubes using free radical polymerization. Physical differences occurred

due to the different technique used, and PHEMA's capability to crosslink; a comparison was discussed between controlled living polymer brushes to uncontrolled polymer brushes on carbon nanotubes. One of these differences resulted from the reactivity of the monomer and hence the polymer layer thickness or content was affected. In the living polymerizations research, this thickness depended on the reaction time. It was found that the PS was much less reactive in comparison to the PMMA. Approximately 80% polymer content of PMMA was achieved in a fifth of the time to produce the PS. In contrast to the PHEMA brushes, the polymer content ranged between 50 to 80%. This was independent of reaction time as the free radical polymerization had terminating reactions that stopped the propagating chain end, unlike the ARGET ATRP procedure, which has a living end. The polymer layer thickness of the three different types of brushes was in the range of 10nm, but this did not reflect the molecular weight as PS, PMMA, and PHEMA all have different densities (e.g. for the same thickness of PMMA and PS, the molecular weight of PMMA is much greater than PS).

Decomposition temperatures were determined and the results of the PS brush carbon nanotubes exhibited a trend, which was an increase in the decomposition temperature with respect to the molecular weight. Overall the CNT-PS decreases by approximately 40^oC when compared to CA-PS, CNT-PMMA increases by 35^oC when compared to CA-PMMA, and CNT-PHEMA decreased by 4^oC when compared to un-filled PHEMA. Furthermore, structurally PHEMA has many similarities to the carbon nanotube in terms of oxygenated moieties. This similarity generates the greatest attraction to the nanotube walls and was unlikely to hinder the decomposition temperature compared to the chemically dis-similar PS or PMMA.

The glass transition temperature increased for all the brushes synthesized, by 14°C for the PS brushes, 17°C for the PMMA brushes and 17°C for the PHEMA brushes. This increase was attributed to the rigidity of the carbon nanotube which was acting as a reinforcing agent.

Spectroscopic techniques were used to determine the chemical structures of the synthesized materials. In particular, FT-IR was used verify the presence of the various polymers, however the nanotubes could not be detected due to the low concentration of specific nanotube functional groups. Raman spectra was used to determine the presence of a charge transfer affect. This affect occurs when unfunctionalized carboxylic acids are present on carbon nanotubes and when functionalized the affect does not occur.[426] It was observed and used to verify the covalent attachment of the polymer brushes. Furthermore, it indicates attachment occurred by covalent means and not solely due to additional forces, such as π-π stacking.

The polymer brush carbon nanotubes are also electrically conductive so the electrical conductance was measured. The results found that the polymer brush carbon nanotubes were less conductive than AR or AC nanotubes and that the strength of conductance was dependent on the polymer content (i.e. more polymer, less conductive). In addition, the preparation technique found that the polymer brush carbon nanotubes can be pressed into films and hence applications exist for conductive coatings or films.

Macro-sized Composites

Using the polymer brush carbon nanotube as a filler in a polymer matrix of the same brush (i.e. PS brush carbon nanotubes in a PS matrix) found that it could enhance the properties of the matrix. Limitations existed as AR nanotubes have a low

limit of dispersion, but due to the presence of the polymer brushes, this increased its architectural similarity to the polymer matrix, increasing the limit of dispersion.

Composites of PS, PMMA, and PHEMA with the corresponding filler in concentrations of 0.10w/w% to 1w/w% were produced. Generally the properties of the PS material gave enhanced results due to the presence of the aromatic groups and hence π-π stacking capabilities. The methacrylate polymers did not possess the π-π stacking capabilities, but experienced greater effects due to a difference in polarity between the nanotube and the polymer. This resulted in a decrease in the storage modulus, however did not affect the glass transition temperature of the materials while still producing an increase in processability. Ultimately for a carbon nanotube to be most affective as a filler that has been functionalized with polymer brushes, aromatic groups within the chains are necessary to help foster its attraction with the matrix (i.e. aided by the π-π stacking capabilities).

Pyrene as a Model System

The model system of Pyrene was used to produce polymer brushes using ARGET ATRP with Pyrene-HEBI as the initiator. The results found that a well initiated polymer of 1.16 polydispersity, produced a 5.9$^\text{o}$C increase in the glass transition temperature, and the decomposition temperature increased with respect to increasing molecular weight. In comparison to the PS brush carbon nanotubes, similar physical changes in the properties occurred (i.e. increased or decreased) and therefore implied that the CNT-PS was also well initiated.

Using the Pyrene-PS material as a filler in a PS matrix found that it did not exhibit a limit of dispersion for concentrations less than 1w/w%. It displayed an increased storage modulus that continued to increase with increasing concentration; at 1w/w% the increase was 130%. Other properties such as glass transition temperature and

processability increased by approximately 20°C and to 64%, respectively. These property changes were very similar to the PS brush carbon nanotube composites, but a limit of dispersion was experienced in the nanotube composite which was not detected in the pyrene composite. This limit occurred at 0.25w/w% PS brush carbon nanotube concentration, but the properties were much more enhanced than for pyrene. 0.25w/w% of PS brush carbon nanotubes in PS had an increase in storage modulus of 180%, 500MPa greater than that experienced with Pyrene-PS, the complex viscosity reduced to 4.5%, and without significantly changing the glass transition temperature. Overall the nanotube played an important part in increasing the storage modulus and increasing the processability that was not matched by the Pyrene.

<u>Nano-sized Composites</u>

In order to produce perpendicularly aligned 30/70 block copolymer melt thin films, a neutral surface was required. Previously, pre-formed living polymer brushes were used, as the specific end functionality (i.e. the living end) could be chemically altered to a hydroxyl group for a "graft to" attachment to silicon wafers.[427,428,429] However, the work in this thesis produced a neutral surface by a new method. Instead of altering the end functionality, a random tripolymer of styrene, MMA and HEMA was produced, with the HEMA monomeric unit supplying the hydroxyl groups. A low concentration of HEMA was used within the polymer chain, which was necessary to avoid significantly disrupting the comparable surface energy to a P(S-b-MMA) polymer. These neutral surfaces successfully produced thin films of lamellae and hexagonal-packed cylindrical phases with perpendicular alignment of P(S-b-MMA).

The hexagonal-packed cylindrical phase was then manipulated to incorporate polystyrene polymer brushes on carbon nanotubes with comparable nanotube length

to the thickness of the film. The resultant material found that the segregation forces of the di-block copolymer melt were not strong enough to orientate/align the nanotubes within the cylindrical domain. This concept was further verified using a bulk di-block copolymer melt. Furthermore, TEM found that the phase formation was disrupted by the presence of the nanotubes and forced the PS phase to align with the carbon nanotube in the systems effort to lower the entropic forces; the carbon nanotubes controlled the orientation, not the polymer melt and had no long-range order.

6.2 Future Work

Macro-sized Composites and Pyrene

The work of this section found that even with polymer brushes the aromatic groups of the carbon nanotube wall can still interfere with the dispersion in methacrylate polymers. It was therefore recommended that polymer brushes containing aromatic groups would be ideal candidates for this application.

To create further understanding of polymer brush carbon nanotubes as fillers more study is required in using other aromatic polymers such as poly(etherether ketone) or the many other styrene derivatives. Further work could also extend to increasing the polymer brush content to near 100% in an attempt to increase the degree of architectural similarity. In addition, the electrical percolation threshold could simultaneously be explored if a high load of polymer brush carbon nanotubes were used.

The complex viscosity plots of AR and AC in a polymer matrix were lower than expected. Usually in the literature it is reported that upon the addition of carbon nanotubes the complex viscosity increases,[430] but has instead decreased. These composites were not explored at great depth as they were used as a controlled/comparative material for the other composites (i.e. polymer brush carbon

nanotube composites). Further research is required to obtain a full understanding as to why the complex viscosity decreased and it is suggested to explore the molecular weight, concentration, and carbon nanotube length dependence. Furthermore, it was also suggested to perform post-processing to the PMMA composites as previous research had shown that this was a technique to increase the dispersibility, storage modulus,[431,432] and in turn could increase the complex viscosity.

The pyrene work found that there was no limit of dispersion when used as a filler for concentrations less than 1w/w%. A limit could be experienced, but at much higher concentrations and therefore to extend on this work, greater concentrations above 1w/w% should be explored to determine the full extent of the property enhancements.

Improvement of Carbon Nanotube Alignment

The nano-sized work found that a block copolymer melt did not create strong enough forces to align a carbon nanotube within the cylindrical domain. To increase these forces an improvement on the carbon nanotubes affinity for a particular phase will be necessary. Di-block copolymer brush carbon nanotubes could enhance this ability, with PS as the first block as PS has proven to be an efficient first block in polymer brush carbon nanotubes, and di-block copolymer chemistry. Using a di-block copolymer brush would aid in the segregation process and limit the disruption as the PS brush nanotube would not solely be surrounded by the PS, but also PMMA, creating a stronger architectural similarity with its surrounding environment. In addition, the molecular weights of the polymer blocks should match that of the di-block copolymer matrix to further increase the architectural symmetry.

It was also recommended that additional forces were necessary to aid in the alignment as the carbon nanotube is a macro-sized molecule that can settle out by gravity. Previous research has shown that a uniform electric field can orientate a

hexagonal-packed cylindrical phase from a parallel orientation to a perpendicular orientation during a polymer melt.[433,434,435] This might be a suitable technique that could be used to effectively stand the nanotubes perpendicularly at the same time as when the PS phase aligns to the electric field lines. Furthermore, the carbon nanotube is encased by the PS brushes, which would also align to the electric field. Research by Martin et al[436] has already shown that multi-walled carbon nanotubes can be aligned using electric fields in epoxy composites, but a regular array was not achieved. In addition, Piao *et al*[437] found that they could produce carbon nanotube alignment using a modulated magnetic field of 2.4 to 12T. The alignment was oriented parallel or perpendicular from a suspension that was either solidified by polymerization or evaporation of a solvent, but had no regular spacing between each nanotube. The use of a block copolymer would help in producing a regularly spaced array of nanotubes aided by either an electric or magnetic field.
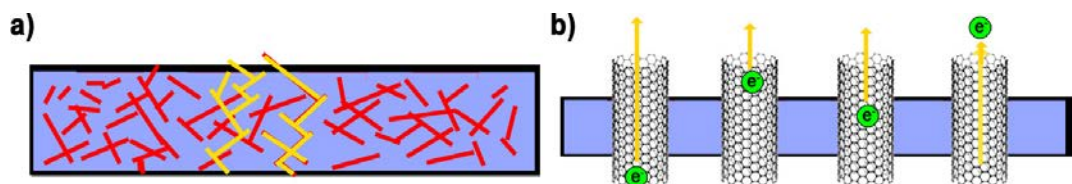
Figure 6. 1: A representative diagram of a) the conductive pathways when the percolation threshold has been reached (each red line is a carbon nanotube) and b) when the thickness of the substrate is smaller than the carbon nanotubes length.

Once the perpendicular alignment of the carbon nanotubes has been established, an additional property that would occur due to the physical dimensions of the composite, is conductivity. Typically the electrical percolation threshold needs to be reached, which is the critical concentration when a carbon nanotube conductive pathway can be found through a composite.[438,439] However, when the composite is thinner than the length of the carbon nanotubes used the threshold can decrease

significantly (see Figure 6. 1). This occurs because the nanotube traverses the matrix creating a conductive pathway between the surfaces.

<u>UV Exposure</u>

Once the perpendicular alignment of the carbon nanotubes has been established further structural work could be carried out that leads towards forming pillars. Previous research has shown that in a P(S-b-MMA) polymer melt, UV exposure can degrade the PMMA phase and leave, while strengthening, the PS phase to create a nanoporous film.[440] With the phases reversed, UV exposure would remove the PMMA and leave the PS pillars with the carbon nanotube inside. A problem could result from pillars being too tall and falling over, but with a carbon nanotube as its backbone, the pillar could remain standing. Futhermore, Leiston-Belanger *et al*[441] produced a thermally stabilized matrix by using a block copolymer melt with the PS phase re-enforced with monomer units of 3-vinylbenzocyclobutene. This would thermally cross-link and strengthen the PS phase for nanoporous film production when subsequently exposed to UV. In the case of forming pillars, using the 3-vinylbenzocyclobutene would increase the strength of the PS pillar and aid in it standing up after the UV treatment.

7. References

[1] Iijima, S. *Nature* **1991**, 354, 56-58

[2] Ebbesen, T. W. *"Carbon Nanotubes"* CRC Press **1997**

[3] Andrews, R.; Jacques, D.; Rao, A. M.; Rantell, T.; Derbyshire, F. *App. Phys. Lett.* **1999**, 75, 1329-1331

[4] Ebbesen, T. W. *Annu. Rev. Mater. Sci.* **1994**, 24, 235-264

[5] Sloan, J.; Kirkland, A. I.; Hutchison, J. K.; Green, M. L. H. *Acc. Chem. Res.* **2002**, 35, 1054-1062

[6] Bethune, D. S. *Physica B* **2002**, 323, 90-96

[7] Koshio, A.; Yudasaka, M.; Iijima, S. *Chem. Phys. Lett.* **2002**, 356, 595-600

[8] Sinnott, S. B.; Andrews, R.; Qian, D.; Rao, A. M.; Mao, Z.; Dickey, E. C.; Derbyshire, F. *Chem. Phys. Lett.* **1999**, 315, 25-30

[9] Ajayan, P. M.; Ebbesen, T. W. *Rep. Prog. Phys.* **1997**, 60, 1025-1062

[10] Ebbesen, T. W.; Ajayan, P. M. *Nature* **1992**, 358, 220-222

[11] Dresselhaus, M. S.; Dresselhaus, G.; Ph. Avouris (Eds.) *"Carbon Nanotubes: Synthesis, Structure, Properties, and Applications"* Springer-Verlag Berlin Heidelberg **2001**

[12] Takikawa, H.; Kusano, O; Sakakibara, T. *J. Phys. D: Appl. Phys.* **1999**, 32, 2433-2437

[13] Bethune, D. S.; Kiang, C. H.; DeVries, M.; Gorman, G.; Savoy, R.; Vazques, J.; Beyers, R. *Nature* **1993**, 363, 605-607

[14] Ren, Z. F.; Huang, Z. P.; Xu, J. W.; Wang, J. H.; Bush, P.; Siegal, M. P.; Provenico, P. N. *Science* **1998**, 282, 1105-1107

[15] Li, W. Z.; Xie, S. S.; Qian, L. X.; Chang, B. H.; Zou, B. S.; Zuo, W. Y.; Zhao, R. A.; Wang, G. *Science* **1996**, 274, 1701-1703

[16] Kusunoki, M.; Suzuki, T.; Ito, M. *Philosophical Mag. Lett.* **1999**, 79, 153-161

[17] Franklin, N. R.; Dai, H. *Adv. Mater.* **2000**, 12, 890-894

[18] Duesberg, G. S.; Graham, A. P.; Liebau, M.; Seidel, R.; Unger, E.; Kreupl, F.; Hoenlein, W. *Nano Letters* **2003**, 3, 257-259

[19] Andrews, R.; Jacques, D.; Qian, D.; Rantell, T. *Acc. Chem. Res.* **2002**, 35, 1008-1017

[20] Pan, Z. W.; Xie, S. S.; Chang, B. H.; Sun, L. F.; Zhou, W. Y.; Wang, G. *Chem. Phys. Lett.* **1999**, 299, 97-102

[21] Hornyak, G. L.; Grigorian, L.; Dillon, A. C.; Parilla, P. A.; Jones, K. M.; Heben, M. J. *J. Phys. Chem. B* **2002**, 106, 2821-2825

[22] Colomer, J-F.; Benoit, J-M.; Stephan, C.; Lefrant, S.; Tendeloo, G. V.; Nagy, J. B. *Chem. Phys. Letts.* **2001**, 345, 11-17

[23] Zhou, O.; Shimoda, H. Gao, B.; Oh, S. Fleming, L.; Yue, G. *Acc. Chem. Res.* **2002**, 35, 1045-1053

[24] Wong, W. K.; Li, C. P.; Au, F. C. K.; Fung, M. K.; Sun, X. H.; Lee, C. S.; Lee, S. T. *J. Phys. Chem. B* **2003**, 107, 1514-1517

[25] Saito, R.; Dresselhaus, G.; Dresselhaus, M. S. *"Physical Properties of Carbon Nanotubes"* Imperial College Press, **1998**

[26] Charlier, J. C. *Acc. Chem. Res.* **2002**, 35, 1063-1069

[27] Dai, H. *Acc. Chem. Res.* **2002**, 35, 1035-1044

[28] Haddon, R. C. *Acc. Chem. Res.* **2002**, 35, 997

[29] Sheeney-Haj-Ichia, L.; Basnar, B.; Willner, I. *Angew. Chem.* **2005**, 117, 80-85

[30] Luong, J. H. T.; Hrapovic, S.; Liu, Y.; Yang, D. Q.; Sacher, E.; Wang, D.; Kingston, C. T.; Enright, G. D. *J. Phys. Chem. B* **2005**, 109, 1400-1407

[31] Zhang, J.; Zuo, H.; Qing, Q.; Tang, Y.; Li, Q.; Liu, Z.; Guo, X.; Du, Z. *J. Phys. Chem. B* **2003**, 107, 3712-3718

[32] Chen, C.-M.; Chen, M.; Peng, Y.-W.; Yu, H.-W.; Chen, C.-F. *Thin Solid Films* **2006**, 498, 202-205

[33] Li, Y.; Zhang, X.; Luo, J.; Huang, W.; Cheng, J.; Luo, Z.; Li, T.; Liu, F.; Xu, G.; Ke, X.; Li, L.; Geise, H. J. *Nanotechnology* **2004**, 15, 1645-1649

[34] Igarashi, H.; Murakami, H.; Murakami, Y.; Maruyama, S.; Nakashima, N. *Chem. Phys. Lett.* **2004**, 392, 529-532

[35] Cai, L.; Bahr, J. L.; Yao, Y.; Tour, J. M. *Chem. Mater.* **2002**, 14, 4235-4241

[36] Colomer, J.-F.; Piedigrosso, P.; Willems, I.; Journet, C.; Bernier, P.; Van Tendeloo, G.; Fonseca, A.; Nagy, B. *J. Chem. Soc., Faraday Trans.* **1998**, 94, 3753-3758

[37] Kuznetsova, A.; Mawhinney, D. B.; Naumenko, V.; Yates, Jr. J. T.; Liu, J., Smalley, R. E. *Chem. Phys. Letts.* **2000**, 321, 292-296

[38] Park, Y. S.; Choi, Y. C.; Kim, K. S.; Chung, D. C.; Bae, D. J.; An, K. H.; Lim, S. C.; Zhu, X. Y.; Lee. Y. H. *Carbon* **2001**, 39, 655-661

[39] Gooding, J. J.; Wibowo, R.; Liu, J.; Yang, W.; Losic, D.; Orbons, S.; Mearns, F. J.; Shapter, J. G.; Hibbert, D. B. *J. Am. Chem. Soc.* **2003**, 125, 9006-9007

[40] Chen, Z.; Ziegler, K. J.; Shaver, J.; Hauge, R. H.; Smalley, R. E. *J. Phys. Chem. B* **2006**, 110, 11624-11627

[41] Banerjee, S.; Wong, S. S. *J. Phys. Chem. B* **2002**, 106, 12144-12151

[42] Razumovski, S. D.; Zaikov, G. E. *"Ozone and its Reactions with Organic Compounds"* Elsevier Science Publishers, **1984**

[43] McMurry, J. *"Organic Chemistry 5th Ed."* Brooks/Cole Thomson Learning, **2000**

[44] Hernadi, K.; Siska, A.; Thien-Nga, L.; Forro, L.; Kiricsi, I. *Solid State Ionics* **2001**, 141-142, 203-209

[45] Aitchison, T. J.; Ginic-Markovic, M.; Matisons, J. G.; Simon, G. P.; Fredericks, P. M. *J. Phys. Chem. B* **2007**, 111, 2440-2446

[46] Solomans, G.; Fryle, C. *"Organic Chemistry 7th Ed. Upgrade"* John Wiley & Sons Inc., **2002**

[47] Cotton, F. A.; Wilkinson, G.; Fryhle, C. *"Basic Inorganic Chemistry 3rd Ed."* John Wiley & Sons Inc., **1995**

[48] Duesberg, G. S.; Burghard, M.; Muster, J.; Philipp, G.; Roth, S. *J. Chem. Soc., Chem. Commun.* **1998**, 435

[49] Semet, V.; Biuh, V.; Vincent, P.; Guillot, D.; Chowalla, M.; Amaratunga, G.; Milne, W. *Appl. Phys. Lett.* **2002**, 81, 343

[50] Bonnard, J.-M.; Salvetat, J. P.; Stockli, T.; Forro, L.; Chatelain, A. *Appli. Phys. A* **1999**, 69, 245

[51] Matarredona, O.; Rhoads, H.; Li, Z.; Harwell, J. H.; Balzano, L.; Resasco, D. E. *J. Phys. Chem. B* **2003**, 107, 13357-13367

[52] Kovtyukhova, N. I.; Mallouk, T. E.; Pan, L.; Dickey, E. C. *J. Am. Chem. Soc.* **2003**, 125, 9761-9769

[53] Lian, Y.; Maeda, Y.; Wakahara, T.; Akasaka, T.; Kazaoui, S.; Minami, N.; Shimizu, T.; Choi, N.; Tokumoto, H. *J. Phys. Chem. B* **2004**, 108, 8848-8854

[54] Ou, Y.-Y.; Huang, M. H. *J. Phys. Chem. B* **2006**, 110, 2031-2036

[55] Lin, Y.; Allard, L. F.; Sun, Y.-P. *J. Phys. Chem. B* **2004**, 108, 3760-3764

[56] Chen, G.-X.; Kim, H.-S.; Park, B. H.; Yoon, J.-S. *J. Phys. Chem. B* **2005**, 109, 22237-22243

[57] Chen, J.; Rao, A. M.; Lyuksyutov, S.; Itkis, M. E.; Hamon, M. A.; Hu, H.; Cohn, R. W.; Eklund, P. C.; Colbert, D. T.; Smalley, R. E.; Haddon, R. C. *J. Phys. Chem. B* **2001,** 105, 2525-2528

[58] Niyogi, S.; Hamon, M. A.; Hu, H.; Zhao, B.; Bhowmik, P.; Sen, R.; Itkis, M. E.; Haddon, R. C. *Acc. Chem. Res.* **2002**, 35, 1105-1113

[59] Hirsch, A. *Angew. Chem. Int. Ed.* **2002**, 41, 1853-1859

[60] Viswanathan, G.; Chakrapani, N.; Yang, H.; Bingqing, W.; Chung, H.; Cho, K.; Tyu, C. Y.; Ajayan, P. M. *J. Am. Chem. Soc.* **2003**, 125, 9258-9259

[61] Wang. Y.; Iqbal, Z.; Mitra, S. *J. Am. Chem. Soc.* **2006**, 128, 95-99

[62] Sinclair, J. M.; Wilkes, G. A.; Krebs, W. A. *"Collins English Dictionary, 4th Australian Ed."* Harper Collins Publishers **1999**

[63] Lindman, B.; Wennerstrom, H *"Topics in Current Chemistry 87: Micelles. Amphiphile Aggregation in Aqueous Solution"* Springer-Verlag New York Inc. **1980**

[64] Tanford, C. *"The hydrophobic effect: Formation of micelles and biological membranes 2nd Ed."* John Wiley & Sons Inc., **1980**

[65] Weiss, R. G.; Terech, P. "Molecular Gels, Materials with Self-Assembled Fibrillar Networks" Springer, **2006**

[66] Yurekli, K.; Mitchell, C. A.; Krishnamoorti, R. *J. Am. Chem. Soc.* **2004**, 126, 9902-9903

[67] Patel, N.; Egorov, S. A. *J. Am. Chem. Soc.* **2005**, 127, 14124-14125

[68] Shvartzman-Cohen, R.; Nativ-Roth, E.; Baskaran, E.; Levi-Kalisman, Y.; Szleifer, I.; Yerushalmi-Rozen, R. *J. Am. Chem. Soc.* **2004**, 126, 14850-14857

[69] Kang, Y.; Taton, T. A. *J. Am. Chem. Soc.* **2003**, 125, 5650-5651

[70] Shin, H.; Min, B. G.; Jeong, W.; Park, C. *Macromol. Rapid Commun.* **2005**, 26, 1451-1457

[71] Bennett, R. D.; Xiong, G. Y.; Ren, Z. F.; Cohen, R. E. *Chem. Mater.* **2004**, 16, 5589-5595

[72] Stewart, S.; Liu, G. *Angew. Chem. Int. Ed.* **2000**, 39, 340-344

[73] Yang, M.; Koutsos, V.; Zaiser, M. *J. Phys. Chem. B* **2005**, 109, 10009-10014

[74] Gao, J.; Itkis, M. E.; Yu, A.; Bekyarova, E.; Zhao, B.; Haddon, R. C. *J. Am. Chem. Soc.* **2005**, 127, 3847-3854

[75] Hill, D. E.; Lin, Y.; Rao, A. M.; Allard, L. F.; Sun, Y. P. *Macromolecules* **2002**, 35, 9466-9471

[76] Liu, Y.; Yao, Z.; Adronov, A. *Macromolecules* **2005**, 38, 1172-1179

[77] Philip, B; Xie, J.; Abraham, J. K.; Varadan, V. K. *Polymer Bulletin* **2005**, 53, 127-138

[78] Gao, C.; Jin, Y. Z.; Kong, H.; Whitby, R. L. D.; Acquah, S. F. A.; Chen, G. Y.; Qian, H.; Hartschuh, A.; Silva, S. R. P.; Henley, S.; Fearon, P.; Kroto, H. W.; Walton, D. R. M. *J. Phys. Chem. B* **2005**, 109, 11925-11932

[79] Li, Q.; Zaiser, M.; Koutsos, V. *Phys. Status Solid A* **2004**, 201, R89

[80] Qin, S.; Qin, D.; Ford, W. T.; Resasco, D. E.; Herrera, J. E. *J. Am. Chem. Soc.* **2004**, 126, 170-176

[81] Biercuk, M. J.; Llaguno, M. C.; Radosavljevic, M.; Hyun, J. K.; Johnson, A. T.; Fischer, J. E. *Appl. Phys. Lett.* **2002**, 80, 2767-2769

[82] Qian, D.; Dickey, E. C.; Andrews, R.; Rantell, T. *Appl. Phys. Lett.* **2000**, 76, 2868

[83] Niu, C.; Sickel, E. K.; Hoch, R.; Moy, D.; Tennent, H. *Appl. Phys. Lett.* **1997**, 70, 1480

[84] Niu, C.; Kupperschmidt, J.; Hock, R. *Proceedings of the 39th Power Sources Conference (Maple Hill, NJ)* **2000**, 314-317

[85] Lee, N. S.; Chung, D. S.; Han, I. T.; Kang, J. H.; Choi, Y. S.; Kim, H. Y.; Park, S. H.; Jin, Y. W.; Yi, W. K.; Yun, M. J.; Jung, J. E.; Lee, C. J. You, J. H.; Jo, S. H.; Lee, C. G.; Kim, J. M. *Diamond Relat. Materials* **2001**, 10, 265-270

[86] Sugie, H.; Tanemura, M.; Filip, V.; Iwata, K.; Takahashi, K.; Okuyama, F. *Appl. Phys. Lett.* **2001**, 78, 2578-2579

[87] Wong, S. S.; Joselevich, A. T.; Woolley A. T.; Chueng, C. L.; Lieber, C. M. *Nature* **1998**, 394, 52

[88] Baughman, R. H.; Zakhidov, A. A.; de Heer, W. A. *Science* **2002**, 297, 787-792

[89] Piao, G.; Kimura, F.; Takahashi, T.; Moritani, Y.; Awano, H.; Nimori, S.; Tsuda, K.; Yonetake, K.; Kimura, T. *Polymer Journal* **2007**, 39, 589-592

[90] Kashiwagi, T.; Grulke, E.; Hilding, J.; Harris, R.; Awad, W.; Douglas, J. *Macromol. Rapid Commun.* **2002**, 23, 761

[91] Li, S.; Qin, Y.; Shi, J.; Guo, Z.-X.; Li, Y.; Zhu, D. *Chem. Mater.* **2005**, 17, 130-135

[92] Philip, B.; Xie, J.; Abraham, J. K.; Varadan, V. K. *Polymer Bulletin* **2005**, 53, 127-138

[93] Gao, J.; Itkis, M. E.; Yu, A.; Bekyarova, E.; Zhao, B.; Haddon, R. C. *J. Am. Chem. Soc.* **2005**, 127, 3847-3854

[94] Salalha, W.; Dror, Y.; Khalfin, R. L.; Cohen, Y.; Yarin, A. L.; Zussman, E. *Langmuir* **2004**, 20, 9852-9855

[95] Lou, X.; Daussin, R.; Cuenot, S.; Duwez, A.-S.; Pagnoulle, C.; Detrembleur, C.; Bailly, C.; Jerome, R. *Chem. Mater.* **2004**, 16, 4005-4011

[96] Deng, J.; Zhang, X.; Wang, K.; Zou, H.; Zhang, Q.; Fu, Q. *J. Membrane Sci.* **2007** 288, 261-267

[97] Blake, R.; Gun'ko, Y. K.; Coleman, J.; Cadek, M.; Fonseca, A.; Nagy, J. B.; Blau, W. J. *J. Am. Chem. Soc.* **2004**, 126, 10226-10227

[98] Frankland, S. J. V.; Caglar, A.; Brenner, D. W.; Griebel, M. *J. Phys. Chem. B* **2002**, 106, 3046-3048

[99] Geng, H.; Rosen, R.; Zheng, B.; Shimoda, H.; Fleming, L.; Liu, J.; Zhou, O. *Adv. Mater.* **2002**, 14, 1387-1390

[100] Gao, J.; Itkis, M. E.; Yu, A.; Bekyarova, E.; Zhao, B.; Haddon, R. C. *J. Am. Chem. Soc.* **2005**, 127, 3847-3854

[101] Bower, C.; Rosen, R.; Jin, L.; Han, J.; Zhou, O. *Appl. Phys. Lett.* **1999**, 74, 3317

[102] Qian, D.; Dickey, E. C. *Appl. Phys. Lett.* **2000**, 76, 2868-2870

[103] Wagner, D. H. *Chem. Phys. Lett.* **2002**, 361, 57

[104] Fragneaud, B.; Masenelli-Varlot, K.; Gonzalez-Montiel, A.; Terrones, M.; Cavaille, J.-Y. *Chem. Phys. Lett.* **2007**, 444, 1-8

[105] Park, M.; Kim, H.; Youngblood, J. P. *Nanotechnology* **2008**, 19, 055705

[106] Mitchell, C. A.; Bahr, J. L.; Arepalli, S.; Tour, J. M.; Krishnamoorti, R. *Macromolecules* **2002**, 35, 8825

[107] Sung, J. H.; Kim, H. S.; Jin, H.-J.; Choi, H. J.; Chin, I.-J. *Macromolecules* **2004**, 37, 9899-9902

[108] Billmeyer, Jr. F. W. *"Textbook of Polymer Science 2nd Ed."* John Wiley and Sons, Inc., **1971**

[109] Webster, O. W. *Science* **1991**, 251, 887-893

[110] Swarc, M. *Nature* **1956**, 178, 1168-1169

[111] Swarc. M.; Levy, M. Milkovich, R. *J. Am. Chem. Soc.* **1956**, 78, 2656

[112] Flory, P. J. *"Principles of Polymer Chemistry"* Cornell Univ. Press., **1953**

[113] Painter, P. C.; Coleman, M. M. *"Fundamentals of Polymer Science, An Introductory Text 2nd Ed."* CRC Press LLC **1997**

[114] Patten, T. E.; Matyjaszewski, K *Adv. Mater.* **1998**, 10, 901-915

[115] Udding, J. H.; Tuijp, K. J. M.; van Zanden, M. N. A.; Hiemstra, H.; Meyerstein, D. *J. Org. Chem.* **1994**, 59, 1993

[116] Metzger, J. O.; Mahler, R. *Angew. Chem. Int. Ed. Engl.* **1995**, 34, 902

[117] Grove, D. M.; van Koten, G.; Verschuuren, A. H. M. *J. Mol. Catal.* **1988**, 45, 169

[118] Tsuji, J.; Sato, K.; Nagashima, H. *Chem. Lett.* **1981**, 1169

[119] Nagashima, H.; Wakamatsu, H.; Ozaki, N.; Ishii, T.; Watanabe, M.; Tajima, T.; Itoh, K. *J. Org. Chem.* **1992**, 57, 1682

[120] Minisci, F. *Acc. Chem. Res.* **1975**, 8, 165

[121] Patten, T. E.; Matyjaszewski, K. *Acc. Chem. Res.* **1999**, 32, 895-903

[122] Uegaki, H.; Kotani, Y.; Kamigaito, M.; Sawamoto, M. *Macromolecules* **1997**, 30, 2249

[123] Ando, T.; Kao, M.; Kamigaito, M.; Sawamoto, M. *Macromolecules* **1996**, 29, 1070

[124] Matyjaszewski, K.; Wei, M.; Xia, J.; McDermott, N. E. *Macromolecules* **1997**, 30, 8161

[125] Matyjaszewski, K.; Patten, T. E.; Xia, J. *J. Am. Chem. Soc.* **1997**, 119, 674

[126] Kotani, Y.; Kamigaito, M.; Sawamoto, M. *Macromolecules* **2000**, 33, 6746

[127] Kotani, Y.; Kamigaito, M.; Sawamoto, M *Macromolecules* **1999**, 32, 2420

[128] Brandts, J. A. M.; van de Geijn, P.; van Faassen, E. E.; Boersma, J.; van Koten, G. *J. Organomet. Chem.* **1999**, 584, 246-253

[129] Matyjaszewski, K.; Davis, K.; Patten, T. E.; Wei, M. L. *Tetrahedron* **1997**, 53, 15321

[130] Wang, J. S.; Matyjaszewski, K. *Macromolecules* **1995**, 28, 7901

[131] Percec, V.; Barboiu, B. *Macromolecules* **1995**, 28, 7970

[132] Matyjaszewski, K; Coessens, V.; Nakagama, Y.; Xia, J.; Qiu, J.; Gaynor, S.; Coca, S.; Jasieczek, C. *ACS Symp. Ser.* **1998**, 704, 16

[133] Destarac, M.; Bessiere, J.-M.; Boutevin, B. *J. Polym. Sci., Part A: Polym. Chem.* **1998**, 36, 2933

[134] Percec, V.; Barboiu, B.; Kim, H.-J. *J. Am. Chem. Soc.* **1998**, 120, 305

[135] Davis, K.; Paik, H.-J.; Matyjaszewski, K. *Macromolecules* **1999**, 32, 1767

[136] Simal, F.; Demonceau, A.; Noels, A. F. *Angew. Chem., Int. Ed. Engl.* **1999**, 38, 538

[137] Teodorescu, M.; Gaynor, S. G.; Matyjaszewski, K. *Macromolecules* **2000**, 33, 2335

[138] Moineau, G.; Minet, M.; Dubois, Ph.; Teyssie, Ph.; Senninger, T.; Jerome, R. *Macromolecules* **1999**, 32, 27-35

[139] Xia, J.; Gaynor, S. G.; Matyjaszewski, K. *Macromolecules* **1998**, 31, 5958

[140] Qin, S.; Qin, D.; Ford, W. T.; Resasco, D. E.; Herrera, J. E. *J. Am. Chem. Soc.* **2004**, 126, 170-176

[141] Zhang, X.; Xia, J.; Matyjaszewski, K. *Macromolecules* **1998**, 31, 5167-5169

[142] Carlmark, A.; Malmstrom, E. E. *Biomacromolecules* **2003**, 4, 1740-1745

[143] Beers, K. L.; Gaynor, S. G.; Matyjaszewski, K. *Macromolecules* **1998**, 31, 9413-9415

[144] Grimaud, T.; Matyjaszewski, K. *Macromolecules* **1997**, 30, 2216

[145] Lecornte, P.; Drapier, I.; Dubois, P.; Teyssie, P.; Jerome, R. *Macromolecules* **1997**, 30, 7631

[146] Moineau, G.; Granel, C.; Dubois, P.; Jeromes, R.; Teyssie, P. *Macromolecules* **1998**, 1, 542

[147] Matyjaszewski, K.; Xia, J. *Chem. Rev.* **2001**, 101, 2921-2990

[148] Kamigaito, M.; Ando, T.; Sawamoto, M. *Chem. Rev.* **2001**, 101, 3689-3745

[149] Jakubowski, W.; Matyjaszewski, K. *Macromolecules* **2005**, 38, 4139-4146

[150] Braunecker, W. A.; Matyjaszewski, K. *Prog. Polym. Sci.* **2007**, 32, 93-146

[151] Tsarevsky, N. V.; Braunecker, W. A.; Tang, W.; Brooks, S. J.; Matyaszewski, K.; Weisman, G. R.; Wong, E. H. *J. Mol. Catal. A: Chem* **2006**, 257, 132-140

[152] Gromada, J.; Matyjaszewski, K. *Macromolecules* **2001**, 34, 7664-7671

[153] Moad, G.; Rizzardo, E.; Solomon, D. H. *Macromolecules* **1982**, 15, 909; Solomon, D. H.; Rizzardo, E.; Cacioli, P., U.S. Patent 4,581,429, March 27, **1985**

[154] Georges, M. K.; Veregin, R. P. N.; Kazmaier, P. M.; Hamer, G. K. *Macromolecules* **1993**, 26, 2987

[155] Hawker, C. J. *Acc. Chem. Res.* **1997**, 30, 373-382

[156] Malmstrom, E. E.; Hawker, C. J. *Macromol. Chem. Phys.* **1998**, 199, 923-935

[157] Greszta, D.; Matyjaszewski, K. *Macromolecules* **1996**, 29, 7661-7670

[158] Hawker, C. J.; Bosman, A. W.; Harth E. *Chem. Rev.* **2001**, 101, 3661-3688

[159] Moad, G.; Rizzardo, E.; Thang, S. H. *Aust. J. Chem.* **2005**, 58, 379-410

[160] Barner-Kowollik, C.; Davis, T. P.; Heuts, J. P. A.; Stenzel, M. H.; Vana, P.; Whittaker, M *J. Polym. Sci. Part A: Polym. Chem.* **2003**, 41, 365-375

[161] Moad, G.; Chong, Y. K.; Postma, A.; Rizzardo, E.; Thang, S. H. *Polymer* **2005**, 46, 8458-8468

[162] Kricheldorf, H. R.; Nuyken, O.; Swift, G. *"Handbook of Polymer Synthesis 2nd Ed."* Marcel Dekker **2005**

[163] Saegusa, T.; Ikeda, H.; Fujii, H. *Macromolecules* **1973**, 6, 315

[164] Webster, O. W.; Hertler, W. R.; Sogah, D. Y.; Farnham, W. B.; RajanBabu, T. V. *J. Am. Chem. Soc.* **1983**, 105, 5706

[165] Sogah, D. Y.; Hertler, W. R.; Webster, O. W.; Cohen, G. M. *Macromolecules* **1988**, 20, 1473

[166] Bates, F. S. *Science* **1991**, 251, 898-905

[167] deGennes, P.-G. *"Scaling Concepts in Polymer Physics"* Cornell Univ. Press **1979**

[168] Flory, P. J. *"Principles of Polymer Chemistry"* Cornell Univ. Press **1953**

[169] Abraham, F. F. *"Homogeneous Nucleation Theory"* Academic **1974**

[170] Cahn, J. W. *J. Chem. Phys.* **1965**, 42, 93

[171] Bates, F. S.; Frederickson, G. H. *Annu. Rev. Phys. Chem.* **1990**, 41, 525-557

[172] Hillmyer, M *Curr. Op. Solid State & Mater. Sci.* **1999**, 4, 559-564

[173] Hamley, I. W. *"Developments in Block Copolymer Science and Technology"* John Wiley & Sons, Ltd **2004**

[174] Wang, J.-L.; Grimaud, T.; Shipp, D. A.; Matyjaszewski, K. *Macromolecules* **1998**, 31, 1527-1534

[175] Matyjaszewski, K.; Shipp, D. A.; McMurtry, G. P..; Gaynor, S. G.; Pakula, T. J. *Polym. Sci., Part A: Polym. Chem.* **2000**, 38, 2023-2031

[176] Tang, W.; Tsarevsky, N. V.; Matyjaszewski, K. *J. Am. Chem. Soc.* **2006**, 128, 1598-1604

[177] Tsarevsky, N. V.; Cooper, B. M.; Wojtyna, O. J.; Jahed, N. M.; Gao, H.; Matyjaszewski, K. Polym. Prep (Am. Chem. Soc., Div. Polym. Chem.) **2005**, 46, 249-250

[178] Leibler, L. Macromolecules **1980**, 13, 1602

[179] Fredrickson, G. H.; Helfand, E. J. Chem. Phys. **1987**, 87, 697

[180] Seminov, A. N. *Sov. Phys. JETP* **1985**, 61, 733

[181] Matsen, M. W.; Schick, M. *Phys. Rev. Lett.* **1994**, 72, 2660

[182] Matsen, M. W.; Bates, F. S. *Macromolecules* **1996**, 29, 1091

[183] Thurn-Albrecht, T.; Stiener, R.; DeRouchey, J.; Stafford, C. M.; Huang, E.; Bal, M.; Tuominen, M.; Harker, C. J.; Russell, T. P. *Adv. Mater.* **2000**, 12, 787

[184] Zhong, Z.; Zheng, S.; Mi, Y. *Polymer* **1999**, 40, 3829-3834

[185] Fox, Jr. T. G.; Flory, P. J. *J. Appl. Physics* **1950**, 21, 581-591

[186] Fornes, T. D.; Paul, D. R. *Polymer* **2003**, 44, 3945-3961

[187] Kim, S. H.; Misner, M. J.; Xu T.; Kimura, M.; Russell, T. P. *Adv. Mater.* **2004**, 16, 226-231

[188] Thurn-Albrecht, T.; Schotter, J.; Kastle, G. A.; Emley, N.; Shibauchi, T.; Krusin-Elbaum, L.; Guarini, K.; Black, C. T.; Tuominen, M. T.; Russell, T. P. *Science* **2000**, 290, 2126

[189] Xu, T.; Zvelindovsky, V.; Sevink, G. J. A.; Lyakhova, K. S.; Jinnai, H.; Russell, T. P. *Macromolecules* **2005**, 38, 10788-10798

[190] Cheng, J. Y.; Ross, C. A.; Thomas, E. L.; Smith, H. I.; Vancso, G. J. *Appl. Phys. Lett.* **2002**, 81, 3657

[191] Villar, M. A.; Rueda, D. R.; Ania, F.; Thomas, E. L. *Polymer* **2002**, 43, 5139

[192] De Rosa, C.; Park, C.; Thomas, E. L.; Lotz, B. *Nature* **2000**, 405, 433

[193] Bodycomb, J.; Funaki, Y.; Kimishima, K.; Hashimoto, T. *Macromolecules* **1999**, 32, 2075

[194] Kim, S. O.; Solar, H. H.; Stoykovich, M. P.; Ferrier, N. J.; de Pablo, J. J.; Nealey, P. F. Nature 2003, 424, 411

[195] Mansky, P.; Russel, T. P.; Hawker, C. J.; Pitsikalis, M.; Mays, J. *Macromolecules* **1997**, 30, 6810-6813

[196] Huang, E.; Rockford, L.; Russell, T. P.; Hawker, C. *Nature* **1998**, 395, 757

[197] Kimura, M.; Misner, M. J.; Xu, T.; Kim, S. H.; Russell, T. P. *Langmuir* **2003**, 19, 9910-9913

[198] Mansky, P.; Liu, Y.; Huang, E.; Russell, T. P.; Hawker, C. *Science* **1997**, 275, 1458-1460

[199] Xu, T.; Hawker, C. J.; Russell, T. P. *Macrmolecules* **2003**, 36, 6178-6182

[200] Lu, J. Q.; Kopley, T. E.; Moll, N.; Roitman, D.; Chamberlin, D.; Fu, Q.; Liu, J.; Russell, T. P.; Rider, D. A.; Manners, I.; Winnik, M. A. *Chem. Mater.* **2005**, 17, 2227-2231

[201] Lu, J. Q.; Rider, D. A.; Onyegam, E.; Wang, H.; Winnik, M. A.; Manners, I.; Cheng, Q.; Fu, Q.; Liu, J. *Langmuir* **2006**, 22, 5174-5179

[202] Zalusky, A. S.; Olayo-Valles, R.; Wolf, J. H.; Hillmyer, M. A. *J. Am. Chem. Soc.* **2002**, 124, 12761-12773

[203] Leiston-Belanger, J. M.; Russel, T. P.; Drockenmuller, E.; Hawker, C. J. *Macromolecules* **2005**, 38, 7676-7683

[204] Goldbach, J. T.; Lavery, K. A.; Panelle, J.; Russell, T. P. *Macromolecules* **2004**, 37, 9639-9645

[205] Drockenmuller, E.; Li, L. Y. T.; Ryu, D. Y.; Harth, E.; Russell, T. P.; Kim, H.-C.; Hawker, C. J. *J. Poly. Sci.: Part A: Poly. Chem.* **2005**, 43, 1028-1037

[206] Park, C.; Yoon, J.; Thomas, E. L. *Polymer* **2003**, 44, 6725-6760

[207] Odegard, G. M.; Gates, T. S.; Wise, K. E.; Park, C.; Siochi, E. J. *Composites Science and Technology* **2003**, 63, 1671-1687

[208] Matyjaszewski, K.; Xia, J. *Chem. Rev.* **2001**, 101, 2921-2990

[209] Patten, T. E.; Matyjaszewski, K. *Acc. Chem. Res.* **1999**, 32, 1172-1179

[210] Bartholome, C.; Beyou, E.; Bourgeat-Lami, E.; Chaumont, P.; Lefebvre, R.; Zydowicz, N.; *Macromolecules* **2005**, 38, 1099-1106

[211] Bartholome, C.; Beyou, E.; Bourgeat-Lami, E.; Cassagnau, P.; Chaumont, P.; David, L.; Zydowics, N. *Polymer* **2005**, 46, 9965-9973

[212] Moad, G.; Rizzardo, E.; Thang, S. H. *Aust J. Chem.* **2005**, 58, 379-410

[213] Matyjaszewski, K.; Jakubowski, W.; Min, K.; Tang, W.; Huang, J.; Braunecker, W. A.; Tsarevsky, N. V. *PNAS* **2006**, 103, 15309-15314

[214] Jin, Z.; Pramoda, K. P.; Xu, G.; Goh, S. H. *Chem. Phys. Lett.* **2001**, 337, 43-47

[215] Andrews, R.; Jacques, D.; Minot, M.; Rantell, T. *Macromol. Mater. Eng.* **2002**, 287, 395-403

[216] Velasco-Santos, C.; Martinez-Hernandez, A. L.; Fisher, F. T.; Ruoff, R.; Castano, V. M. *Chem. Mater.* **2003**, 15, 4470-4475

[217] Park, C.; Ounaies, Z.; Watson, K. A.; Crooks, R. E.; Smith, Jr. J.; Lowther, S. E.; Connell, J. W.; Siochi, E. J.; Harrison, J. S.; St. Clair, T. L. *Chem. Phys. Lett.* **2002**, 364, 303-308

[218] Li, S.; Qin, Y.; Shi, J. Guo, Z.-X.; Li, Y.; Zhu, D. *Chem. Mater.* **2005**, 17, 130-135

[219] Chiu, J. J.; Kim, B. J.; Kramer, E. J.; Pine, D. J. *J. Am. Chem. Soc.* **2005**, 127, 5036-5037

[220] Kong, H.; Gao, C.; Yan, D. *J. Mater. Chem.* **2004**, 14, 1401-1405

[221] Yao, Z.; Braidy, N.; Botton, G. A.; Adronov, A. *J. Am. Chem. Soc.* **2003**, 125, 16015-16024

[222] Hong, C.Y.; You, Y. Z.; Wu, D.; Liu, Y.; Pan, C. Y. *Macromolecules* **2005**, 38, 2606

[223] You, Y. Z.; Hong, C. Y.; Pan, C. Y. *Macromol. Rapid Commun.* **2006**, 27, 2001-2006

[224] Wichterle, O.; Lim, D. *Nature* **1960**, 185, 117-118

[225] Young, C.-D.; Wu, J.-R.; Tsou, T.-L. *Biomaterials* **1998**, 19, 1745-1758

[226] Jiang, X.; Lok, M. C.; Hennik, W. E. *Bioconjugate Chem.* **2007**, 18, 2077-2084

[227] Kumar, N. A.; Ganapathy, H. S.; Kim, J. S.; Jeong, Y. S.; Jeong, Y. T. *European Polymer Journal* **2008**, 44, 3, 579-586

[228] Billmeyer, Jr. F. W. *"Textbook of Polymer Science 2nd Ed."* John Wiley and Sons, Inc., **1971**

[229] Matyjaszewski, K; Xia, J. *Chem. Rev.* **2001**, 101, 2921-2990

[230] Hawker, C. J.; Bosman, A. W.; Harth, E. *Chem. Rev.* **2001**, 101, 3667-3688

[231] Moad, G.; Rizzardo, E.; Thang, S. H. *Aust. J. Chem.* **2005**, 58, 379-470

[232] Min, K.; Gao, H.; Matyjaszewski, K. *Macromolecules* **2007**, 40, 1789-1791

[233] Matyjaszewski, K.; Dong, H.; Jakubowski, W.; Pietrasik, J.; Kusumo, A. *Langmuir* **2007**, 23, 4528-2531

[234] Braunecker, W. A.; Matyjaszewski, K. *Prog. Polym. Sci.* **2007**, 32, 93-146

[235] Matyjaszewski, K.; Jakubowski, W.; Min, K.; Tang, W.; Huang, J.; Braunecker, W. A.; Tsarevsky, N. V. *PNAS* **2006**, 103, 15309-15314

[236] Jakubowski, W.; Min, K.; Matyjaszewski, K. *Macromolecules* **2006**, 39, 39-45

[237] Mueller, L.; Jakubowski, W.; Tang, W.; Matyjaszewski, K. *Macromolecules* **2007**, 40, 6464-6472

[238] Cheng, G. L.; Hu, C. P.; Ying, S. K. *Macromol. Rapid Commun.* **1999**, 20, 303

[239] Wang, G. L.; Hu, C. P.; Ying, S. K. *Polymer* **1999**, 40, 2167

[240] Kickelbick, G.; Matyjaszewski, K. *Macromol. Rapid Commun.* **1999**, 20, 341

[241] Amass, A. J.; Wyres, C. A.; Colclough, E.; Hohn, I. M. *Polymer* **1999**, 41, 1697

[242] Haddleton, D. M.; Jasieczek, C. B.; Hannon, M. J.; Shooter, A. J. *Macromolecules* **1997**, 30, 2190

[243] Queffelec, J.; Gaynor, S. G.; Matyjaszewski, K. *Macromolecules* **2000**, 33, 8629-8639

[244] Jakubowski, W.; Min, K.; Matyjaszewski, K. *Macromolecules* **2006**, 39, 39-45

[245] Mueller, L; Jakubowski, W.; Tang, W.; Matyjaszewski, K *Macromolecules* **2007**, 40, 6464-6472

[246] Plackett, D.; Jankova, K.; Egsgaard, H.; Hvilsted, S. *Biomacromolecules* **2005**, 6, 2474-2484

[247] Tao, Y.; Yun, W.; Dairen, L.; Ruke, B.; Weiqi, L. Front. Chem. Eng. China **2007**, 2, 140-145

[248] Liu, L.; Wang, W. Polymer Bulletin **2009**, 62, 315-325

[249] Silverstein, R. M.; Bassler, C. G.; Morrill, T. C. *Spectrometric Identification of Organic Compounds 3rd Ed.*, John Wiley & Sons Inc. **1974**

[250] Hwu, J. M.; Jiang, G. J.; Gao, Z. M.; Xie, W.; Pan, W. P. *J. App. Polymer Sci.* **2002**, 83, 1702-1710

[251] Huang, X.; Brittain, W. J. *Macromolecules* **2001**, 34, 3255-3260

[252] Xiao, P.; Xiao, M.; Gong, K. *Polymer* **2001**, 42, 4813-4816

[253] Fredrickson, G. H.; Bates, F. S. *Annu. Rev. Mater. Sci.* **1996**, 26, 501-550

[254] Matyjaszewski, K.; Shipp, D. A.; Wang, J. L.; Grimaud, T.; Pattern, T. E. *Macromolecules* **1998**, 31, 6836-6840

[255] Ramakrishnan, A.; Dhamodharan, R. *Macromolecules* **2003**, 36, 1039-1046

[256] Tsarevsky, N. V.; Cooper, B. M.; Wojtyna, O. J. Jahed, N. M.; Gao, H.; Matyjaszewski, K. Polym. Prep. (Am. Chem. Soc., Div. Polym. Chem.) **2004**, 46, 249-250

[257] Wang, X. –S.; Luo, N.; Ying, S. –K. J. Polym. Sci., Part A: Polym. Chem. **1999**, 37, 1255-1263

[258] Charleux, B.; Nicolas, J.; Guerret, O. Macromolecules **2005**, 38, 5485-5492

[259] Nicolas, J.; Dire, C.; Mueller, L.; Belleney, J.; Charleux, B.; Marque, S. R. A.; Bertin, D.; Magnet, S.; Couvreur, L. Macromolecules **2006**, 39, 8274-8282

[260] Fox, Jr. T. G.; Flory, P. J. J. Appl. Phys. **1950**, 21, 581-591

[261] Holoubek, J.; Lednicky, F.; Baldrian, J. European Polymer Journal **2006**, 42, 2236-2246

[262] Ebbesen, T. W. *Annu. Rev. Mater. Sci.* **1994**, 24, 235-264

[263] Majumder, M.; Chopra, N.; Hinds, B. J. *J. Am. Chem. Soc.* **2005**,127, 9062-9070

[264] Mitchell, C. A.; Bahr, J.L.; Arepalli, S.; Tour, J.M.; Krishnamoorti, R. *Macromolecules* **2002**, 35, 8825-8830

[265] Jin, Z.; Promoda, K. P.; Xu, G.; Goh, S. H. *Chem. Phys. Lett.* **2001**, 337, 43-47

[266] Haggenmueller, R.; Gommans, H. H.; Rinzler, A. G.; Fischer, J. E.; Winey, K. I. *Chem. Phys. Lett.* **2000**, 330, 219-225

[267] Sung, J. H.; Kim, H. S.; Jin, H. J.; Choi, H. J.; Chin, I. J. *Macromolecules* **2004**, 37, 9899-9902

[268] Ginic-Markovic, M.; Matisons, J. G.; Cervini, R.; Simon, G. P.; Fredericks, P. M. *Chem. Mater.* **2006**, 18, 6258-6265

[269] Kong, H.; Gao, C.; Yan, D. J. *Mater. Chem.* **2004**, 14, 1401-1405

[270] Yao, Z.; Braidy, N.; Botton, G. A.; Adronov, A. *J. Am. Chem. Soc.* **2003**, 125, 16015-16024

[271] Hong, C. Y.; You, Y. Z.; Wu, D.; Liu, Y.; Pan, C. Y. *Macromolecules* **2005**, 38, 2606-2611

[272] You, Y. Z.; Hong, C. Y.; Pan, C. Y. *Macromol. Rapid Commun.* **2006**, 27, 2001-2006

[273] Fragneaud, B.; Masenelli-Varlot, K.; Gonzalez-Montiel, A.; Terrones, M.; Cavaille, J. Y. *Chem. Phys. Lett.* **2007**, 444, 1-8

[274] Matrab, T.; Chancolon, J.; L'hermite, M. M.; Rouzaud, J. N.; Deniau, G.; Boudou, J. P.; Chehimi, M. M.; Delamar, M. *Colloids and Surfaces A: Physicochem. Eng. Aspects* **2006**, 287, 217-221

[275] Qin, S.; Qin, D.; Ford, W. T.; Resasco, D. E.; Herrera, J. E. *J. Am. Chem. Soc.* **2004**, 126, 170-176

[276] Baskaran, D.; Mays, J. W.; Bratcher, M. S. *Angew. Chem. Int. Ed.* **2004**, 43, 2138-2142

[277] Yamada, M.; Nishino, H.; Ueda, M. JP 2006028421 A 20060202

[278] Dehonor, M.; Masenelli-Varlot, K.; Gonzalez-Montiel, A.; Gautheir, C.; Cavaille, J. Y.; Terrones, H.; Terrones, M. *Chem. Commun.* **2005**, 42, 5349-5351

[279] Pei, X.; Hao, J.; Liu, W. *J. Phys. Chem. C* **2007**, 111, 2947-2952

[280] Xu, G.; Wu, W. T.; Wang, Y.; Pang, W.; Zhu, Q.; Wang, P.; You, Y. *Polymer* **2006**, 47, 5909-5918

[281] Guo, G.; Yang, D.; Wang, C.; Yang, S. *Macromolecules* **2006**, 39, 9035-9040

[282] Jakubowski, W.; Mueller, L.; Matyjaszewski, K. *Polymer Preprints* **2007**, 48, 256-257

[283] Aitchison, T. J.; Ginic-Markovic, M.; Matisons, J. G.; Simon, G. P.; Fredericks, P. M. *J. Phys. Chem. C* **2007**, 111, 2440-2446

[284] Bates, F. S.; Frederickson, G. H. *Annu. Rev. Phys. Chem.* **1990**, 41, 525-57

[285] Matyjaszewski, K.; Dong, H.; Jakubowski, W.; Pietrasik, J.; Kusumo, A. *Langmuir* **2007**, 23, 4528-4531

[286] Matyjaszewski, K.; Xia, J. *Chem. Rev.* **2001**, 101, 2921-2990

[287] von Werne, T. A.; Germack, D. S.; Hagberg, E. C.; Sheares, V. V.; Hawker, C. J.; Carter, K. R. *J. Am. Chem. Soc.* **2003**, 125, 3831-3838

[288] Carlmark, A.; Malmstrom, E. E. *Biomacromolecules* **2003**, 4, 1740-1745

[289] Ejaz, M.; Yamamoto, S.; Ohno, K.; Tsujii, Y.; Fukuda, T. *Macromolecules* **1998**, 31, 5934-5936

[290] Matyjaszewski, K.; Miller, P. J.; Shukla, N.; Immaraporn, B.; Gelman, A.; Luokala, B. B.; Siclovan, T. M.; Kickelbick, G.; Vallant, T.; Hoffmann, H.; Pakula, T. *Macromolecules* **1999**, 32, 8716-8724

[291] Queffelec, J.; Gaynor, S. G.; Matyjaszewski, K. *Macromolecules* **2000**, 33, 8629-8639

[292] Carlmark, A.; Malmstrom E. E. *Biomacromolecules* **2003**, 4, 1740-1745

[293] Ajayan, P. M.; Ebbesen, T. W. *Rep. Prog. Phys.* **1997**, 60, 1025-1062

[294] Dresselhaus, M. S.; Dresselhaus, G.; Ph. Avouris (Eds.) *"Carbon Nanotubes: Synthesis, Structure, Properties, and Applications"* Springer-Verlag Berlin Heidelberg **2001**

[295] Zhang, J.; Zuo, H.; Qing, Q.; Tang, Y.; Li, Q.; Liu, Z.; Guo, X.; Du, Z. *J. Phys. Chem. B* **2003**, 107, 3712-3718

[296] Gooding, J. J.; Wibowo, R.; Liu, J.; Yang, W.; Losic, D.; Orbons, S.; Mearns, F. J.; Shapter, J. G.; Hibbert, D. B. *J. Am. Chem. Soc.* **2003**, 125, 9006-9007

[297] White, M. A.; Johnson, J. A.; Koberstein, J. T.; Turro, N. J. *J. Am. Chem. Soc.* **2006**, 128, 11356-11357

[298] Silverstein, R. M.; Bassler, C. G.; Morrill, T. C. *Spectrometric Identification of Organic Compounds 3rd Ed.*, John Wiley & Sons Inc. **1974**

[299] Mawhinney, D. B.; Naumenko, B.; Kuznetsova, A.; Yates, Jr. J. T. *J. Am. Chem. Soc.* **2000**, 122, 2383-2384

[300] Braunecker, W. A.; Matyjaszewski, K. *Prog. Polym. Sci.* **2007**, 32, 93-146

[301] Jakubowski, W.; Matyjaszewski, K. *Macromolecules* **2005**, 38, 4139-4146

[302] Hicks, J. C.; Jones, C. W. *Langmuir* **2006**, 22, 2676-2681

[303] Kong, H.; Gao, C.; Yan, D. *Macromolecules* **2004**, 37, 4022-4030

[304] Li, L.; Lukehart, C. M. *Chem. Mater.* **2006**, 18, 94-99

[305] Pietrasik, J; Dong, H.l Matyjaszewski, K. *Macromolecules* **2006**, 39, 6384-6390

[306] Silverstein, R. M.; Bassler, C. G.; Morrill, T. C. *Spectrometric Identification of Organic Compounds 3rd Ed.*, John Wiley & Sons Inc. **1974**

[307] Wei, C.; Srivastava, D.; Cho, K. *Nano* Lett. **2002**, 2, 647

[308] Wild, S.; Kesmodel, L. L.; Apai, G. *J. Phys. Chem. B* **2000**, 104, 3179-3182

[309] Hiura, H.; Ebbesen, T. W.; Tanigaki, K. *Chem. Phys. Lett.* **1993**, 202, 509-512

[310] Bahr, J. L.; Yang, J.; Kosynkin, D. V.; Bronikowski, M. J.; Smalley, R. E.; Tour, J. M. *J. Am. Chem. Soc.* **2001**, 123, 6536-6542

[311] Veloso, M. V.; Filho, A. G. S.; Filho, J. M.; Fagan, S. B.; Mota, R. *Chem. Phys. Lett.* **2006**, 430, 71-74

[312] Barros, E. B.; Filho, A. G. S.; Lemos, V.; Filho, J. M.; Fagan, S. B.; Herbst, M. H.; Rosolen, J. M.; Luengo, C. A.; Huber, J. G. *Carbon* **2005**, 43, 2495-2500

[313] Wu, H.-X.; Tong, R.; Qiu, X.-Q.; Yang, H.-F.; Lin, Y.-H.; Cai, R.-F.; Qian, S.-X. *Carbon* **2007**, 45, 152-159

[314] Curran, S. A.; Talla, J.; Dias, S.; Zhang, D.; Carroll, D.; Birx, D. *J. Appl. Phys.* **2009**, 105, 079711-073715

[315] Brandrup, J.; Immergut, E. H.; Grulke, E. A. *"Polymer Handbook 4th Ed."* John Wiley and Sons **2003**

[316] Chowdhury, S. R.; Chen, Y.; Wang, Y.; Mitra, S. *J. Mater. Sci.* **2009**, 44, 1245-1250

[317] Billmeyer, Jr. F. W. *"Textbook of Polymer Science 2nd Ed."* John Wiley and Sons, Inc., **1971**

[318] Webster, O. W. *Science* **1991**, 251, 887-893

[319] Kovtyukhova, N. I.; Mallouk, T. E.; Pan, L.; Dicky, E. C. *J. Am. Chem. Soc.* **2003**, 125, 9761-9769

[320] Cai, L.; Bahr, J. L.; Yao, Y. Tour, J. M. *Chem. Mater.* **2002**, 14, 4235-4241

[321] Solomons, T. W. G.; Fryhle, C. B. *"Organic Chemistry 9th Ed."*, John Wiley and Sons, Inc., **2008**

[322] Roesky, H. W.; Andruh, M. Coordination Chemistry Reviews **2003**, 236, 91-119

[323] Silverstein, R. M.; Bassler, C. G.; Morrill, T. C. *Spectrometric Identification of Organic Compounds 3rd Ed.*, John Wiley & Sons Inc. **1974**

[324] Robinson, K. L.; Khan, M. A.; de Paz Banez, M. V.; Wang, X. S.; Armes, S. P. *Macromolecules* **2001**, 34, 3155-3158

[325] Jakubowski, W.; Min, K.; Matyjaszewski, K. *Macromolecules* **2006**, 39, 39-45

[326] Erdogan, M.; Hepuzer, Y.; Cianga, I.; Yagci, Y.; Pekcan, O. *J. Phys. Chem. A* **2003**, 107, 8363-8370

[327] Fernandez, J. E. *"Organic Chemistry: An Introduction"* Prentice-Hall, Inc., **1982**

[328] Piao, G.; Kimura, F.; Takahashi, T.; Moritani, Y.; Awano, H.; Nimori, S.; Tsuda, K.; Yonetake, K.; Kimura, T. *Polymer Journal* **2007**, 39, 589-592

[329] Kashiwagi, T.; Grulke, E.; Hilding, J.; Harris, R.; Awad, W.; Douglas, J. *Macromol. Rapid Commun.* **2002**, 23, 761

[330] Li, S.; Qin, Y.; Shi, J.; Guo, Z.-X.; Li, Y.; Zhu, D. *Chem. Mater.* **2005**, 17, 130-135

[331] Philip, B.; Xie, J.; Abraham, J. K.; Varadan, V. K. *Polymer Bulletin* **2005**, 53, 127-138

[332] Gao, J.; Itkis, M. E.; Yu, A.; Bekyarova, E.; Zhao, B.; Haddon, R. C. *J. Am. Chem. Soc.* **2005**, 127, 3847-3854

[333] Salalha, W.; Dror, Y.; Khalfin, R. L.; Cohen, Y.; Yarin, A. L.; Zussman, E. *Langmuir* **2004**, 20, 9852-9855

[334] Lou, X.; Daussin, R.; Cuenot, S.; Duwez, A.-S.; Pagnoulle, C.; Detrembleur, C.; Bailly, C.; Jerome, R. *Chem. Mater.* **2004**, 16, 4005-4011

[335] Deng, J.; Zhang, X.; Wang, K.; Zou, H.; Zhang, Q.; Fu, Q. *J. Membrane Sci.* **2007** 288, 261-267

[336] Blake, R.; Gun'ko, Y. K.; Coleman, J.; Cadek, M.; Fonseca, A.; Nagy, J. B.; Blau, W. J. *J. Am. Chem. Soc.* **2004**, 126, 10226-10227

[337] Fragneaud, B.; Masenelli-Varlot, K.; Gonzalez-Montiel, A.; Terrones, M.; Cavaille, J.-Y. *Chem. Phys. Lett.* **2007**, 444, 1-8

[338] Park, M.; Kim, H.; Youngblood, J. P. *Nanotechnology* **2008**, 19, 055705

[339] Andrews, R.; Jacques, D.; Minot, M.; Rantell, T. *Macromol. Mater. Eng.* **2002**, 287, 395-403

[340] Velasco-Santos, C.; Martinez-Hernandez, A. L.; Fisher, F. T.; Ruoff, R.; Castano, V. M. *Chem. Mater.* **2003**, 15, 4470-4475

[341] Park, C.; Ounaies, Z.; Watson, K. A.; Crooks, R. E.; Smith, Jr. J.; Lowther, S. E.; Connell, J. W.; Siochi, E. J.; Harrison, J. S.; St. Clair, T. L. *Chem. Phys. Lett.* **2002**, 364, 303-308

[342] Jin, Z.; Pramoda, K. P.; Xu, G.; Goh, S. H. *Chem. Phys. Lett.* **2001**, 337, 43-47

[343] Seymour, R. W.; Cooper, S. L. *Macromolecules* **1973**, 6, 48-53

[344] Weston, J. E.; Steele, B. C. H. *Solid State Ionics* **1981**, 2, 347-354

[345] Odegard, G. M.; Gates, T. S.; Wise, K. E.; Park, C.; Siochi, E. J. *Composites Science and Technology* **2003**, 63, 1671-1687

[346] Tobolsky, A. V.; Rogers, C. E.; Brickman, R. D. *J. Am. Chem. Soc.* **1960**, 82, 1277-1280

[347] Zhu, S.; Tian, Y.; Hamielec, A. E.; Eaton, D. R. *Macromolecules* **1990**, 23, 1144-1150

[348] Zhu, S.; Tian, Y.; Hamielec, A. E.; Eaton, D. R. *Polymer* **1990**, 31, 1726-1734

[349] Balke, S. T.; Hamielec, A. E. *J. App. Poly. Sci.* **1973**, 17, 905-949

[350] Gabbott, P. *Principles and Applications of Thermal Analysis* **2008**, Blackwell, United Kingdom

[351] Ishihara, N.; Seimiya, T.; Kuramoto, M. Uoi, M. *Macromolecules* **1986**, 19, 2464-2465

[352] Kriz, J.; Masar, B.; Plestil, J.; Tuzar, Z.; Pospisil, H.; Doskocilova, D. *Macromolecules* **1998**, 31, 41-51

[353] Wilkes, C. E.; Summers, J. W.; Daniels, C. A *PVC Handbook* **2005**, Carl Hanser Verlag, Germany

[354] Tagle, L. H.; Diaz, F. R.; Vega, R. J. *Poylmer Bulletin* **1984**, 11, 523-524

[355] Couchman, P. R. *Polymer Engineering and Science* **1981**, 21, 377-380

[356] Sung, J. H.; Kim, H. S.; Jin, H.-J.; Choi, H. J.; Chin, I.-J. *Macromolecules* **2004**, 37, 9899-9902

[357] Park, S. J.; Cho, M. S.; Lim, S. T.; Choi, H. J.; Jhon, M. S. *Macromol. Rapid Commun.* **2003**, 24, 1070-1073

[358] Mitchell, C. A.; Bahr, J. L.; Arepalli, S.; Tour, J. M.; Krishnamoorti, R. *Macromolecules* **2002**, 35, 8825

[359] Ma, S. X.; Cooper, S. L. *Macromolecules* **2001**, 34, 3294-3301

[360] Georgelos, A. N.; Torkelson, J. M. J. Non-Newtonian Fluid Mechanics **1988**, 27, 191-204

[361] Kota, A. K.; Cipriano, B. H.; Duesterberg, M. K.; Gershon, A. L.; Powell, D.; Raghavan, S. R.; Bruck, H. A. Macromolecules **2007**, 40, 7400-7406

[362] McClory, C.; McNally, T.; Baxendale, M.; Potschke, P.; Blau, W.; Ruether, M. *European Polymer Journal* **2010**, 46, 854-868

[363] Fangming, D.; Scogna, R. C.; Zhou, W.; Brand, S.; Fischer, J. E.; Winey, K. I. *Macromolecules* **2004**, 37, 9048-9055

[364] Jakubowski, W.; Min, K.; Matyjaszewski, K. *Macromolecules* **2006**, 39, 39-45

[365] Frankland, S. J. V.; Caglar, A.; Brenner, D. W.; Griebel, M. *J. Phys. Chem. B* **2002**, 106, 3046-3048

[366] Geng, H.; Rosen, R.; Zheng, B.; Shimoda, H.; Fleming, L.; Liu, J.; Zhou, O. *Adv. Mater.* **2002**, 14, 1387-1390

[367] Gao, J.; Itkis, M. E.; Yu, A.; Bekyarova, E.; Zhao, B.; Haddon, R. C. *J. Am. Chem. Soc.* **2005**, 127, 3847-3854

[368] Yang, M.; Koutsos, V.; Zaiser, M. *J. Phys. Chem. B* **2005**, 109, 10009-10014

[369] Ma, A. W. K.; Mackley, M. R.; Rahatekar, S. S. *Rheol Acta* **2007**, 46, 979-987

[370] Smoluchowski, M. *Z Phys Chem* **1917**, 92, 129-168

[371] Warren, L. J. *Chemtech* **1981**, 11, 180-185

[372] Zollars, R. I.; Ali, S. I. *J. Colloid Interface Sci.* **1986**, 114, 149-166

[373] Geng, H.; Rosen, R.; Zheng, B.; Shimoda, H.; Fleming, L.; Liu, J.; Zhou, O. *Adv. Mater.* **2002**, 14, 1387-1390

[374] Gao, J.; Itkis, M. E.; Yu, A.; Bekyarova, E.; Zhao, B.; Haddon, R. C. *J. Am. Chem. Soc.* **2005**, 127, 3847-3854

[375] Gorga, R. E.; Cohen, R. E.; *J. Polym. Sci. Part B: Polym. Phys.* **2004**, 42, 2690-2702

[376] Wei, C.; Srivastava, D.; Cho, K. *Nano Lett.* **2002**, 2, 647

[377] Majumder, M.; Chopra, N.; Hinds, B. J. *J. Am. Chem. Soc.* **2005**, 127, 9062

[378] Gelves, G. A.; Lin, B.; Sundararaj, U.; Haber, J. A. *Nanotechnology* **2008**, 19, 215712

[379] Robinson, K. L.; Khan, M. A.; de Paz Banez, M. V.; Wang, X. S.; Armes, S. P. *Macromolecules* **2001**, 34, 3155-3158

[380] Li, S.; Qin, Y.; Shi, J. Guo, Z.-X.; Li, Y.; Zhu, D. *Chem. Mater.* **2005**, 17, 130-135

[381] Holly, F. J.; Refojo, M. F. *Journal of Biomedical Materials Research* **1975**, 9, 315-326

[382] Robinson, K. L.; Khan, M. A.; de Paz Banez, M. V.; Wang, X. S.; Armes, S. P. *Macromolecules* **2001**, 34, 3155-3158

[383] Caykara, T.; Guven, O *Polymer Degradation and Stability* **1998**, 62, 267-270

[384] Mohomed, K.; Abourahma, H.; Zaworotko, M. J.; Harmon, J. P. *Chem. Commun.* **2005**, 3277-3279

[385] El-Tahlawy, K.; Hudson, S. M. *Journal of Applied Polymer Science* **2001**, 82, 683-702

[386] Ruoff, R. S.; Lorents, D. C. *Carbon* **1995**, 33, 925-930

[387] Bates, F. S. *Science* **1991**, 251, 898-905

[388] Zalusky, A. S.; Olayo-Valles, R.; Wolf, J. H.; Hillmyer, M. A. *J. Am. Chem. Soc.* **2002**, 124, 12761-12773

[389] Leiston-Belanger, J. M.; Russel, T. P.; Drockenmuller, E.; Hawker, C. J. *Macromolecules* **2005**, 38, 7676-7683

[390] Goldbach, J. T.; Lavery, K. A.; Panelle, J.; Russell, T. P. *Macromolecules* **2004**, 37, 9639-9645

[391] Drockenmuller, E.; Li, L. Y. T.; Ryu, D. Y.; Harth, E.; Russell, T. P.; Kim, H.-C.; Hawker, C. J. *J. Poly. Sci.: Part A: Poly. Chem.* **2005**, 43, 1028-1037

[392] Xu, T.; Zvelindovsky, V.; Sevink, G. J. A.; Lyakhova, K. S.; Jinnai, H.; Russell, T. P. *Macromolecules* **2005**, 38, 10788-10798

[393] Mansky, P.; Liu, Y.; Huang, E.; Russell, T. P.; Hawker, C. *Science* **1997**, 275, 1458-1460

[394] Lu, J. Q.; Kopley, T. E.; Moll, N.; Roitman, D.; Chamberlin, D.; Fu, Q.; Liu, J.; Russell, T. P.; Rider, D. A.; Manners, I.; Winnik, M. A. *Chem. Mater.* **2005**, 17, 2227-2231

[395] Lu, J. Q.; Rider, D. A.; Onyegam, E.; Wang, H.; Winnik, M. A.; Manners, I.; Cheng, Q.; Fu, Q.; Liu, J. *Langmuir* **2006**, 22, 5174-5179

[396] Odegard, G. M.; Gates, T. S.; Wise, K. E.; Park, C.; Siochi, E. J. *Composites Science and Technology* **2003**, 63, 1671-1687

[397] Chiu, J. J.; Kim, B. J.; Kramer, E. J.; Pine, D. J. *J. Am. Chem. Soc.* **2005**, 127, 5036-5037

[398] Li, H. J.; Lu, W. G.; Li, J. J.; Bau, X. D.; Gu, C. Z. *Phys. Rev. Lett.* **2005**, 95, 086601

[399] Hummer, G.; Rasaiah, J. C.; Noworyta, J. P. *Nature* **2001**, 414, 188-190

[400] Carlmark, A.; Malmstrom E. E. *Biomacromolecules* **2003**, 4, 1740-1745

[401] Yu, W. H.; Kang, E. T.; NeohShiping Zu, K. G. *J. Phys. Chem. B* **2003**, 107, 10198

[402] Xu, T.; Hawker, C. J.; Russell, T. P. *Macromolecules* **2003**, 36, 6178-6182

[403] Xu, T.; Kim, H. C.; DeRouchey, J; Sney, C.; Levesque, C.; Martin P.; Stafford C. M.; Russell, T. P. *Polymer* **2001**, 42, 9091-9095

[404] Mansky, P.; Liu, Y.; Huang, E.; Russell, T. P.; Hawker, C. *Science* **1997**, 275, 1458

[405] Robinson, K. L.; Khan, M. A.; de Paz Banez, M. V.; Wang, X. S.; Armes, S. P. *Macromolecules* **2001**, 34, 3155-3158

[406] Billmeyer, F. W. *"Textbook of Polymer Science 3rd Ed."*, John Wiley and Sons, New York, 1984 (Chapter 5)

[407] Meyer, V. E.; Lowry, G. G. *J. Polym. Sci. **1965**, A3, 2843-2851*

[408] Meyer, V. E.; Chan, R. K. S. *Am. Chem. Soc. Div. Polym. Chem. Prepr.* **1967**, 8, 209-215

[409] Plackett, D.; Jankova, K.; Egsgaard, H.; Hvilsted, S. *Biomacromolecules* **2005**, 6, 2474-2484

[410] Tao, Y.; Yun, W.; Dairen, L.; Ruke, B.; Weiqi, L. Front. Chem. Eng. China **2007**, 2, 140-145

[411] Silverstein, R. M.; Bassler, C. G.; Morrill, T. C. *Spectrometric Identification of Organic Compounds 3rd Ed.*, John Wiley & Sons Inc. **1974**

[412] Manksy, P.; Russell, T. P.; Hawker, C. J.; Pitsikalis, M.; Mays, J. *Macromolecules* **1997**, 30, 6810-6813

[413] Brandrup, J.; Immergut, E. H.; Grulke, E. A. *"Polymer Handbook 4th Ed."* John Wiley and Sons **2003**

[414] Owens, D. K.; Wendt, R. C. *J. App. Poly. Sci.* **1969**, 13, 1741-1747

[415] Liu, L.; Wang, W. Polymer Bulletin **2009**, 62, 315-325

[416] Xu, T.; Kim, H.-C.; DeRouchey, J.; Seney, C.; Levesque, C.; Martin, P.; Stafford, C. M.; Russell, T. P. *Polymer* **2001**, 42, 9091-9095

[417] Li, S.; Qin, Y.; Shi, J. Guo, Z.-X.; Li, Y.; Zhu, D. *Chem. Mater.* **2005**, 17, 130-135

[418] Bockstaller, M. R.; Lapetnikov, Y.; Margel, S.; Thomas, E. L. *J. Am. Chem. Soc.* **2003**, 125, 5276-5277

[419] Lacier, C. S. T.; Chastek, T. Q.; Lodge, T. P.; Taton, T. A. *Macromolecules* **2005**, 38, 9749-9756

[420] Min, K.; Gao, H.; Matyjaszewski, K. *Macromolecules* **2007**, 40, 1789-1791

[421] Matyjaszewski, K.; Dong, H.; Jakubowski, W.; Pietrasik, J.; Kusumo, A. *Langmuir* **2007**, 23, 4528-2531

[422] Matyjaszewski, K; Xia, J. *Chem. Rev.* **2001**, 101, 2921-2990

[423] Hawker, C. J.; Bosman, A. W.; Harth, E. *Chem. Rev.* **2001**, 101, 3667-3688

[424] Moad, G.; Rizzardo, E.; Thang, S. H. *Aust. J. Chem.* **2005**, 58, 379-470

[425] Kong, H.; Gao, C.; Yan, D. *Macromolecules* **2004**, 37, 4022-4030

[426] Aitchison, T. J.; Ginic-Markovic, M.; Matisons, J. G.; Simon, G. P.; Fredericks, P. M. *J. Phys. Chem. C* **2007**, 111, 2440-2446

[427] Xu, T.; Hawker, C. J.; Russell, T. P. *Macrmolecules* **2003**, 36, 6178-6182

[428] Xu, T.; Kim, H. C.; DeRouchey, J; Sney, C.; Levesque, C.; Martin P.; Stafford C. M.; Russell, T. P. *Polymer* **2001**, 42, 9091-9095

[429] Mansky, P.; Liu, Y.; Huang, E.; Russell, T. P.; Hawker, C. *Science* **1997**, 275, 1458

[430] Mitchell, C. A.; Bahr, J. L.; Arepalli, S.; Tour, J. M.; Krishnamoorti, R. *Macromolecules* **2002**, 35, 8825

[431] Gorga, R. E.; Cohen, R. E.; *J. Polym. Sci. Part B: Polym. Phys.* **2004**, 42, 2690-2702

[432] Velasco-Santos, C.; Martinez-Hernandez, A. L.; Fisher, F. T.; Ruoff, R.; Castano, V. M. *Chem. Mater.* **2003**, 15, 4470-4475

[433] Xu, T.; Zvelindovsky, A. V.; Sevink, G. J. A.; Lyakhova, K. S.; Jinnai, H.; Russell, T. P. *Macromolecules* **2005**, 38, 10788-10798

[434] Morkved, T. L.; Lu, M.; Urbas, A. M.; Ehrichs, E. E.; Jaeger, H. M.; Mansky, P.; Russell, T. P. *Science* **1996**, 273, 931-933

[435] Thurn-Albrecht, T.; DeRouchey, J.; Russell, T. P. *Macromolecules* **2000**, 33, 3250-3253

[436] Martin, C. A.; Sandler, J. K. W.; Windle, A. H.;; Schwarz, M.-K.; Bauhofer, W.; Schulte, K.; Shaffer, M. S. P. *Polymer* **2005**, 46, 877-886

[437] Piao, G.; Kimura, F.; Takahashi, T.; Moritani, Y.; Awano, H.; Nimori, S.; Tsuda, K.; Yonetake, K.; Kimura, T. *Polymer Journal* **2007**, 39, 589-592

[438] Fragneaud, B.; Masenelli-Varlot, K.; Gonzalez-Montiel, A.; Terrones, M.; Cavaille, J.-Y. *Chem. Phys. Lett.* **2007**, 444, 1-8

[439] Park, M.; Kim, H.; Youngblood, J. P. *Nanotechnology* **2008**, 19, 055705

[440] Thurn-Albrecht, T.; Steiner, R.; DeRouchey, J.; Stafford, C. M.; Huang, E.; Bal, M.; Tuominen, M.; Hawker, C. J.; Russell, T. P. *Adv. Mater.* **2000**, 12, 787-791

[441] Leiston-Belanger, J. M.; Russell, T. P.; Drockenmuller, E.; Hawker, C. J. *Macromolecules* **2005**, 38, 7676-7683